ANALYSIS OF SMS-2 ATTITUDE SENSOR BEHAVIOR

INCLUDING OABIAS RESULTS

Prepared for

GODDARD SPACE FLIGHT CENTER

By

COMPUTER SCIENCES CORPORATION

Under

Contract NAS 5-11999
Task Assignment 396

Prepared by:

Dr. L. C. Chen — Date 9/23/75

Dr. J. R. Wertz — Date

Approved by:

M. Joseph
Section Manager — Date 4/23/75

R. D. Cardwell
Technical Area Manager — Date

ORIGINAL PAGE IS
OF POOR QUALITY

ABSTRACT

The Synchronous Meteorological Satellite-2 (SMS-2) spacecraft was launched on February 6, 1975. For the first four days of the mission an extensive program of attitude and bias determination was carried out using primarily the Multisatellite Attitude Determination/Optical Aspect Bias Determination System (MSAD/OABIAS). This memorandum presents the results of this analysis, and makes specific recommendations for the support of future missions.

All necessary biases for accurate determination of attitude for SMS-2 were successfully determined in near real-time. No biases in excess of 0.4 degrees were found. New statistical and geometrical procedures implemented for predicting and measuring the determinability of biases were effective in both planning and carrying out an extensive program of bias determination which resulted in obtaining sensor bias measurements for all five SMS-2 Earth horizon sensors and Sun sensor 2 used during the first days of the mission. A systematic anomaly referred to as the "pagoda effect" appeared in the horizon sensor data wherever the scan of a sensor entered or left the disk of the Earth. This effect could degrade attitude and bias determination activities on future missions.

PRECEDING PAGE BLANK NOT FILMED

PAGE 11 INTENTIONALLY BLANK

ABSTRACT

The Synchronous Meteorological Satellite-2 (SMS-2) spacecraft was launched on February 6, 1975. For the first four days of the mission an extensive program of attitude and bias determination was carried out using primarily the Multisatellite Attitude Determination/Optical Aspect Bias Determination System (MSAD/OABIAS). This memorandum presents the results of this analysis, and makes specific recommendations for the support of future missions.

All necessary biases for accurate determination of attitude for SMS-2 were successfully determined in near real-time. No biases in excess of 0.4 degrees were found. New statistical and geometrical procedures implemented for predicting and measuring the determinability of biases were effective in both planning and carrying out an extensive program of bias determination which resulted in obtaining sensor bias measurements for all five SMS-2 Earth horizon sensors and Sun sensor 2 used during the first days of the mission. A systematic anomaly referred to as the "pagoda effect" appeared in the horizon sensor data whereever the scan of a sensor entered or left the disk of the Earth. This effect could degrade attitude and bias determination activities on future missions.

ACKNOWLEDGMENTS

The authors wish to acknowledge the assistance of L. Gunshol of the Orbit Determination Area and L. Hooper of the Attitude Determination Area in the review and preparation of this document for publication.

IV INTENTIONALLY BLANK

PRECEDING PAGE BLANK NOT FILMED

TABLE OF CONTENTS

Section 1 - Background 1-1

1.1 MSAD/OABIAS System Description 1-1
1.2 Bias Determination and Confirmation Procedures 1-4
1.2.1 Preliminary Analysis 1-4
1.2.2 Bias Determination 1-4
1.2.3 Confirmation 1-5
1.3 Real-Time Reporting Procedures 1-6

Section 2 - Prelaunch Analysis 2-1

2.1 Sensor Coverage 2-1
2.2 Bias and Attitude Determination Geometry 2-7
2.2.1 Description of Geometry Plots 2-7
2.2.2 Geometry at AMF Attitude 2-14
2.2.3 Geometry During Erection to Orbit Normal 2-18
2.3 Effect of Change of Launch Date 2-27
2.4 Nominal Bias Determination Sequence 2-28

Section 3 - Postlaunch Analysis 3-1

3.1 Bias Determination Sequence of Events 3-1
3.2 Data Quality 3-6
3.3 Pagoda Effect 3-19
3.4 Sensor Biases 3-57
3.4.1 Summary of Sensor Biases 3-57
3.4.2 Systematic Behavior of Results 3-61
3.4.3 Earth Horizon Sensor Biases 3-66
3.4.4 Sun Sensor Biases 3-139
3.5 Determination of Uncertainties 3-144

Section 4 - Conclusions and Recommendations 4-1

4.1 Conclusions 4-1
4.2 Recommendations 4-4

Appendix A - SMS Attitude Determination Hardware Description

References

PRECEDING PAGE BLANK NOT FILMED

PAGE vi INTENTIONALLY BLANK

LIST OF ILLUSTRATIONS

Figure

1-1	MSAD/OABIAS Functional Subsystems	1-2
1-2	Report Form for OABIAS Results	1-7
2-1	Horizon Sensor Coverage for SMS-2 Transfer Orbit	2-2
2-2	Horizon Sensor Coverage for SMS-2 Drift Orbit	2-3
2-3	Attitude Determination Geometry for Transfer Orbit and AMF Attitude	2-8
2-4	Determining Approximate AOS and LOS Locations From the Geometry	2-11
2-5	SMS-2 Attitude and Bias Geometry for AMF Attitude During Both Transfer Orbit and Drift Orbit Viewed From R.A. = 90^{o}, dec. = $+30^{o}$	2-15
2-6	SMS-2 Attitude and Bias Geometry for AMF Attitude During Both Transfer Orbit and Drift Orbit Viewed From R.A. = 150^{o}, dec. = 0^{o}	2-16
2-7	SMS-2 Attitude and Bias Geometry for AMF Attitude During Both Transfer Orbit and Drift Orbit Viewed From R.A. = 300^{o}, dec. = 0^{o}	2-17
2-8	Attitude Determination Geometry in the Drift Orbit at an Attitude of $\alpha = 19^{o}$, $\delta = -20^{o}$	2-19
2-9	Attitude Determination Geometry in the Drift Orbit at an Attitude of $\alpha = 19^{o}$, $\delta = -30^{o}$	2-20
2-10	Attitude Determination Geometry in the Drift Orbit at an Attitude of $\alpha = 19^{o}$, $\delta = -40^{o}$	2-21
2-11	Attitude Determination Geometry in the Drift Orbit at an Attitude of $\alpha = 19^{o}$, $\delta = -50^{o}$	2-22
2-12	Attitude Determination Geometry in the Drift Orbit at an Attitude of $\alpha = 19^{o}$, $\delta = -60^{o}$	2-23
2-13	Attitude Determination Geometry in the Drift Orbit at an Attitude of $\alpha = 19^{o}$, $\delta = -70^{o}$	2-24
2-14	Attitude Determination Geometry in the Drift Orbit at an Attitude of $\alpha = 19^{o}$, $\delta = -80^{o}$	2-25
3-1	DS# SMSB65 Data Plots Showing Unaveraged Raw Data	3-11
3-2	DS# SMSB66 Data Plots Showing Data From Figure 3-1 After Averaging	3-14
3-3	Sun Angle Measurements During Transfer Orbit	3-18
3-4	DS# SMSB56 Rotation Angle Data Showing Pagoda Effect	3-20
3-5	DS# SMSB56 Earth Width Data Showing Pagoda Effect	3-23

LIST OF ILLUSTRATIONS (Cont'd)

Figure

3-6 DS# SMSB56 OASYS Sun Angle/Mid-Scan Dihedral Angle Solution Showing Pagoda Effect 3-26
3-7 DS# SMSB56 Rotation Angle Plot for OASYS Solution for Center of Earth Ellipse 3-27
3-8 DS# SMSB56 Rotation Angle Plot for OABIAS Solution for Center of Earth Ellipse 3-29
3-9 DS# SMSB56 Earth Width Plot for OABIAS Solution for Center of Earth Ellipse 3-32
3-10 DS# SMSB60A Rotation Angle Data Showing Pagoda Effect 3-34
3-11 DS# SMSB60A Earth Width Data Showing Pagoda Effect 3-37
3-12 DS# SMSB60A Sun Angle Data Showing Absence of Pagoda Effect 3-40
3-13 DS# SMSB60A Spin Rate Showing Absence of Pagoda Effect 3-41
3-14 DS# SMSB60A Rotation Angle Plot for OABIAS Solution for Center of Earth Ellipse 3-43
3-15 DS# SMSB60B Rotation Angle Plot for OABIAS Solution for Center of Earth Ellipse 3-47
3-16 DS# SMSB60B Earth Width Plot for OABIAS Solution for Center of Earth Ellipse 3-50
3-17 DS# SMSB63 Earth Width Data Showing Visually Undetectable Pagoda Effect at Center of Data Span 3-53
3-18 DS# SMSB63 Earth Width Plot for OABIAS Solution Omitting Data From Center of Data Span 3-54
3-19 DS# SMSB67 Sun Sensor Switch Experiment 3-62
3-20 DS# SMSB52 Data Plots 3-71
3-21 DS# SMSB51 Comparison of OASYS Solutions With Nominal and OABIAS Parameters 3-74
3-22 DS# SMSB51 Earth Width Plots for Nominal and OABIAS Solutions 3-76
3-23 DS# SMSB60 Data Plots 3-78
3-24 DS# SMSB60 Comparison of OASYS Solutions With Nominal and OABIAS Parameters 3-86
3-25 DS# SMSB60 Rotation Angle and Earth Width Plots for Nominal and OABIAS Solutions 3-90
3-26 DS# SMSB64 Data Plots 3-96

LIST OF ILLUSTRATIONS (Cont'd)

Figure

3-27	DS# SMSB64 Comparison of OASYS Solutions With Nominal and OABIAS Parameters	3-99
3-28	DS# SMSB64 Earth Width Plots for Nominal and OABIAS Solutions	3-101
3-29	DS# SMSB63 Data Plots	3-104
3-30	DS# SMSB63 Comparison of OASYS Solutions With Nominal and OABIAS Parameters	3-107
3-31	DS# SMSB63 Earth Width Plots for Nominal and OABIAS Solutions	3-109
3-32	DS# SMSB53 Data Plots	3-114
3-33	DS# SMSB53 Comparison of OASYS Solutions With Nominal and OABIAS Parameters	3-117
3-34	DS# SMSB53 Earth Width Plot for Nominal and OABIAS Solutions	3-119
3-35	DS# SMSB52 Data Plots	3-123
3-36	DS# SMSB52 Comparison of OASYS Solutions With Nominal and OABIAS Parameters	3-126
3-37	DS# SMSB52 Earth Width Plot for Nominal and OABIAS Solutions	3-128
3-38	DS# SMSB59 Data Plots	3-129
3-39	DS# SMSB59 Comparison of OASYS Solutions With Nominal and OABIAS Parameters	3-132
3-40	DS# SMSB59 Earth Width Plot for Nominal and OABIAS Solutions	3-136
3-41	Sun Sensor Switch Experiments	3-141

LIST OF TABLES

Table

2-1	SMS-2 Nominal Parameters of January 10, 1975	2-9
3-1	Data Sets Used for Bias Determination on SMS-2	3-3
3-2	SMS-2 Bias Determination Summary	3-59
3-3	Comparison of Drift Orbit 2 and Drift Orbit 3	3-64
3-4	Earth Sensor-1 Bias Determination Results	3-69
3-5	Earth Sensor-2 Bias Determination Results	3-103
3-6	Earth Sensor-3 Bias Determination Results	3-113
3-7	Earth Sensor-4 Bias Determination Results	3-121
3-8	Earth Sensor-5 Bias Determination Results	3-138
3-9	OABIAS Bias Result for Sun Sensor-2	3-140

SECTION 1 - BACKGROUND

1.1 MSAD/OABIAS SYSTEM DESCRIPTION

The principal analytic tool for the determination of sensor biases on SMS-B is the Multi-Satellite Attitude Determination System/Optical Aspect Bias Determination System, MSAD/OABIAS (Reference 1). MSAD/OABIAS is a multi-satellite system designed to determine biases in the alignment or performance of optical horizon sensors used for spacecraft attitude determination. Specifically, MSAD/OABIAS uses any combination of eight observation models to process data from a single onboard horizon sensor and a Sun sensor to determine simultaneously the two components of the attitude of the spacecraft, the initial phase of the Sun sensor, the spin rate, seven sensor biases, and the orbital in-track error associated with the spacecraft ephemeris information supplied to the system. In addition, the MSAD/OABIAS system provides a data simulator for system and performance testing, an independent deterministic attitude system for preprocessing and independent testing of biases determined, and a multi-purpose data prediction and comparison system. The deterministic preprocessor used in MSAD/OABIAS is a modified version of the Optical Aspect Attitude Determination System, OASYS, which is also used within the SMSADS Attitude Determination System. (See Reference 2 for a description of the OASYS System.) It should be noted that the bias determination subsystem (OABIAS) and the deterministic preprocessing subsystem (OASYS) use completely different logic, coding, and processing techniques and, therefore, can serve as independent checks on any result obtained. The major components of the MSAD/OABIAS System are shown in Figure 1-1.

MSAD/OABIAS is intended primarily for use in an interactive graphics mode and makes use of the Graphics Executive Support System, GESS, to supply graphics and executive services. MSAD/OABIAS is a multi-satellite system capable of supporting Small Scientific Satellite (S^3), Radio Astronomy Explorer (RAE),

PAGE XII INTENTIONALLY BLANK PRECEDING PAGE BLANK NOT FILMED

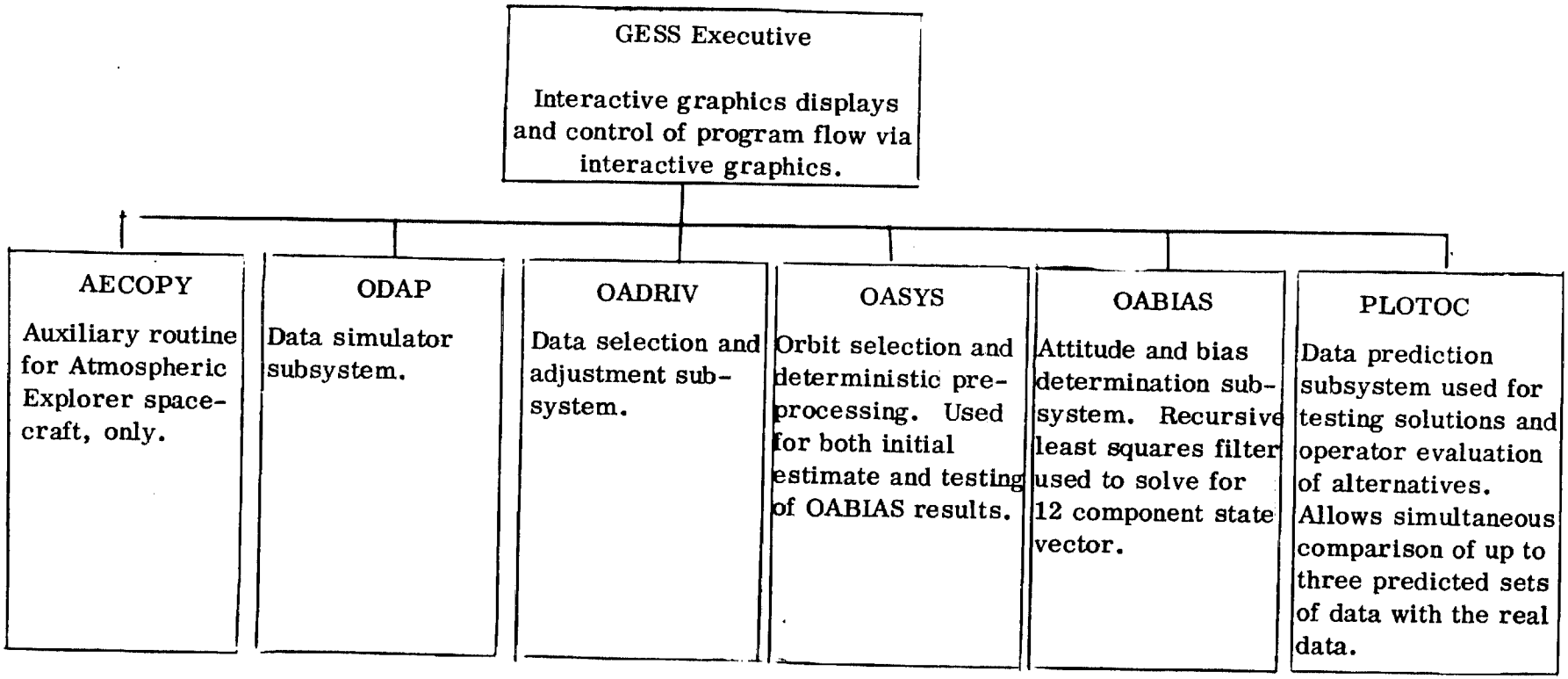
GESS Executive
Interactive graphics displays and control of program flow via interactive graphics.
AECOPY
Auxiliary routine for Atmospheric Explorer spacecraft, only.
ODAP
Data simulator subsystem.
OADRIV
Data selection and adjustment subsystem.
OASYS
Orbit selection and deterministic preprocessing. Used for both initial estimate and testing of OABIAS results.
OABIAS
Attitude and bias determination subsystem. Recursive least squares filter used to solve for 12 component state vector.
PLOTOC
Data prediction subsystem used for testing solutions and operator evaluation of alternatives. Allows simultaneous comparison of up to three predicted sets of data with the real data.

Figure 1-1. MSAD/OABIAS Functional Subsystems

NOTE: Program flow ordinarily progresses from left to right, starting at ODAP of OADRIV. AECOPY is not used for SMS missions. Note that this is not a baseline diagram of the MSAD/OABIAS System.

Interplanetary Monitoring Platform (IMP), Atmospheric Explorer (AE), and Synchronous Meteorological Satellite (SMS) missions or any similar missions using optical horizon scanners and providing attitude data in a form which can be read by the MSAD/OABIAS System.

1.2 BIAS DETERMINATION AND CONFIRMATION PROCEDURES

1.2.1 Preliminary Analysis

The preliminary analysis for bias determination consists of two phases: (1) prelaunch analysis of the distinguishability of observables and (2) data selection. The tests and procedures used to determine the distinguishability of observables are presented in Section 2. These procedures may be carried out prior to launch for nominal mission conditions.

After a particular pass of data has been received from the spacecraft and passed to MSAD/OABIAS, interactive graphics displays are used to examine the data, delete bad points, and select an appropriate subset for processing. This is ordinarily a rapid part of data processing. However, whenever any substantial anomalistic behavior of the data is observed this becomes an important and time-consuming part of attitude analysis. In particular, the large "pagoda effect" on SMS-2, described in detail in Section 3.3, required that more time than anticipated be spent in data selection.[1] The only effective way that bad data due to the pagoda effect can be identified is through runs of the attitude and bias programs. In such runs, systematic residuals were observed on both ends of each Earth ellipse of the SMS-2 data. This information was then used to eliminate data points corresponding to the large systematic residuals. The validity of this procedure was tested by checking for consistency among different data sets and by examination of predicted versus observed rotation angle plots.

1.2.2 Bias Determination

After a data pass is selected and invalid frames deleted, the data is passed to the OASYS subsystem of MSAD/OABIAS which computes a deterministic attitude

[1] The actual process of removing data can be done ordinarily in less than a minute. The time consuming element is the ongoing process of determining which data should be removed.

with nominal parameters. This solution is used as an initial estimate of the attitude state vector for bias determination and is also used for comparison with OASYS runs made using the parameters determined by OABIAS.

After OASYS processing, the data set is processed by the OABIAS subsystem for the determination of attitude and biases. Multiple runs of the OABIAS subsystem are used to determine uncertainties and test the convergence characteristics of the solutions. Use of the prelaunch analysis of the distinguishability of observables speeds this process considerably. Thus, in the transfer orbit, a preliminary report of OABIAS results (i.e., after a converged solution had been obtained but before the confirmation procedures discussed in Section 2) was made available for one data set within 15 minutes of the time that the OABIAS data set was written. Note that since this data set did not include any small Earth widths, it was not necessary to attempt to identify bad data due to the pagoda effect.

1.2.3 Confirmation

There are two main purposes of the confirmation procedures used to test bias results: (1) to test the degree to which the determined parameters have improved the fit to the data and the consistency of attitude solutions, and (2) to estimate the remaining systematic residuals in the data and determine their effect on attitude and bias uncertainties. The two procedures ordinarily used for confirmation of the results are a comparison of predicted and observed rotation angles and Earth widths and a re-analysis of the data with the OASYS deterministic subsystem using the parameters determined by the OABIAS subsystem. In both procedures a comparison is made between nominal parameters and OABIAS parameters to determine how much of the systematic residuals remain.

1.3 REAL-TIME REPORTING PROCEDURES

Figure 1-2 shows the report form used for results of OABIAS analysis during launch support. Since the last two pages consist entirely of information on uncertainties and confirmation results, the first page by itself may be used for preliminary reporting of results.

The statistical uncertainties given in Part IV of the form are at the 95% confidence level (2σ) and represent the minimum uncertainties for the set of parameters solved for. These uncertainties will depend on the noise on the data, the fit to the data, and the choice of parameters solved for. In general, the statistical uncertainties will be reduced by lower noise, a better fit, or solving for fewer parameters.

Part V of the form gives a comparison of the OABIAS results with attitude solutions based on nominal parameters, when both are processed with the OASYS deterministic subsystem. This comparison shows the size of the attitude shift caused by the biases and the improvement in the consistency of the results. An improved fit is indicated by more points remaining after automatic residual editing and by smaller standard deviations.

Part VI measures the fit of the nominal and OABIAS solutions to the data. For both nominal and OABIAS solutions, two parameters are given to indicate the presence of systematic residuals. "% of Good Fit" is an operator estimate of the percentage of the predicted data that lies within the noise on the observed data. The "Maximum Deviation" is the operator estimate of the largest variation between the predicted value and the mean of the observed values.

REPORT OF OABIAS RESULTS

Preliminary_____ Final Realtime_____

Stage of Processing (for Preliminary)_____

Date_____ Operator(s)_____ Sensors_____

I. Data Set Information

OABIAS Data Set No.:	No. of Frames Used:
Data Set Source:	Record Numbers:
Data Span (GMT): : / / to : / /	
Time Data Set Was Written (Local): : / /	
Time of OABIAS Run (Local): : / /	
Nominal Sensor Mounting Angle (Deg):	
Nominal Azimuth for Central Body Triggering (Deg):	
Sun Angle from Data (Deg):	Spin Rate from Data (Deg):

II. Orbit Information

a (Km):	S/C Ephemeris Source:
e:	Fortran Unit #:
i (Deg):	Disk or Tape:
M_o (Deg):	Tape # / File #:
ω (Deg):	Level:
Ω (Deg):	Solar Ephemeris Source:
Epoch (GMT):	

III. OABIAS Results (Deg)

Right Ascension, α	
Declination, δ	
Bias on Sensor Mounting Angle, Δr	
Bias on Central Body in Triggering, $\Delta\phi^i$	
Bias on Central Body out Triggering, $\Delta\phi^o$	
Bias on Central Body Angular Radius, $\Delta\rho$	
Bias on Sun Angle, $\Delta\beta$	
In-track Orbit Correction, Δt	

Figure 1-2. Report Form for OABIAS Results (1 of 3)

OABIAS SOLUTION CONFIDENCE LEVEL AND VERIFICATION

IV. OABIAS Uncertainties

Parameter	Value[1] (Deg)	Statistical Uncertainty[2] (95% Confid.=2 σ)	Comments
α			
δ			
$\Delta\gamma$			
$\Delta\phi^I$			
$\Delta\phi^0$			
$\Delta\rho$			
$\Delta\beta$			
Δt			

[1] Bracket = fixed at previously determined value; Brace = $\Delta\phi^I$ constrained to equal $\Delta\phi^0$; N.O. = not observable = fixed at 0.0 or nominal value.

[2] Statistical uncertainty is the minimum uncertainty for the set of parameters solved for. Any unkown correlated systematic variation will increase the uncertainty.

V. OASYS Deterministic Results

		Using Nominal Parameters	Using OABIAS Results
Right Ascension, α (Deg)			
Declination, δ (Deg)			
No. of Data Points before Editing			
No. of Data Points after Editing			
Standard Deviation	Arc Length		
	α		
	δ		

VI. Fit to Data

		OASYS Results with Nom. Param.	OABIAS Results
Rot. Angle	Mean Residual		
	STDV		
	% of Good Fit[3]		
	Maximum Deviation[4]		

Figure 1-2. Report Form for OABIAS Results (2 of 3)

VI. Fit to Data (Continued)			
		OASYS Results with Nom. Param.	OABIAS Results
Central Body Width	Mean Residual		
	STDV		
	% of Good Fit[3]		
	Maximum Deviation[4]		

[3]Percentage of predicted data within observed noise (operator estimate).

[4]Maximum deviation of predicted value from mean observed value (operator estimate).

"% of good fit" and "Max. deviation" are used to indicate the presence of systematic errors such as residual orbit errors or unmodeled parameters.

VII. Comments

Figure 1-2. Report Form for OABIAS Results (3 of 3)

SECTION 2 - PRELAUNCH ANALYSIS

2.1 SENSOR COVERAGE

Figures 2-1 and 2-2 show line-printer plots of the SMS-2 orbit with horizon sensor coverage indicated by numbers along the orbit. The small inner circle is the disk of the Earth. The letter S on the disk indicates the direction relative to the center of the Earth of the projection of the Sun line into the orbit plane. The large ellipse is the satellite orbit. The transfer orbit is shown in Figure 2-1 and the post-Apogee Motor Firing (AMF) drift orbit is shown in Figure 2-2. The numbers 1 through 5 indicate the regions of coverage of the five Earth horizon sensors ES1 to ES5. The approximate sensor mounting angles are: ES1, +4 degrees; ES2, -4 degrees; ES3, +20 degrees; ES4, -25 degrees; and ES5, -48 degrees. An unprimed number marks the location where the sensor acquires the Earth and a primed number marks the location where it loses the Earth. The plots were generated by a utility program developed with the OSAG System (Reference 3).

Figure 2-1 shows the sensor coverage in the transfer orbit for the Apogee Motor Firing attitude. The spacecraft is at this attitude from midway through the first outbound leg through Apogee Motor Firing at second apogee. The spacecraft is out of contact with the ground near perigee. Therefore, the only sensor coverage of interest is that from a true anomaly of about 90 degrees to a true anomaly of about 270 degrees. There is only one region where no sensor coverage is available. This is the small span from the loss of ES2 after apogee to the acquisition of ES4.

Figure 2-2 shows the sensor coverage in the post-AMF drift orbit for AMF attitude and the two intermediate attitudes at which data was collected while the spacecraft was being brought to orbit normal. An important feature that is evident from both Figures 2-1 and 2-2 is that there is a great deal of overlap in the coverage of ES1 and ES2, the two sensors which see the Earth when

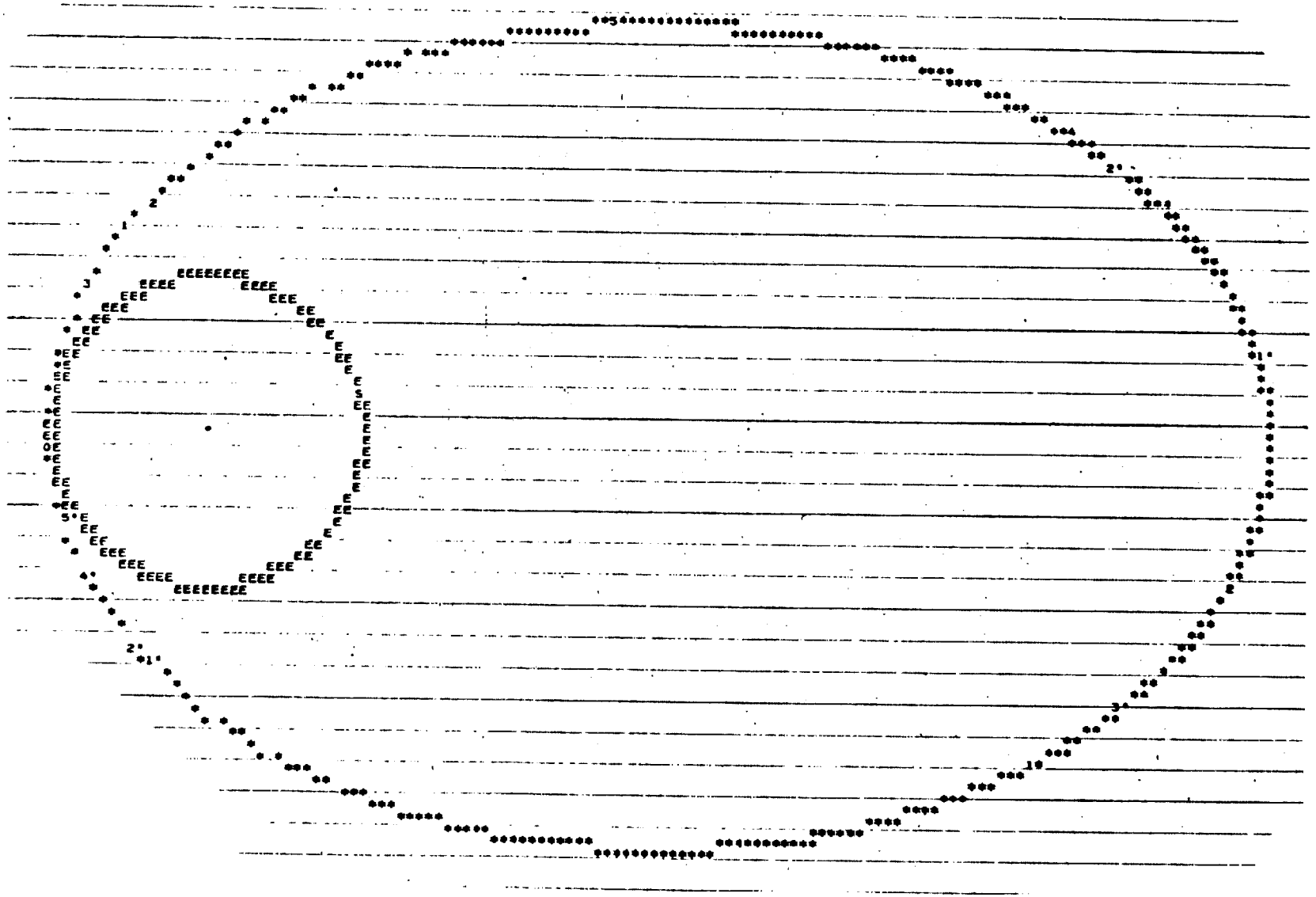

Figure 2-1. Horizon Sensor Coverage for SMS-2 Transfer Orbit

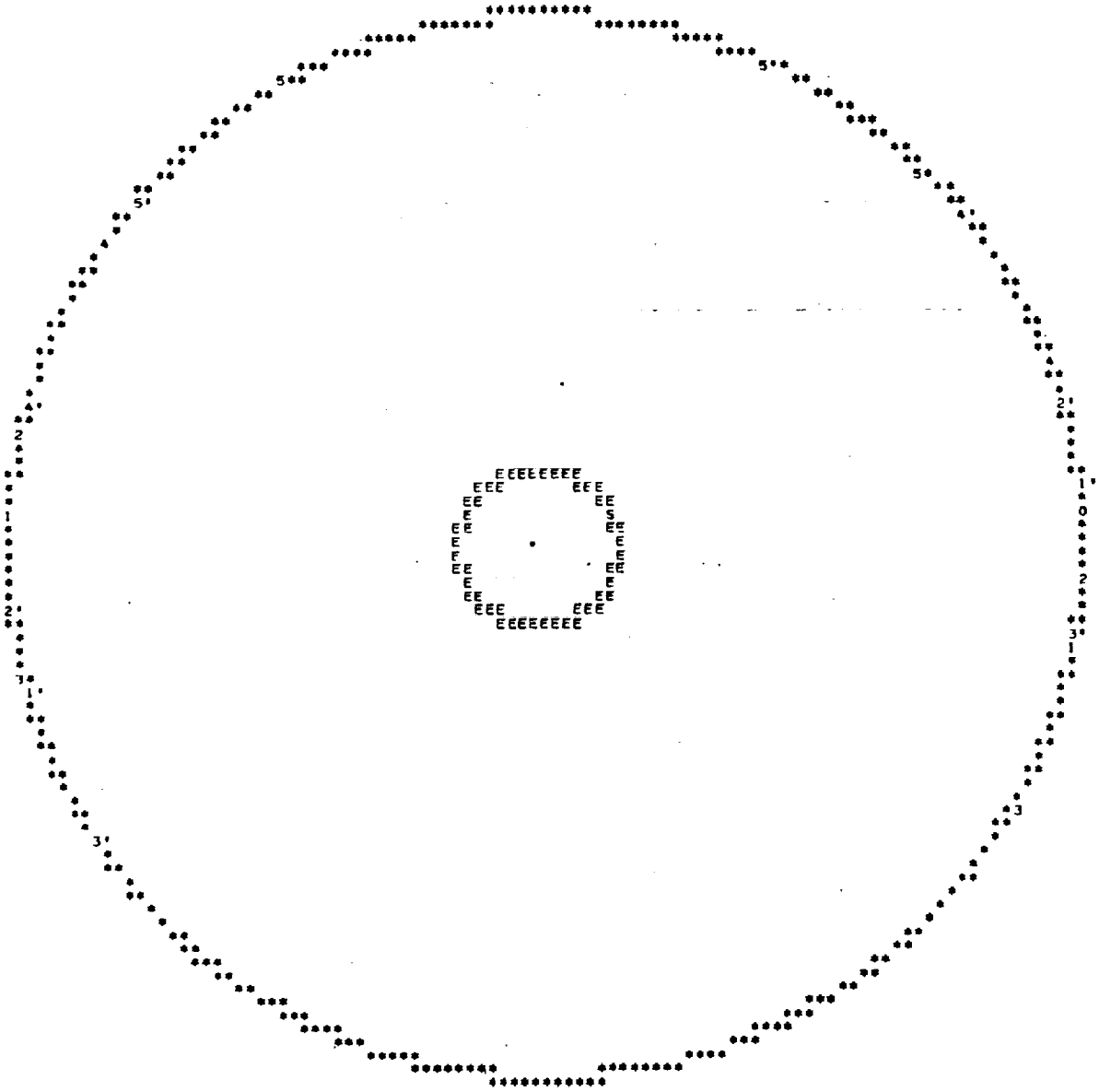

Figure 2-2. Horizon Sensor Coverage for SMS-2 Drift Orbit (1 of 3)

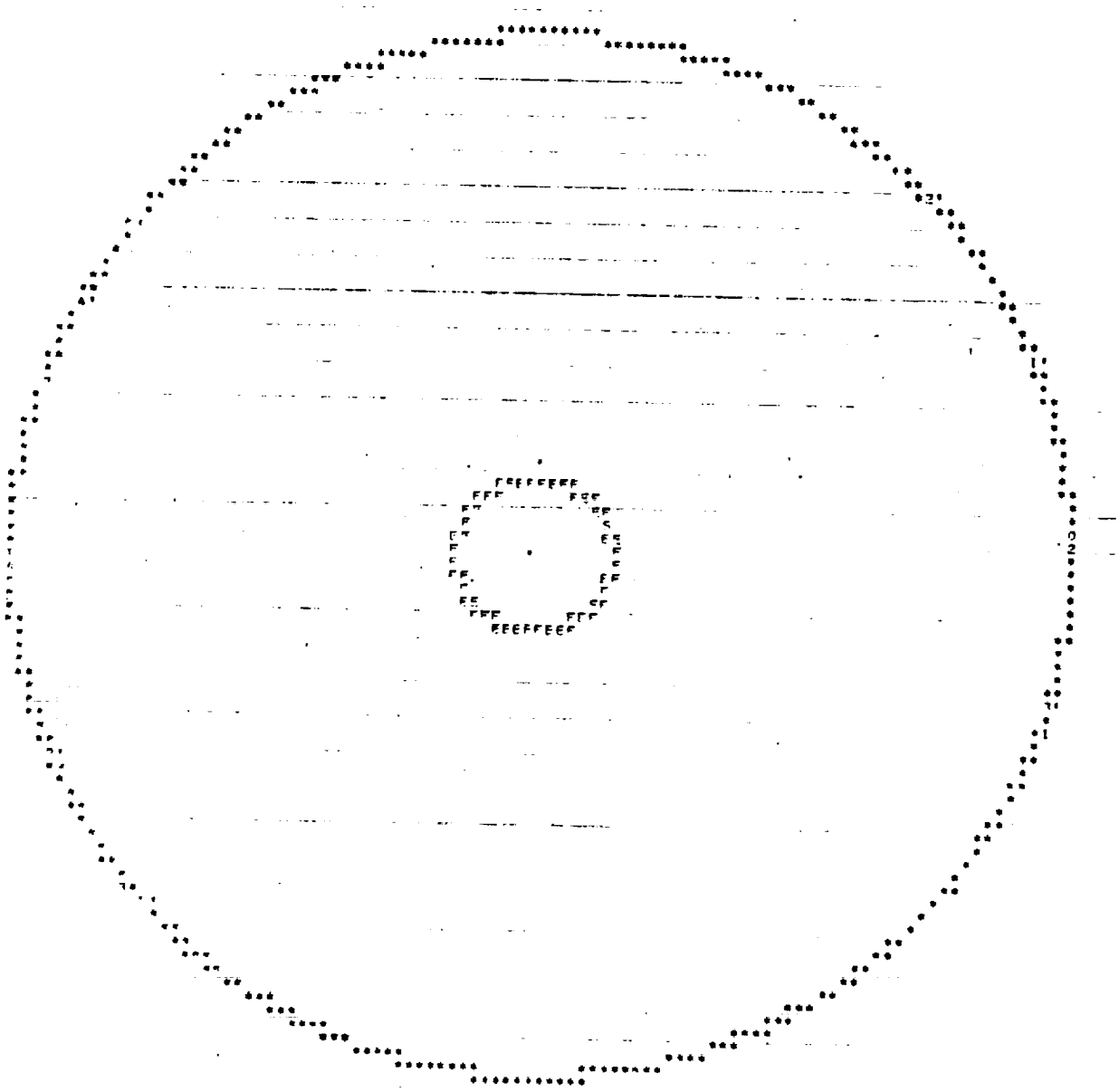

Figure 2-2. Horizon Sensor Coverage for SMS-2 Drift Orbit (2 of 3)

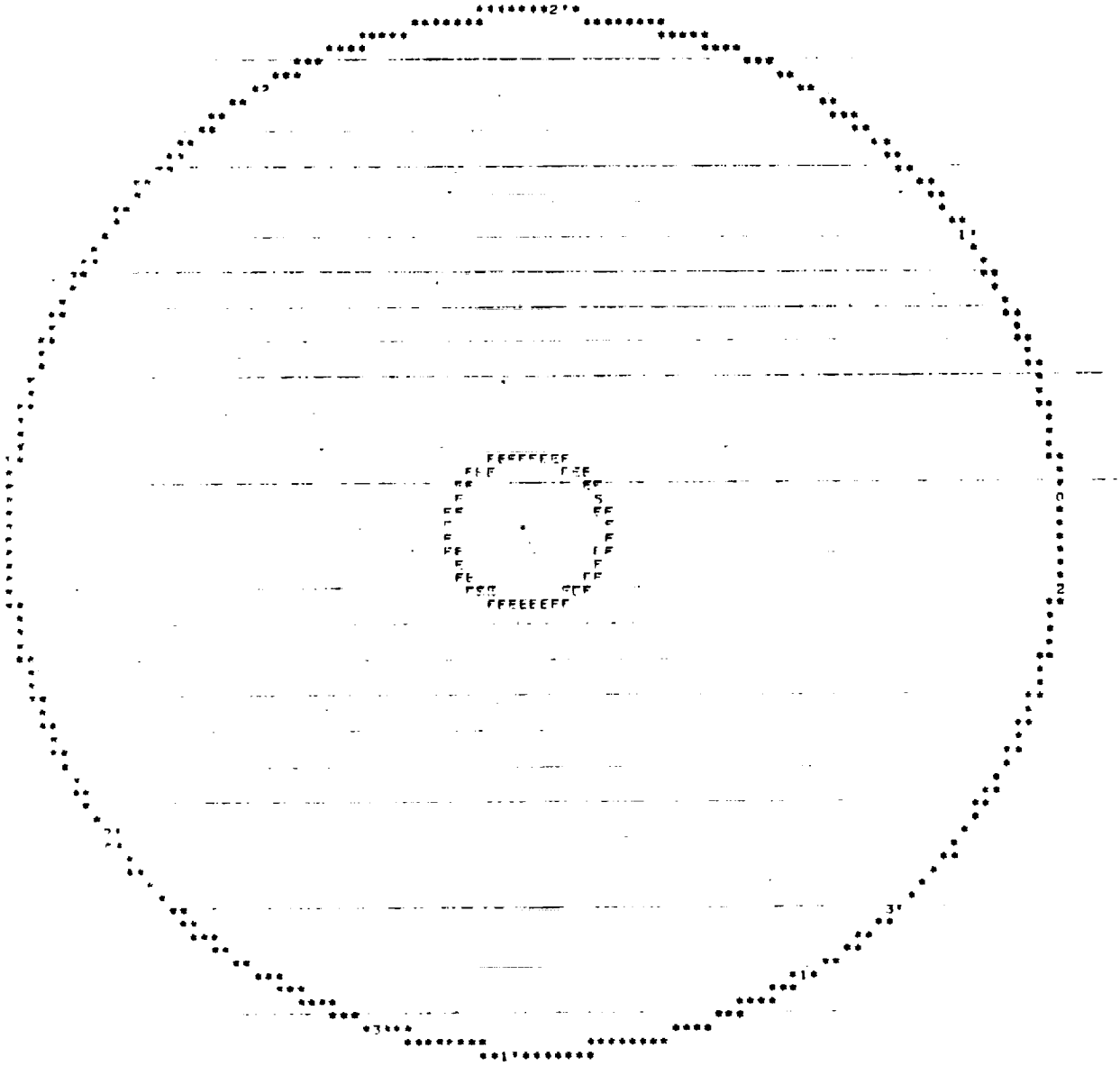

Figure 2-2. Horizon Sensor Coverage for SMS-2 Drift Orbit (3 of 3)

the spacecraft is in mission orbit at orbit normal. Thus, it is not possible to obtain a complete set of data for bias determination for both sensors without doubling the time required for data collection. The alternative chosen was to designate ES1 as the prime sensor for use in mission orbit and concentrate the bias determination efforts on that sensor.

2.2 BIAS AND ATTITUDE DETERMINATION GEOMETRY

An important analytic tool for the prelaunch analysis of the observability of sensor biases is a global plot of the celestial sphere showing regions where particular parameters are highly correlated. These are then regions of "poor geometry" in the sense that the correlated parameters are difficult to distinguish from each other and observation models based on these parameters will yield poor solutions. For example, in a region where the Sun angle bias and azimuth bias are highly correlated the Sun angle/Earth mid-scan dihedral angle observation model will give high uncertainties.

Section 2.2.1 describes the global geometry plots and the information contained on them. Section 2.2.2 presents and discusses plots for the spacecraft at Apogee Motor Firing attitude in both the transfer orbit and the post-AMF drift orbit. Finally, Section 2.2.3 describes the change in geometry as the attitude is maneuvered to orbit normal.

2.2.1 Description of Geometry Plots

Figure 2-3 is a plot of the celestial sphere showing the attitude and bias determination geometry for the SMS-2 spacecraft in the transfer orbit and oriented toward Apogee Motor Firing (AMF) attitude. All the celestial sphere plots in Section 2.2 are constructed with the nominal orbit parameters listed in Table 2-1. The effect of the change in launch date is discussed in Section 2.3.

In all the celestial sphere plots the spacecraft is assumed to be at the center of the sphere. Figure 2-3 is centered at 90^{o} right ascension and 30^{o} declination. Heavy solid lines show the orbit of the Earth around the spacecraft as seen from the spacecraft. The Earth (as viewed from the spacecraft) is moving toward increasing right ascension, that is, from left to right on the plots. Tick marks are times from apogee in 10 minute intervals. AP marks the location of apogee. P marks the location of perigee on plots where it is

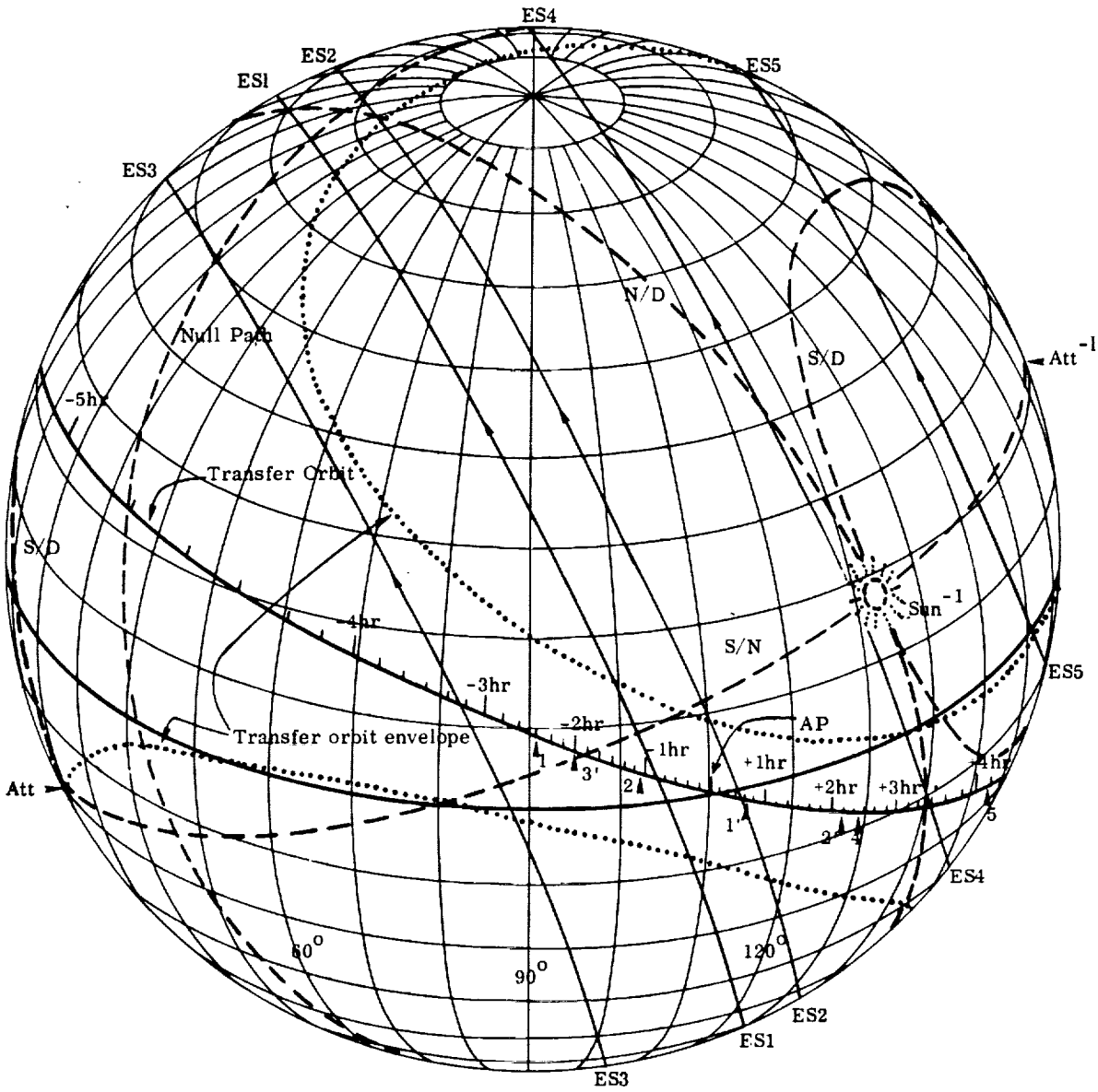

Figure 2-3. Attitude Determination Geometry for Transfer Orbit and AMF Attitude

Table 2-1. SMS-2 Nominal Parameters of January 10, 1975. (These parameters are used for all figures in Section 2-2.)

Sun location:	RA = 313^{o}
	Dec = -17.5^{o}
Attitude at AMF:	RA = 18.890^{o}
	Dec = -20.030^{o}
Sensor mounting angles:	ES1 = $+4^{o}$ (86^{o} from +z axis)
	ES2 = -4^{o} (94^{o})
	ES3 = $+20^{o}$ (70^{o})
	ES4 = -25^{o} (115^{o})
	ES5 = -48^{o} (138^{o})

Orbital Elements	Transfer Orbit	Post-AMF (Drift) Orbit
a (km)	24826.0	42740.357
e	0.73563	0.0034652
i (deg)	23.8	0.974
M_o (deg)	0.0	179.417
ω (deg)	179.90	202.776
Ω (deg)	290.0	268.388
Period (min)	649	1466
Epoch	1/30/75 22:30:10	1/31/75 14:42:22

visible. The dotted line surrounding the orbit marks the envelope of the disk of the Earth as it moves across the sky. S marks the location of the Sun and S^{-1} marks the anti-solar point. Att marks the location of the AMF attitude and Att^{-1} marks the direction of the negative attitude axis (anti-attitude). The small circles labeled ES1 to ES5 and centered on Att and Att^{-1} (approximately straight lines going from upper left to lower right in Figure 2-3) are the field of view (FOV) lines of the five Earth horizon sensors as the spacecraft spins about the Att-Att^{-1} axis. Arrowheads on the FOV lines indicate the direction in which the sensors scan the sky. Acquisition and loss of the Earth by each sensor are indicated by arrowheads with primed numbers (LOS) or unprimed numbers (AOS) along the orbit. These locations may be determined approximately from the plots by the method shown in Figure 2-4, although the points marked on the plots are those obtained from runs of the programs OSAG and ODAP (References 2-3 and 2-4). Inaccuracies in the geometrical procedures of Figure 2-4 occur because the sensor field of view and the envelope of the Earth are not great circles.

Dashed curves on the plots are regions of poor geometry for attitude and bias determination due to a strong correlation among attitude determination procedures or, equivalently, among biases. S/N (Sun/Nadir) is the great circle containing the attitude and the Sun vector. Where this curve intersects the orbit the Sun vector, nadir vector, and attitude are coplanar; the Sun angle/nadir angle (or Sun angle/Earth width) attitude solutions have large uncertainties; and the Sun angle bias and sensor mounting angle bias are highly correlated. Figure 2-3 shows this occurs about 40 minutes after AOS for the region of coverage of ES1 near apogee in the transfer orbit. The large correlation and uncertainties were independently confirmed by runs of both the OASYS and OABIAS attitude systems. Since the attitude/Sun vector plane is at a small inclination to the equator, the principle attitude uncertainty is in the right ascension component

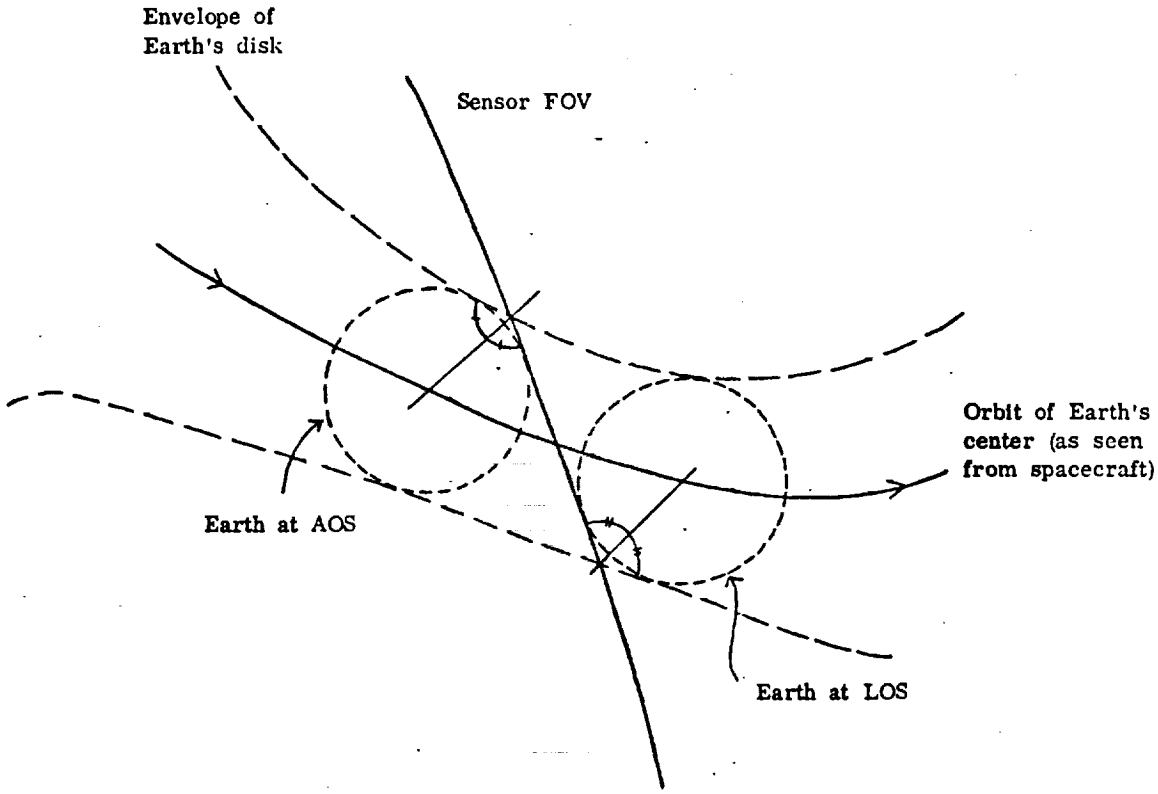

Figure 2-4. Determining Approximate AOS and LOS Locations From the Geometry

NOTE: At AOS the Earth's disk must be tangent to both the sensor FOV (field of view) and the envelope of the Earth's disk. Let A be the angle formed by the intersection of the sensor FOV and the envelope of the Earth's disk. Then, if the area surrounding A is sufficiently small that both curves may be treated as segments of great circles, the great circle which bisects A will intersect the Earth's orbit at the location of the center of the Earth when AOS occurs.

if the Sun angle and sensor mounting angle biases are assumed to be unknown and in the declination component if these biases are fixed. Again, this result is in agreement with OASYS and OABIAS results. The major result of this correlation is that ES1 data from the transfer orbit cannot be used for determination of the Sun angle bias and sensor mounting angle bias simultaneously. Thus, if a large Sun angle bias is suspected from the initial data, it must be determined with data from a sensor other than ES1.

If the Earth lies on the great circle labeled N/D, then, at that point in the orbit, the nadir angle and Sun-Earth midscan dihedral angle are highly correlated, that is, the same information is being obtained from both measurements. This implies that the sensor mounting angle bias and azimuth bias are highly correlated.

The dashed curve labeled S/D passing through the Sun and the attitude or Sun^{-1} and Att^{-1} shows the location of the Earth for which the Sun angle and Sun-Earth midscan dihedral angle are highly correlated. This does not occur at all for the transfer orbit. Thus, in the transfer orbit, correlations between Sun angle and azimuth bias will not be a major difficulty for bias determination.

Again, the presence of correlations between both nadir angle/midscan dihedral angle and Sun angle/midscan dihedral angle have been confirmed by runs of OASYS and OABIAS. At least for the SMS-2 geometry, these correlations do not cover as wide an area of the celestial sphere as does the Sun angle/nadir angle correlation. That is, the regions of poor geometry are narrower around the N/D or S/D curves than around the S/N curve.

Finally, the great circle labeled Null path is the locus of the Sun vector/nadir vector cross product, as the spacecraft moves around the Earth. This great circle is perpendicular to the Sun axis and is the same for all orbits. When the spacecraft attitude is near the Null path, there are

regions of the orbit where dihedral angle measurements are poor due to a low dihedral angle density. This is not a problem for the AMF attitude. References 5 and 6 contain a more extended discussion of attitude and bias determination geometry.

2.2.2 Geometry at AMF Attitude

Figures 2-5, 2-6, and 2-7 are plots of the celestial sphere showing the attitude and bias determination geometry for the SMS-2 spacecraft oriented toward AMF attitude in both the transfer orbit and the post AMF drift orbit. In the nominal sequence of events, the spacecraft goes to near AMF attitude on the first outbound leg[1] and remains near this attitude for about 1 1/4 revolutions in the transfer orbit through AMF, and for approximately one revolution in the post AMF drift orbit.

The major conclusion from the geometry plots is that in the transfer orbit a Sun angle bias and a sensor mounting angle bias are effectively indistinguishable for ES1, the prime attitude sensor in the drift and mission orbits. The same problem is encountered in one of the two Earth ellipses seen by both ES3 and ES4 at AMF attitude in the drift orbit. However, these sensors are of little practical interest, since they cannot view the Earth in mission orbit and attitude. In addition, the azimuth bias and the sensor mounting angle bias are highly correlated and, therefore, difficult to separate for ES4 in one of the two Earth ellipses in the drift orbit and in the early data furthest from perigee in the transfer orbit. Other correlations exist which are of little interest to mission operations.

Figure 2-5 is centered at right ascension 90°, declination $+30^{\circ}$. Thus, it is the same as Figure 2-1 with the drift orbit added. Figure 2-6 is centered at right ascension 150°, declination 0°. Figure 2-7 is centered at right ascension 300°, declination 0°. Note that Figure 2-7 covers a region in which the spacecraft is normally out of contact with the Earth while in the transfer orbit. Thus, this figure is for use primarily in the determination of drift orbit geometry.

As previously discussed in Section 2.2.1, Earth sensor-1 in the transfer orbit

[1] "Outbound leg" refers to the portion of the orbit from perigee to apogee and "inbound leg" refers to the portion from apogee to perigee.

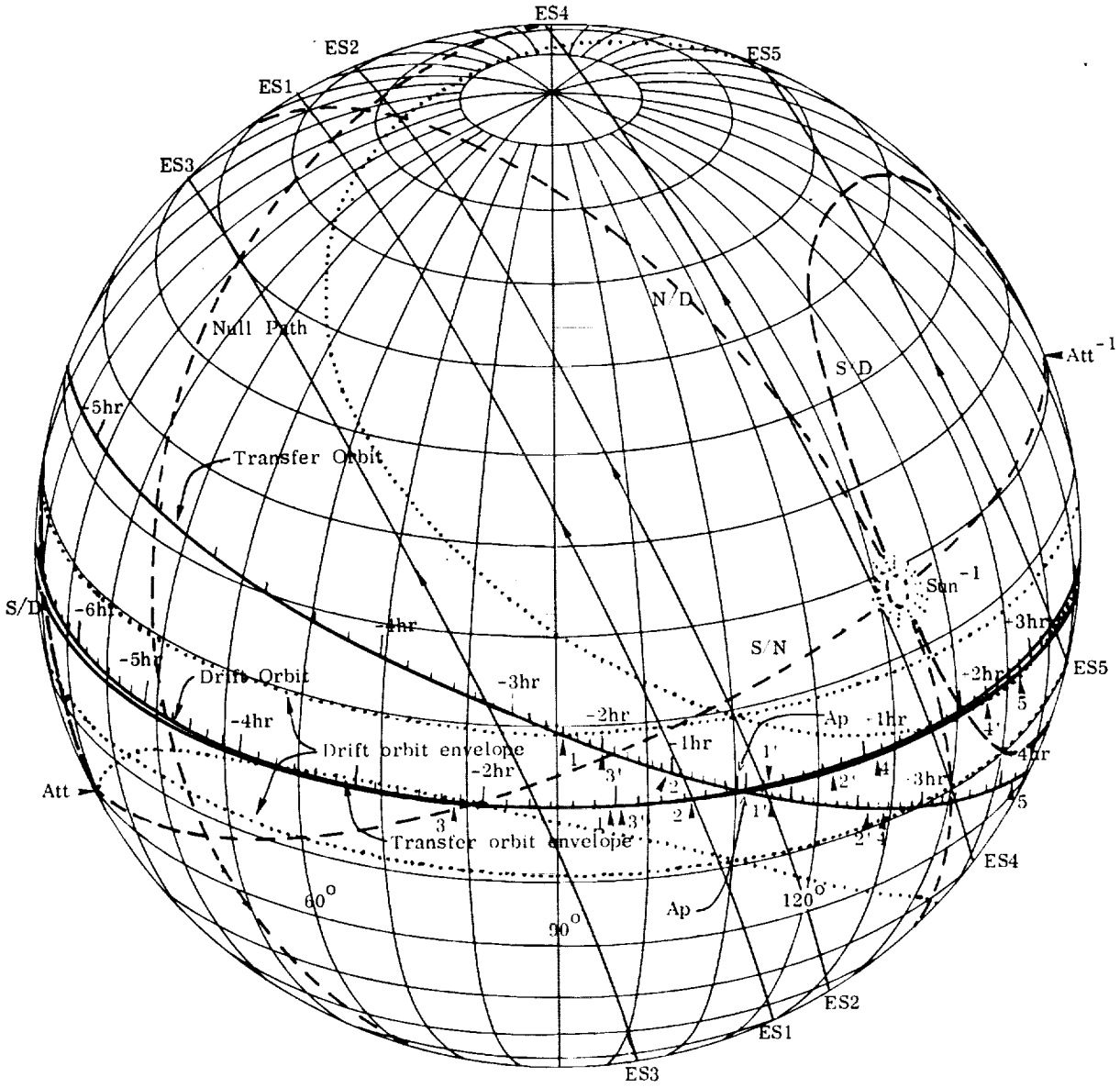

Figure 2-5. SMS-2 Attitude and Bias Geometry for AMF Attitude During Both Transfer Orbit and Drift Orbit Viewed From R.A. = 90°, dec. = +30°

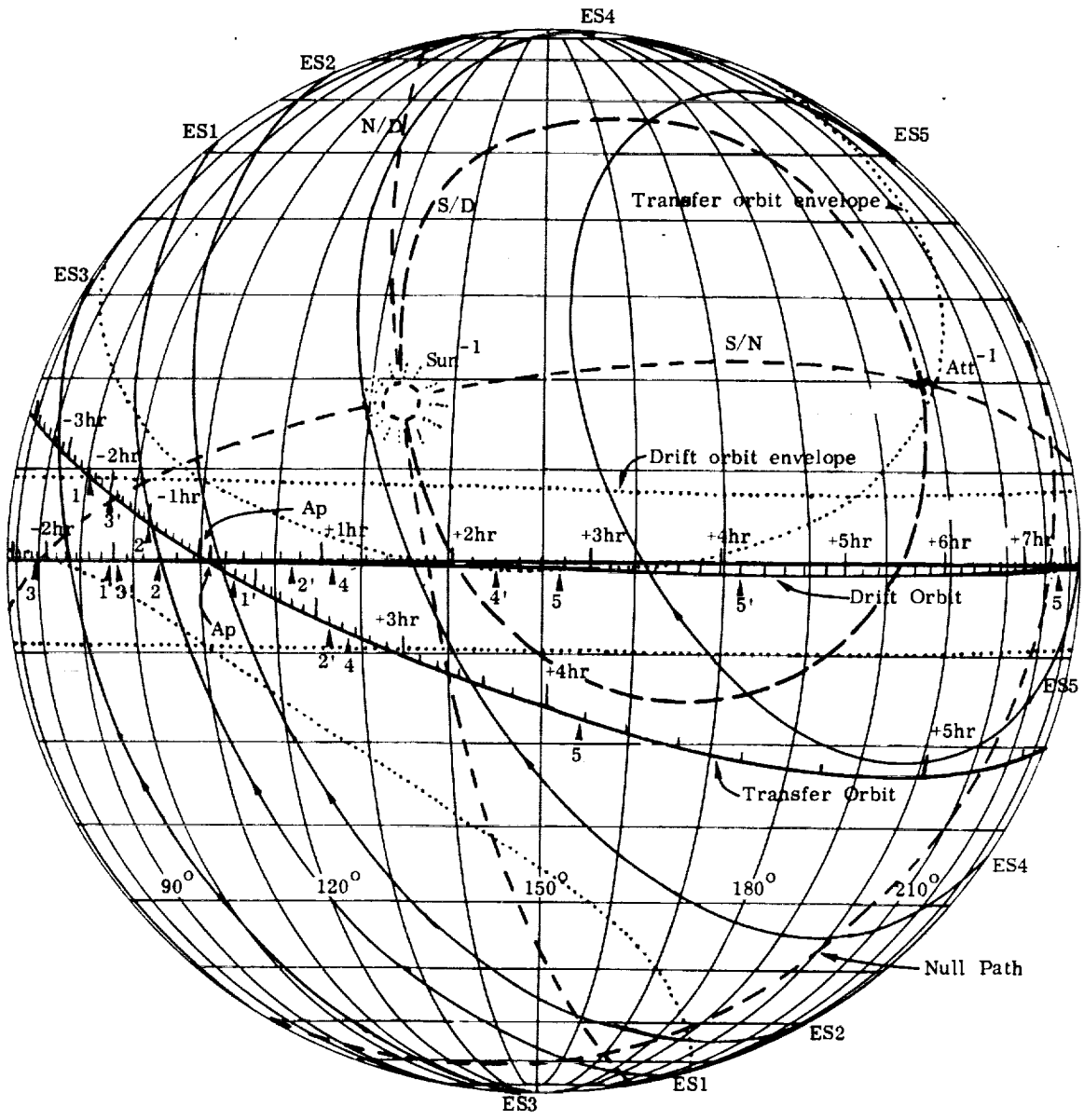

Figure 2-6. SMS-2 Attitude and Bias Geometry for AMF Attitude During Both Transfer Orbit and Drift Orbit Viewed From R.A. = 150°, dec. = 0°

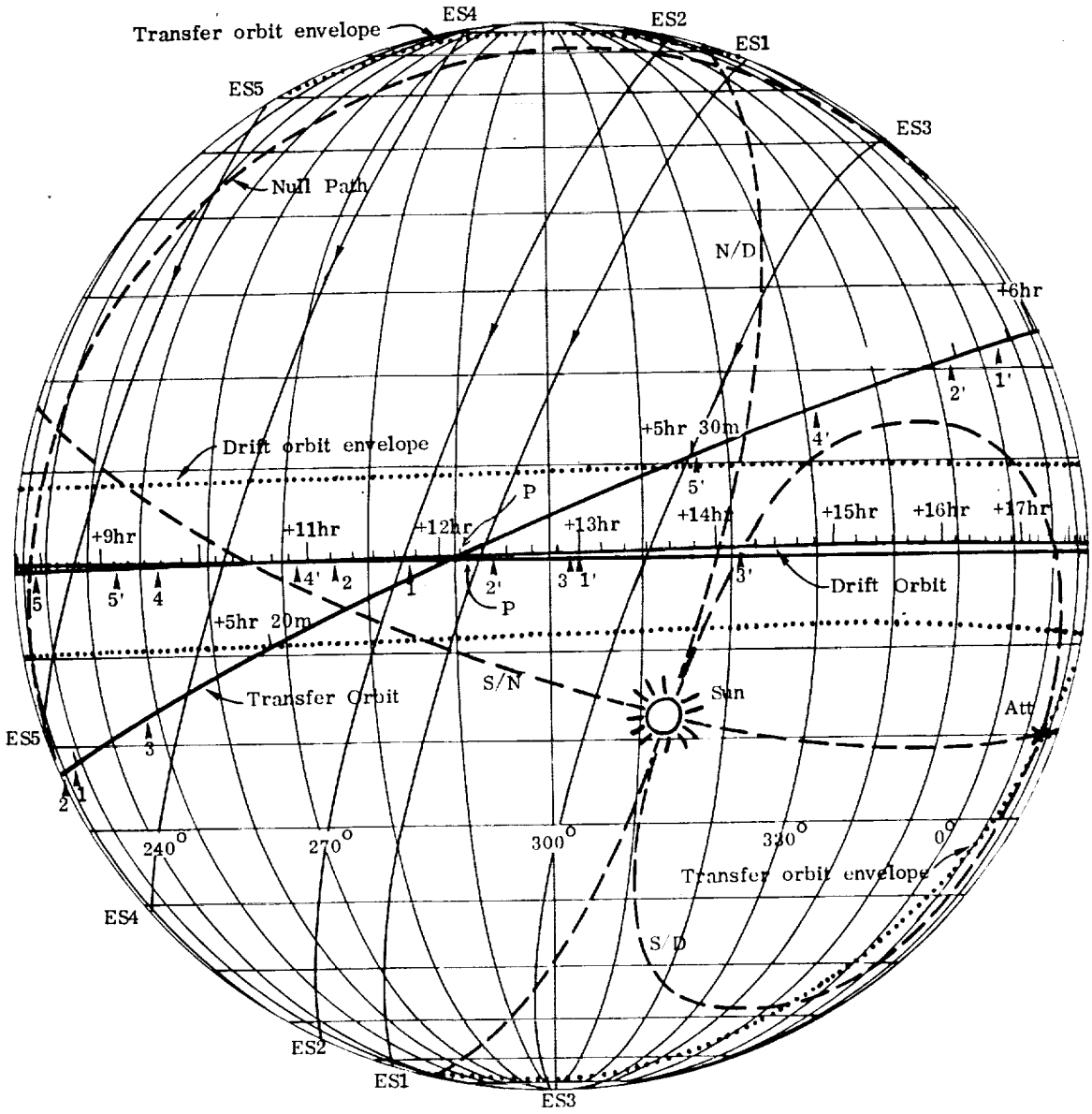

Figure 2-7. SMS-2 Attitude and Bias Geometry for AMF Attitude During Both Transfer Orbit and Drift Orbit Viewed From R.A. = 300°, dec. = 0°

NOTE: During most of the time covered by this figure the spacecraft is out of contact with the Earth when in the transfer orbit.

sees the Earth in a region of poor geometry due to the high correlation between the Sun angle and the nadir angle. This implies that in the transfer orbit, a Sun angle bias cannot be distinguished from a sensor mounting angle bias with ES1 data. However, if the Sun angle is determined using other Earth sensor data and held fixed during the processing of ES1 data, then this data can be used to determine the sensor mounting angle and azimuth bias. (Note that these conclusions based on the geometry plot of Figure 2-5 were confirmed on OASYS and OABIAS runs with simulated data and, subsequently, with real data.) This problem also occurs for ES3 and ES4 at AMF attitude in the drift orbit. However, these sensors are of substantially less interest and some ambiguities may be resolved, if necessary, by the second Earth ellipse seen by each sensor.

The sensor mounting-angle bias and azimuth bias are highly correlated along the curve labeled N/D. This occurs in the region of coverage of ES4 for both the transfer orbit and one of the two Earth ellipses in the drift orbit. Correlations between the Sun angle bias and azimuth bias (the S/D curves on the plots) do not occur at all for the transfer orbit and in regions of little interest for the drift orbit. Specifically, for the drift orbit the S/D curve passes through one Earth ellipse for ES4 and at the end of one Earth ellipse for ES3. Thus, correlations between Sun angle and azimuth biases are not a major difficulty for bias determination.

2.2.3 Geometry During Erection to Orbit Normal

Figures 2-8 through 2-14 show the SMS-2 geometry in the post-AMF drift orbit from AMF attitude to within 10 degrees of orbit normal in increments of 10 degrees. True orbit normal is at a declination of 89 degrees. However, for purposes of examining the geometry plots, it is sufficient to think of orbit normal as at the celestial pole. The nominal sequence of events calls for maneuvering the attitude from AMF attitude to orbit normal in three stages with data collected between each stage for sensor bias determination. The

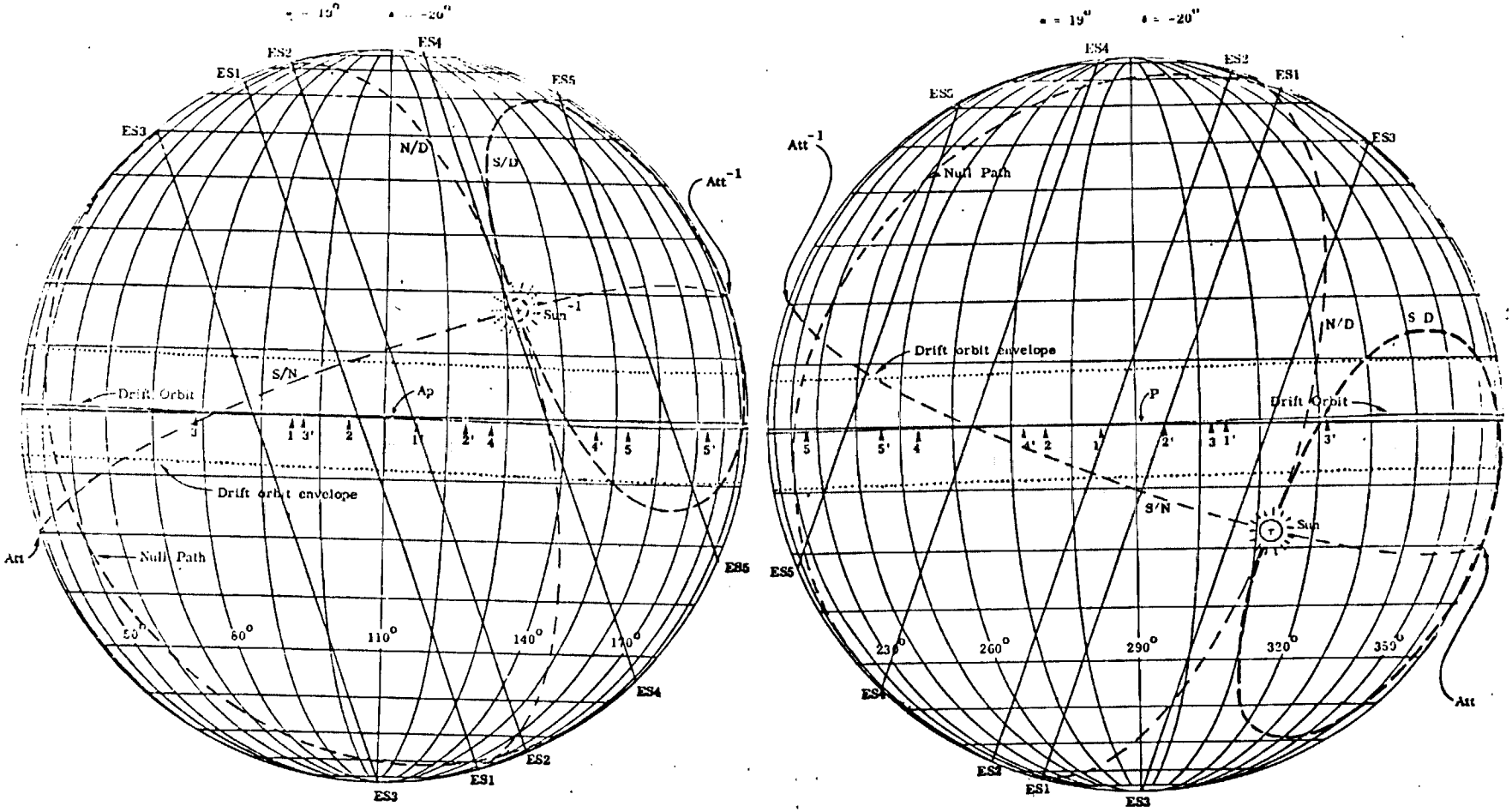

Figure 2-8. Attitude Determination Geometry in the Drift Orbit at an Attitude of $\alpha = 19^{o}$, $\delta = -20^{o}$

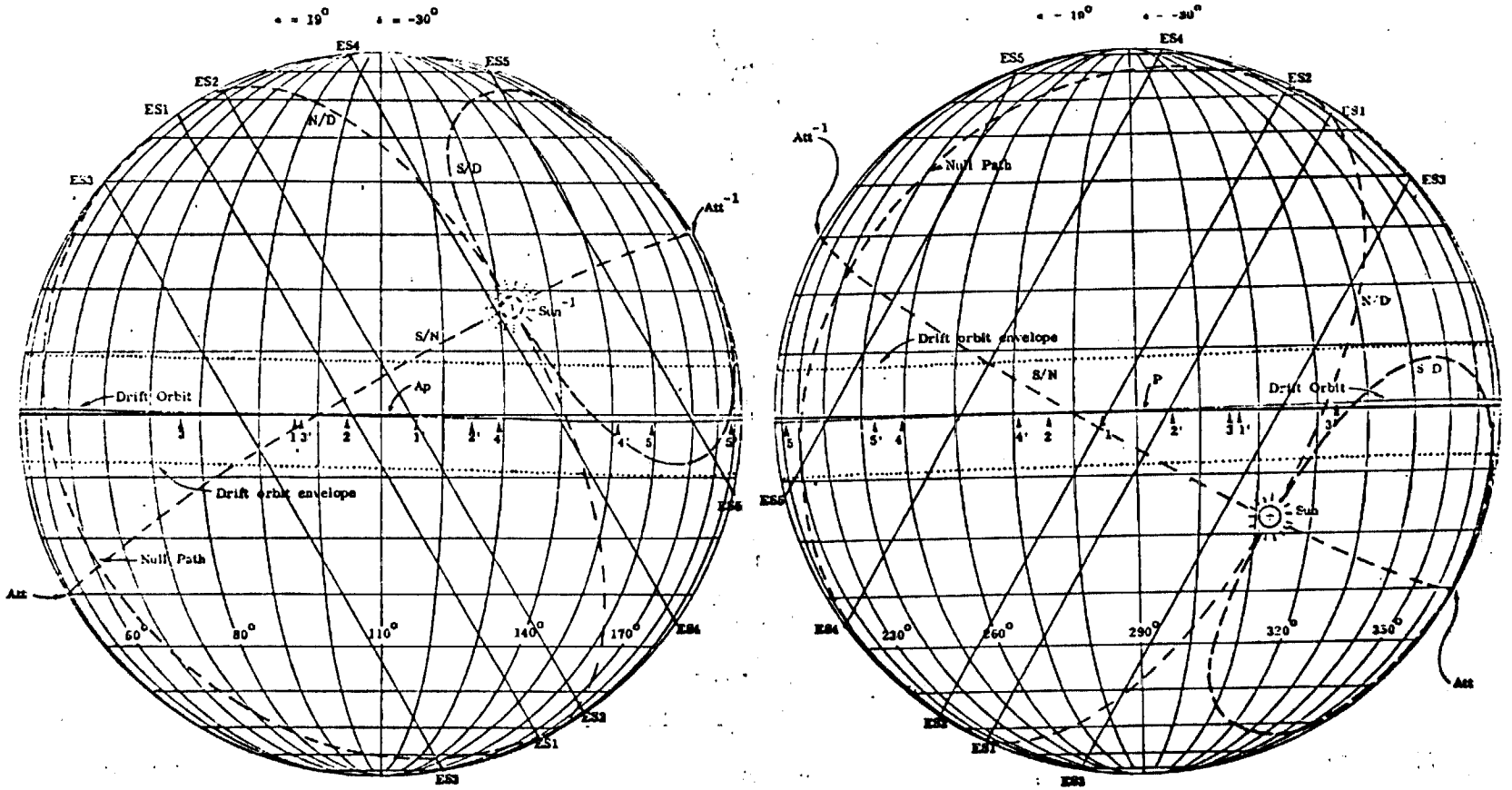

Figure 2-9. Attitude Determination Geometry in the Drift Orbit at an Attitude of $\alpha = 19^{o}$, $\delta = -30^{o}$

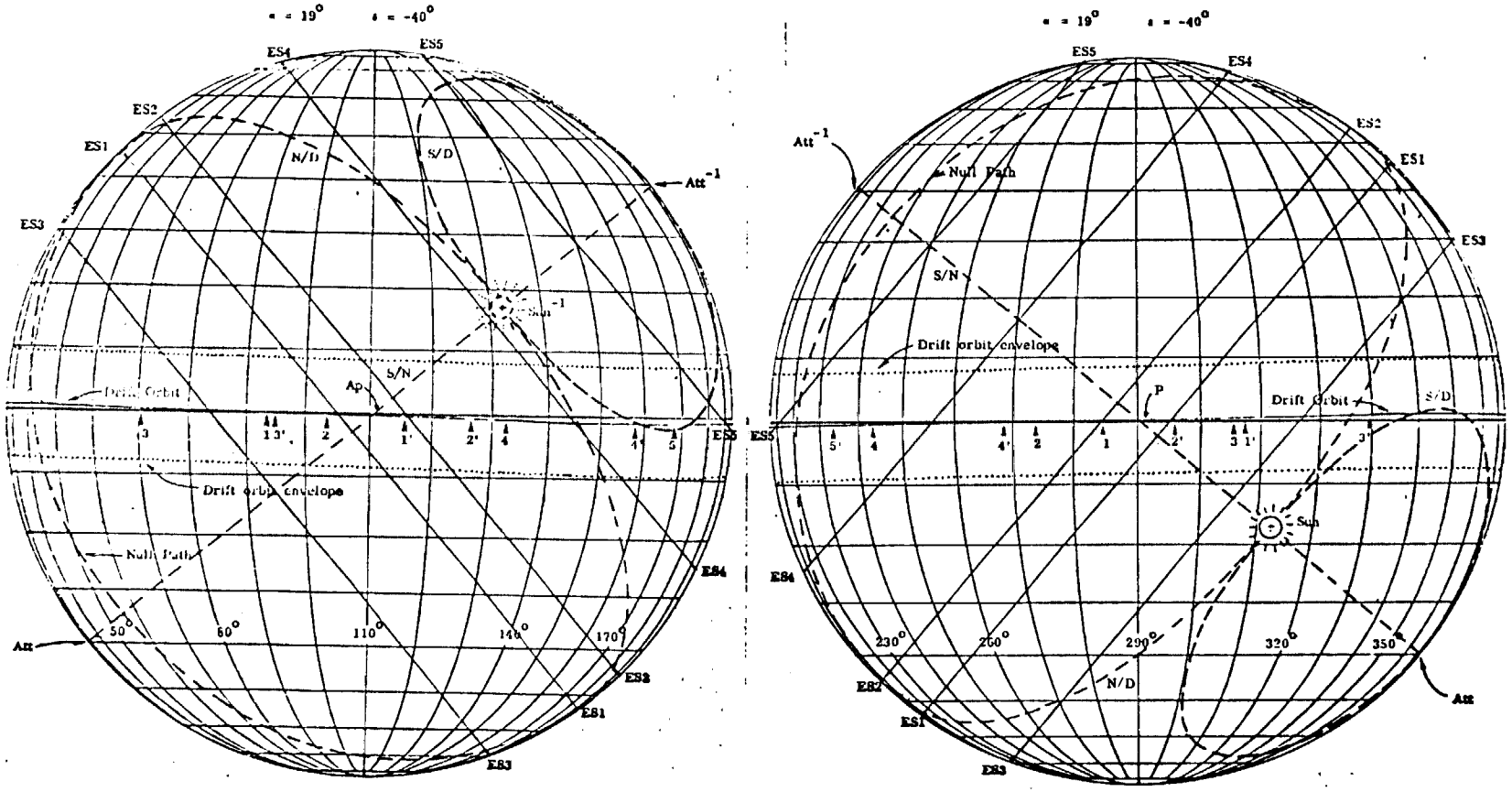

Figure 2-10. Attitude Determination Geometry in the Drift Orbit at an Attitude of $\alpha = 19^{o}$, $\delta = -40^{o}$

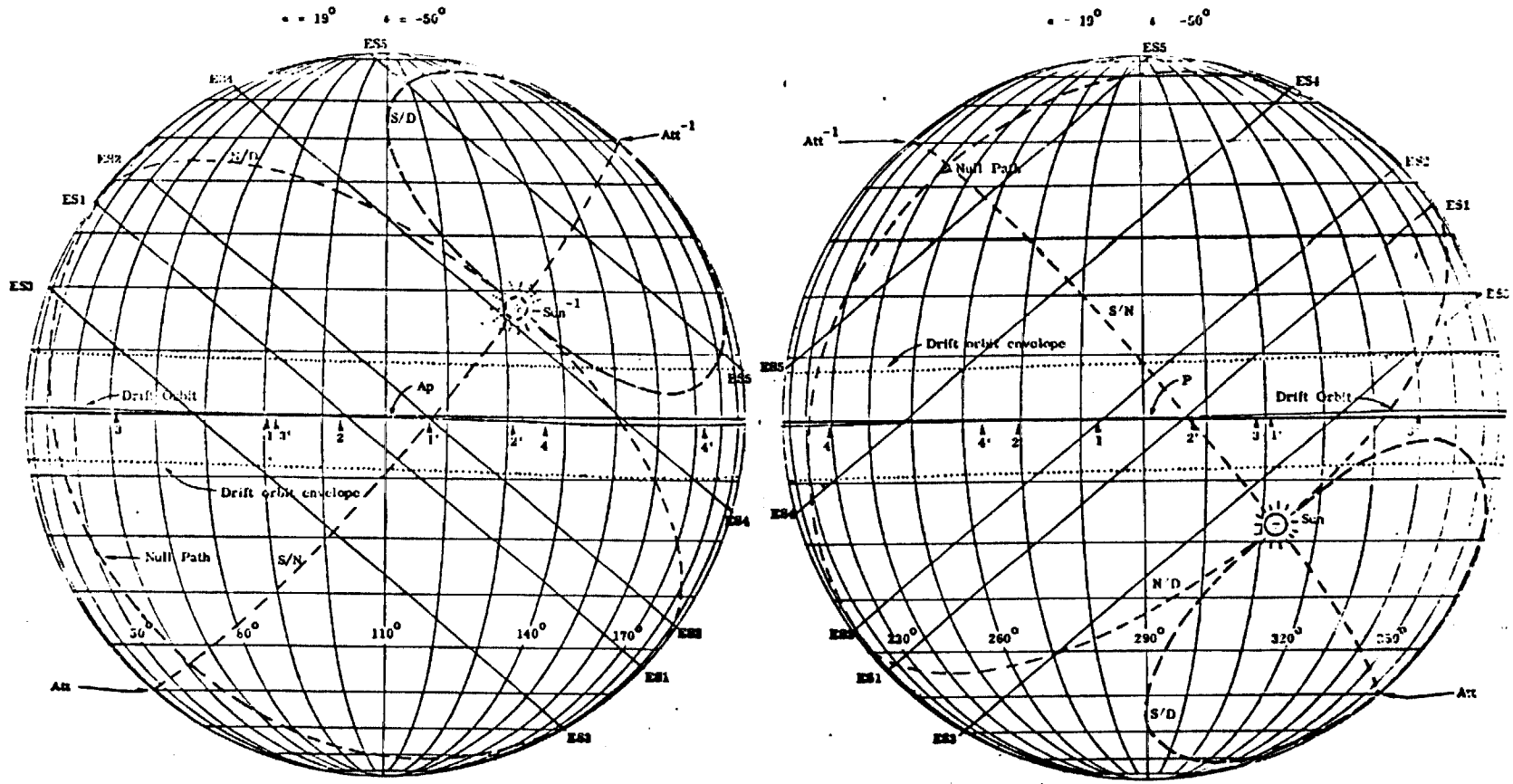

Figure 2-11. Attitude Determination Geometry in the Drift Orbit at an Attitude of $\alpha = 19^{o}$, $\delta = -50^{o}$

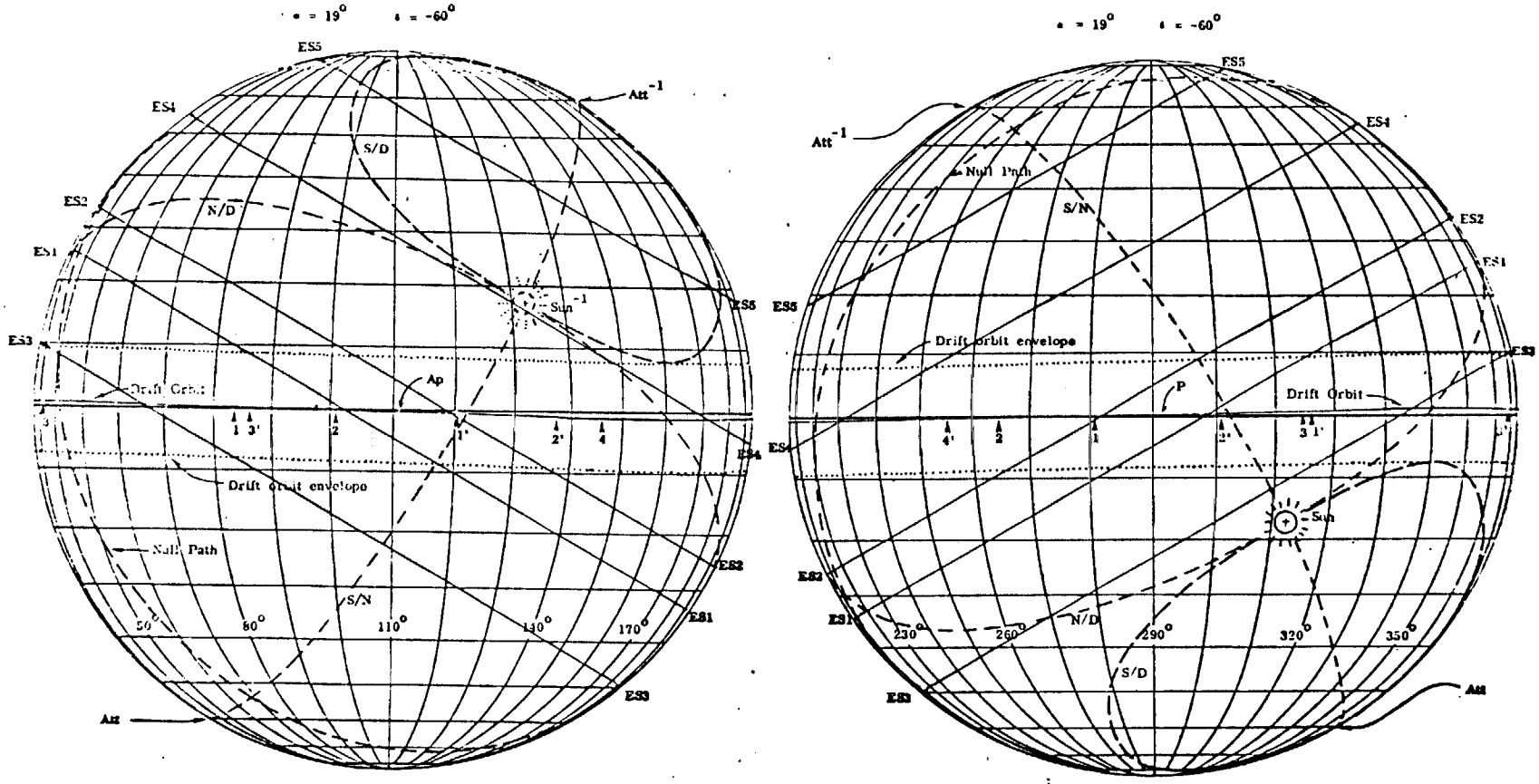

Figure 2-12. Attitude Determination Geometry in the Drift Orbit at an Attitude of $\alpha = 19^{o}$, $\delta = -60^{o}$

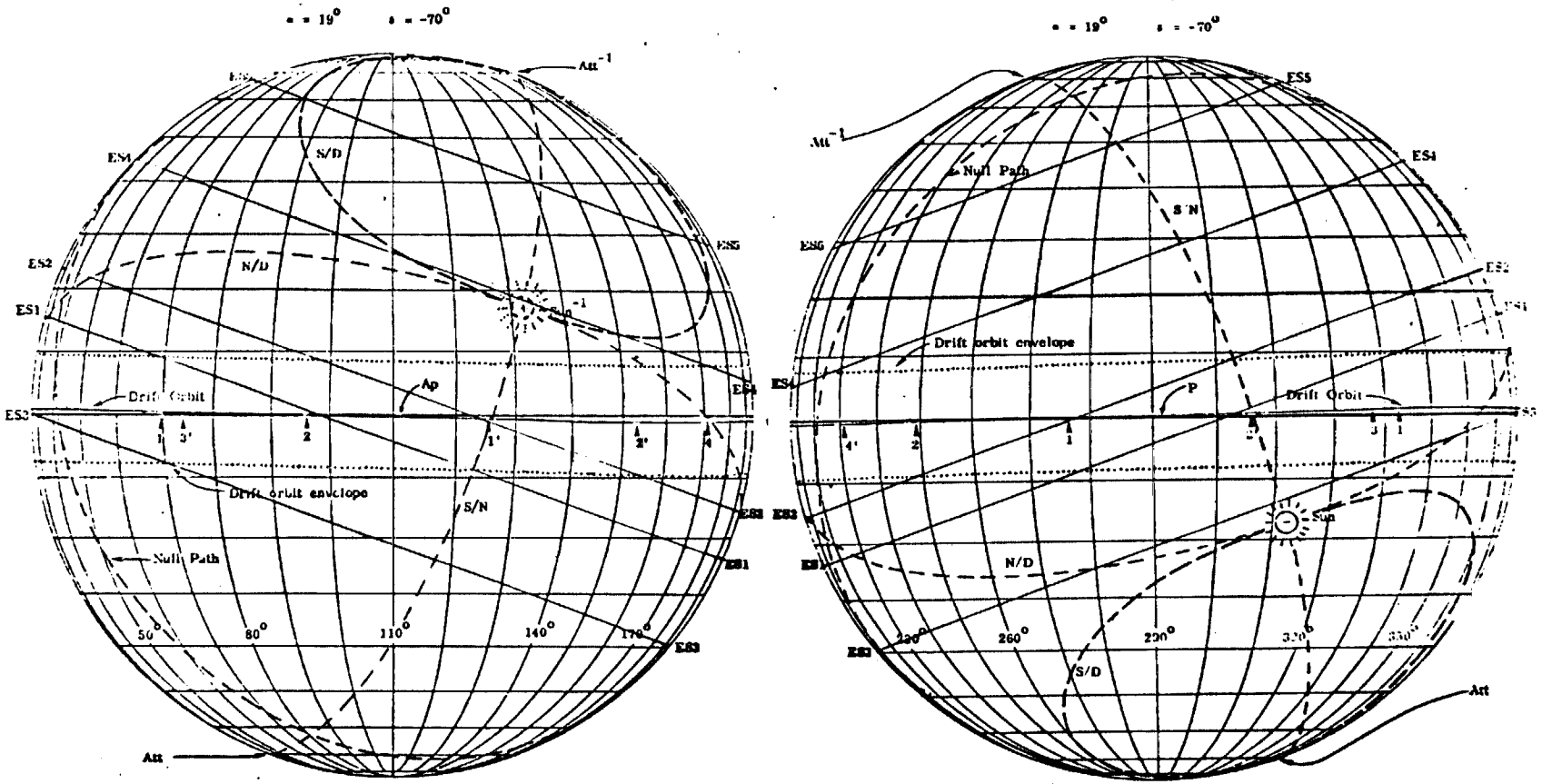

Figure 2-13. Attitude Determination Geometry in the Drift Orbit at an Attitude of $\alpha = 19^{o}$, $\delta = -70^{o}$

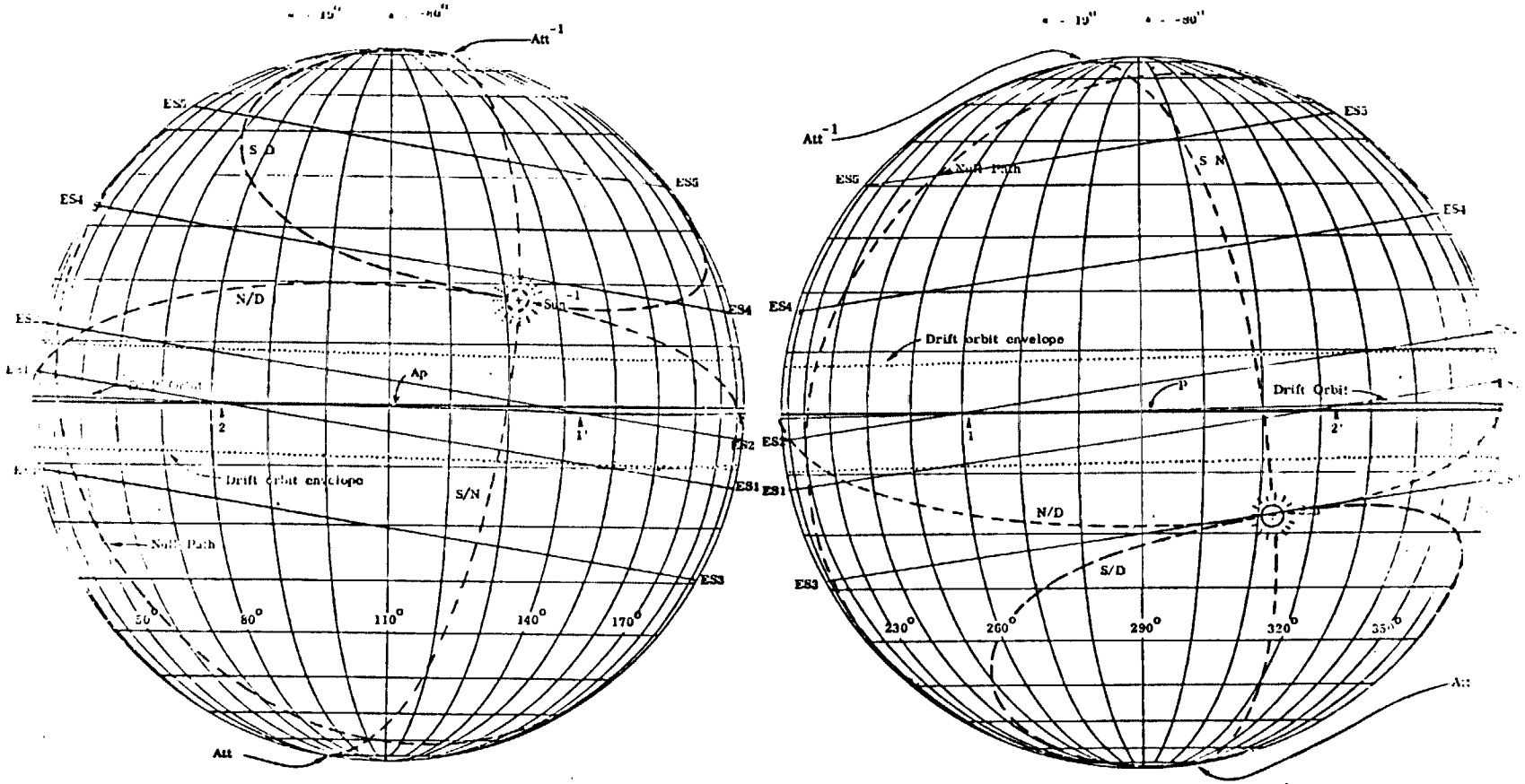

Figure 2-14. Attitude Determination Geometry in the Drift Orbit at an Attitude of $\alpha = 19^{o}$, $\delta = -80^{o}$

purpose of the plots in this section is to determine the most effective way to carry out this procedure.

There are two major conclusions to be drawn from the plots. Intermediate attitudes in the range of 40 degrees to 60 degrees from orbit normal are poor for bias determination because of the strong correlation between Sun angle bias and sensor mounting-angle bias. Again, these results were confirmed by runs of the OASYS and OABIAS attitude determination subsystems on simulated data. Secondly, ES1 and ES2 have equivalent attitude and bias determination geometries and, therefore, there is no reason to prefer one of the two sensors as a prime sensor because of conditions during the drift orbit. Since the sensors are symmetrically placed with respect to the satellite spin plane, this conclusion is always true for a satellite in a circular orbit and a correlation region which forms a great circle on the celestial sphere. However, it is not necessarily true for non-circular orbits or correlations such as the one between Sun angle and azimuth biases which do not form great circles on the celestial sphere.

For the SMS-2 geometry, the principal correlation for ES1 and ES2 is that between Sun angle, and nadir angle or, equivalently, between the Sun angle bias and the sensor mounting angle bias. At AMF attitude, the S/N great circle passes just outside the region of sensor coverage. As the attitude is shifted toward orbit normal, the S/N great circle moves through the region of sensor coverage. This correlation is greatest in the vicinity of 50 degrees from orbit normal (declination of -40 degrees) where it passes near the center of both Earth ellipses for each of the two sensors. As the attitude goes to 20 degrees to 30 degrees from orbit normal (declination of -60 degrees to -70 degrees), the Earth ellipses become considerably longer and the S/N correlation becomes less dominant. As the attitude approaches orbit normal, a problem arises which does not appear on the geometry plots. This is the problem of data

redundancy. With the attitude parallel to orbit normal and a circular orbit, all of the measurements of a given type are equivalent. For example, all of the Earth width observations are providing the same information repeatedly. In this case, it is effectively impossible to do sensor bias determination. Runs with the OSAYS and OABIAS systems on simulated data indicate that for SMS-2 data, bias determination is still possible when there are two separate Earth ellipses. However, an orbital in-track error cannot be distinguished from an azimuth bias with spacecraft data when the attitude is near orbit normal, i.e., at declinations below about -70 degrees.

The geometry of ES1 and ES2 is of principal concern for SMS-2. However, data from the other sensors may be used to determine attitude, Sun angle bias, or orbital in-track error to aid in the processing of ES1 and ES2 data or to confirm results. As can be seen from Figure 2-8, both ES3 and ES4 cross regions of poor geometry at AMF attitude. However, both Earth ellipses from ES5 avoid poor geometry regions and do not overlap any of the coverage of ES1 or ES2. Thus, ES5 is a particularly valuable sensor for obtaining information in the drift orbit at AMF attitude. When the attitude has been maneuvered to within 30 degrees of orbit normal (declination of -60 degrees), ES5 no longer sees the Earth. ES3 and ES4 will supply good data for bias determination with only a small overlap with the coverage of ES1. Although both sensors include the N/D region of correlation between sensor mounting angle and azimuth bias, the scan of the Earth is sufficiently long to incorporate large regions of good geometry where attitude and biases are distinguishable.

2.3 EFFECT OF CHANGE OF LAUNCH DATE

The geometry plots of Section 2.2 were based on a nominal launch date of January 30, 1975. Since the spacecraft was subsequently launched on

February 6th, it is of interest to consider the effect of the change of the launch date on the geometrical analysis and the resulting conclusions on the observability of various parameters.

As the launch data is shifted by a few days, the AMF attitude is shifted so that it maintains nearly the same geometry relative to the orbit. Thus, for purposes of attitude and bias determination geometry, the only change in geometry is the relative motion of the Sun with respect to the attitude vector. For the first week in February, the Sun in increasing its right ascension by 1.01 degrees/day. During this same period, the right ascension of the nominal AMF attitude is increasing by 0.92 degrees/day (Reference 7). Thus, the relative motion is only 0.09 degrees/day. In declination the Sun is moving 0.30 degrees/day, the AMF attitude is moving -0.01 degrees/day, and their relative motion is 0.31 degrees/day. Therefore, the major effect on the geometry is the motion of the Sun of about 1/3 of a degree per day toward the celestial equator.

In the 7-day interval from the time for which the geometry plots were constructed and the actual launch date, the principal effect is a shift of the Sun by just over 2 degrees toward the equator. The plots in Section 2.2 show that this will have only a small effect on location of the regions of the poor geometry and will not alter the conclusions of that section.

2.4 NOMINAL BIAS DETERMINATION SEQUENCE

The sequence of events for the determination of SMS-2 sensor biases has been determined primarily from the results of the geometric analysis of Section 2.2. Specifically, ES1 is the most important sensor for the transfer orbit, since this sensor will be used during AMF. However, as discussed in Section 2.2, the Sun angle bias is not determinable from the data for this sensor. Therefore, the nominal sequence of events calls for collection of data from ES1 during first apogee in the transfer orbit, collecting and

processing data from ES4 on the inbound leg of the first orbit to determine a Sun angle bias, and then using this Sun angle bias to process the ES1 data and determine the other ES1 biases.

During the transfer orbit, the active nutation damper will be firing and will cause the spacecraft attitude to drift in an unpredictable manner. This results in large uncertainties for any biases determined. Furthermore, once the spacecraft has been brought to orbit normal, bias determination will not be possible. Therefore, the principal data for bias determination must be in the drift orbit before the spacecraft has been brought fully to orbit normal. Three different attitudes will be used to average over systematic variations, such as orbit residuals. One of these attitudes will be the AMF attitude since this provides the best geometry. Since intermediate attitudes in the vicinity of 50 degrees from orbit normal (-40 degrees declination) provide particularly poor geometry, the first attitude maneuver should go past this region. Thus, the nominal sequence calls for the second set of post-AMF data to be collected at a declination of about -60 degrees. The last data set will be collected at an attitude such that ES1 just maintains two separate Earth ellipses. This will occur at a declination of about -74 degrees.

Based on the above analysis, the following nominal bias determination sequence was established:

- Collect data from ES1 during first apogee in the transfer orbit.
- During the coverage of ES2 immediately after first apogee, switch to the alternate Sun sensor for approximately 30 minutes and then switch back to determine the relative reading of the two Sun sensors.
- Collect data from ES4 for as long as possible on the inbound leg. (Poor geometry at the beginning of ES4

coverage makes data near perigee relatively important.) Process this data to determine the best estimate of the Sun angle bias.

- Use the Sun angle bias from ES4 to process the previously collected ES1 data and determine the remaining biases on ES1. These biases may then be used for providing the best attitude for AMF.

- After AMF, remain at AMF attitude for one full orbit and collect and process data for two Earth ellipses for both ES1 and ES5. (See discussion of ES5 data in Section 2.2.3.) Use the ES5 results to either aid in processing or confirm results for ES1 processing.

- Maneuver the attitude to 30 degrees from orbit normal (declination of -60 degrees) and remain there for one full orbit to collect and process data from two Earth ellipses for ES1, ES3, and ES4. (See discussion of data quality in Section 2.2.3.) Again, the attitude and Sun angle biases from the alternate sensors, ES3 and ES4, are used to confirm the attitude and biases obtained from ES1 and to check on the overall consistency of results. This also provides a check on the validity of the uncertainties obtained.

- Maneuver the attitude to a declination of approximately -74 degrees and remain at this attitude for one full orbit to obtain two complete Earth ellipses from ES1. The attitude here is not critical since complete separation of the two Earth ellipses is not necessary for accurate bias determination. At least for the SMS-2 geometry, a

strong narrowing in Earth width between two Earth width peaks is as good as having two separate ellipses. When this data is processed, the resulting attitude may be used for accurate evaluation of the final maneuver to orbit normal.

Note that throughout this nominal sequence of events, ES1 data should be given precedence. That is, ES1 data should be collected from acquisition of the Earth to loss of the Earth even though this may cut off part of the coverage of other sensors.

SECTION 3 - POSTLAUNCH ANALYSIS

3.1 BIAS DETERMINATION SEQUENCE OF EVENTS

SMS-2 was launched into a transfer orbit and brought near to Apogee Motor Firing (AMF) attitude on the first outbound leg. It remained close to this attitude through AMF (with some drift due to the active nutation damper and a small trim maneuver just prior to AMF) and into the initial drift orbit. The spacecraft was brought to orbit normal via a sequence of three attitude maneuvers with bias determination data obtained at AMF attitude and two intermediate attitudes prior to the maneuver to orbit normal. For convenience, the following nomenclature is established: Drift orbit-1 refers to the orbit after AMF during which the spacecraft remained at AMF attitude; drift orbit-2 refers to the orbit during which the spacecraft was at the first intermediate attitude; and drift orbit-3 refers to the orbit during which the spacecraft was oriented toward the final intermediate attitude before erection to orbit normal. Thus, data was obtained at the following approximate attitudes:

- Transfer orbit, R.A. = 25^{o}, Dec. = -20^{o}
- Drift orbit-1 R.A. = 25^{o}, Dec. = -20^{o}
- Drift orbit-2 R.A. = 38^{o}, Dec. = -64^{o}
- Drift orbit-3 R.A. = 35^{o}, Dec. = -77^{o}

The nominal sequence of events for bias determination was described in Section 2.4. The actual sequence followed the nominal plan in most respects with some changes in the amount of data collected. An additional data set was collected during the transfer orbit from ES3. A second additional data set was obtained during drift orbit-3 from ES2. Two data sets were lost: approximately half of the data from ES1 during drift orbit-1 and all of the data from ES3 during drift orbit-2. Thus, a total of eight different data sets were used for postlaunch analysis of biases. Three of the data sets were from the prime sensor, ES1, two data sets were from ES4, with one data set from each of the other three Earth sensors.

Table 3-1 lists the basic characteristics of the bias determination data sets obtained. Several characteristics common to all of the data sets are not included in the table. Specifically, Sun sensor-2 was used with all of the data and is the reference azimuth for the azimuth angles given in the table. Spacecraft ephemeris data was obtained from a GTDS orbit file. The orbit parameters listed in Table 3-1 were obtained from the header of that file. The algebraic routine SUN1 was used as the source of solar ephemeris data. The data was written on an OABIAS data file on disk storage by the SMS Attitude Determination System, SMSADS. The SMSADS System provides preaveraging of the data before it is written to OABIAS for most of the data collected. Each data record written to OABIAS is the average of up to 8 data points. Thus, a single record covers a time span of approximately 4 seconds. Date Set number 64 (DS#64) was obtained to test the consequences of the preaveraging. This data set is identical to DS#62, except that it was written such that up to 40 data points are averaged to obtain a single OABIAS record. For OABIAS processing, records were sifted as necessary to provide a uniform distribution of approximately 200 records over the data interval being processed.

The chronological sequence of events for bias determination was as follows:

- A whole Earth ellipse of data from ES1 was collected during first apogee in the transfer orbit (DS#51).
- During the coverage of ES2 immediately after first apogee, a switch to Sun sensor-1 was made. Data was collected for approximately 35 minutes before switching back to Sun sensor-2. Although an estimate of the relative readings of the Sun sensors was made, an accurate measurement was not possible due to the rapid change in the attitude of the spacecraft, apparently due to the active nutation damper.
- Data was collected from ES4 on the inbound leg of the transfer

FOLDOUT FRAME 1

OABIAS Data Set No. (DS#)	51	52	53
Sensor	ES1	ES4	ES3
Orbit	Transfer	Transfer	Transfer
Date(s)	2/7/75	2/7/75	2/7/75
Start Time of Data (GMT)	1:30	6:21	9:58
Stop Time of Data (GMT)	4:16	8:15	11:45
Nominal Sensor Mounting Angle (deg.)	86.02	114.98	70.00
Nominal Azimuth Angle[2] (deg.)	-77.1655	96.445	96.4428
Sun Angle From Data (deg.)	60.8	61.4	61.0
Spin Rate From Data (deg./sec.)	567	567	567
Orbit:	Transfer Orbit		
a (km)	24881.479		426
e	0.735744		0.0
i (deg.)	23.9186		1.0
M_o (deg.)	0.225183		215
ω (deg.)	180.259 + 0.642°/day		170
Ω (deg.)	296.470 - 0.369°/day		272
Epoch (GMT)	22:30:00, 2/6/75		14:4

[1] DS#64 is equivalent to DS#62 except that different averaging was used in creating the da

[2] Relative to Sun sensor No. 2.

FOLDOUT FRAME 2

Table 3-1. Data Sets Used for Bias Determination on SMS-2

	55	59	60	62[1]	63	64[1]
	ES5	ES4	ES1	ES1	ES2	ES1
	Drift 1	Drift 2	Drift 2	Drift 3	Drift 3	Drift 3
	2/7/75	2/8/75 - 2/9/75	2/9/75	2/10/75	2/9/75 - 2/10/75	2/10/75
	17:42	18:57 (2/8)	3:27	3:28	17:32 (2/9)	3:28
	23:10	0:51 (2/9)	16:28	17:10	19:38 (2/10)	17:10
	137.99	114.98	86.02	86.02	94.01	86.02
	168.9834	96.445	-77.1655	-77.1655	-77.180	-77.1655
	62.5	70.6	70.5	72.0	71.9	72.0
	561	558.9	558.9	558.2	558.2	558.2
	rift Orbit No. 1	Drift Orbit No. 2		Drift Orbit No. 3		
	3.975	42568.835		42561.285		
	0382	0.011695		0.011804		
	0781	1.063		1.065		
	080927	189.964		243.442		
	720 + 0.0258°/day	173.943 + 0.026°/day		173.999 + 0.026°/day		
	095 - 0.0129°/day	272.179 - 0.013°/day		272.847 - 0.013°/day		
	:37, 2/7/75	13:35:00, 2/8/75		17:31:00, 2/9/75		

1 sets.

orbit (DS#52). This data was processed to obtain a value for the Sun angle bias.

- The Sun angle bias from ES4 data was then used to process the ES1 data and obtain an initial measurement of the sensor biases. The largest bias obtained was the azimuth bias which was subsequently used to improve the attitude for AMF.

- On the second outbound leg of the transfer orbit, an unanticipated data set (DS#53) was obtained from ES3 and processed. All of the transfer orbit data sets were processed and attitude and biases determined prior to AMF.

- After AMF, the spacecraft was kept at AMF attitude for less than the planned time to prevent an adverse effect on the orbit by the attitude maneuver.

- Two Earth ellipses for ES5 were obtained during drift orbit 1 (DS#55), but only one Earth ellipse from ES1 was obtained. This single ellipse was insufficient for bias determination processing. In addition, the two Earth ellipses from ES5 were substantially degraded at the ends of the ellipses. (See the discussion of the "pagoda effect" in Section 3.3.)

- The attitude was maneuvered to approximately R. A. = 38^{o}, Dec. = -64^{o} to obtain data from drift orbit 2. Two full Earth ellipses were obtained from ES4 (DS#59) and ES1 (DS#60). (See comment on ES4 data below.) This data was processed for attitude and biases. Data from ES3 was of bad quality and lost.

- The attitude was maneuvered to its final intermediate value of approximately R. A. = 38^{o}, Dec. = -77^{o}. Two full Earth ellipses of data from ES1 were obtained and processed. (DS#62 and the

equivalent data set DS#64.) An additional data set containing parts of three Earth ellipses was obtained from ES2 and processed (DS#63). The resulting biases from ES2 were used in the final maneuver to bring the spacecraft to orbit normal.

Because the attitude for drift orbit-2 was nearer to orbit normal than expected, the two Earth ellipses obtained for ES4 are not totally distinct. Rather than leaving the Earth entirely between the two maxima, the sensor dipped just slightly below the diameter of the Earth's disk and a single continuous set of data was obtained. This did not affect the quality of the results. Similarly, for ES2 in drift orbit 3 the sensor did not fully leave the Earth between the first two ellipses. However, the Earth width became so narrow that some data between the ellipses had to be discarded due to the pagoda effect discussed in Section 3.3.

3.2 DATA QUALITY

Figure 3-1 shows a segment of unaveraged raw data from Sun sensor 2 and Earth sensor 1 in the drift orbit for about 1.7 minutes. The peak-to-peak noise levels on this data pass are about 0.3° for Sun angle and Earth width, 0.2° for spin rate and 0.15° for rotation angles. Note that since the data transmission rate is faster than the spacecraft spin rate, some data values are repeated in the raw data

In contrast to the raw data of Figure 3-1, the data sets processed by OABIAS have all been written with the data averaging capability of the SMSADS System. This means that each OABIAS data point represents an average of up to 8 points of raw data (except for DS#64). Duplicate data points in the raw data are removed prior to averaging. In order to show the effect of this pre-averaging on the data, the same data shown in Figure 3-1 was rewritten with 8-point averaging and is shown in Figure 3-2. The peak-to-peak noise levels on this data set are about the same as for all other drift orbit data processed by OABIAS and are approximately 0.1° for Sun angle, 0.05° for spin rate and rotation angles, and 0.15° for the Earth width. Thus, the effect of using 8-point averaging in the pre-averaging system

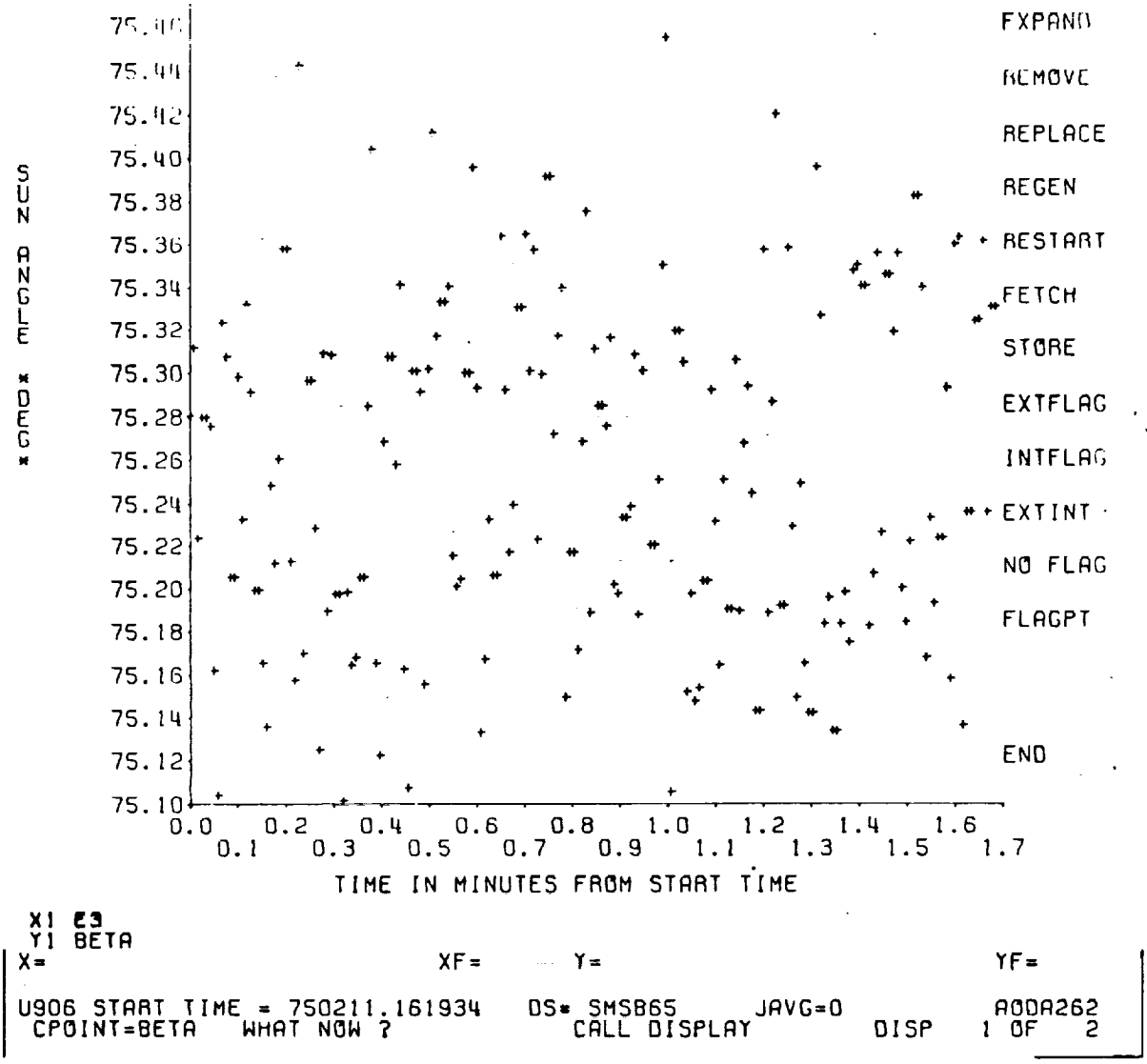

Figure 3-1. DS# SMSB65 Data Plots Showing Unaveraged Raw Data (1 of 5)

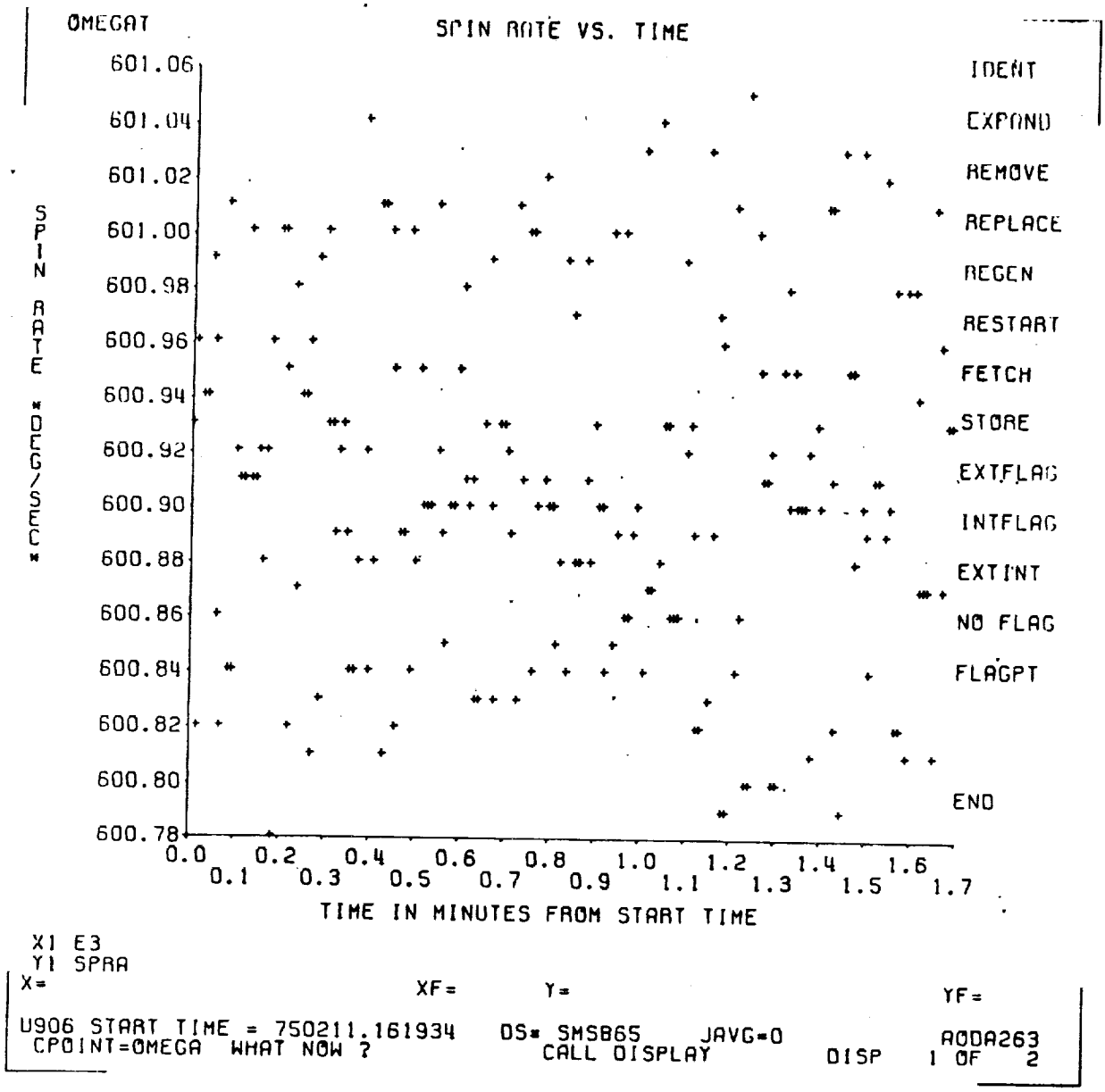

Figure 3-1. DS# SMSB65 Data Plots Showing Unaveraged Raw Data (2 of 5)

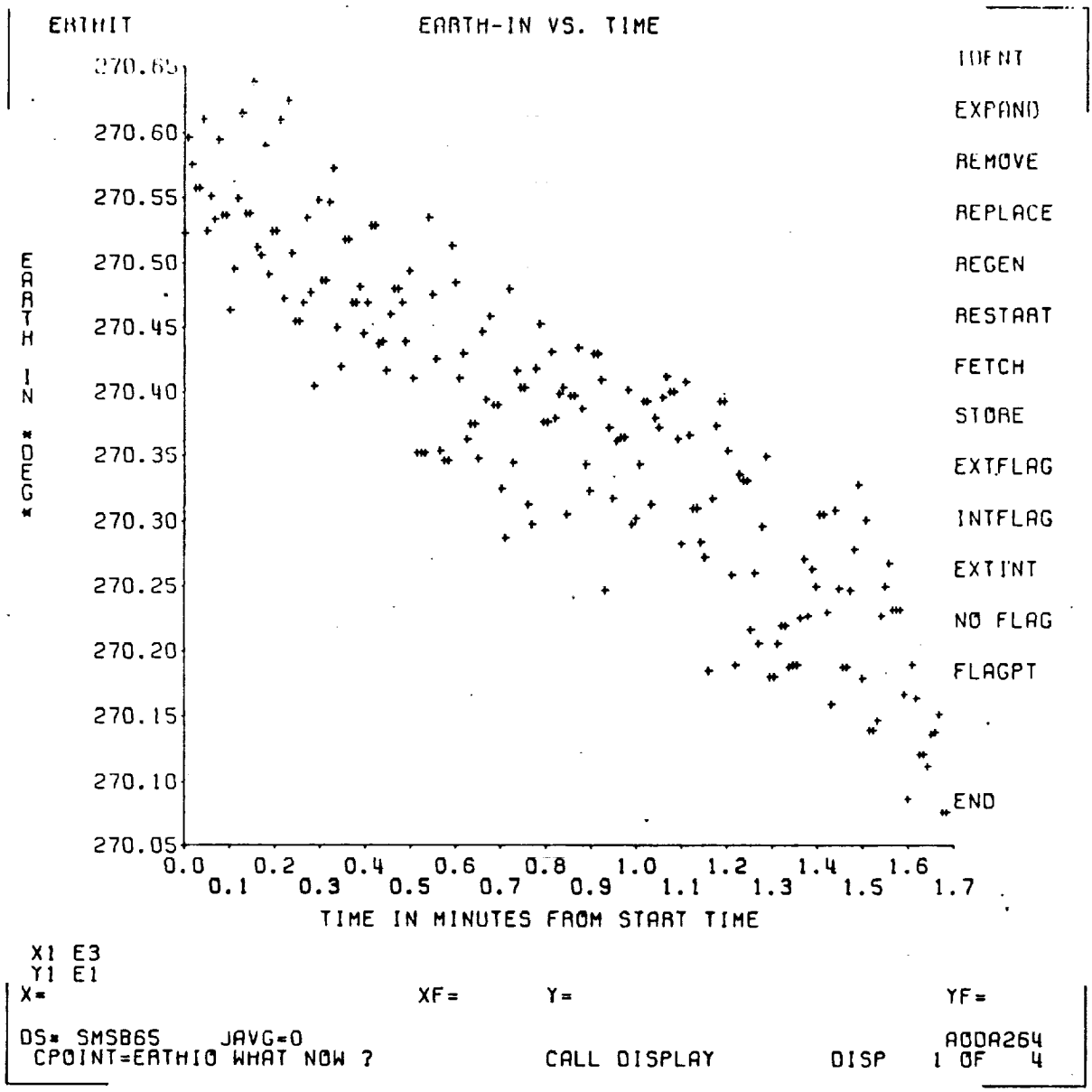

Figure 3-1. DS# SMSB65 Data Plots Showing Unaveraged Raw Data (3 of 5)

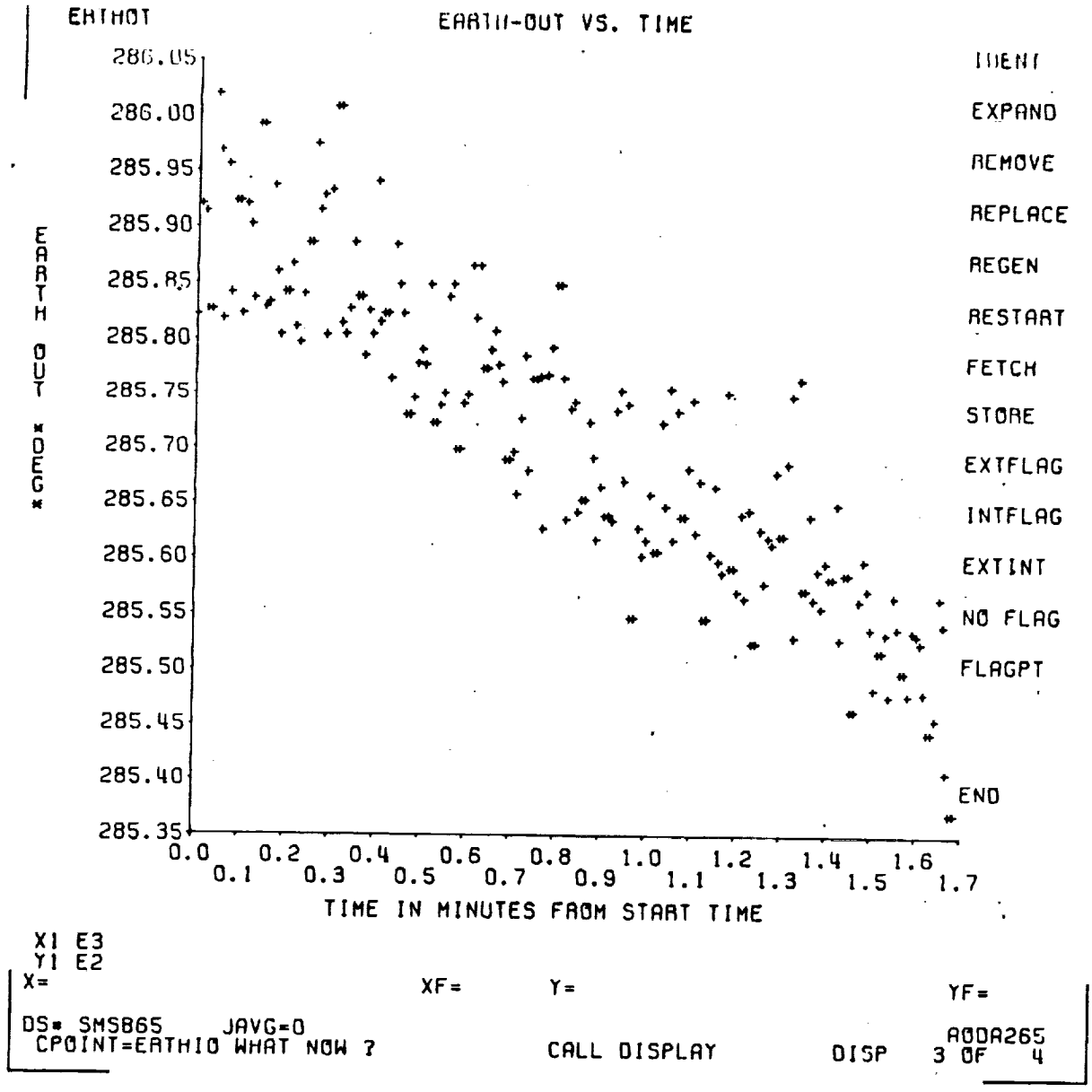

Figure 3-1. DS# SMSB65 Data Plots Showing Unaveraged Raw Data (4 of 5)

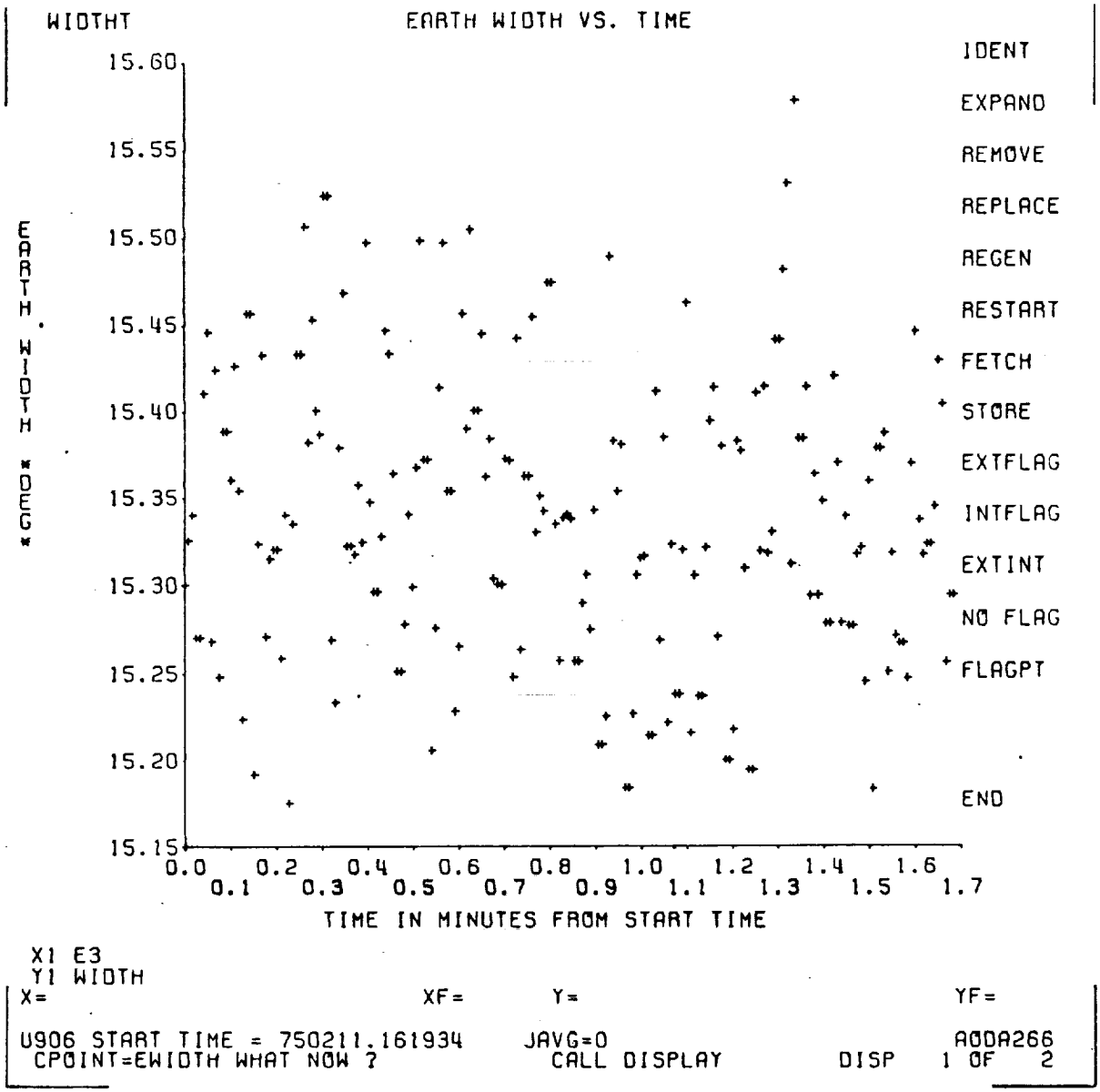

Figure 3-1. DS# SMSB65 Data Plots Showing Unaveraged Raw Data (5 of 5)

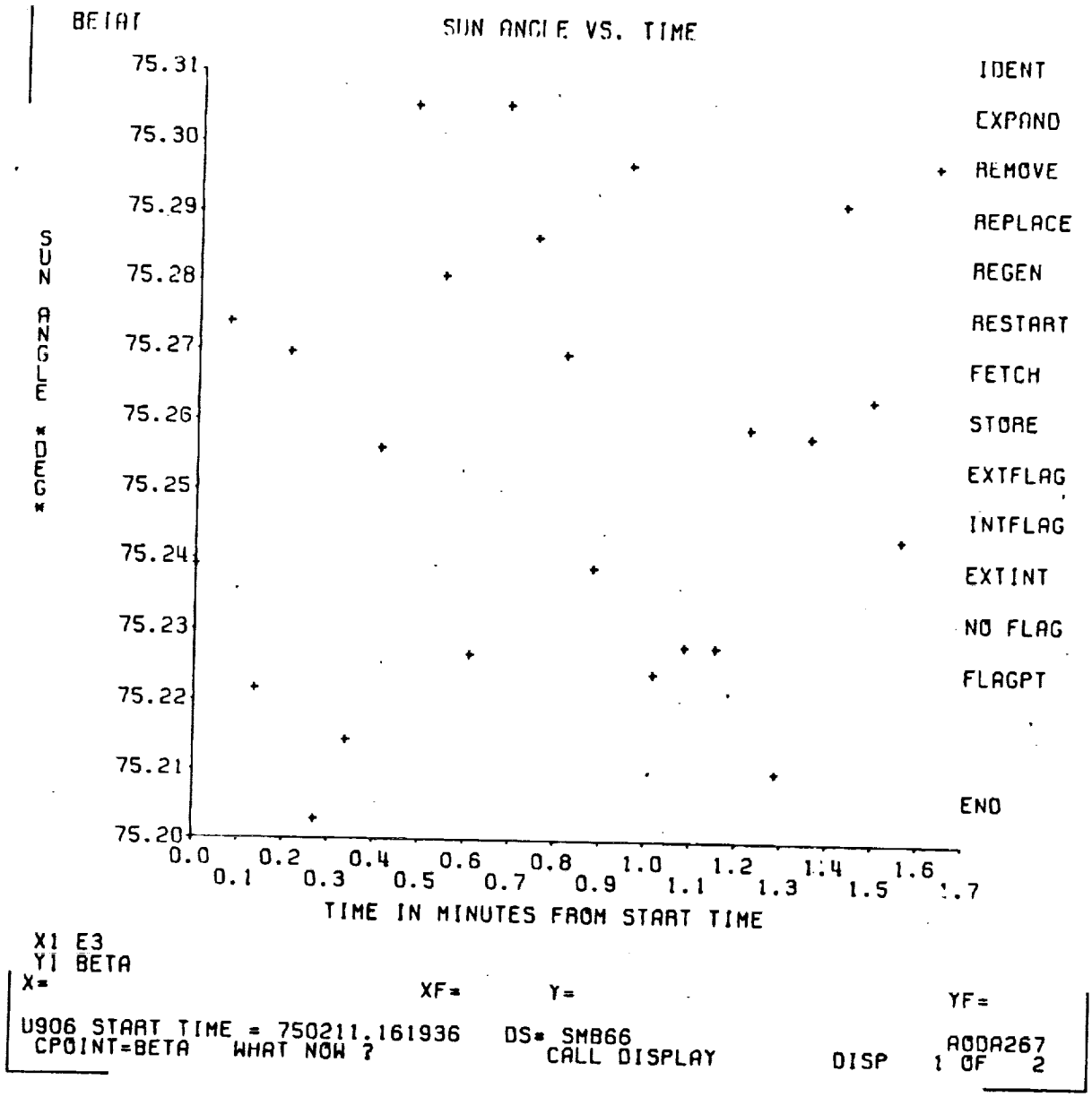

Figure 3-2. DS# SMSB66 Data Plots Showing Data From Figure 3-1 After Averaging (1 of 5)

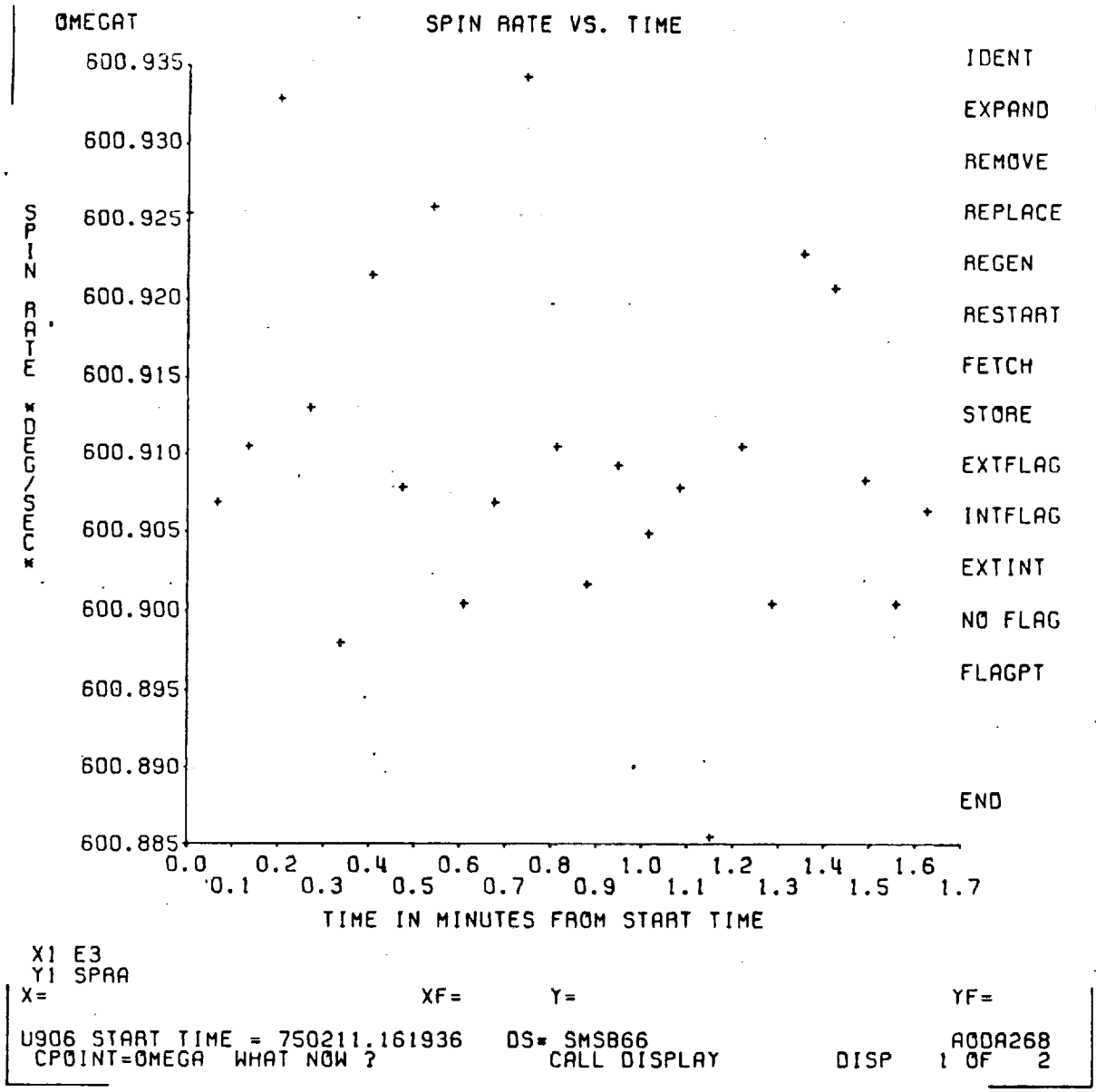

Figure 3-2. DS# SMSB66 Data Plots Showing Data From Figure 3-1 After Averaging (2 of 5)

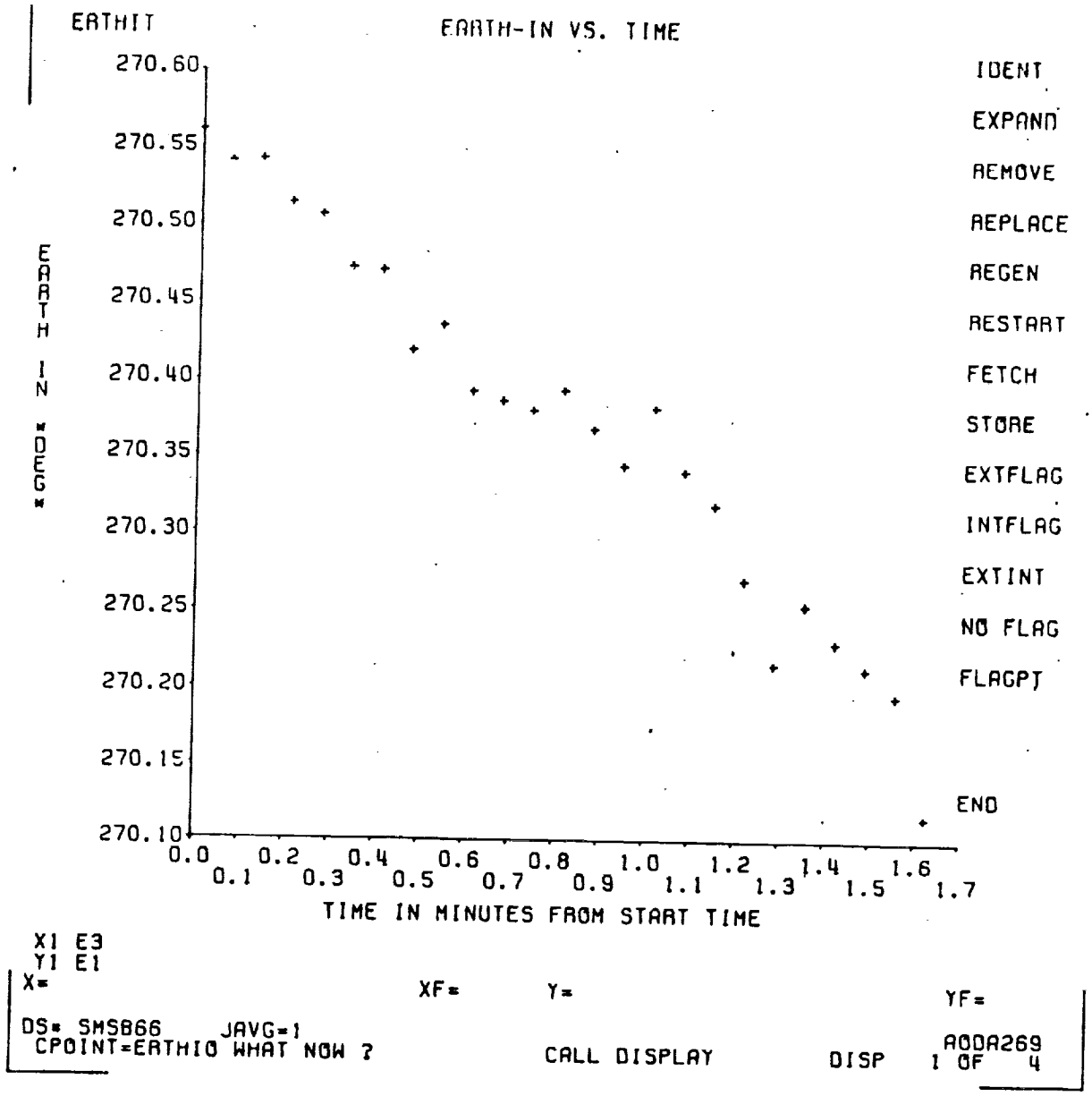

Figure 3-2. DS# SMSB66 Data Plots Showing Data From Figure 3-1 After Averaging (3 of 5)

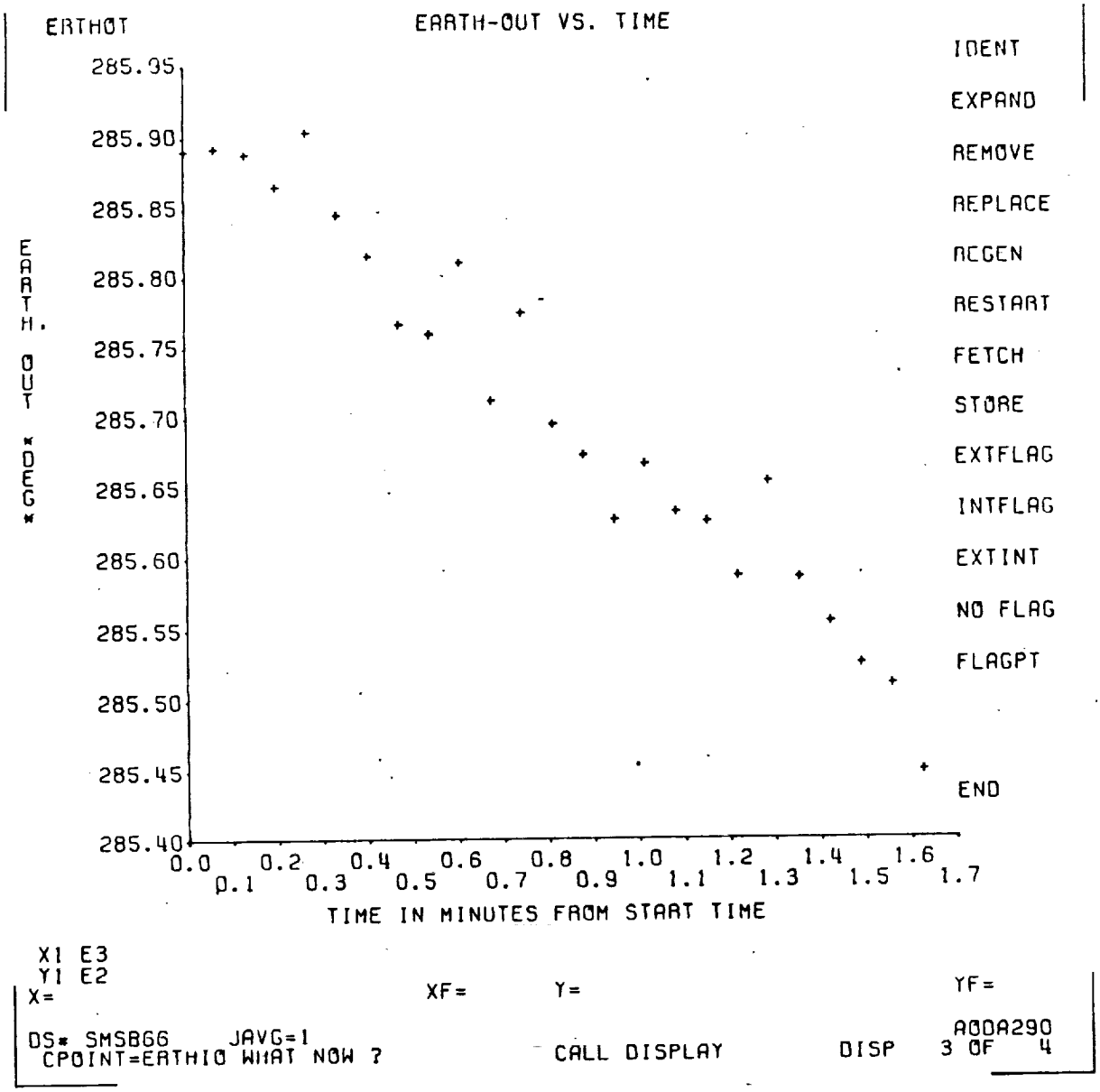

Figure 3-2. DS# SMSB66 Data Plots Showing Data From Figure 3-1 After Averaging (4 of 5)

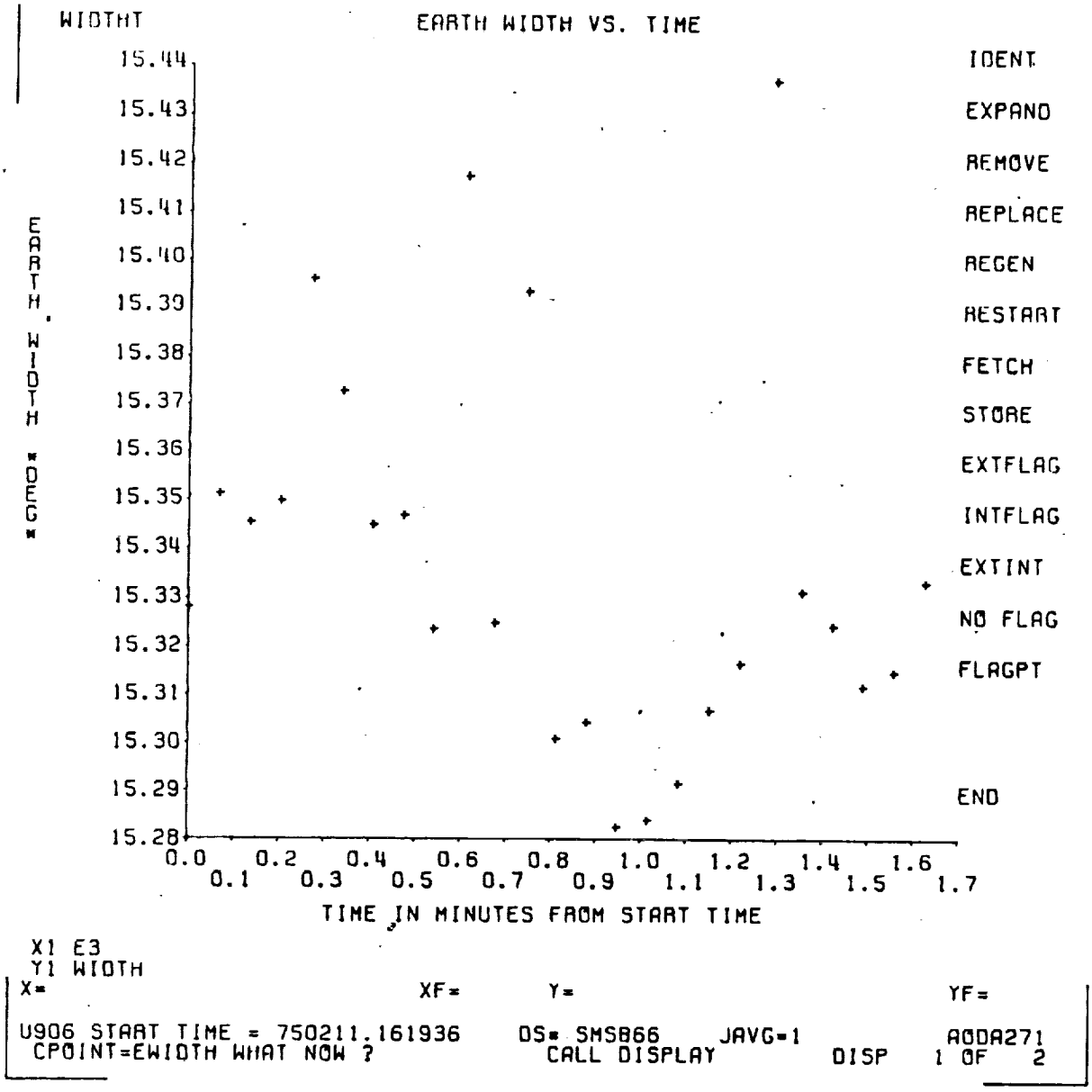

Figure 3-2. DS# SMSB66 Data Plots Showing Data From Figure 3-1 After Averaging (5 of 5)

is a reduction of the data noise levels by a factor of approximately 3, as expected.

The quality of the transfer orbit data (DS# less than 55) is much worse than the drift orbit data. The transfer orbit data is, in general, noisier. The noise levels on these data sets are approximately 0.2^{o} for Sun angle, spin rate, and Earth width, and 0.1^{o} for rotation angles.

Aside from the higher noise levels, the data in the transfer orbit is much less stable than that in the drift orbit. In the drift orbit, the mean Sun angle drifts with the normal rate due to the motion of the Sun (see, for instance, Figure 3-29 (1) in Section 3.4.3.2) while in the transfer orbit the Sun angle shows large abnormal variations (see, for instance, Figure 3-20 (1) in Section 3.4.3.1) which indicate some strong systematic variations such as the motion of the spin axis due to firing of the active nutation damper. Figure 3-3 shows the Sun angle measurements obtained from the three transfer orbit data sets. It can be seen that the variation on Sun angle is as high as 0.9^{o} in 3 hours while the normal drift rate of Sun angle due to the motion of the Sun should be about 0.1^{o} in 3 hours.

One major systematic irregularity which occurred in the SMS-2 data is the "pagoda effect." This effect gives erroneous horizon data at small Earth widths. This effect is discussed in detail in Section 3.3.

It is found that there are glitches[1] of about 0.1^{o} in the Sun angle data on DS#59 (see Figure 3-38 (2) in Section 3.4.3.4) with no apparent reason. The glitches are sufficiently small that they give negligible effects on the OABIAS attitude and bias determination results. Another glitch is found near the top of the second Earth-width data on DS#60 (see Figure 3-23(8) in Section 3.4.3.1). Again, this glitch is too small to affect the attitude and bias determination results from OABIAS.

[1] The word "glitch" refers to a small jump or discontuity in the data.

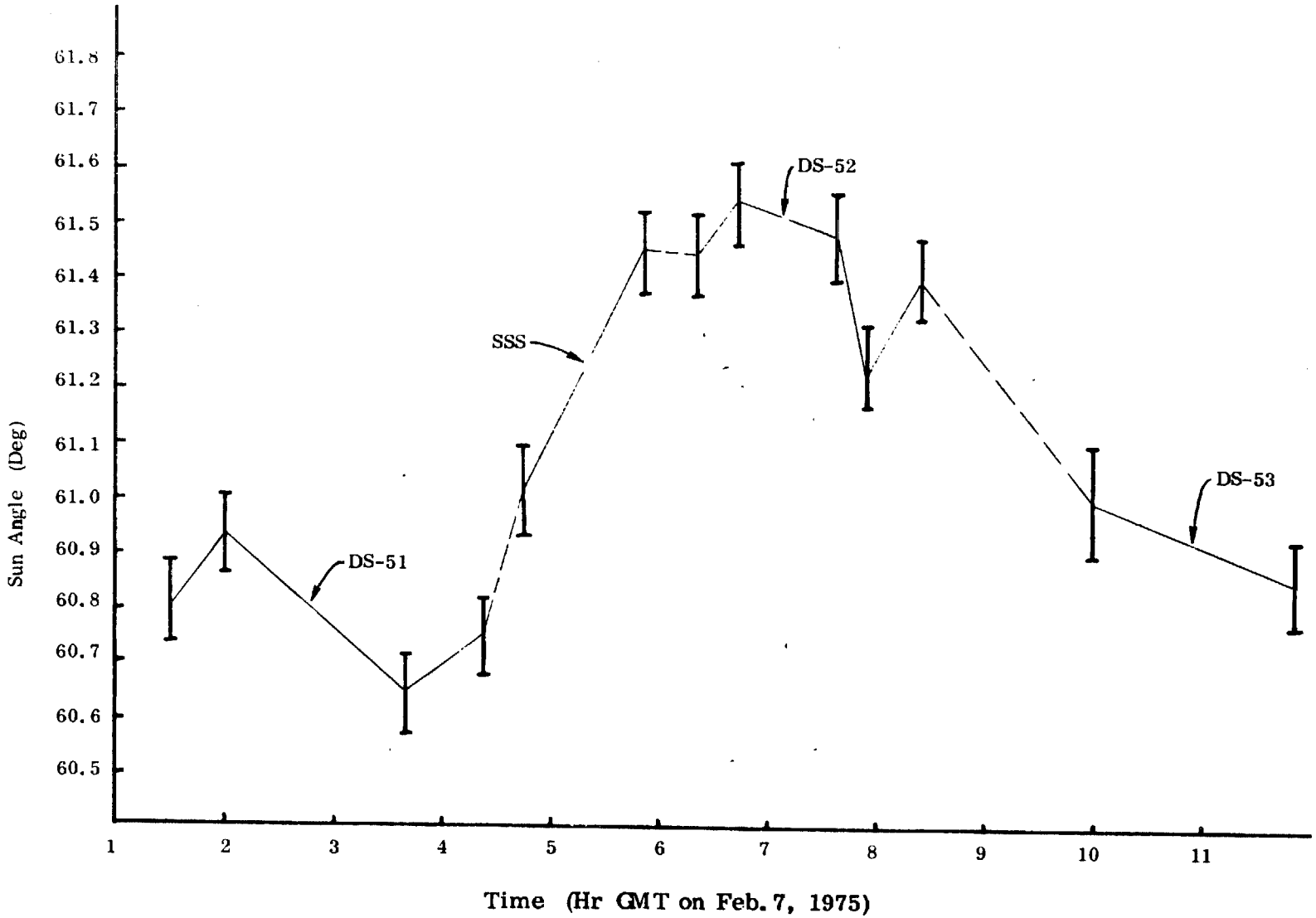

Figure 3-3. Sun Angle Measurements During Transfer Orbit

3.3 PAGODA EFFECT

A major anomaly in the SMS-2 data is the systematic variation between the observed data and its predicted behavior at small Earth widths. This is referred to as the pagoda effect and is most easily seen in the sharp upturn in Earth-out data as the scan of the sensor enters or leaves the disk of the Earth. Figure 3-4 shows the rotation angle data for the first Earth ellipse from ES5 in drift orbit-1. The anomalistic behavior of the data at the ends of the ellipse is evident. The effect is common to all of the data sets from SMS-2 which include small Earth widths. This includes data from all of the SMS-2 Earth horizon sensors except ES3 for which no data was obtained while the scan was entering or leaving the disk of the Earth. A similar effect was observed in data from the SMS-1 spacecraft.

Figure 3-5 shows the Earth width data for the first ES5 Earth ellipse. Although the pagoda effect can be seen here, it is not as prominent as in the rotation angle data. The effect is not observable at all in either Sun angle data or spin rate data.

The central question for bias and attitude determination purposes is to determine how far into the Earth ellipse the anomalistic behavior extends. Note that this cannot be determined from a simple examination of the data itself. The only procedure for determining how far the bad data extends into the Earth ellipse is to observe the resulting attitude solutions for systematic variations or to compare the observed data with predicted data based on the best value of the attitude and bias parameters. Neither method is independent of the observed data. Nonetheless, consistent results for the extent of the region of bad data have been obtained by use of several different procedures. Specifically, four different interactive graphics displays have been used to judge the extent of the bad data due to the pagoda effect. These are as follows:

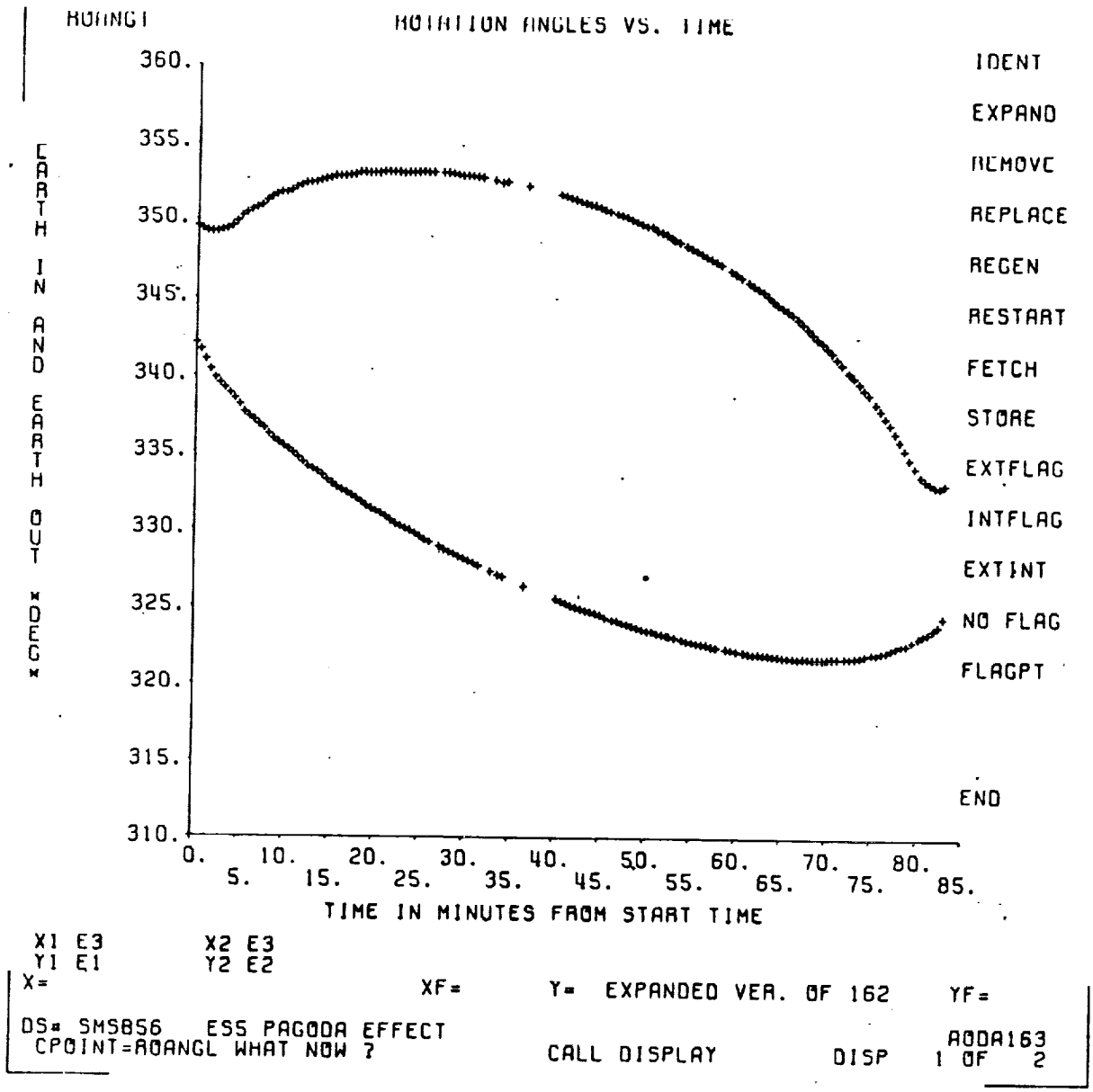

Figure 3-4. DS# SMSB56 Rotation Angle Data Showing Pagoda Effect (1 of 3)

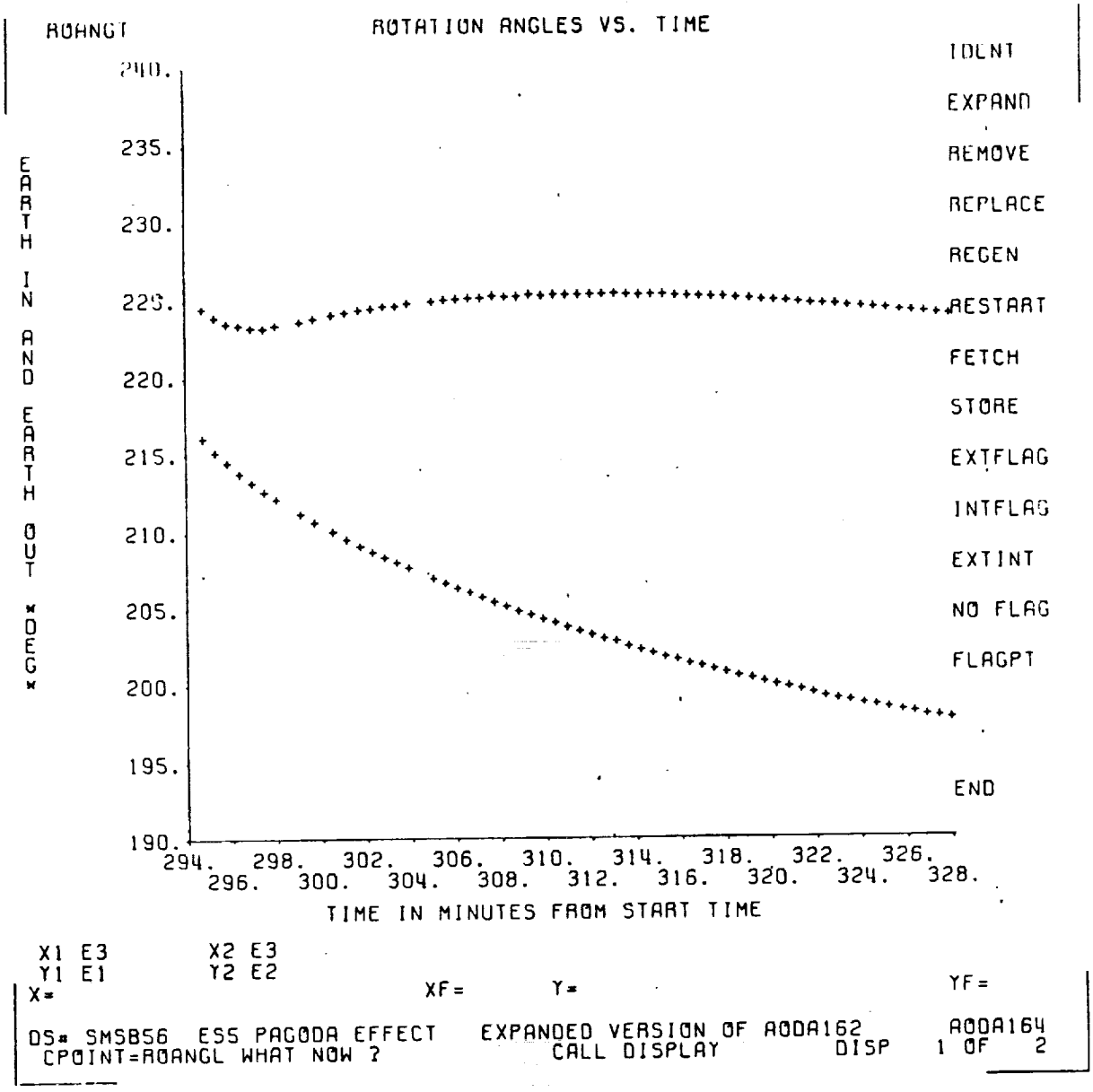

Figure 3-4. DS# SMSB56 Rotation Angle Data Showing Pagoda Effect (2 of 3)

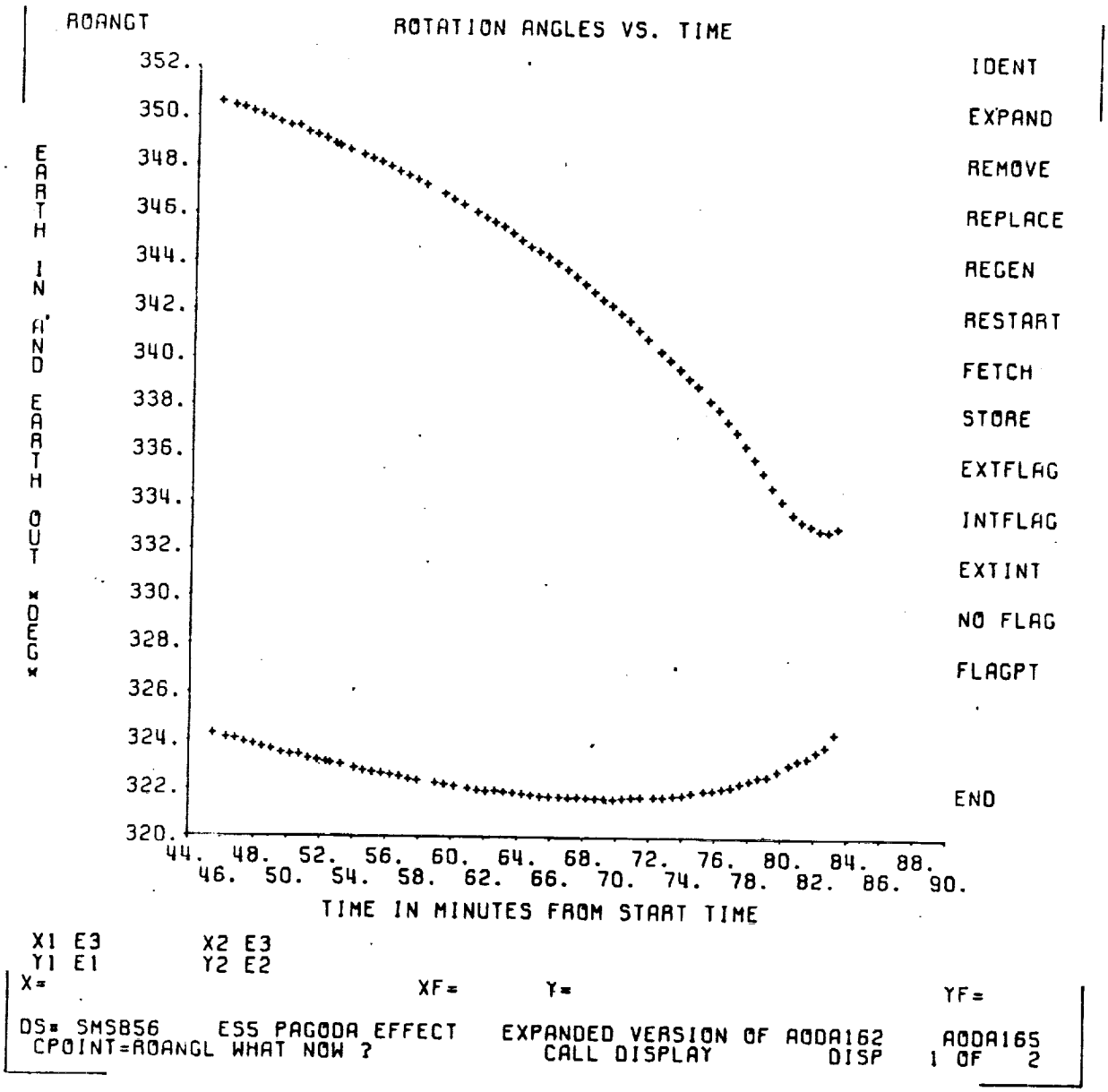

Figure 3-4. DS# SMSB56 Rotation Angle Data Showing Pagoda Effect (3 of 3)

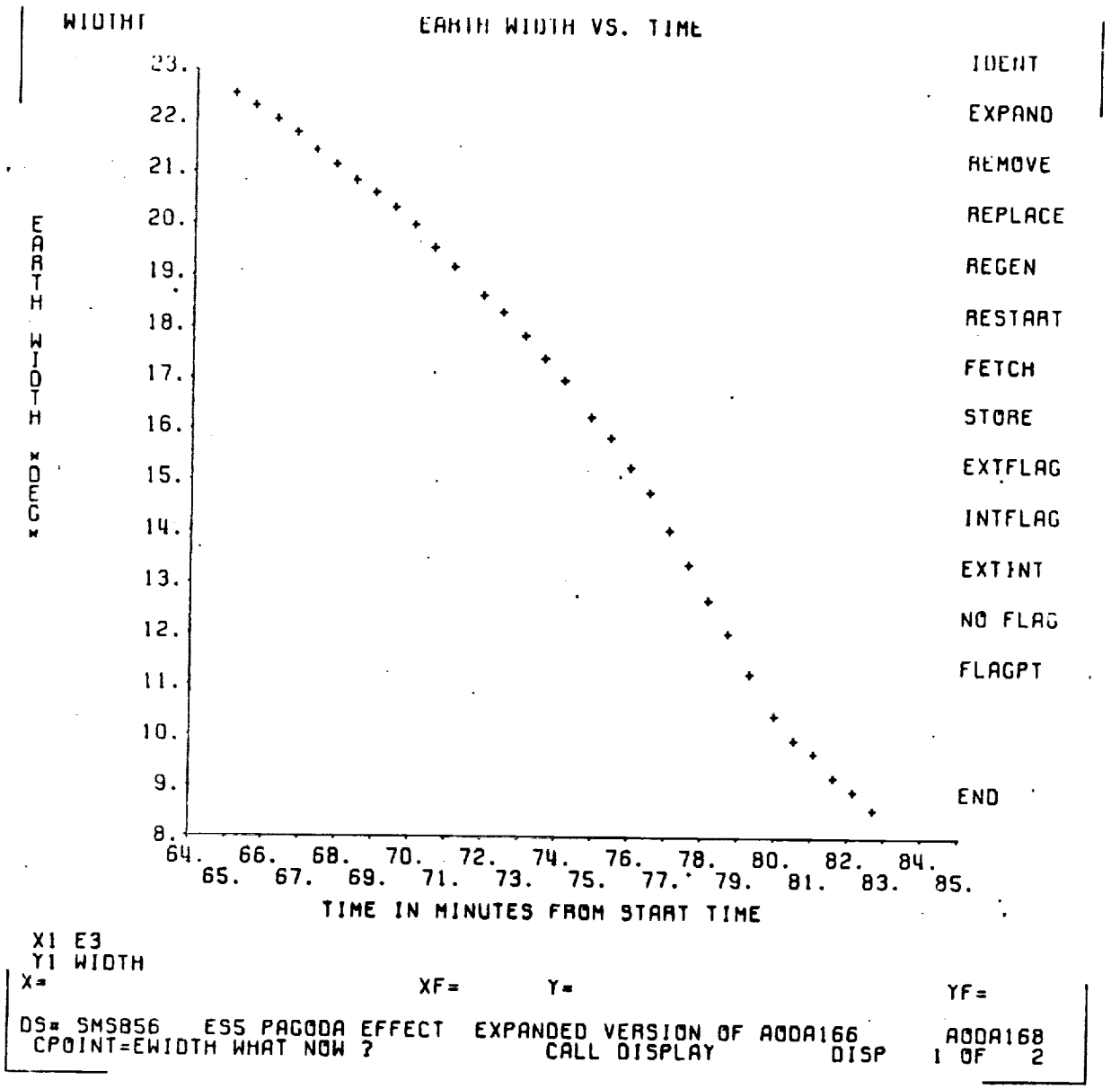

Figure 3-5. DS# SMSB56 Earth Width Data Showing Pagoda Effect (2 of 2)

PRECEDING PAGE BLANK NOT FILMED

- Plots of frame by frame deterministic attitude solutions from the OASYS subsystem of MSAD/OABIAS
- Plots of state vector element values vs frame number from OABIAS
- Plots of residuals from OABIAS
- Plots of predicted vs observed data from subsystem PLOTOC

The most direct procedure for identifying bad data is the examination of the OASYS attitude solution plots. An example of this for the ES5 data is shown in Figure 3-6. The portion of the plot to the right of the spike near the center is from a second Earth ellipse for that data pass and may be ignored. Thus, frames 1 to 140 cover the first Earth ellipse shown in the data plots in Figures 3-4 and 3-5. From the figure it can be seen that a systematic variation in the data extends for approximately 30 frames into either end of the Earth ellipse. Thus, the anomalistic behavior is not confined to the small curl at the end of the Earth ellipse, but extends more deeply into the data.

A better procedure than the OASYS plots for determining the character and extent of the data anomaly is to compare the observed data with predicted data based on the best estimate of the attitude and bias parameters. Since this entails a comparison of predicted and observed data, the results will depend on the accuracy of the parameters used for the prediction. Solutions used for the comparison should not be based on the bad data at ends of the Earth ellipse. Thus, an iterative procedure must be used whereby more data is removed in successive iterations until a good fit to the remaining data is obtained. The bad data is then put back into the data set and can be compared with predicted data which is based on attitude and bias parameters obtained from data at the center of the Earth ellipse.

Accurate modeling of attitude and bias parameters is essential for the above procedure. As an example, Figure 3-7 shows the predicted and observed rotation angles for the ES5 data based on the nominal sensor parameters. The symbol +

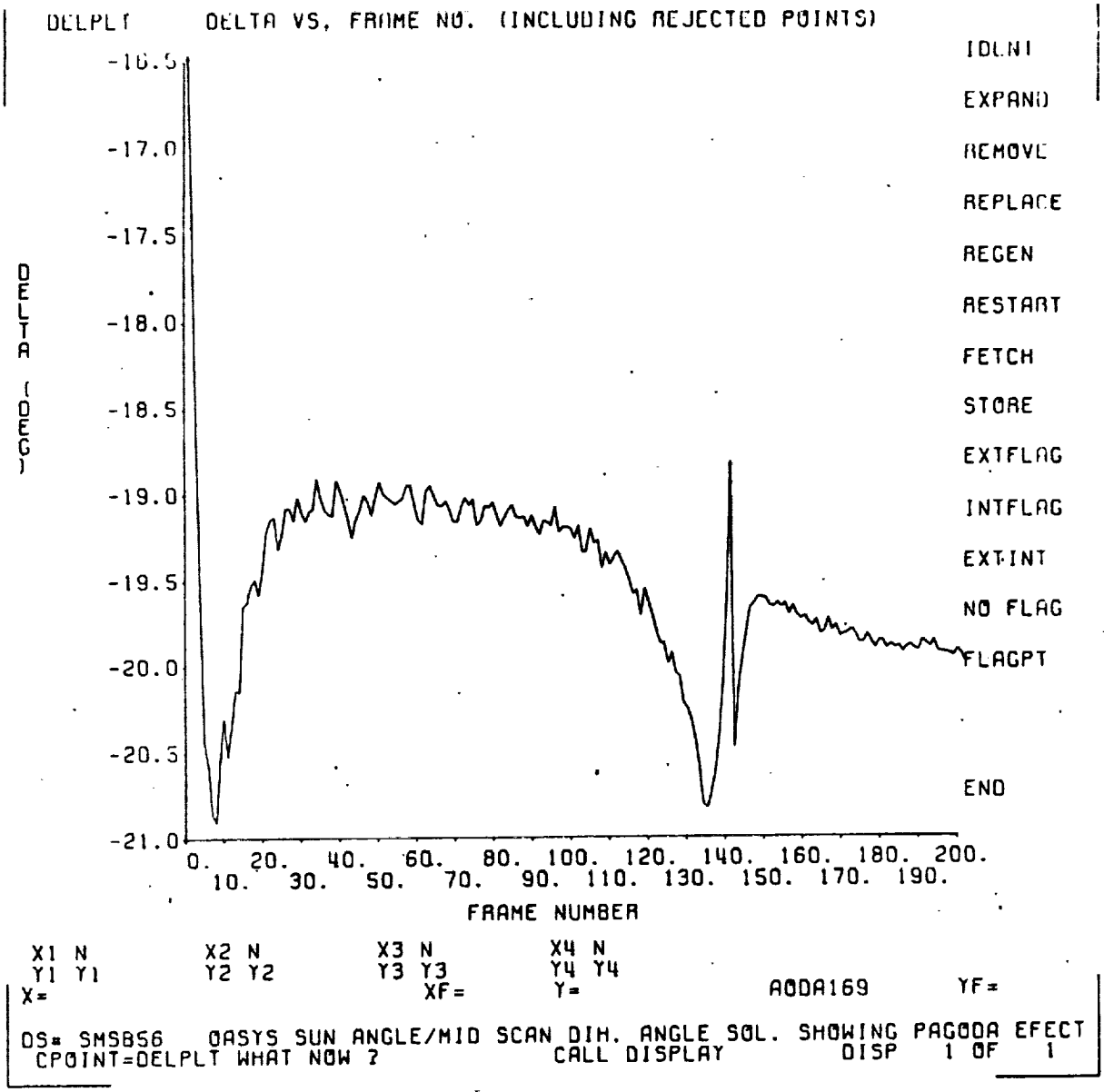

Figure 3-6. DS# SMSB56 OASYS Sun Angle/Mid-Scan Dihedral Angle Solution Showing Pagoda Effect

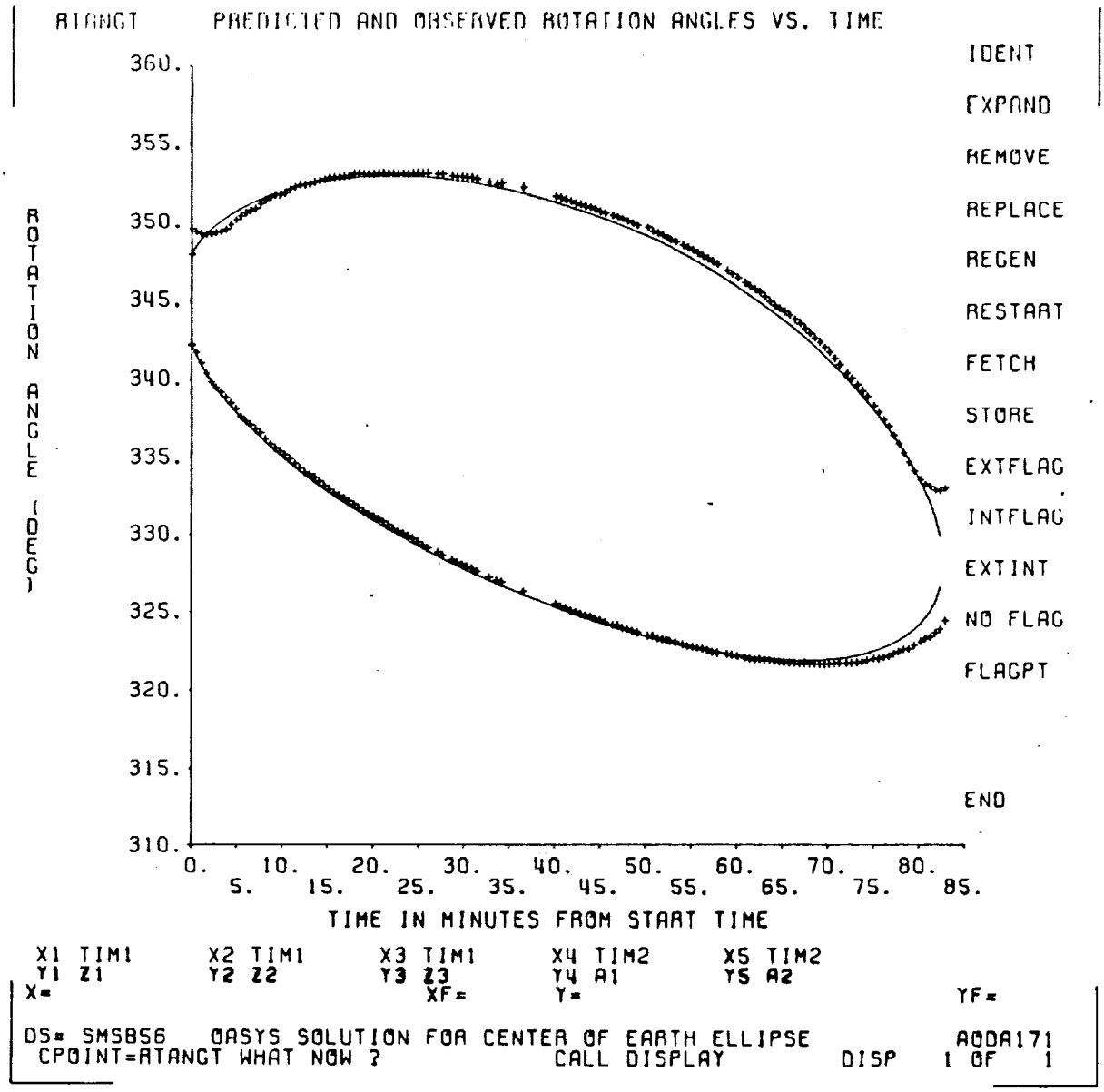

Figure 3-7. DS# SMSB56 Rotation Angle Plot for OASYS Solution for Center of Earth Ellipse

indicates observed data and the smooth curve is the predicted behavior. Even though the solution is based only on the data at the center of the pass, the fit to the data is poor and it is difficult to identify the region of bad data associated with the pagoda effect. (The solution based on the entire data pass is somewhat worse.)

When the OABIAS solution for the center of the data span is used, the fit to the data is improved and the region of bad data due to the pagoda effect is more easily identified. The OABIAS solution for the ES5 data is shown in Figures 3-8 and 3-9. The overall view in Figure 3-8(1) is better for judging the fit to the data in the center of the Earth ellipse and the expanded views in Figures 3-8(2) and 3-8(3) are better for judging the extent of the systematic variations in the data.

From these figures, both the extent and the characteristics of the anomalistic behavior can be seen. Both Earth-in and Earth-out data begin a systematic variation from their predicted behavior at an Earth width of approximately 20 degrees*. Both events occur progressively earlier than anticipated as the scan goes from the center to the edge of the disk of the Earth. For the observed Earth-in data, the behavior proceeds uniformly, becoming progressively worse relative to the predicted values. The difference between predicted and observed Earth-in values increases to approximately 0.5^{o} when the Earth width has dropped to 11.5^{o}. The variation in Earth-out data advances uniformly until an Earth width of approximately 11.5^{o} is reached. At Earth-widths less than this value, the Earth-out curve turns sharply upward to produce the "pagoda" characteristic of this anomaly. At the turning point in the Earth-out curve, the observed data is approximately 0.8^{o} in advance of the predicted data. Is should be emphasized that all of the numbers given here to indicate the size of the pagoda effect are necessarily

* Note that the Earth widths and rotation angles are in dihedral angle degrees, and not degrees of arc. The Earth width dihedral angle is a correct measure of the Earth chord width in arc degrees only for a 90 degree sensor mounting angle.

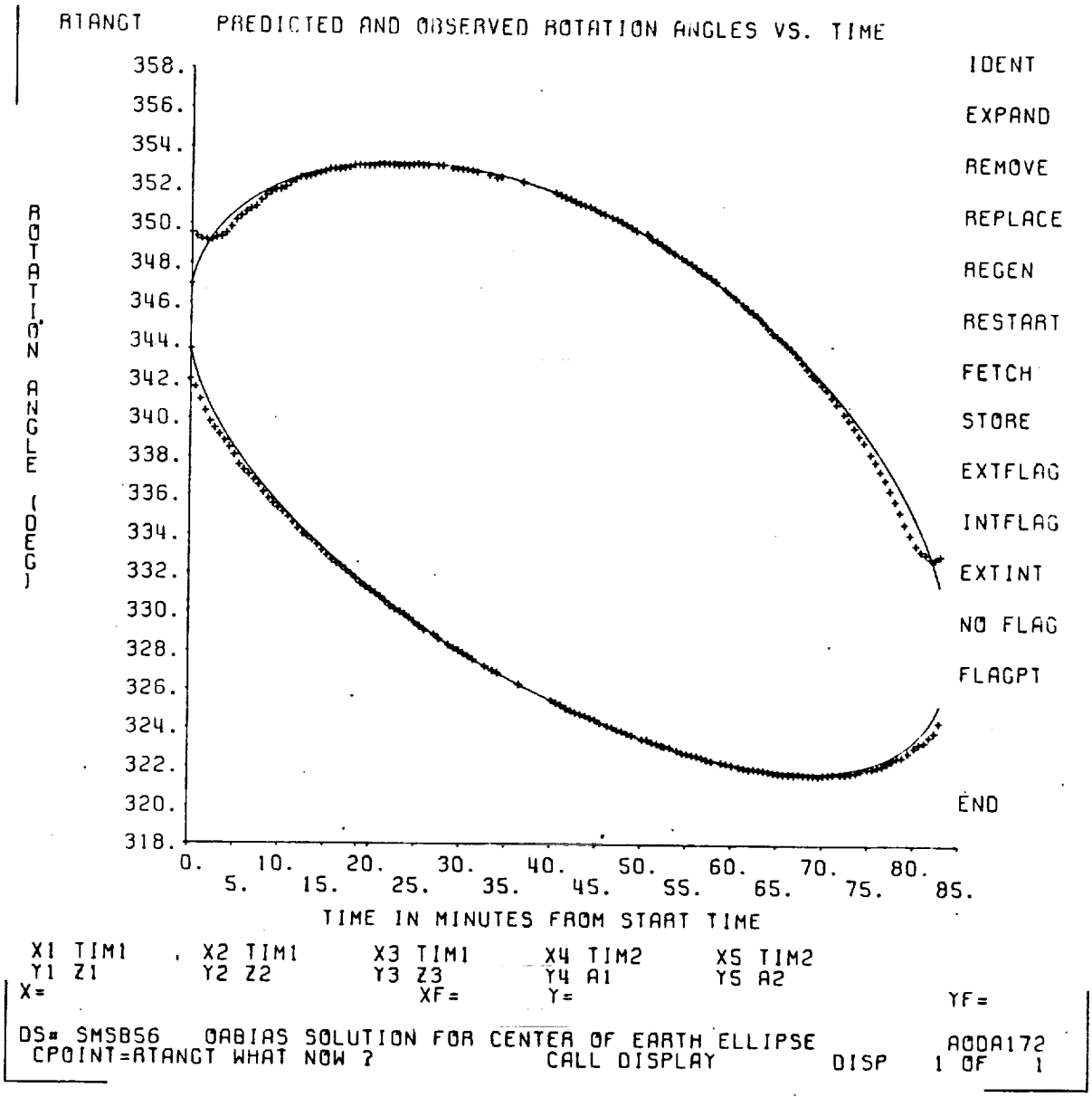

Figure 3-8. DS# SMSB56 Rotation Angle Plot for OABIAS Solution for Center of Earth Ellipse (1 of 3)

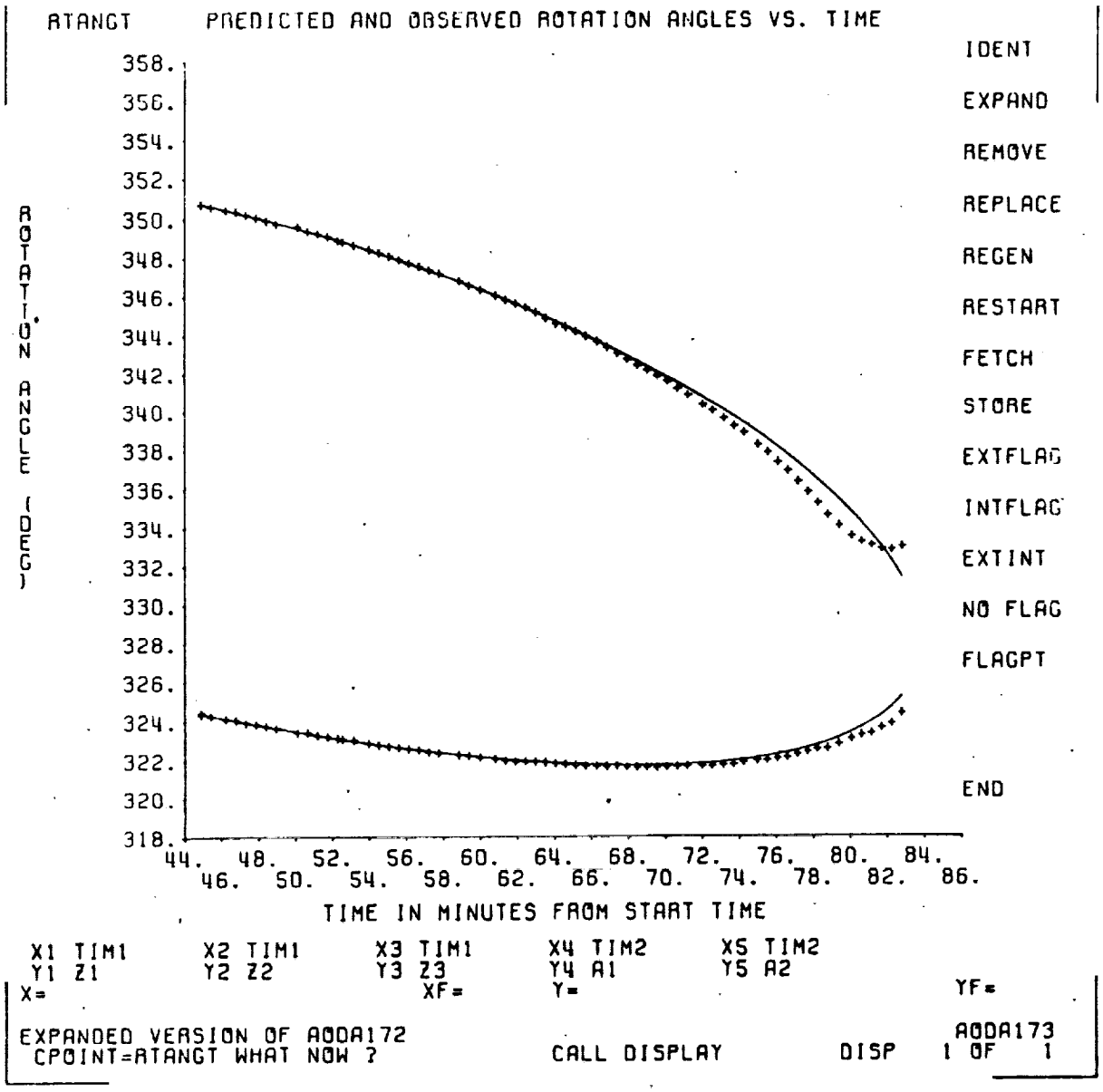

Figure 3-8. DS# SMSB56 Rotation Angle Plot for OABIAS Solution for Center of Earth Ellipse (2 of 3)

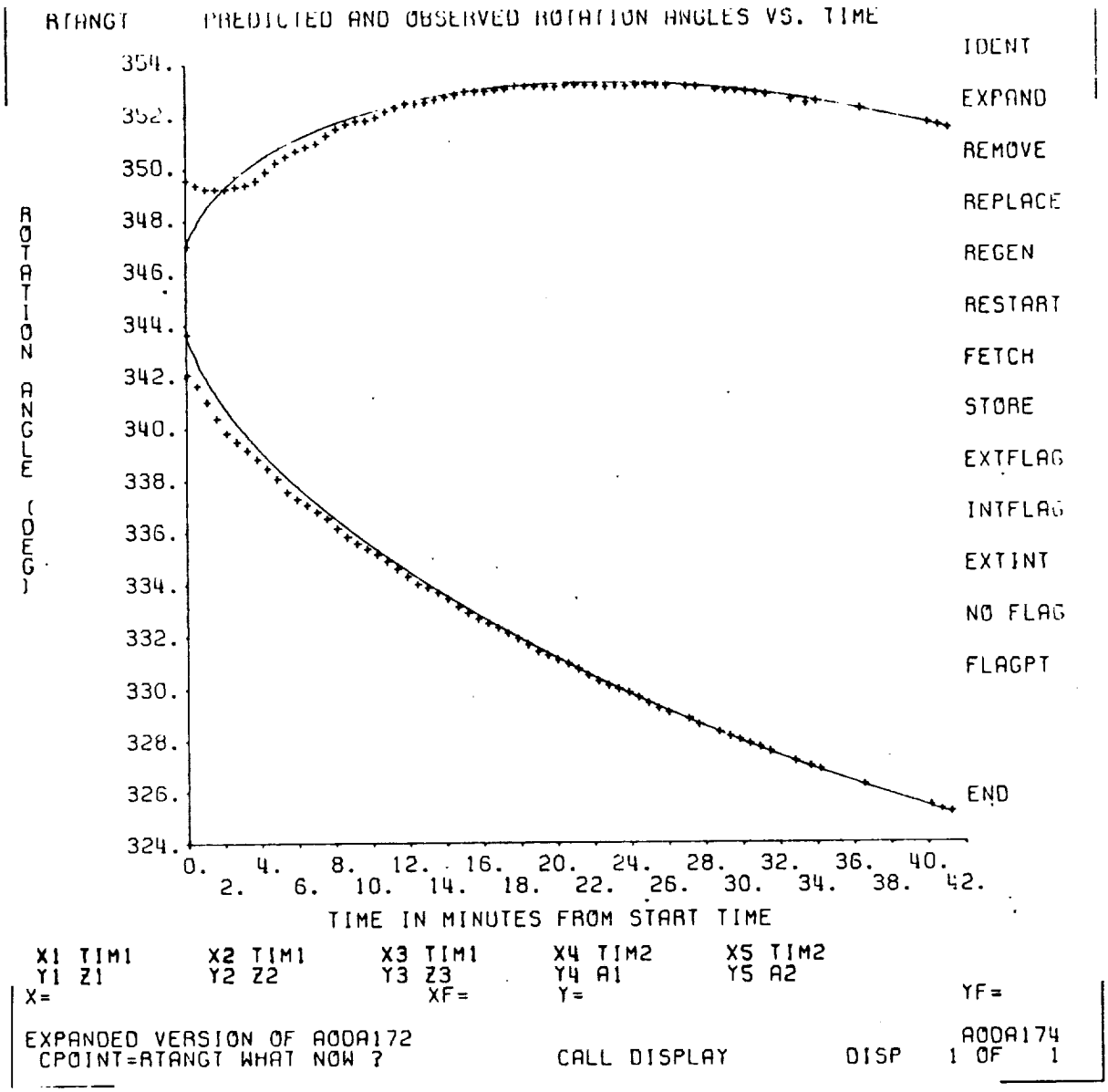

Figure 3-8. DS# SMSB56 Rotation Angle Plot for OABIAS Solution for Center of Earth Ellipse (3 of 3)

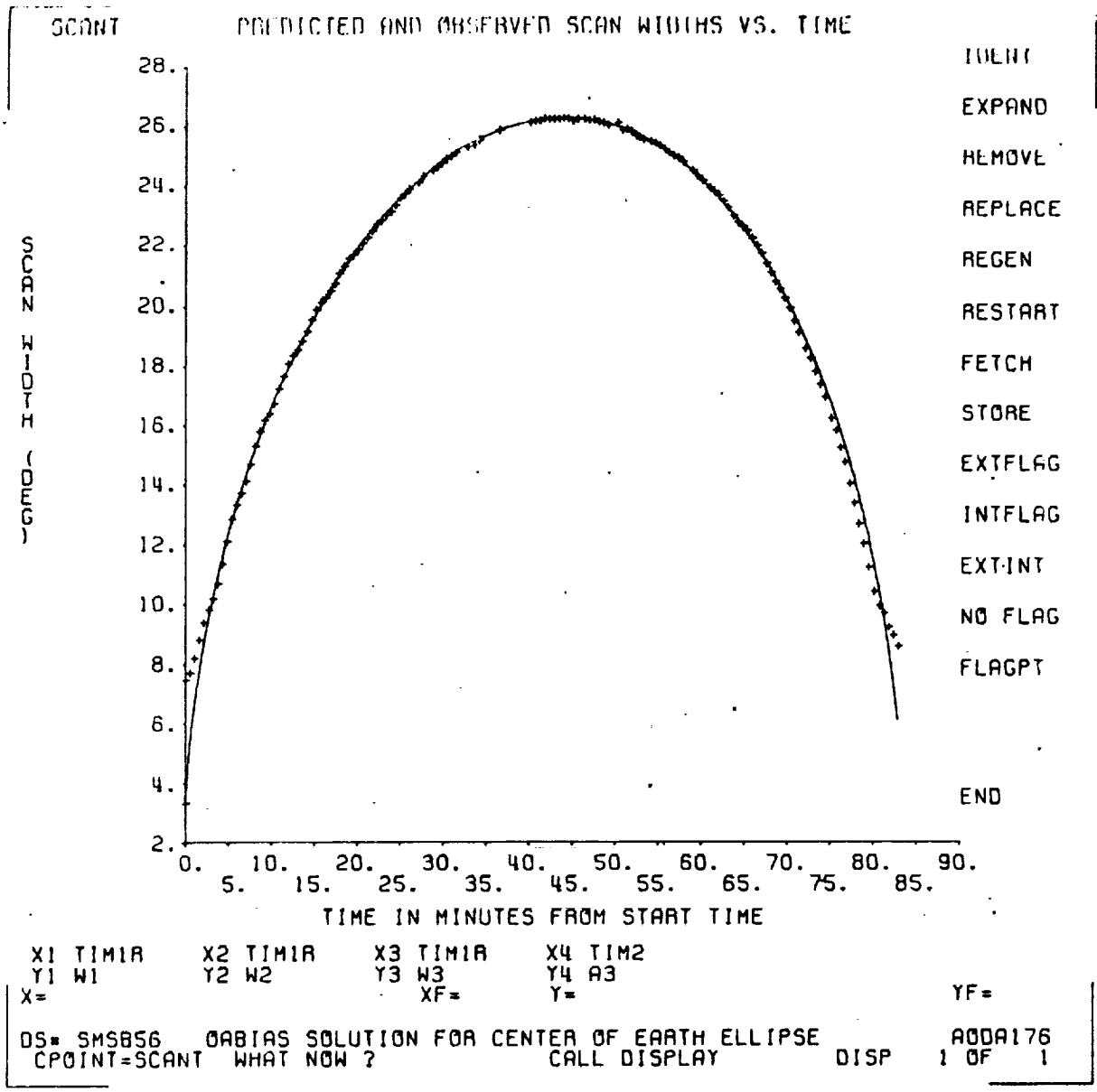

Figure 3-9. DS# SMSB56 Earth Width Plot for OABIAS Solution for Center of Earth Ellipse

approximate values since they depend strongly on the parameters used for data prediction. They are given here to provide an estimate of the magnitude of the anomaly and its effect on the data.

In terms of the data available for bias and attitude determination, the pagoda effect is a major problem. For ES5, all data for Earth widths of less than 21^{o} was discarded for purposes of attitude and bias determination. This Earth-width is 80% of the Earth's diameter of 26.3^{o} as seen by ES5. Of the 83 minutes of data covering the first Earth ellipse of ES5, 28 minutes of data have been eliminated. Although this is only one third of the data, it includes most of the variation in Earth width and, therefore, most of the information due to the variation in the geometry. This effect seriously interfered with bias determination efforts for ES5.

As previously indicated, the pagoda effect occurs in all of the SMS-2 Earth horizon sensor data sets where it would be expected to appear. In particular, Figures 3-10 and 3-11 show the rotation angle and Earth width data in drift orbit 2 for the prime Earth horizon sensor, ES1. Again, the pagoda is clearly present in the data. Figures 3-12 and 3-13 have been included to show the Sun angle and spin rate data, respectively, for the same time span. It can be seen that the anomaly does not appear in either the Sun angle or spin rate data. Figures 3-10 through 3-13 show only the first Earth ellipse for this ES1 data pass. The data from the second Earth ellipse is essentially identical in its overall characteristics to that from the first Earth ellipse except that some small gaps occur in data from the second Earth ellipse. Note that the upturn in the rotation angle data occurs at Earth widths of approximately 7^{o} and that the Earth width plot is noticeably distorted below Earth widths of 6.5^{o} to 7^{o}.

As in the case of ES5, the most effective procedure for determining the characteristics and extent of the pagoda effect is a plot of observed data and predicted data, where the predicted data is based on the OABIAS solution obtained from the central

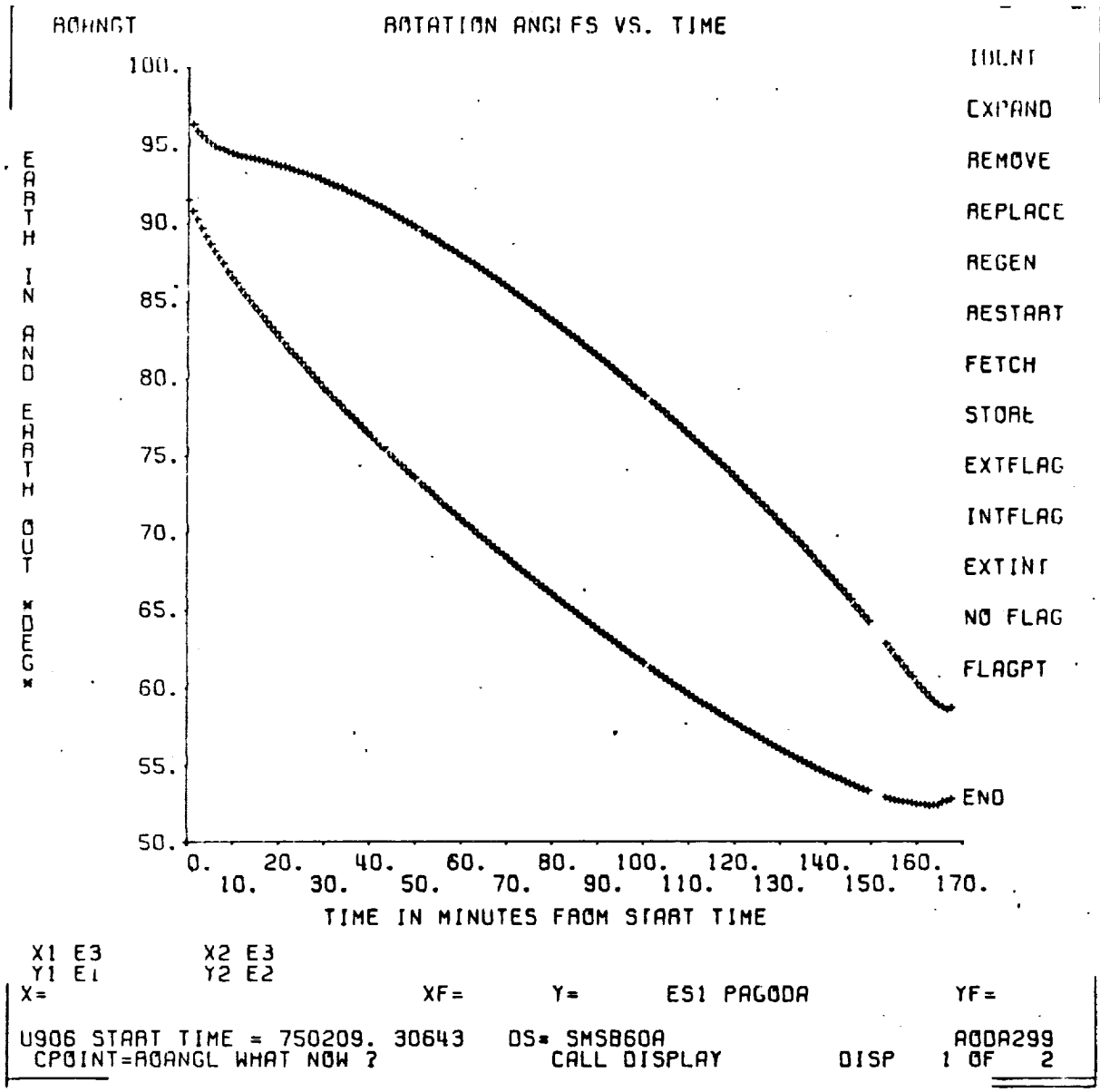

Figure 3-10. DS# SMSB60A Rotation Angle Data Showing Pagoda Effect (1 of 3)

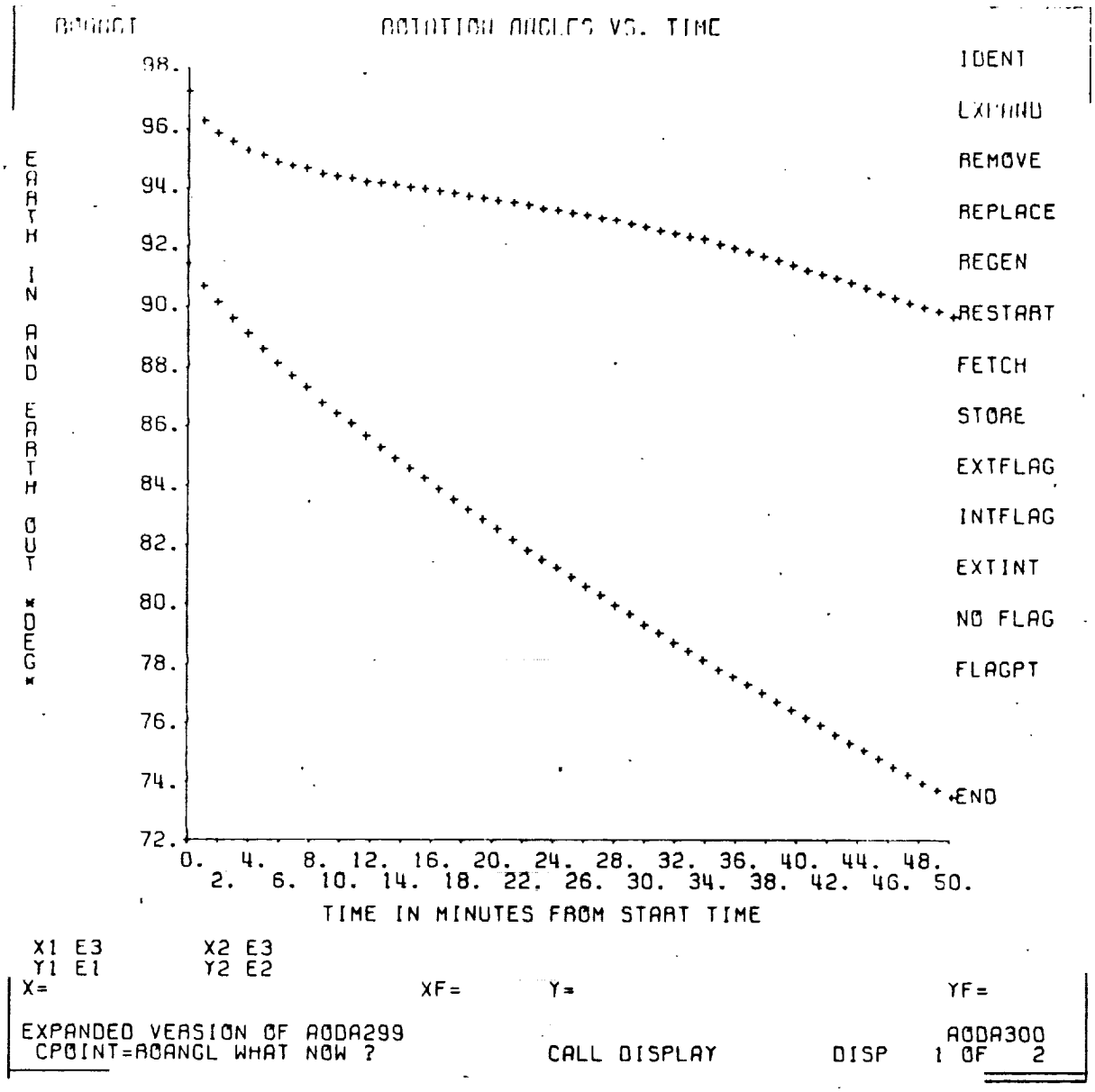

Figure 3-10. DS# SMSB60A Rotation Angle Data Showing Pagoda Effect (2 of 3)

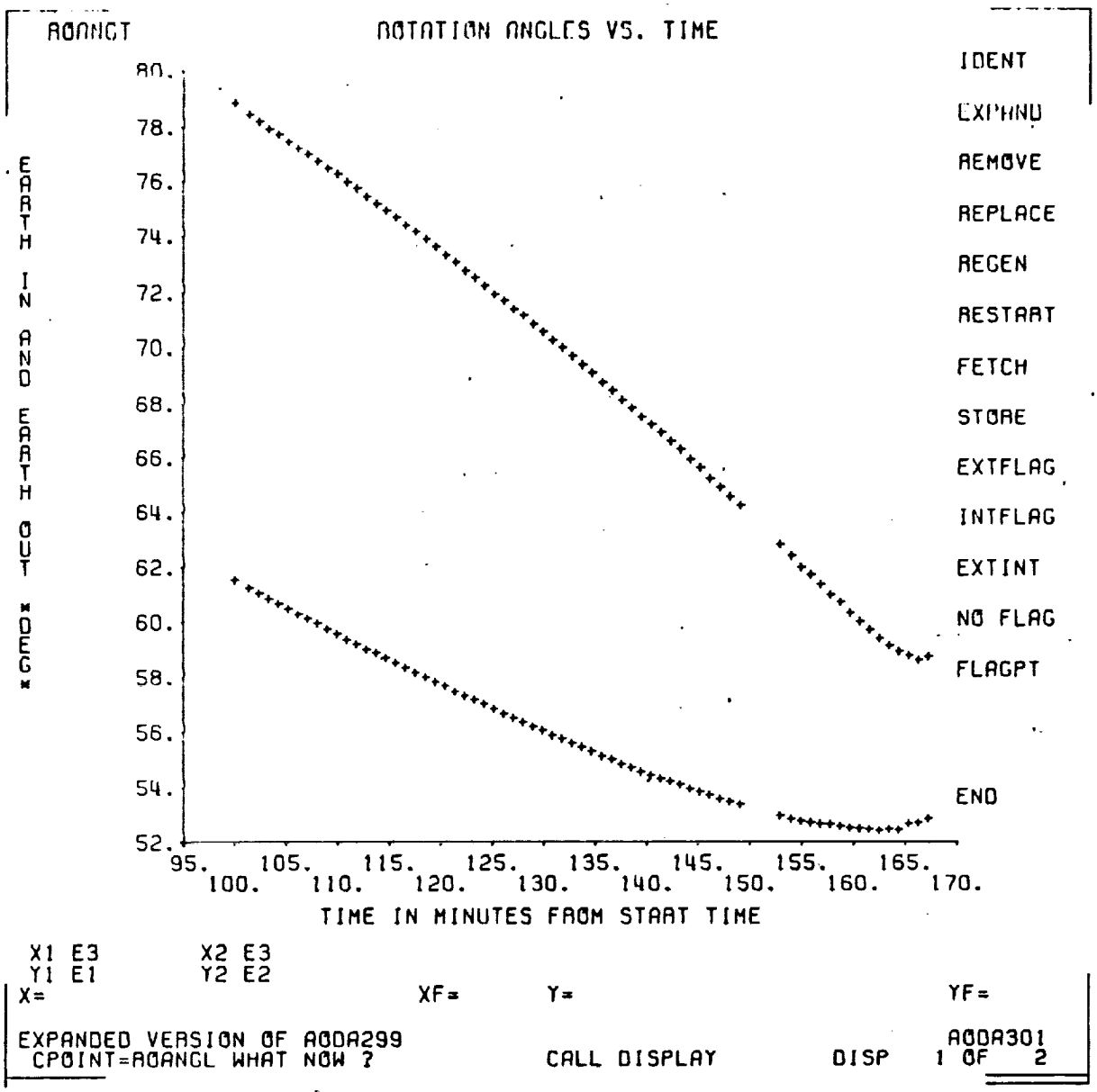

Figure 3-10. DS# SMSB60A Rotation Angle Data Showing Pagoda Effect (3 of 3)

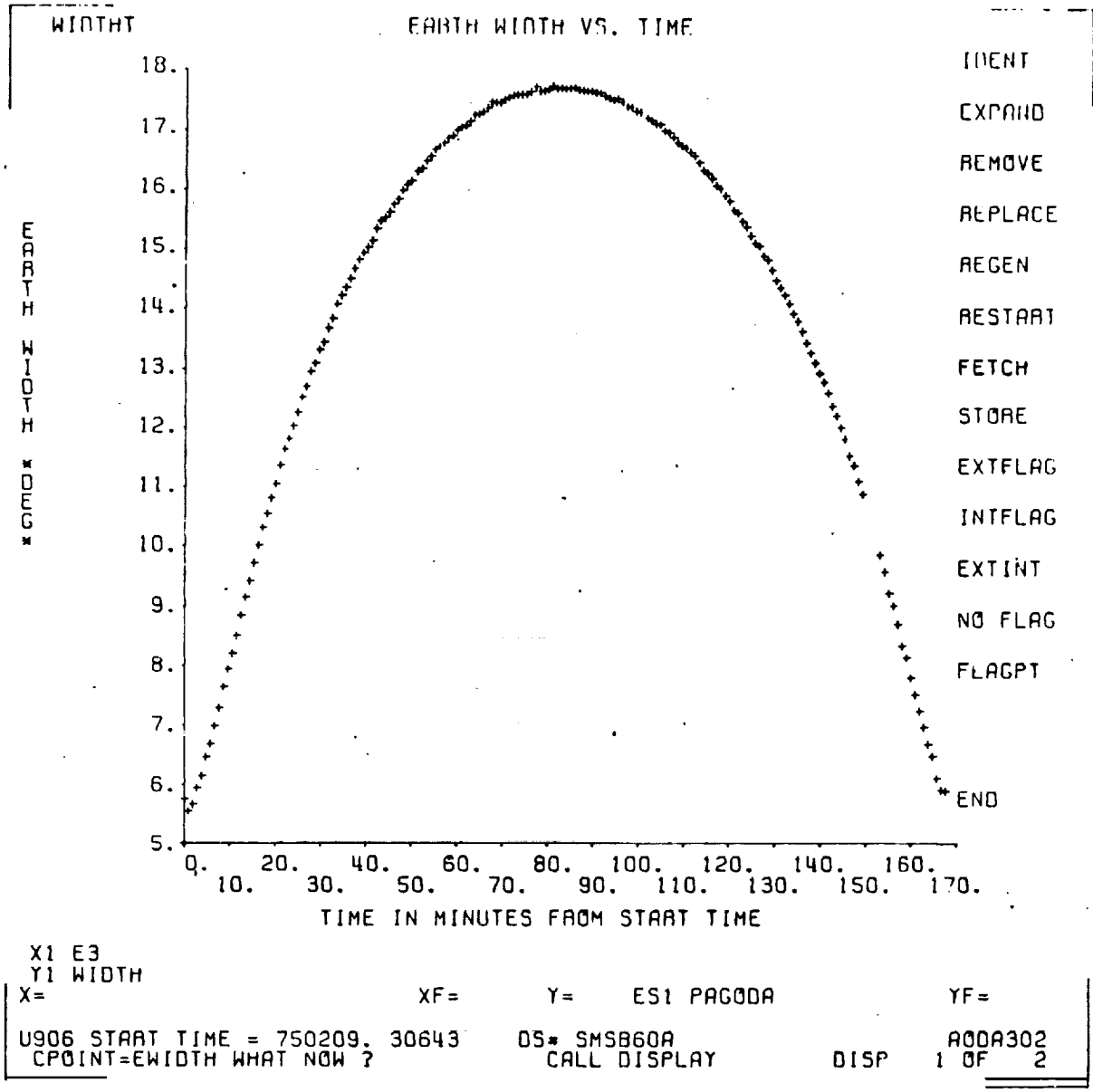

Figure 3-11. DS# SMSB60A Earth Width Data Showing Pagoda Effect (1 of 3)

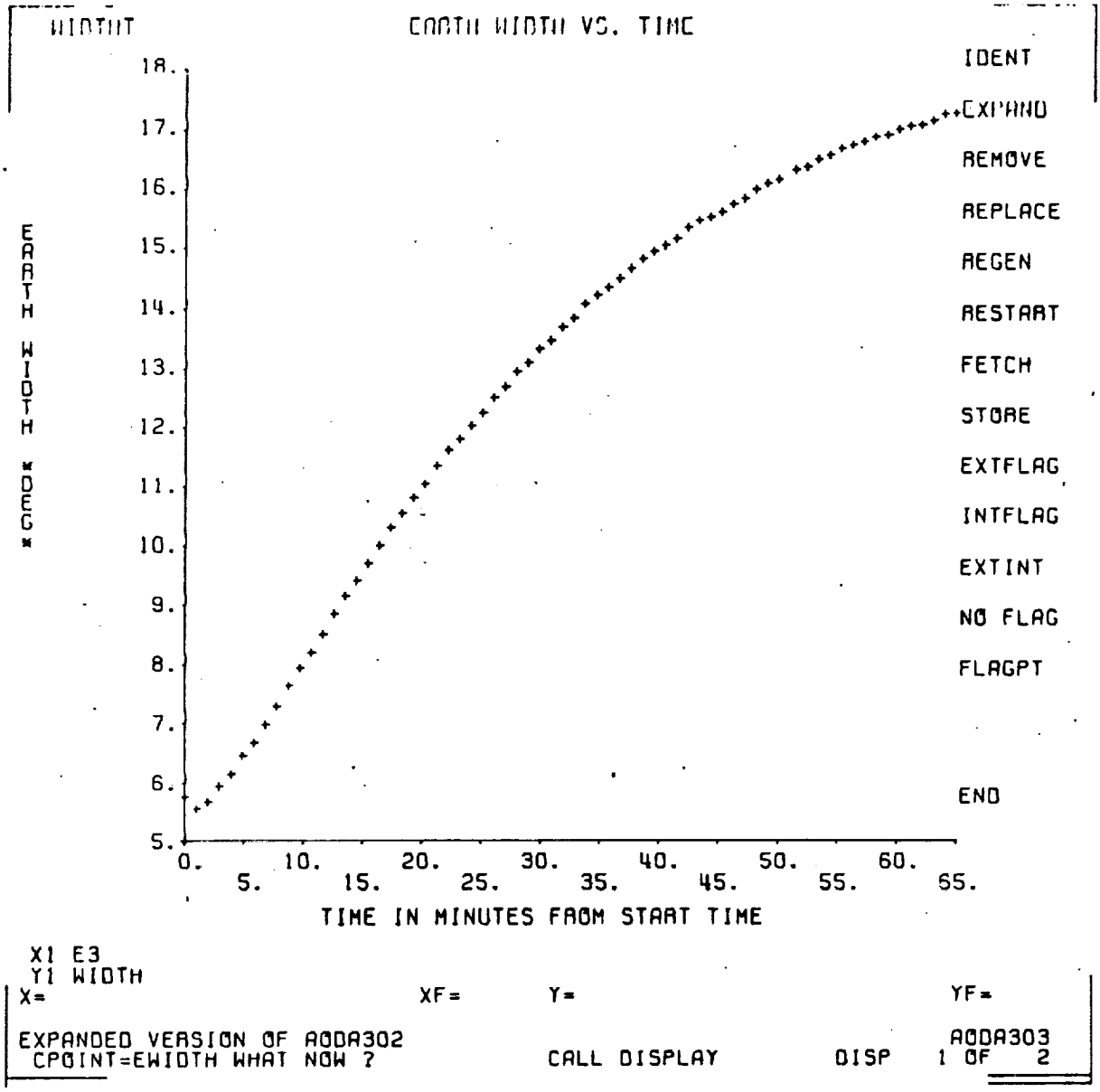

Figure 3-11. DS# SMSB60A Earth Width Data Showing Pagoda Effect (2 of 3)

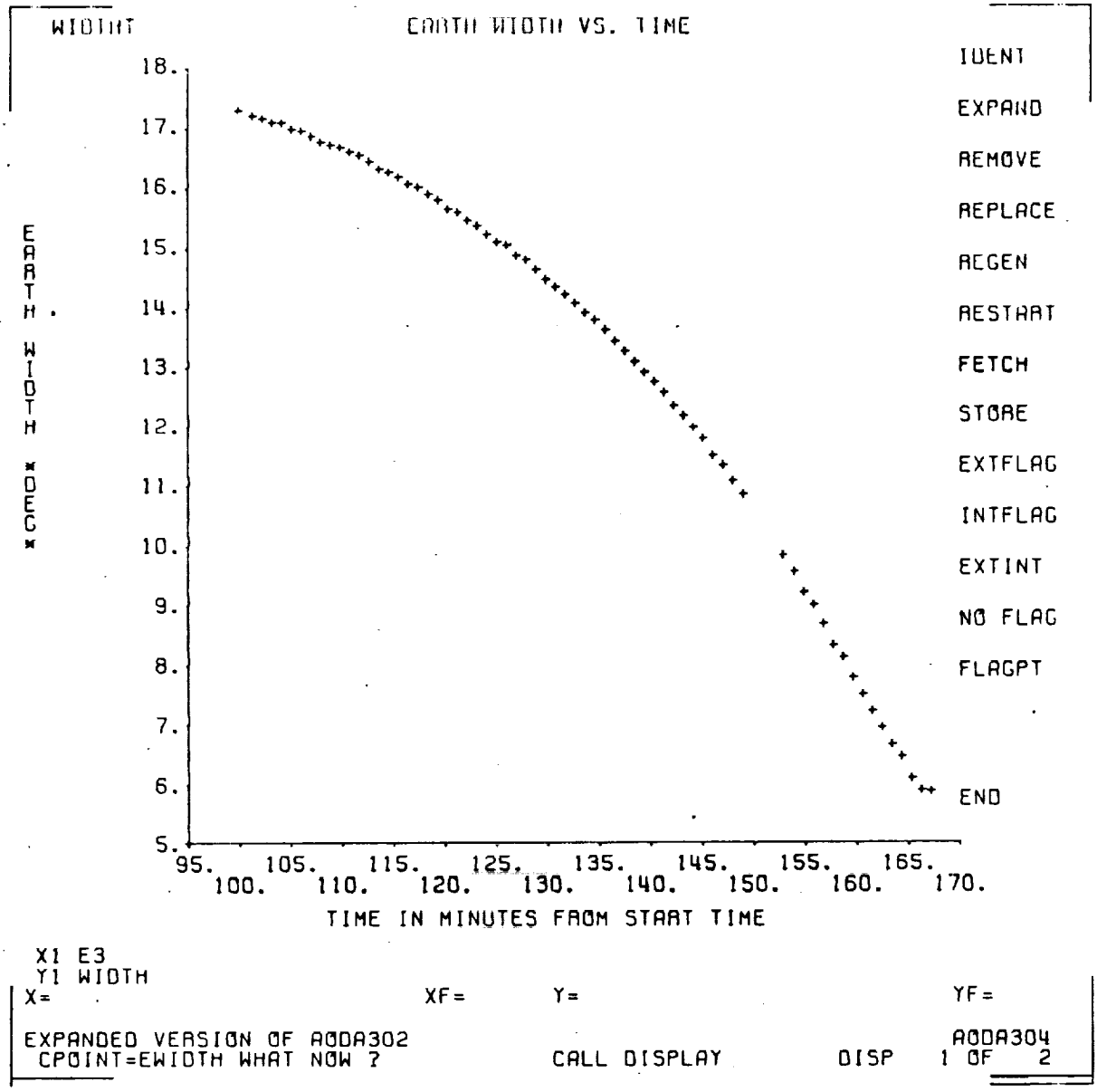

Figure 3-11. DS# SMSB60A Earth Width Data Showing Pagoda Effect (3 of 3)

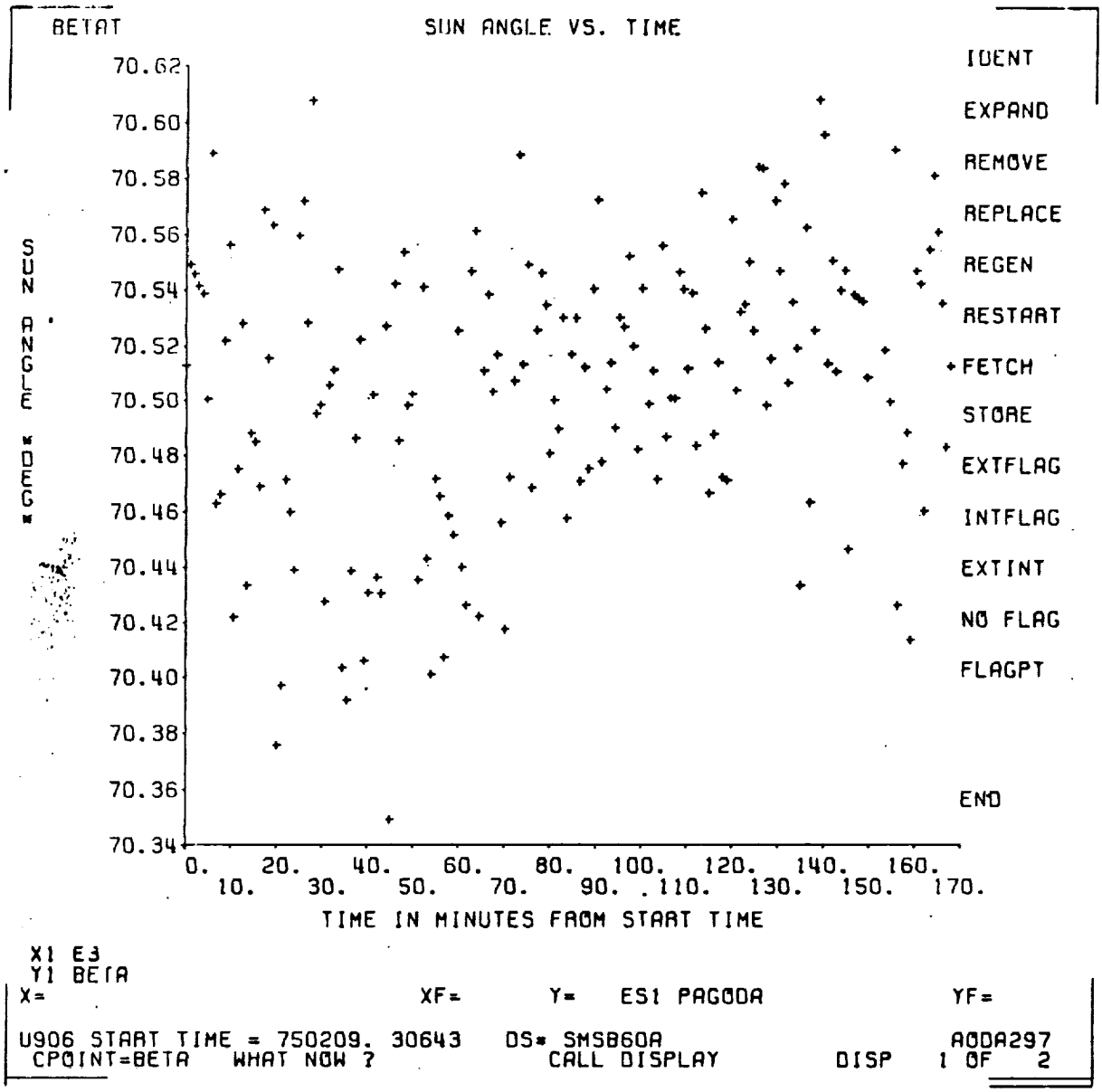

Figure 3-12. DS# SMSB60A Sun Angle Data Showing Absence of Pagoda Effect

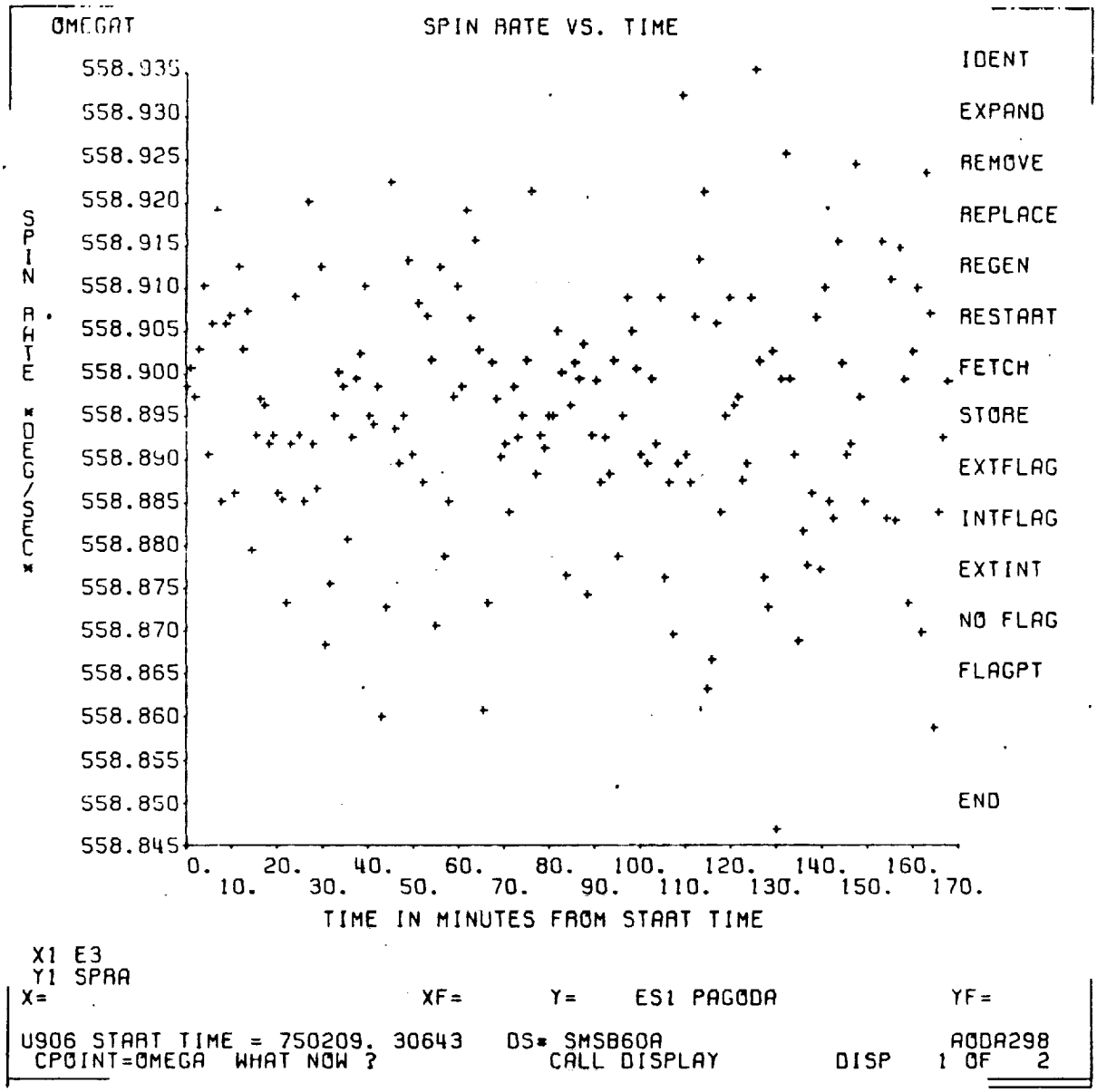

Figure 3-13. DS# SMSB60A Spin Rate Data Showing Absence of Pagoda Effect

data in both ES1 Earth ellipses. The rotation angle plots for the first Earth ellipse (corresponding to the data in Figures 3-10 through 3-13) are shown in Figure 3-14. Again, expanded plots are provided to show the anomalistic behavior. The qualitative behavior of the pagoda effect on ES1 is similar to that of ES5. However, its behavior relative to the predicted data is different in that for the first Earth ellipse of ES1 all of the observed data lies outside of the predicted ellipse as the sensor scans off the Earth (i.e., on the right hand side of Figure 3-14(1) and 3-14(3)). Since the relative behavior of the observed and predicted data in this region is particularly sensitive to the shape and position of the predicted Earth ellipse, this difference in behavior may be due entirely to residual errors in the values of the prediction parameters.

From Figure 3-14 it can be seen that the systematic variation in the data begins at an Earth width of approximately 12.0^{o}. This is 68% of the Earth diameter of 17.7^{o}. The upturn in Earth-out data begins at an Earth width of approximately 7.5^{o}.

The above numerical results for ES1 are about 40% lower than the comparable dihedral angle measurements associated with the ES5 pagoda effect. However, the measurements are very close when considered in terms of chord length on the disk of the Earth. Since the scan of the ES1 sensor is nearly a great circle, the dihedral angle measurements for ES1 are effectively equal to arc length measurements along a chord of the disk of the Earth. That is, for ES1, the start of the systematic variation occurs when the sensor scans a chord of the Earth's disk 12.0^{o} in length and a major change in the behavior occurs when the sensor scans a chord 7.5^{o} in length. Translating the measurements from ES5 into chord length measurements along an arc of a great circle, the results show that the systematic variation for ES5 starts when the sensor scans a chord on the Earth's disk 13.9^{o} in length and the upturn in the pagoda occurs at a chord length of 7.6^{o}. The spin rate for the ES5 data and the ES1 data is

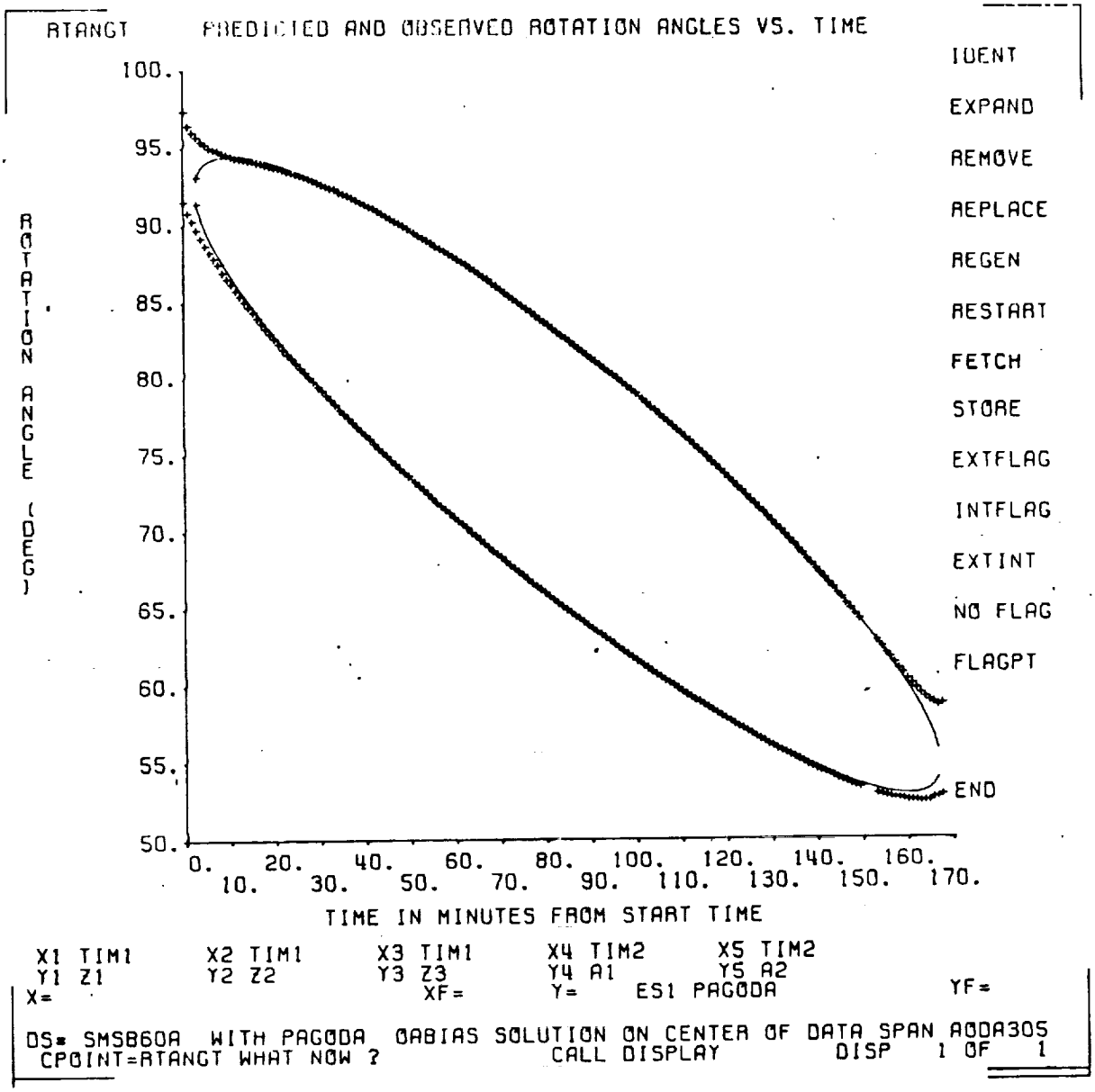

Figure 3-14. DS# SMSB60A Rotation Angle Plot for OABIAS Solution for Center of Earth Ellipse (1 of 3)

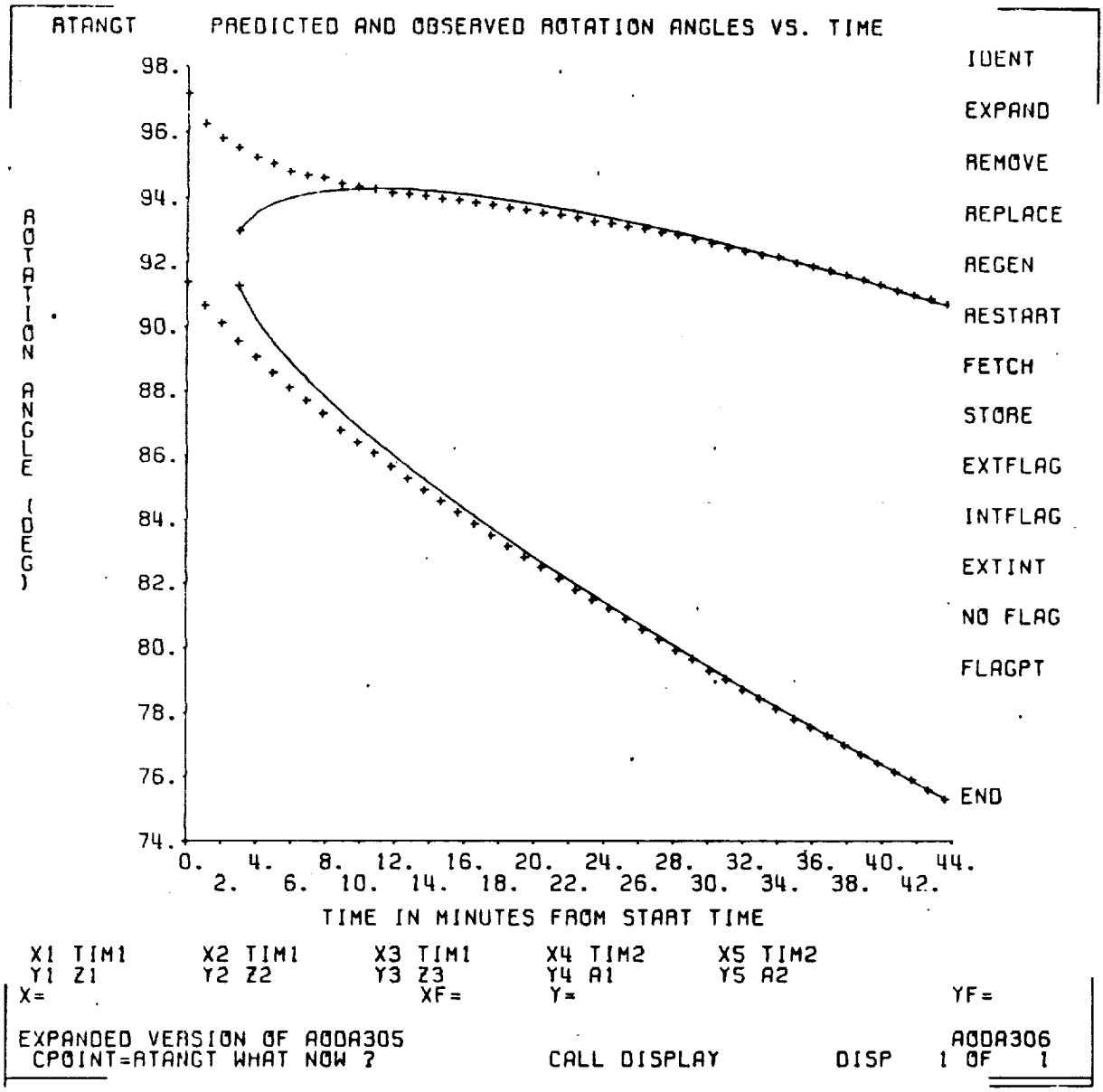

Figure 3-14. DS# SMSB60A Rotation Angle Plot for OABIAS Solution for Center of Earth Ellipse (2 of 3)

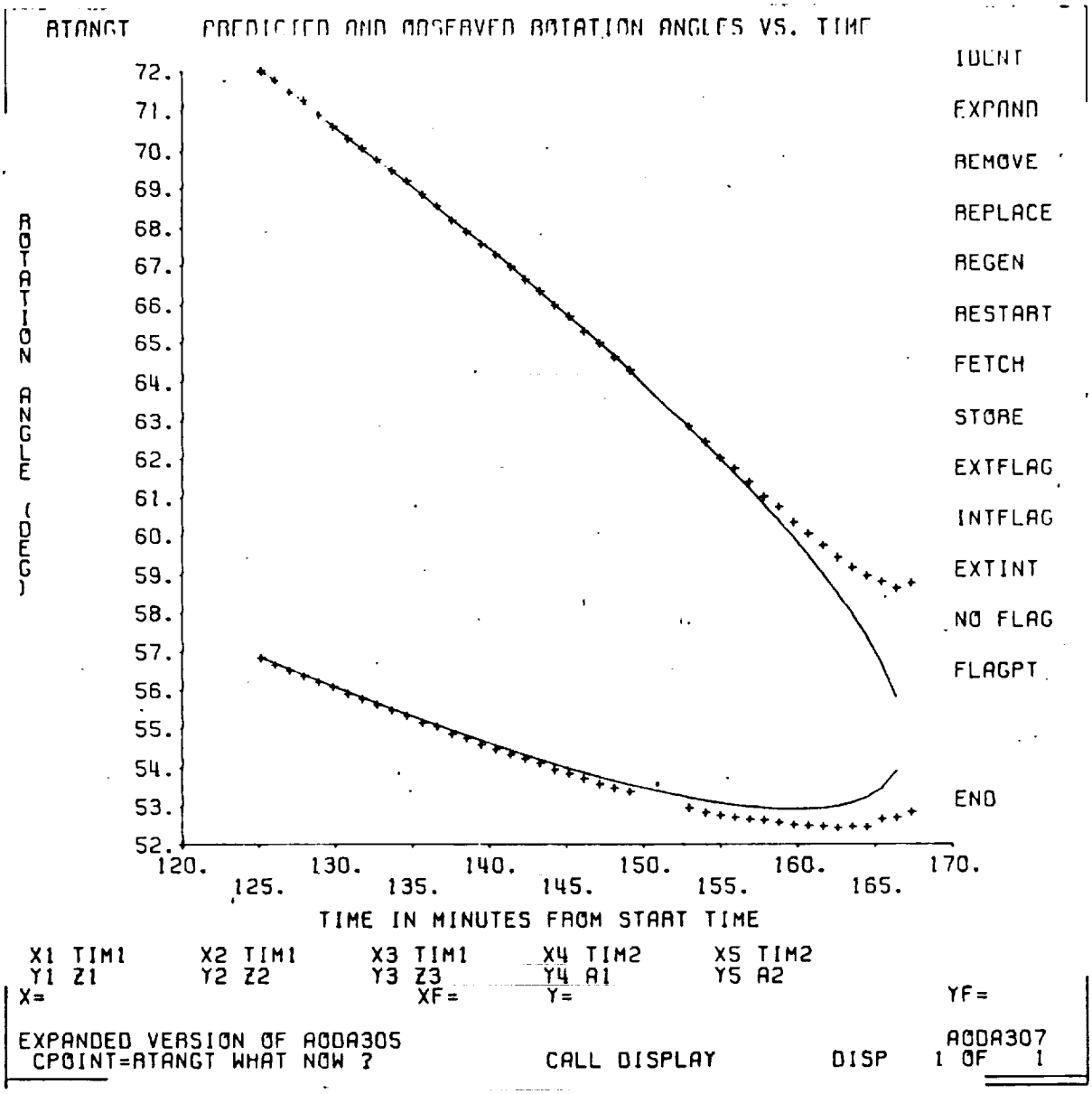

Figure 3-14. DS# SMSB60A Rotation Angle Plot for OABIAS Solution for Center of Earth Ellipse (3 of 3)

essentially the same. Therefore, the dihedral angle measurement is proportional to the time from Earth-in triggering to Earth-out triggering. Thus, it can be concluded that for a fixed spin rate the pagoda effect is approximately a chord length phenomenon rather than a time phenomenon.

For comparison with the first ES1 Earth ellipse, Figures 3-15 and 3-16 show the predicted and observed data for the second Earth ellipse for the ES1 data set in drift orbit 2. The prediction parameters are the same as those used for the first Earth ellipse. It can be seen from Figure 3-15(1) that the pagoda effect produces an advance of observed Earth-out data ahead of predicted Earth-out data for the start of the anomaly at both ends of the Earth ellipse, as was the case for ES5. The variations in the fit to the predicted data can be seen by comparing the right hand portion of the Earth-out curve in Figures 3-8(1), 3-14(1), and 3-15(1). The numerical results are similar to those for the first Earth ellipse from ES1, except that the pagoda effect starts at an Earth width of approximately 13.5°, as can be seen from the rotation angle plots of Figure 3-14. Figure 3-16 clearly shows the strong variation in Earth width behavior caused by the pagoda effect. The variation in Earth width first becomes noticeable at an Earth width of 9.0° to 10.0°. Note that there is a small segment of bad data at the top of the curve in Figure 3-16(1).

As a last example of the pagoda effect, Figure 3-17 shows the Earth width data for ES2 in drift orbit 3. Here the sensor has not dropped fully off of the Earth while going between the two Earth ellipses. The pagoda effect causes a particularly serious problem here in that it cannot be identified at all in a simple examination of the data. Without previous experience with the pagoda effect, there would be no reason to suspect, prior to processing, that some of the data should be deleted. Figure 3-18 shows a plot of predicted and observed Earth widths for this set of data. The prediction was based on attitude and bias parameters obtained from an OABIAS solution based on the two ends of the data pass. In Figure 3-18, the existence of the pagoda effect is clear. From Figure 3-18(2), it can be seen that the anomaly first becomes noticeable at an

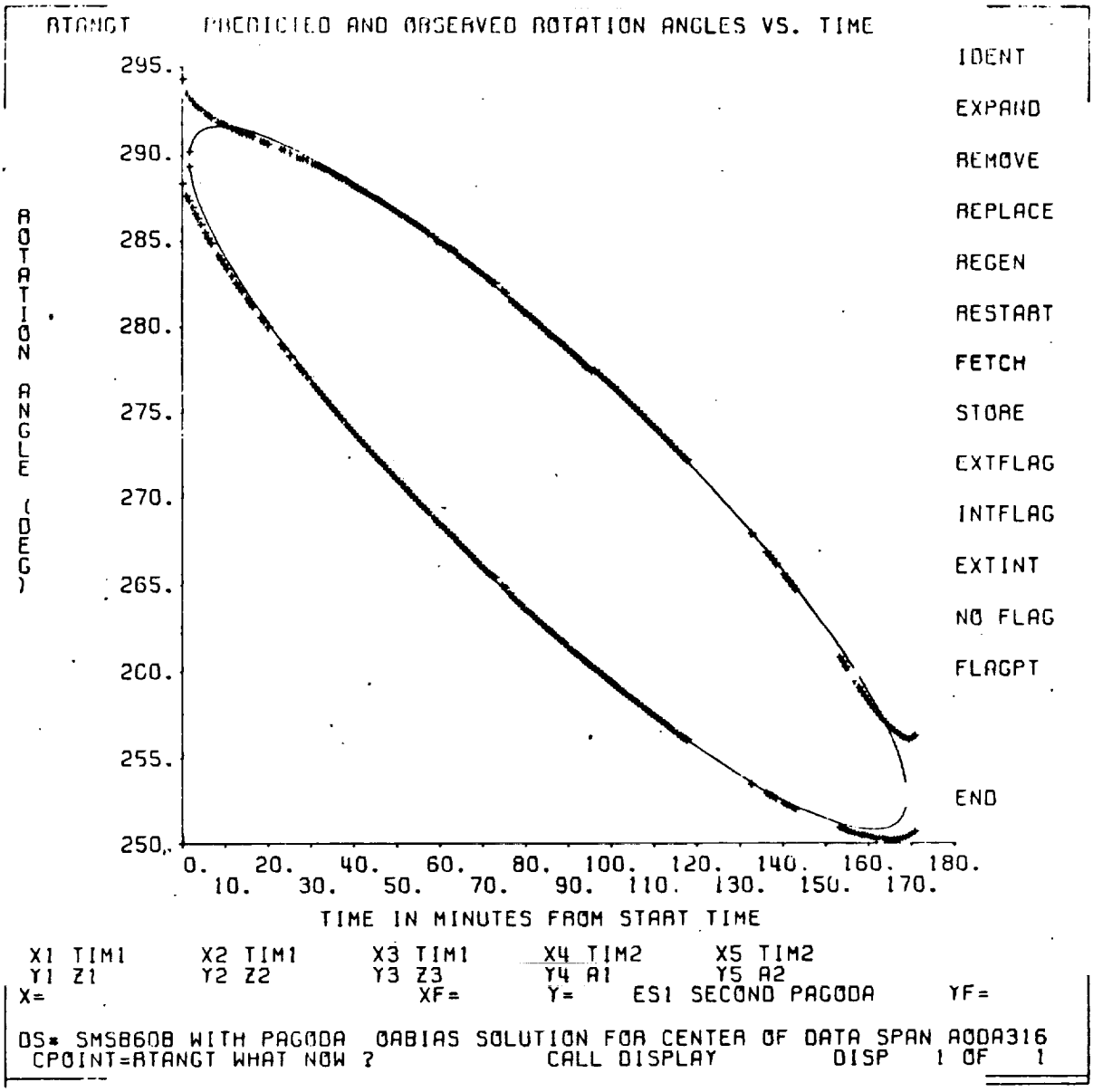

Figure 3-15. DS# SMSB60B Rotation Angle Plot for OABIAS Solution for Center of Earth Ellipse (1 of 3)

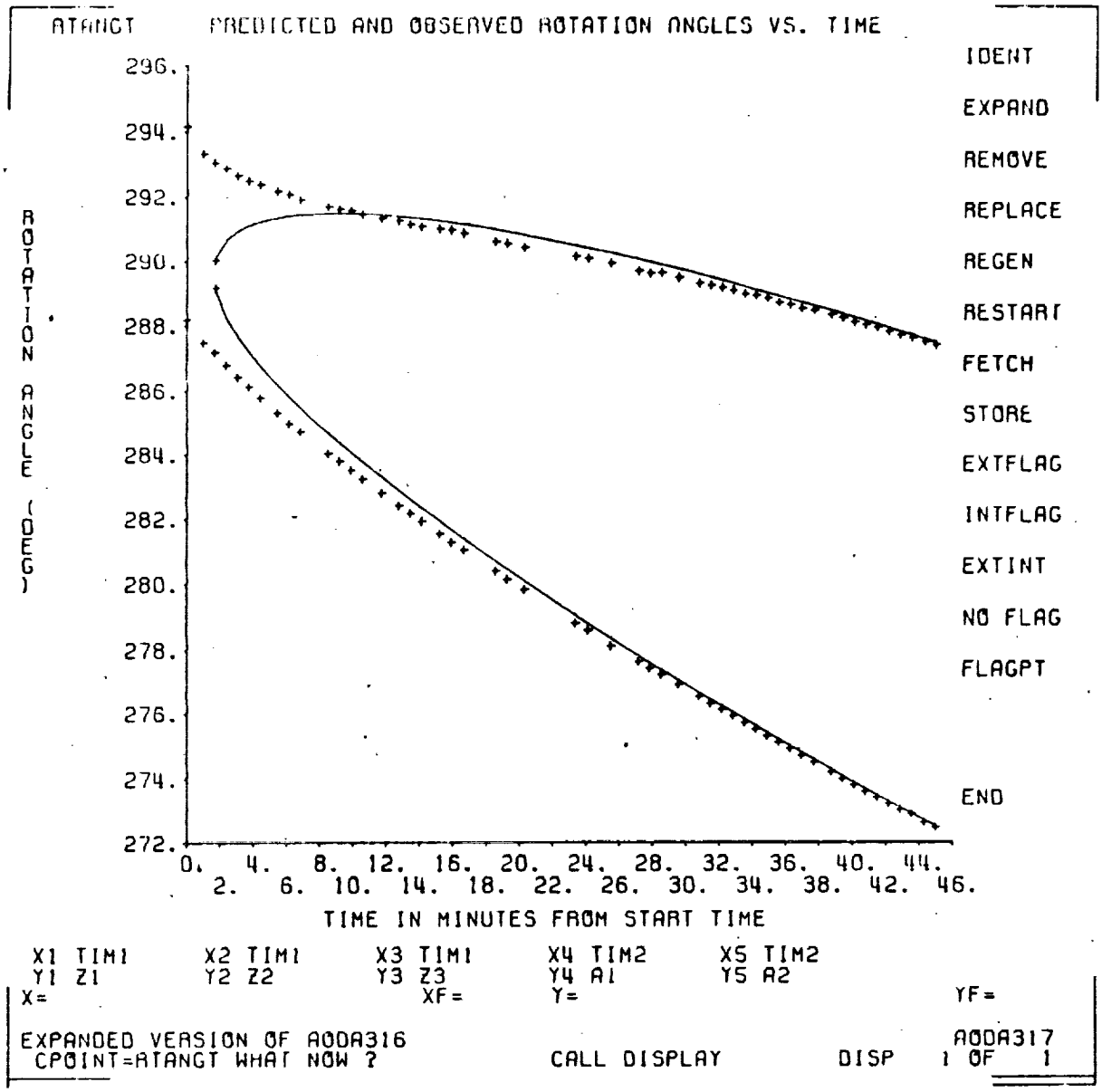

Figure 3-15. DS# SMSB60B Rotation Angle Plot for OABIAS Solution for Center of Earth Ellipse (2 of 3)

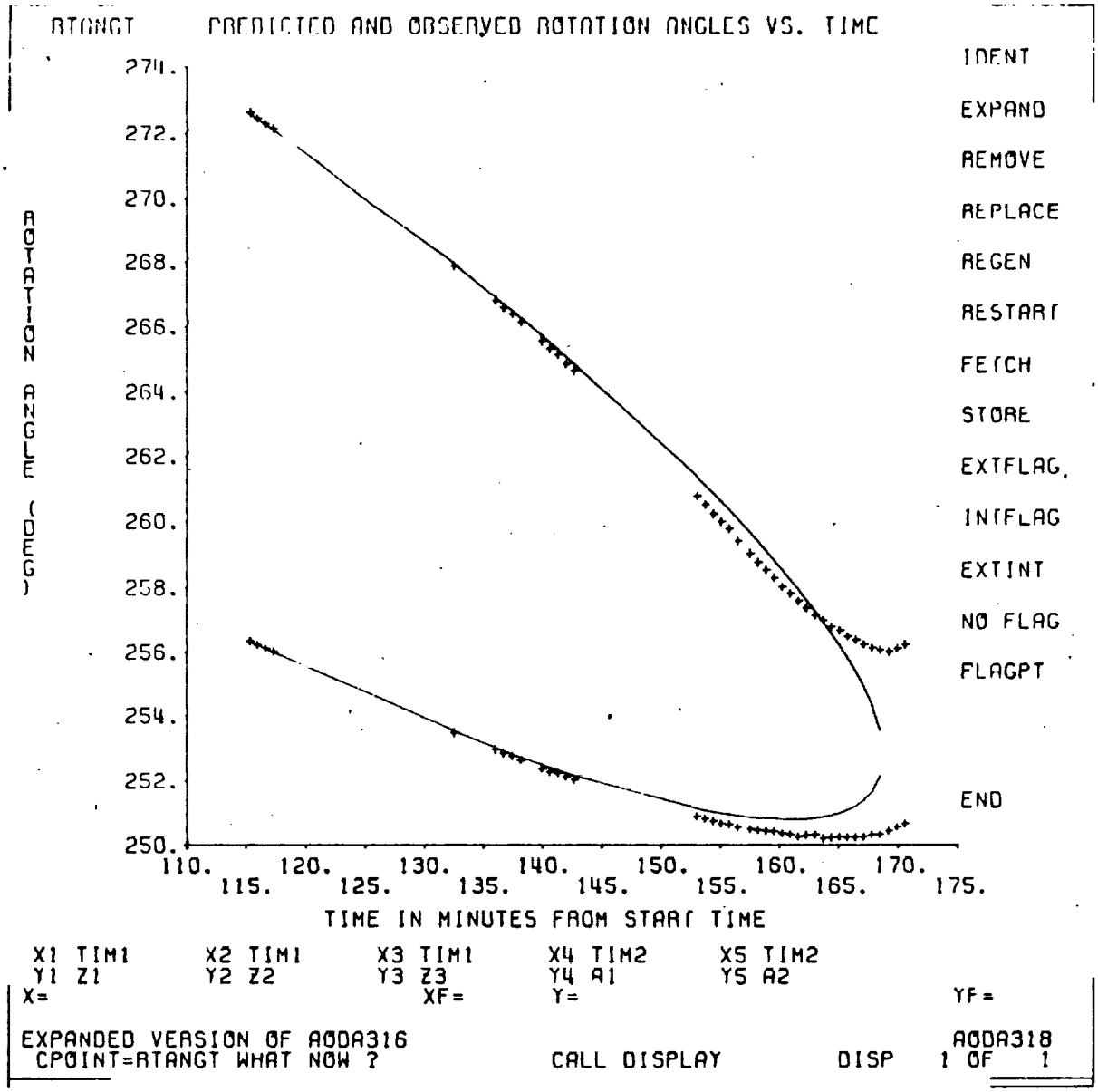

Figure 3-15. DS# SMSB60B Rotation Angle Plot for OABIAS Solution for Center of Earth Ellipse (3 of 3)

C-2

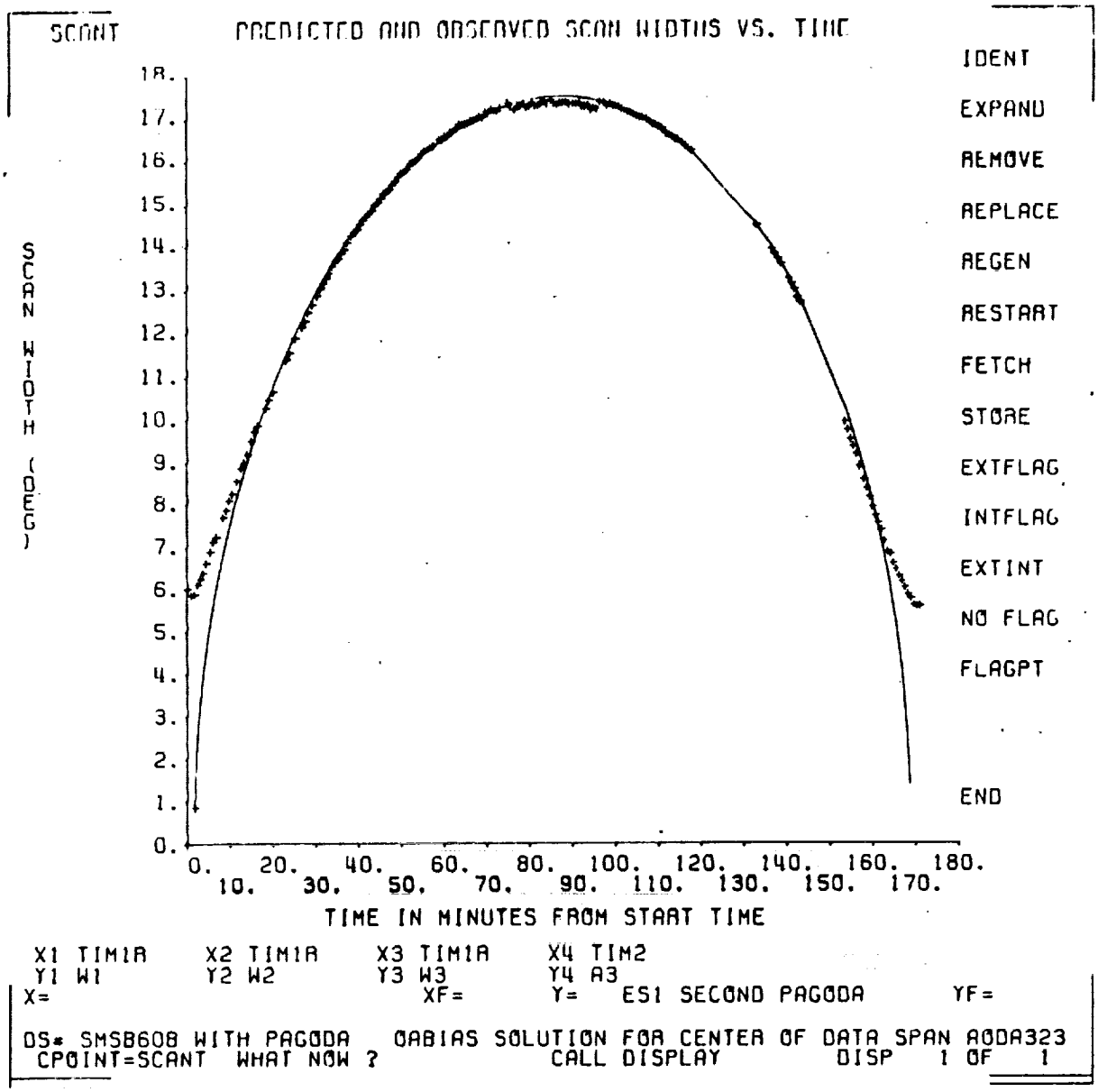
SCANT
PREDICTED AND OBSERVED SCAN WIDTHS VS. TIME
IDENT
EXPAND
REMOVE
REPLACE
REGEN
RESTART
FETCH
STORE
EXTFLAG
INTFLAG
EXTINT
NO FLAG
FLAGPT
END
SCAN WIDTH (DEG)
0. 1. 2. 3. 4. 5. 6. 7. 8. 9. 10. 11. 12. 13. 14. 15. 16. 17. 18.
0. 10. 20. 30. 40. 50. 60. 70. 80. 90. 100. 110. 120. 130. 140. 150. 160. 170. 180.
TIME IN MINUTES FROM START TIME
X1 TIM1A X2 TIM1A X3 TIM1A X4 TIM2
Y1 W1 Y2 W2 Y3 W3 Y4 A3
X= XF= Y= ES1 SECOND PAGODA YF=
DS# SMSB60B WITH PAGODA OABIAS SOLUTION FOR CENTER OF DATA SPAN A0DA323
CPOINT=SCANT WHAT NOW ? CALL DISPLAY DISP 1 OF 1

Figure 3-16. DS# SMSB60B Earth Width Plot for OABIAS Solution for Center of Earth Ellipse (1 of 3)

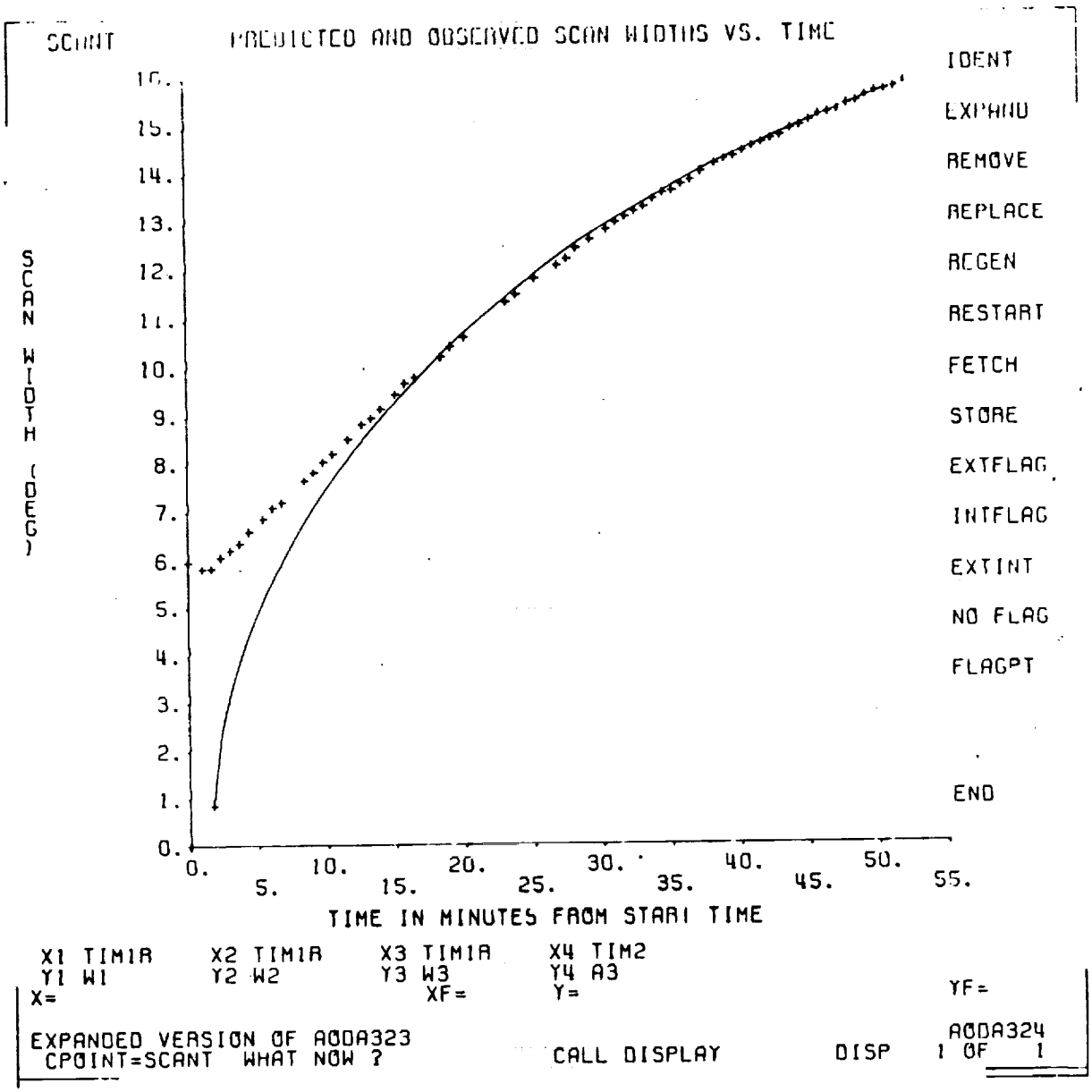

Figure 3-16. DS# SMSB60B Earth Width Plot for OABIAS Solution for Center of Earth Ellipse (2 of 3)

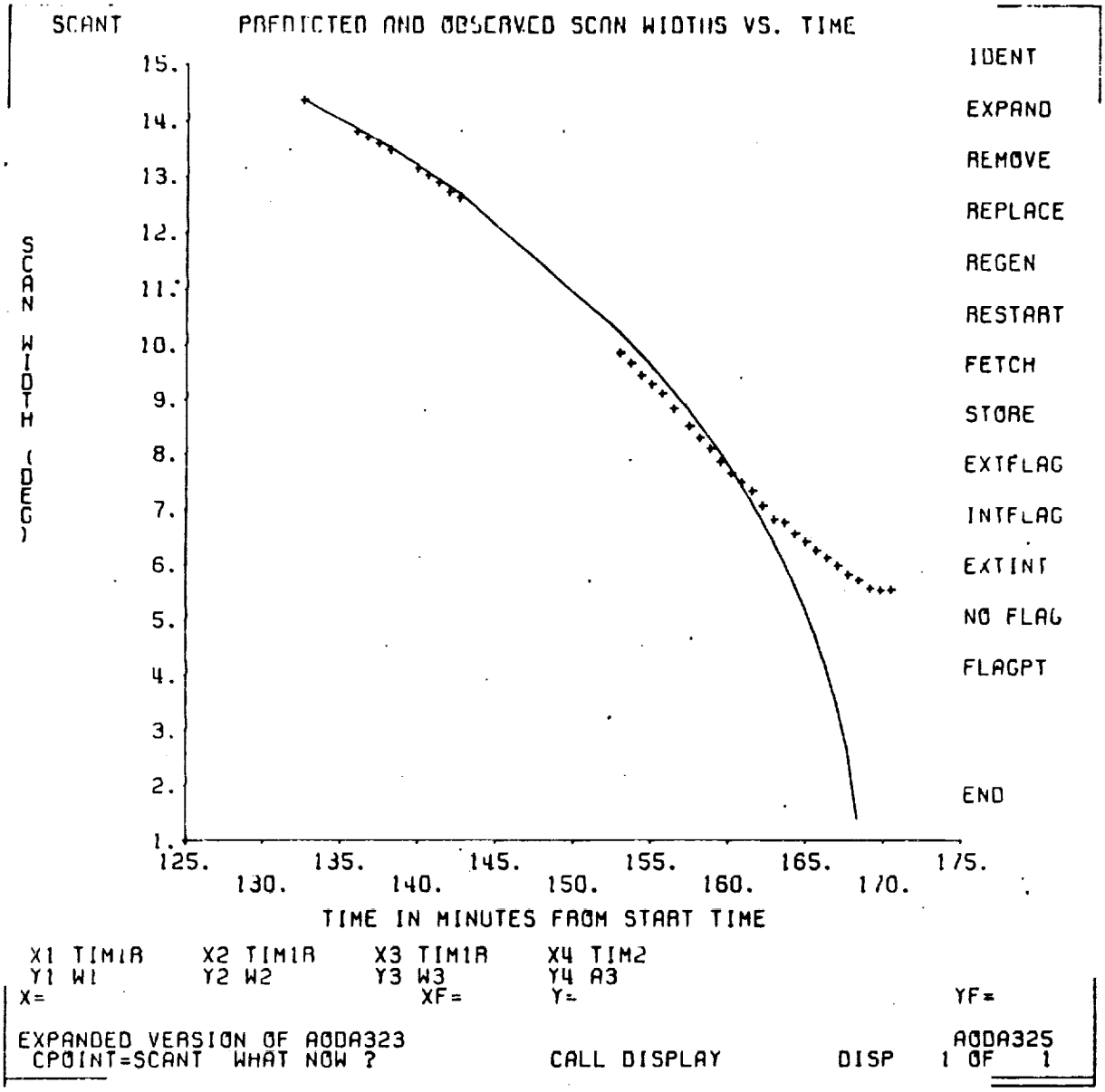

Figure 3-16. DS# SMSB60B Earth Width Plot for OABIAS Solution for Center of Earth Ellipse (3 of 3)

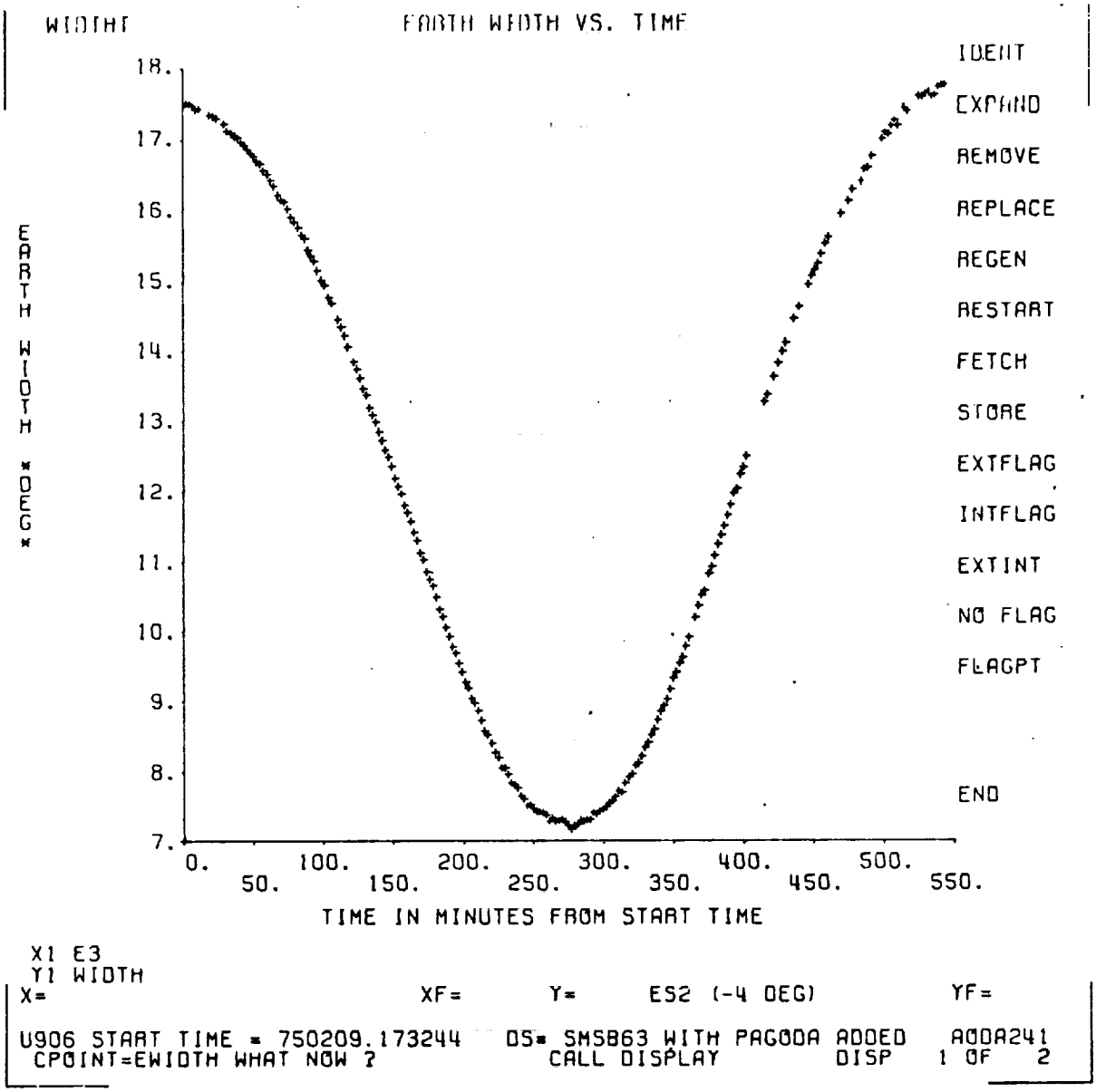

Figure 3-17. DS# SMSB63 Earth Width Data Showing Visually Undetectable Pagoda Effect at Center of Data Span

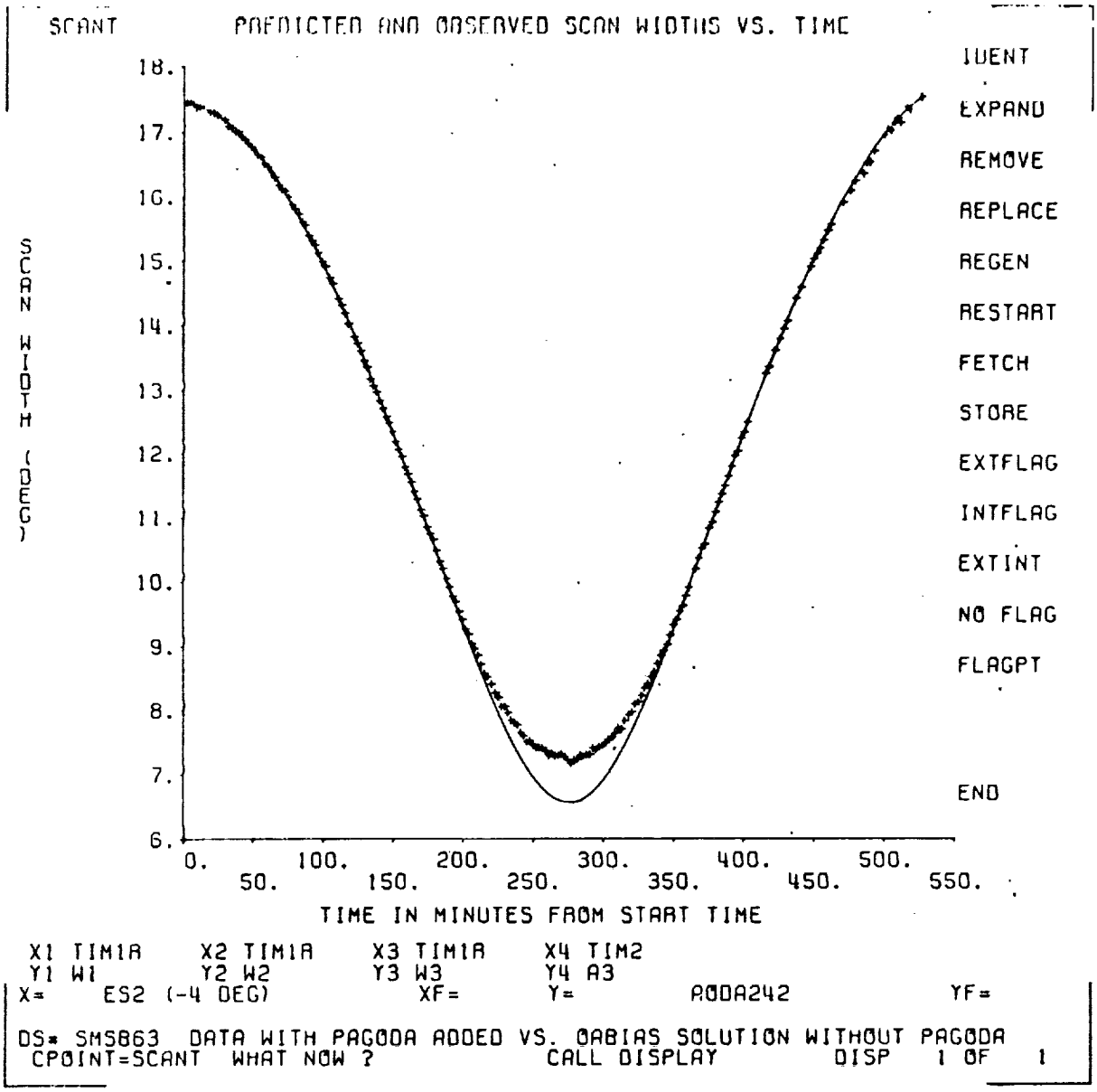

Figure 3-18. DS# SMSB63 Earth Width Plot for OABIAS Solution Omitting Data From Center of Data Span (1 of 2)

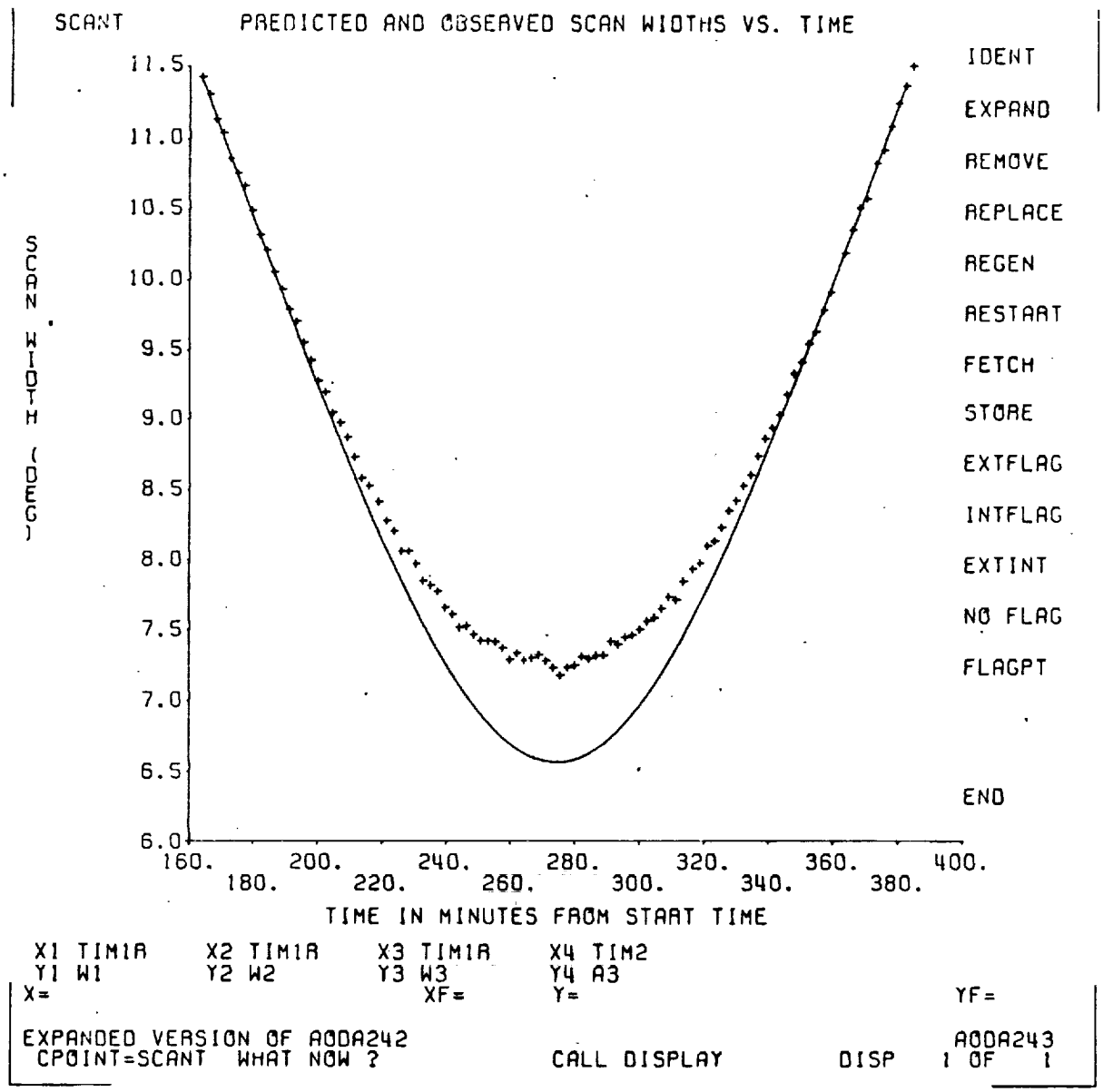

Figure 3-18. DS# SMSB63 Earth Width Plot for OABIAS Solution Omitting Data From Center of Data Span (2 of 2)

Earth width of 9.0^{o} to 9.5^{o}, in agreement with the results for Earth width data from ES1.

It is important to understand the cause of the pagoda effect in order to insure that all of the anomalistic data has indeed been removed or, if possible, to model the pagoda effect in such a way that much of the discarded data can be used in solving for attitude and bias parameters. In the case of SMS-2, the large quantity of good data was sufficient to overcome the problem of data loss due to the pagoda effect except for the relatively unimportant sensor ES5. Nonetheless, it was necessary to discard some data at Earth widths of up to 80% of the diameter of the Earth's disk. Thus, either a reduced data quality or a slightly larger pagoda effect could seriously interfere with or eliminate systematic bias determination activities on future missions if an adequate model of the pagoda effect is not available.

At present, the behavior of the pagoda effect is in good qualitative agreement with the behavior predicted by a procedure which models the response of the sensor electronics. Qualitatively, the pagoda effect agrees with the expected behavior if the sensor triggering level is lower than anticipated. A low triggering level would cause an overall advance in triggering times. At small Earth widths, the wide Earth-in pulse from the electronics would delay the Earth-out pulse, thus producing an upturn at the ends of the Earth ellipse. It is possible that the overall advance in triggering times could be responsible for the negative azimuth biases found in most of the horizon sensors (see Section 3.3). This possible qualitative explanation is intended only to suggest one possible explanation of the very strong anomaly observed in the SMS-2 data. A quantitative model clearly is needed which explains the observed behavior. Work is in progress on obtaining a quantitative model based on modeling the response of the sensor electronics.

3.4 SENSOR BIASES

This section presents the results of the bias determination activities for SMS-B. Section 3.4.1 summarizes the sensor biases. Section 3.4.2 then discusses the systematic behavior of the resulting biases. Section 3.4.3 discusses the biases for each Earth horizon sensor individually and Section 3.4.4 discusses the Sun sensor biases.

3.4.1 Summary of Sensor Biases

Eight different data sets encompassing data from the transfer orbit and three different attitudes in the drift orbit were used for bias determination on SMS-2. Three of these data sets were from the prime sensor ES1; two data sets were from ES4; and one data set was from each of the other three Earth horizon sensors.

The results of the SMS-2 bias determination work are summarized in Table 3-2. The symbols used for sensor biases are as follows: $\Delta\beta$ = Sun angle bias; $\Delta\gamma$ = sensor mounting angle bias; $\Delta\phi^{I}$ = Earth-in azimuth bias; $\Delta\phi^{O}$ = Earth-out azimuth bias; and $\Delta\rho$ = bias on the angular radius of the Earth = triggering level bias. Square brackets around a number indicate that the number was held fixed at the given value in order to solve for the remaining parameters in that data set. Braces around azimuth angle biases are used to indicate that the azimuth angle biases were constrained to have the same value. The numbers reported for sensor biases are the measured values (from OABIAS) minus the nominal pre-launch values (listed in Table 3-1). The uncertainties quoted are 95% confidence level (2σ) and incorporate both the statistical noise on the data and the systematic variation between data sets. It is important to note that the relative values of the uncertainties are more accurate than the absolute values of the uncertainties (see Section 3.5). The bottom of the table gives the weighted mean of the attitude and bias results. Parameters which had been fixed at a given value were not used in determining the mean. No mean value of the attitude in the transfer orbit is given since the

systematic shifts in the Sun angle indicate that the attitude was not constant in the transfer orbit (see Section 3.2).

Of primary interest are those biases which are not consistent with zero to within the uncertainties given. Biases are not consistent with zero if the weighted mean in Table 3-2 differs from zero by more than the uncertainty in the mean. This is equivalent to saying that the measured sensor parameter differs from its nominal value in Table 3-1 by more than the uncertainty. Counting both Earth-in and Earth-out azimuth biases as a single parameter, then there are seven sensor parameters and one measurement of the orbital in-track error which differ from their nominal value by more than the uncertainty in the data. These are:

- Sun sensor 2:

  $\Delta \beta = -0.19 \pm 0.04$ degrees

- Earth horizon sensor 1, ES1:

  $\Delta \gamma = +0.08 \pm 0.05$ degrees

  $\Delta \phi = -0.37 \pm 0.08$ degrees

- Earth horizon sensor 2, ES2:

  $\Delta \phi = -0.38 \pm 0.32$ degrees

- Earth horizon sensor 4, ES4:

  $\Delta \phi = -0.36 \pm 0.15$ degrees

- Earth horizon sensor 5, ES5:

  $\Delta \gamma = +0.27 \pm 0.07$ degrees

  $\Delta \phi = -0.24 \pm 0.17$ degrees

- Orbital in-track error for drift orbit 1:

  $\Delta t = -36 \pm 21$ seconds

The systematic behavior of this list is discussed in the next section.

FOLDOUT FRAME

Param. / DS#	Attitude (Degrees)								$\Delta\beta$	ES1			
	Transfer Orbit		Drift Orbit 1		Drift Orbit 2		Drift Orbit 3			$\Delta\gamma$	$\Delta\phi^I$	$\Delta\phi^O$	$\Delta\rho$
	R.A.	Dec.	R.A.	Dec.	R.A.	Dec.	R.A.	Dec.					
51	23.94 ±.531	-20.34 ±.472							[-.26]	.11 ±.531	-.33 ±.354	-.33 ±.354	.02 ±.177
52	24.66 ±.531	-19.45 ±.472							-.29 ±.472				
53	24.33 ±.531	-19.92 ±.649							-.23 ±.530				
55			26.35 ±.065	-19.73 ±.065					[-.185]				
59					37.97 ±.177	-63.55 ±.177			-.13 ±.088				
60					37.97 ±.136	-63.44 ±.236			-.14 ±.088	.13 ±.076	-.29 ±.195	-.49 ±.195	-.04 ±.077
63							35.22 ±.307	-76.57 ±.443	-.25 ±.141				
64							35.18 ±.224	-76.76 ±.106	-.22 ±.071	.05 ±.059	-.33 ±.089	-.41 ±.089	.02 ±.030
Weighted Mean			26.35	-19.73	37.97	-63.51	35.15	-76.74	-.185	.080	-.32	-.42	.01
Unc. of the Mean			±.065	±.065	±.108	±.142	±.181	±.103	±.044	±.046	±.079	±.079	±.028

2.

FOLDOUT FRAME

Table 3-2. SMS-2 Bias Determination Summary

Sensor Biases																Orbital In-Track Error, (sec.)	
ES2				ES3				ES4				ES5				Drift Orbit 1	Drift Orbit 2
$\Delta\gamma$	$\Delta\phi^I$	$\Delta\phi^O$	$\Delta\rho$	$\Delta\gamma$	$\Delta\phi^I$	$\Delta\phi^O$	$\Delta\rho$	$\Delta\gamma$	$\Delta\phi^I$	$\Delta\phi^O$	$\Delta\rho$	$\Delta\gamma$	$\Delta\phi^I$	$\Delta\phi^O$	$\Delta\rho$		
								.04 ±.484	-.20 ±.330	-.20 ±.330	-.06 ±.177						
				.30 ±.65	.23 ±.41	.23 ±.41	.01 ±.24										
												.27 ±.065	-.15 ±.171	-.32 ±.171	-.01 ±.065	-36 ±21	
								-.01 ±.130	-.40 ±.165	-.40 ±.165	.03 ±.089						-16 ±21
.38 .566	-.38 ±.319	-.38 ±.319	.06 ±.236														
.38	-.38	-.38	.06	.30	.23	.23	.01	.020	-.360	-.360	.012	.27	-.15	-.32	-.01	-36	-16
.566	±.319	±.319	±.236	±.65	±.41	±.41	±.24	±.128	±.148	±.148	±.080	±.065	±.171	±.171	±.065	±21	±21

3.4.2 Systematic Behavior of Results

Examination of the bias list in the previous section shows that the major non-zero biases are azimuth biases and that they have remarkably similar values. The only azimuth bias not in the above list is that on ES3, which has a value of +0.23 ± 0.41 degrees. This measurement on ES3 comes entirely from transfer orbit data, as is reflected in the high uncertainty in the measurement.

The coincidence in measured azimuth bias angles suggests that the observed azimuth bias as on the different Earth horizon sensors result from the same cause. Two possible causes which would affect all of the horizon sensors are an azimuthal misalignment of Sun sensor 2 (the azimuth reference used for bias determination on all five horizon sensors) and an advance in the triggering time of the sensor electronics. The later possibility has been previously discussed as a possible explanation for the large pagoda effect, (see Section 3.3) and is currently being investigated in more detail. If a common azimuth bias is due to a misalignment of the Sun sensor used as a reference, then this misalignment is common to both Sun sensors. Figure 3-19 shows the Earth-in rotation angles during a Sun sensor switch experiment. Sun sensor 2 is on from 0 to 13 minutes and from 47 minutes to the end. Sun sensor 1 is on in the intervening interval. Note that there is no noticeable jump in azimuth angles. The dashed line on the plot shows the shift necessary to account for an azimuth difference between the two sensors of 0.35 degrees. Of course, a correct explanation of the azimuth biases observed on SMS-2 may contain both a component common to all of the sensors and some azimuth bias for each sensor individually.

If it is assumed that the azimuth biases are all produced by some common cause, then the azimuth bias measurements for each of the different sensors are independent measurements of the common azimuth bias. Thus, these measurements could be combined in the usual way to give a measured value of the "common azimuth bias". Combining the measurements for the five sensors

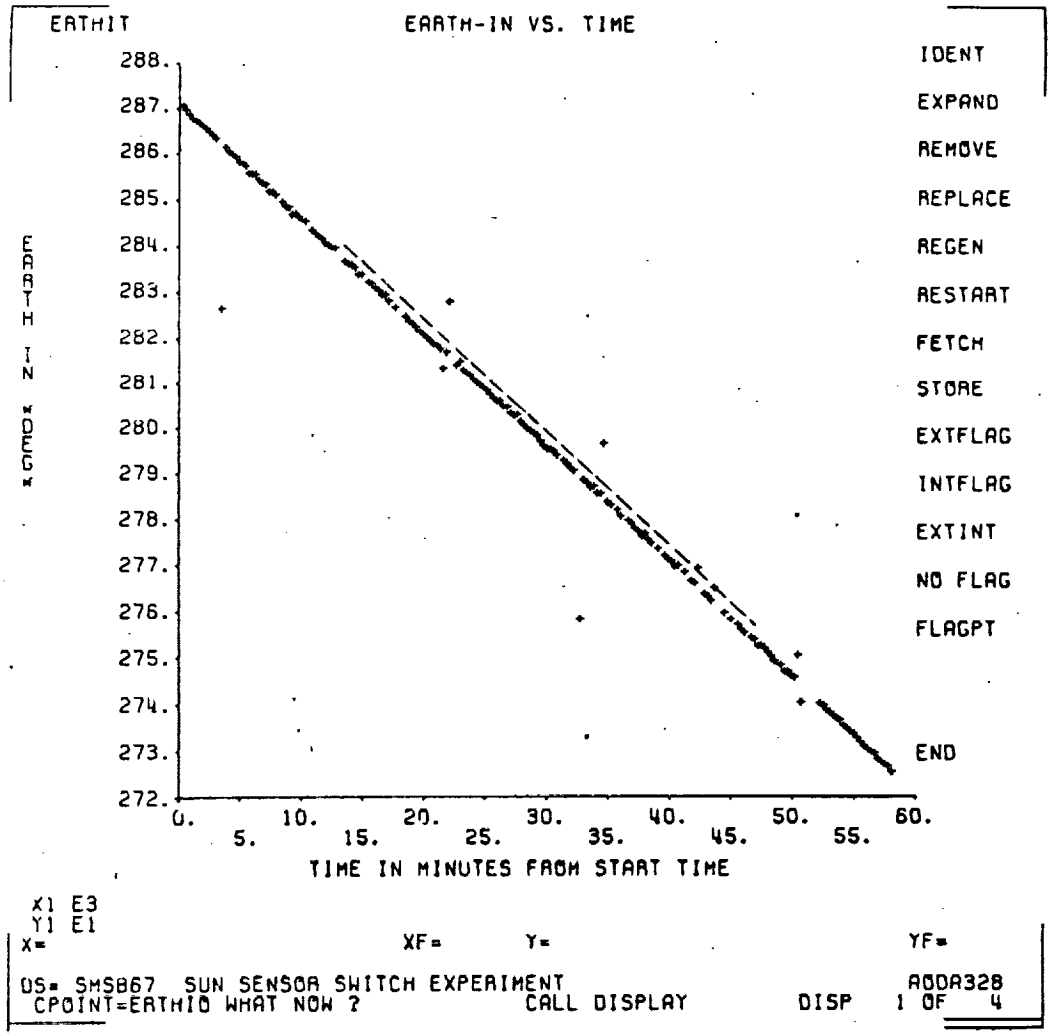

Figure 3-19. DS# SMSB67 Sun Sensor Switch Experiment

gives a weighted mean and uncertainty of -0.35 ± 0.06 degrees. (If the ES3 measurement is omitted, the result is -0.36 ± 0.06 degrees.) This value is well within the uncertainties of all of the measurements except that for ES3. Clearly, this value for a "common azimuth bias" only has meaning to the extent that there is a real azimuth bias component common to all of the SMS-2 horizon sensors.

An additional small systematic variation in the results can be identified by comparing the results obtained during drift orbit 2 with the results obtained during drift orbit 3. This entails a comparison of the results from the four data sets DS#59, 60, 63, and 64. For convenience, the relevant information has been collected into Table 3-3. It is important to note that the uncertainties given in Table 3-3 are the statistical uncertainties due to the noise on the data and not the overall uncertainties as given in Table 3-2. In comparing DS#59 and DS#60 it can be seen that the attitude and Sun angle bias from ES4 and ES1 for drift orbit 2 agree to within the uncertainty due to the noise. Similarly, DS#63 and DS#64 show good agreement between ES2 and ES1 data for drift orbit 3.. However, in comparing the results for drift orbit 2 with the results for drift orbit 3, the value of the Sun angle bias and the sensor mounting angle bias for ES1 disagree by several times the statistical uncertainty. It is possible that the Sun angle bias is a function of Sun angle and, therefore, has truly different values for the two different attitudes. This is unlikely to be the cause since the Sun angle has changed by only 1.5 degrees and since the sensor mounting angle bias for ES1 shows a shift of the same magnitude. The remaining conclusion is that the small difference between the two orbits is due to residual errors in the orbit parameters. Thus, from the comparison of these four data sets, it appears likely that under some conditions, the spacecraft attitude sensor data is providing sufficiently accurate information that the attitude and bias uncertainties are due primarily to the systematic residual errors in the orbit parameters. This implies that information that could be used for further

Table 3-3. Comparison of Drift Orbit 2 and Drift Orbit 3

DS#	Sensor	Attitude				$\Delta\beta$	Δ (ES1 only)
		Drift 2		Drift 3			
		R.A.	Dec.	R.A.	Dec.		
59	ES4	37.97 ±.10	63.55 ±.04			-.13 +.04	
60	ES1	37.97 ±.02	-63.44 ±.11			-.14 ±.02	.13 ±.02
63	ES2			35.22 ±.04	-76.57 ±.07	-.25 ±.02	
64	ES1			35.18 ±.04	-76.76 ±.02	-.22 ±.01	.05 ±.01

NOTE: Uncertainties given are statistical uncertainties due to the noise on the data and not overall uncertainties.

refinement of the orbit parameters is available in the attitude sensor data, at least when both orbit and attitude estimates are based on approximately one orbit of data.

3.4.3 Earth Horizon Sensor Biases

The biases determined for each of the five Earth horizon sensors are presented and discussed individually in the following subsections. In each subsection, a table is given to summarize the bias determination results of that particular Earth sensor (see, for instance, Table 3-4 in Section 3.4.3.1 for Earth sensor 1).

The upper part of the table gives the orbit, the biases, and their uncertainties for each data set, and then lists the weighted mean and the uncertainty of the mean for each of the biases. The four biases are: $\Delta\gamma$ = sensor mounting angle bias; $\Delta\phi^I$ = Earth-in azimuth bias; $\Delta\phi^0$ = Earth-out azimuth bias; and $\Delta\rho$ = bias on angular radius of the Earth. Note that $\Delta\phi$ will be used for $\Delta\phi^I$ and $\Delta\phi^0$ if they share the same value. For each bias determination result, two different uncertainties are quoted in the table. One is the statistical uncertainty obtained directly from the OABIAS processing results which gives the uncertainty of the parameter due to the statistical noise on the data and the quality of the fit to the data. This is a minimum uncertainty for the set of parameters solved for. Any unknown correlated systematic variation will increase the true uncertainty. The second uncertainty quoted on the table is the estimated total uncertainty which includes both the statistical uncertainty and the systematic uncertainties from orbit to orbit. The weighted mean and the uncertainty of the mean are based on the total uncertainties. A discussion of the methods used in obtaining the total uncertainties, the weighted mean and the uncertainty of the mean is given in Section 3.5.

The lower part of the table for each sensor gives a comparison of OABIAS and nominal parameters. For each data set, the OASYS deterministic results and the goodness of the fit to the data are compared by using nominal parameters and OABIAS parameters. In the "Fit to Data" for rotation angle and central body width, the "percent of good fit" and the "maximum deviation" are the operators estimates on the percentage of predicted data within observed noise and the maximum deviation of

predicted value from mean observed value. These estimates are used to indicate the presence of systematic errors such as residual orbit errors or unmodeled parameters.

In addition to the table of results, three figures (each includes a set of plots) are included for each data set to show the data and the quality of the solution (refer to Figures 3-23 to 3-25 in Section 3.4.3.1 where a complete set of plots is given for DS#60). The first figure shows the data on Sun angle, spin rate, Earth-in and Earth-out dihedral angles, and Earth width. Note that the data plotted in this section is the data actually used in OABIAS processing. Therefore the pagoda effect has already been removed from all the data sets (except Figure 3-20 in Section 3.4.3.1 where the data plots were generated before removing the pagoda effect). The second figure shows the OASYS deterministic results for right ascension and declination with nominal parameters and OABIAS parameters respectively. The four curves on each plot represent the attitude solutions obtained through four different models. In principle, for a good attitude and bias solution, the four curves should all give horizontal lines and coincide to within the noise of the data. Thus, an examination of the behavior of these curves usually can give a good estimate of the quality of the solution obtained. The last figure attached to each data set is a set of PLOTOC plots showing the comparison of the data with the predicted values obtained with nominal parameters (OASYS solution) and OABIAS parameters. From the goodness of the fit, one can judge the overall reliability of the attitude and bias results.

In order to limit the size of the present report, a complete set of plots as described above is given only for DS#60 as an example. For the rest of the data sets, selected plots will be presented. The plots omitted generally give less relevant information, such as the spin rate plot in the data plots, the right ascension plots in the OASYS deterministic plots, and the Earth-in and Earth-out (rotation angle) plots in the PLOTOC plots. For those interested in the omitted plots, a complete set of plots for all the SMS-2 data sets is given in Reference 11.

3.4.3.1 Earth Sensor 1 Biases

The Earth sensor 1 (ES1) biases were obtained from three data sets, DS#51, 60, and 64. Note that DS#64 is equivalent to DS#62 except for different preaveraging values. Here the DS#64 results are used because of slightly better convergence characteristics than DS#62.

The ES1 bias determination results are summarized in Table 3-4. In obtaining the biases from DS#51, the Sun angle bias was fixed at $-.26^{\circ}$ as previously determined from DS#52 and 53. In addition, $\Delta\phi^{I}$ was fixed at the same value as $\Delta\phi^{0}$ in order to get convergence. $\Delta\phi^{I}$, $\Delta\phi^{0}$, and $\Delta\beta$ were allowed to vary independently in DS#60 and 64. Note that due to the poor data quality, smaller geometrical variation, and attitude drift in the transfer orbit data as discussed in Section 3.2, the bias results obtained from DS#51 have considerably higher uncertainties that the drift orbit results and thus are weighted lightly in obtaining the mean.

As can be seen from the comparison results for the three data sets shown in the lower part of the table, the OABIAS results obtained from DS#51 did not significantly improve the quality of the fit. Although the mean residual and the standard deviation of the rotation angle, and the standard deviation of the Earth width are slightly reduced, the standard deviation of the arc length and the attitude, and the mean residual of the Earth width are even slightly higher. This indicates a low reliability for the OABIAS results obtained in DS#51, which is consistent with the high uncertainties and low weight for this data set. On the other hand, it is obvious from the table that the OABIAS results obtained from the two data sets in drift orbits substantially improved the attitude solutions and the fit to the data. This is also apparent from the solution plots shown below.

Figures 3-20 to 3-22 are the three sets of plots for DS#51 as previously described before. Figure 3-20 shows the data in this data set. Note that there are strong systematic variations in the Sun angle data which implies a changing spin axis attitude in the transfer orbit. Due to the pagoda effect, data with Earth-width

FOLDOUT FRAME /

OABIAS Bias Result

DS#	51		
Orbit	Transfer		
Biases	Val.	Statistical Unc.	Total Unc.
$\Delta\gamma$	.11	.090	.531
$\Delta\phi^I$	-.33	.060	.354
$\Delta\phi^\circ$	-.33	.060	.354
$\Delta\rho$	.02	.030	.177

Comparison of OABIAS and Nominal Parameters

				Using Nominal Parameters	Using OABIAS Results
OASYS Deterministic Results	Right Ascension, α (Deg)			24.30	23.95
	Declination, δ (Deg)			-20.86	-20.34
	Standard Deviation		Arc Length	.21	.30
			α	.13	.13
			δ	.17	.28
Fit to Data	Rot. Angle		Mean Residual	-.007	-.006
			STDV	.145	.134
			% of Good Fit	50%	40%
			Maximum Deviation	.4°	.2°
	Central Body Width		Mean Residual	.016	.019
			STDV	.222	.121
			% of Good Fit	0%	40%
			Maximum Deviation	.2°	.1°

FOLDOUT FRAME 2

Table 3-4. Earth Sensor-1 Bias Determination Results

60			64			Weighted Mean	Unc. of the Mean
Drift 2			Drift 3				
Val.	Statistical Unc.	Total Unc.	Val.	Statistical Unc.	Total Unc.		
.13	.013	.076	.05	.010	.059	.080	.046
-.29	.033	.195	-.33	.015	.089	-0.32	.079
-.49	.033	.195	-.41	.015	.089	-0.42	.079
-.04	.013	.077	.02	.005	.030	.01	.028

ing Nominal arameters	Using OABIAS Results	Using Nominal Parameters	Using OABIAS Results
38.03	37.96	35.24	35.04
-64.42	-63.45	-77.54	-76.84
.41	.19	.72	.12
.15	.12	.82	.17
.41	.19	.70	.11
-.047	-.021	.082	-.007
.179	.092	.189	.087
70%	100%	70%	100%
.5°	-	.5°	-
-.048	.029	.022	.007
.280	.071	.313	.047
20%	100%	20%	90%
5°	-	.7°	.05°

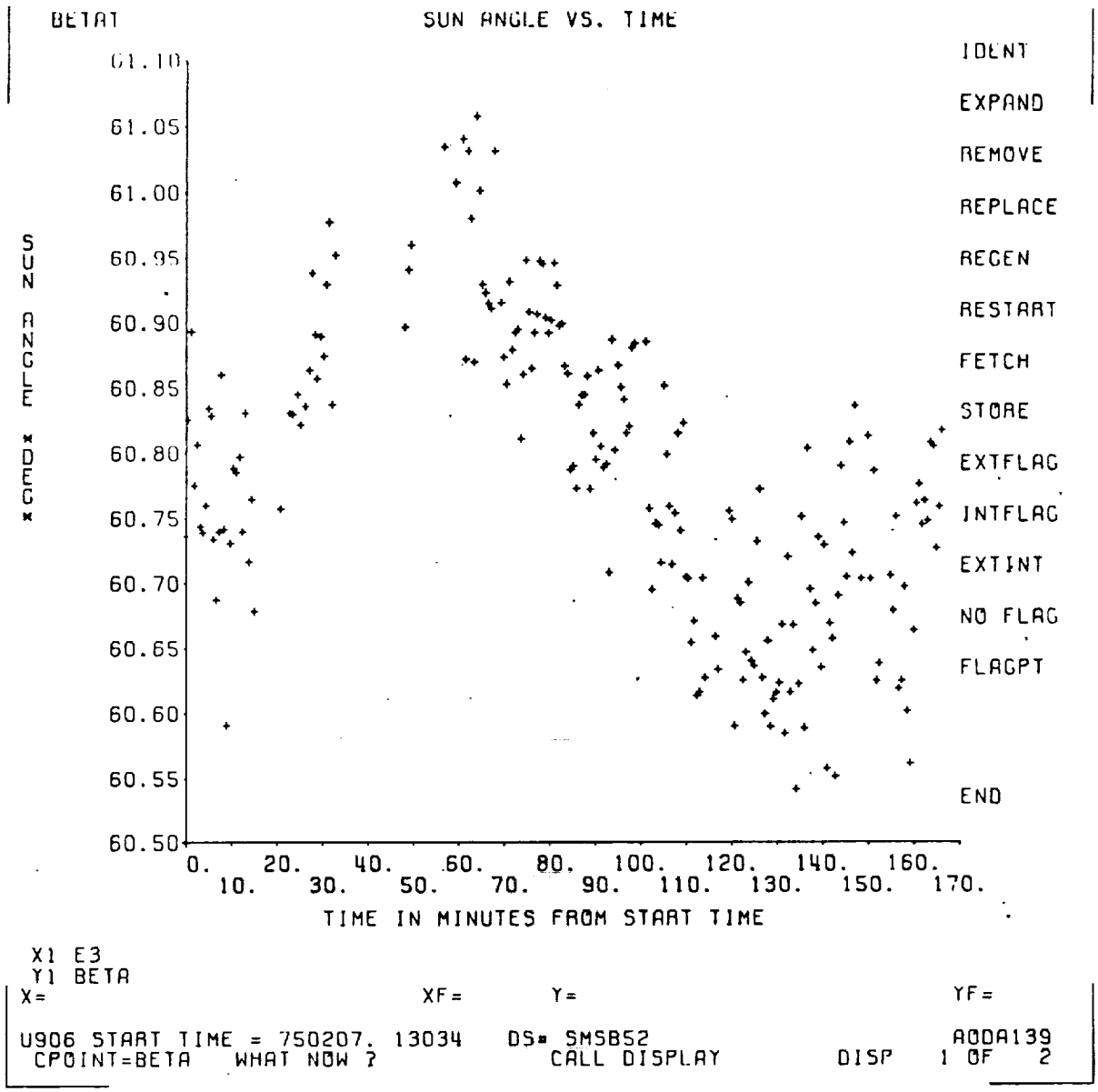

Figure 3-20. DS# SMSB52 Data Plots (1 of 3)

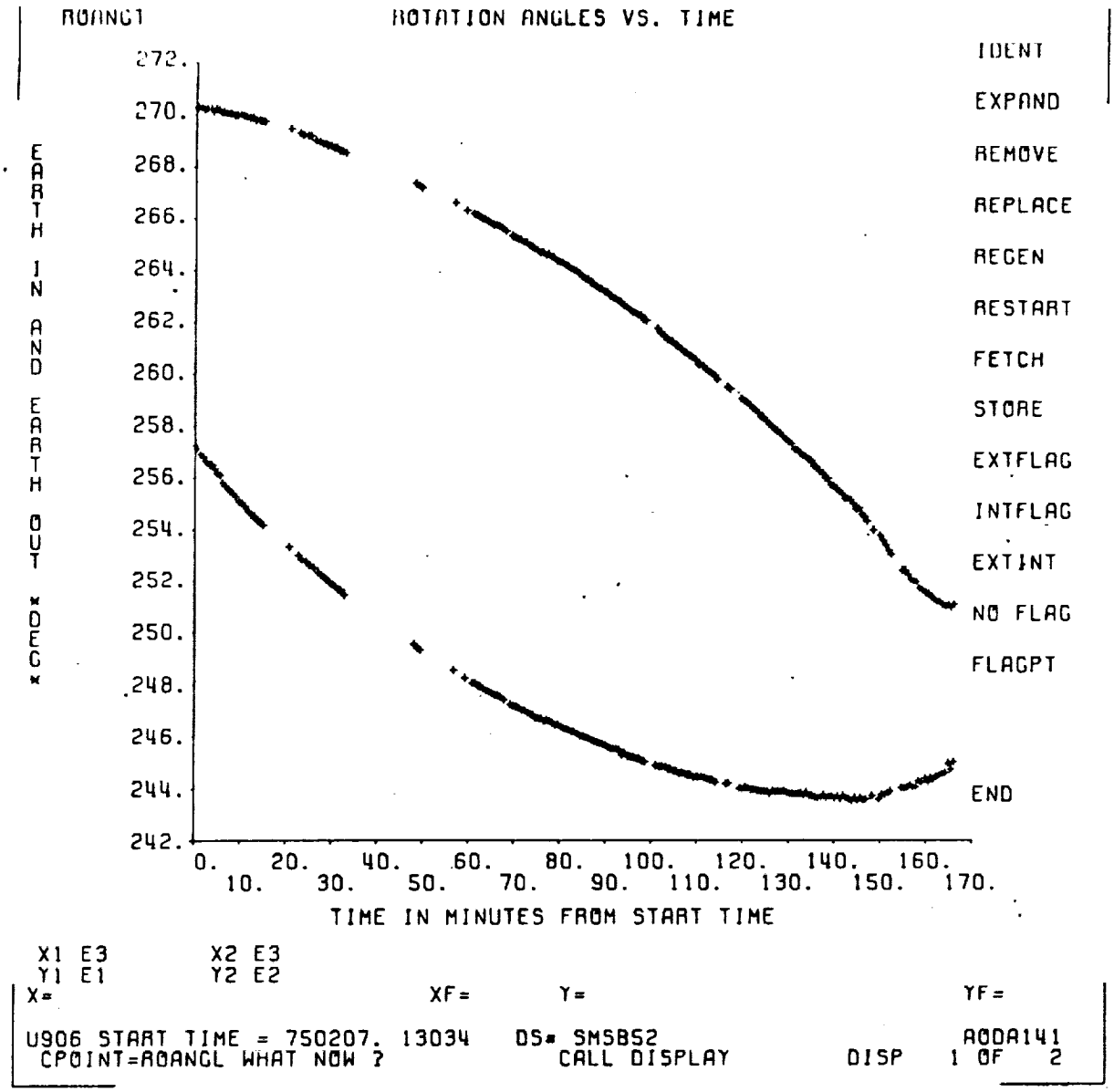

Figure 3-20. DS# SMSB52 Data Plots (2 of 3)

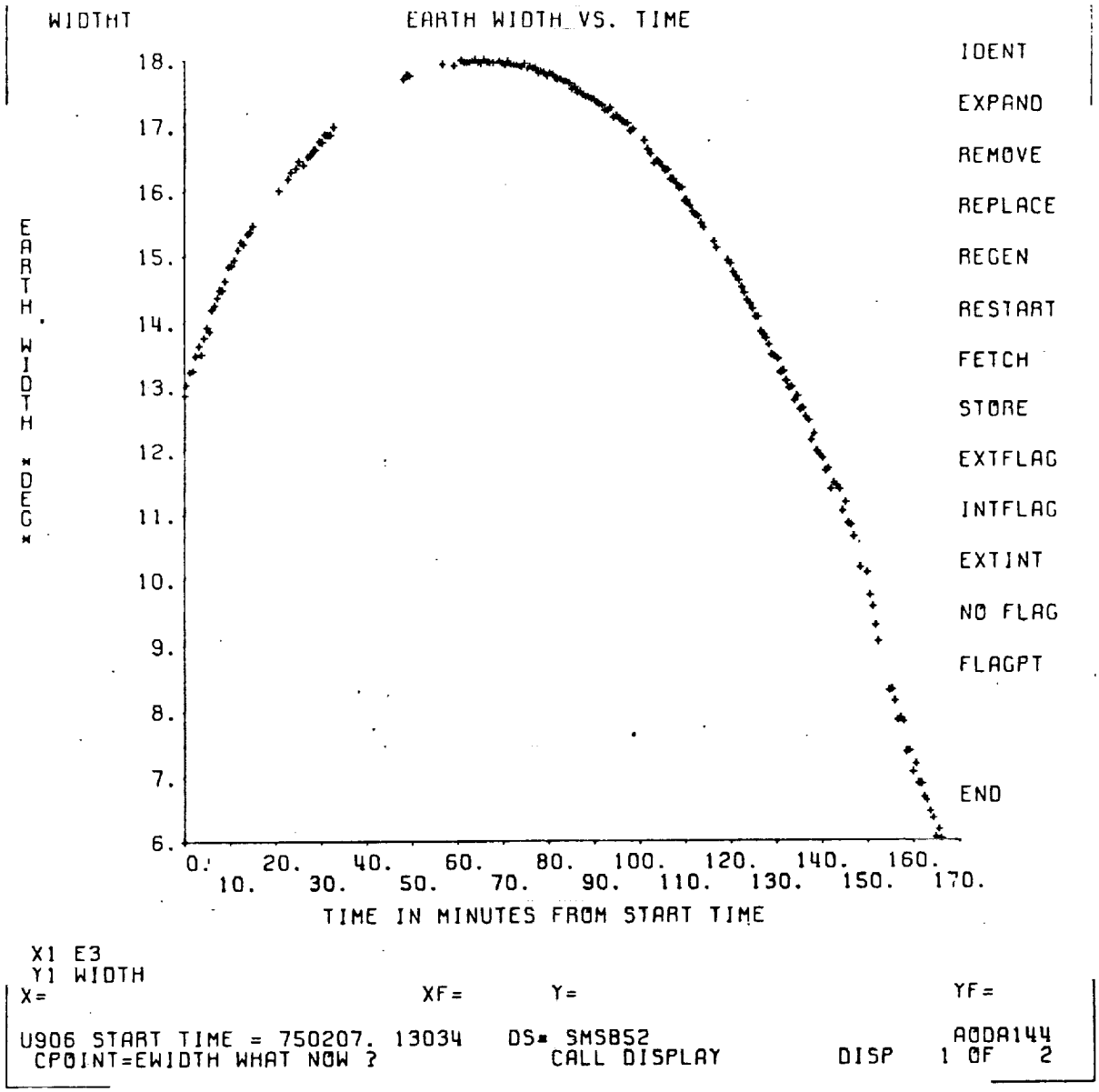

Figure 3-20. DS# SMSB52 Data Plots (3 of 3)

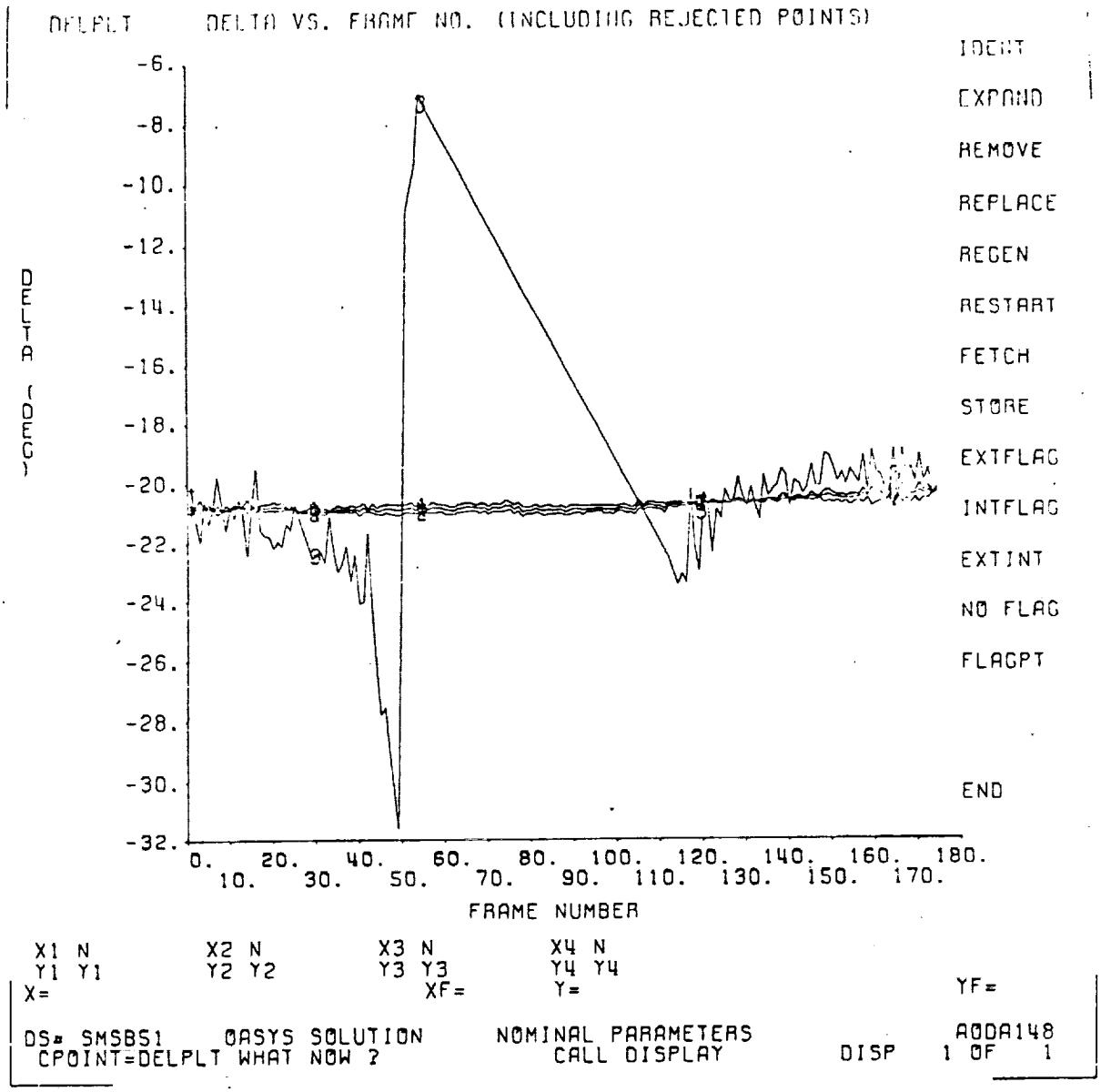

Figure 3-21. DS# SMSB51 Comparison of OASYS Solutions With Nominal and OABIAS Parameters (1 of 2)

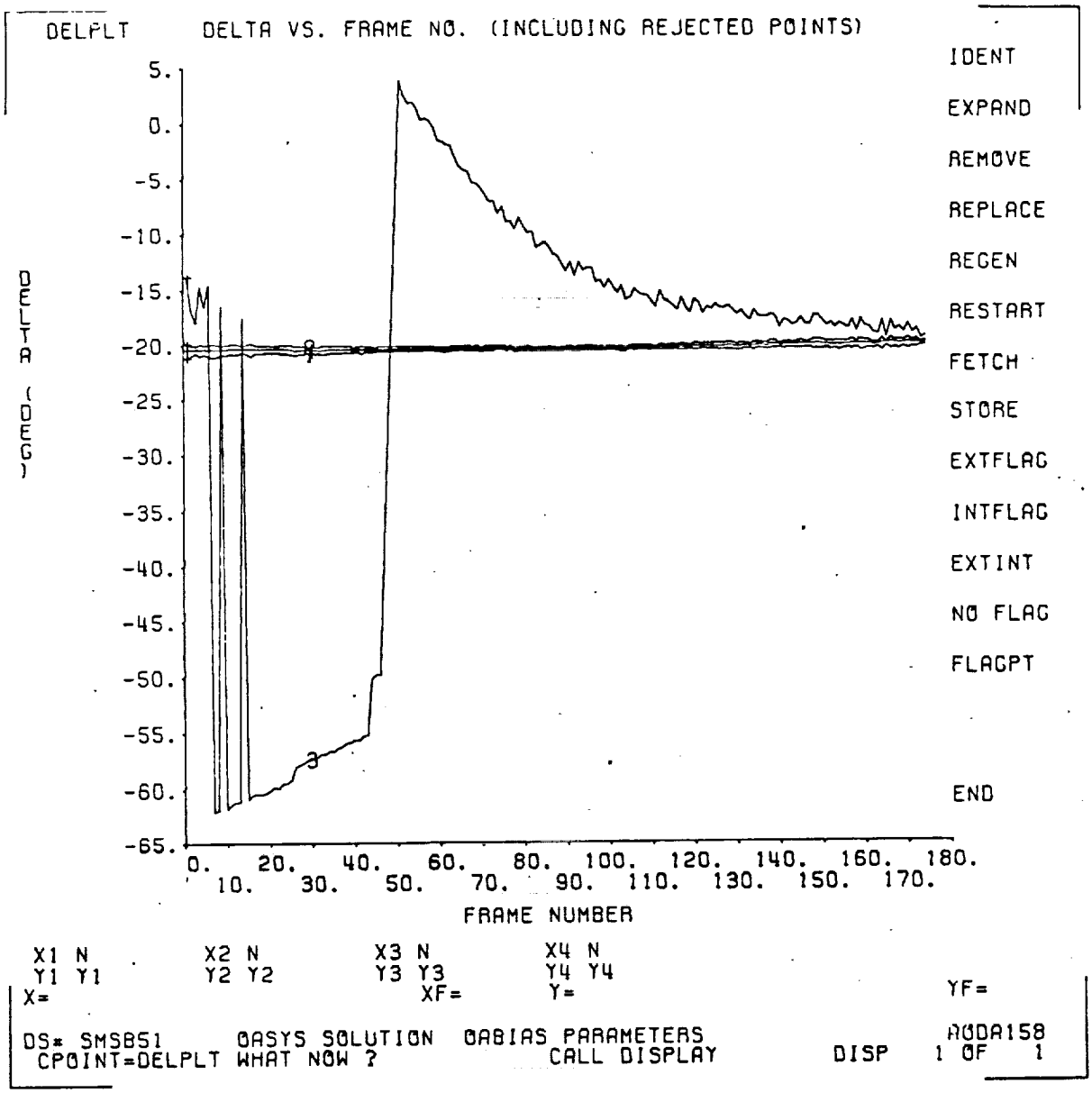

Figure 3-21. DS# SMSB51 Comparison of OASYS Solutions With Nominal and OABIAS Parameters (2 of 2)

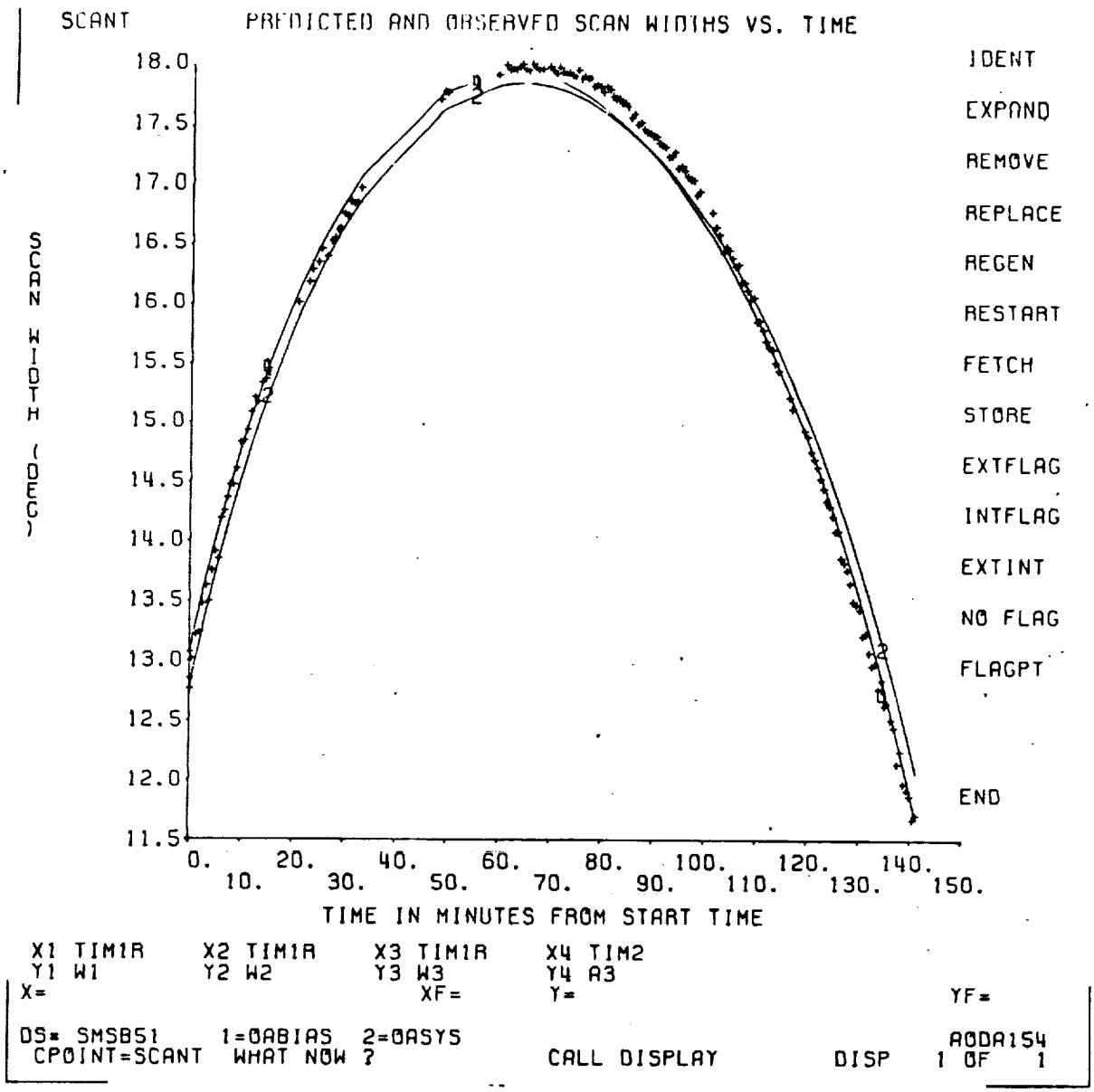

Figure 3-22. DS# SMSB51 Earth Width Plots for Nominal and OABIAS Solutions

below 11.5^{o} was cut off before the processing. This makes the already short data pass even shorter. Figure 3-21 shows the OASYS deterministic results on the declination with nominal and OABIAS determined parameters. The difference between these two parameter sets is small in these plots. Figure 3-22 shows the PLOTOC prediction plot for Earth-width. It is clear from this figure that the OABIAS results indeed give a better fit to the data than the nominal solutions. Nonetheless the fit is not nearly as good as one would expect from a good set of data.

The corresponding plots for DS#60 and 64 are shown in Figure 3-23 to 3-25 and 3-26 to 3-28, respectively. Again, the data points with Earth-width below 11^{o} have been removed due to the pagoda effect. Notice that both of these data sets have two entire Earth ellipses which gives a range of geometrical conditions for bias and attitude determination. No strong systematic variations are observed in these two data sets except the small glitch in the Earth-width data as shown in Figure 3-23 (8). For these two data sets, the superiority of the OABIAS solution over the OASYS solution with nominal parameters is clear from the OASYS deterministic plots (Figures 3-24 and 3-27) and the PLOTOC data prediction plots (Figures 3-25 and 3-28). In Figures 3-23 and 3-26, the attitude solutions determined from the four different models vary over a wide range with nominal parameters but show strong consistency with OABIAS determined parameters (notice the very different vertical scales used in these plots). In Figures 3-25 and 3-28, the Earth widths predicted with OABIAS solutions apparently give much better fits to the data than with nominal parameters. The OABIAS solutions from these two data sets give nearly 100 percent fit to the data within the noise levels. The glitch in the Earth-width data of DS#60 did not affect the OABIAS solution as can be seen from Figure 3-25 (6).

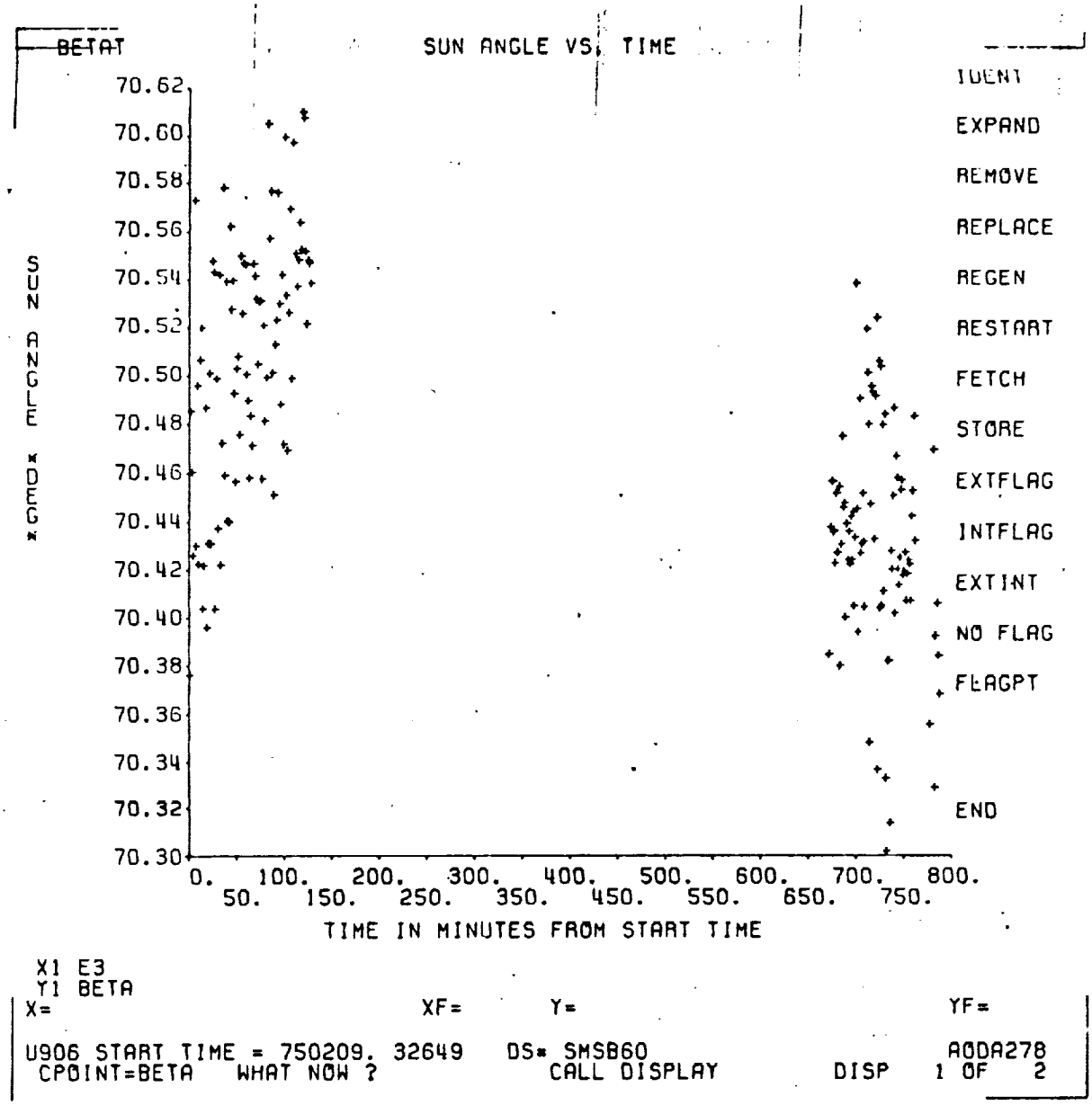

Figure 3-23. DS# SMSB60 Data Plots (1 of 8)

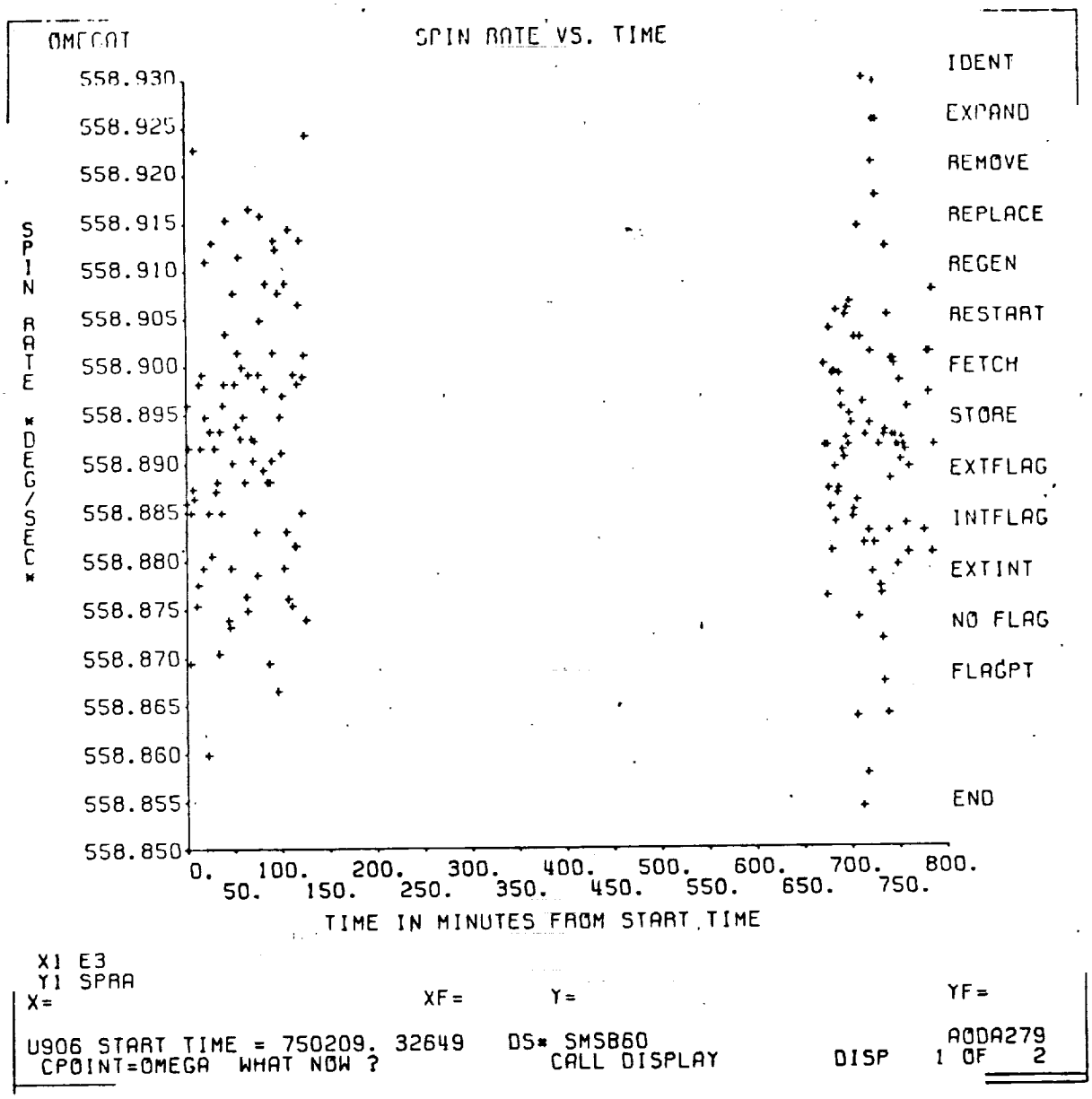

Figure 3-23. DS# SMSB60 Data Plots (2 of 8)

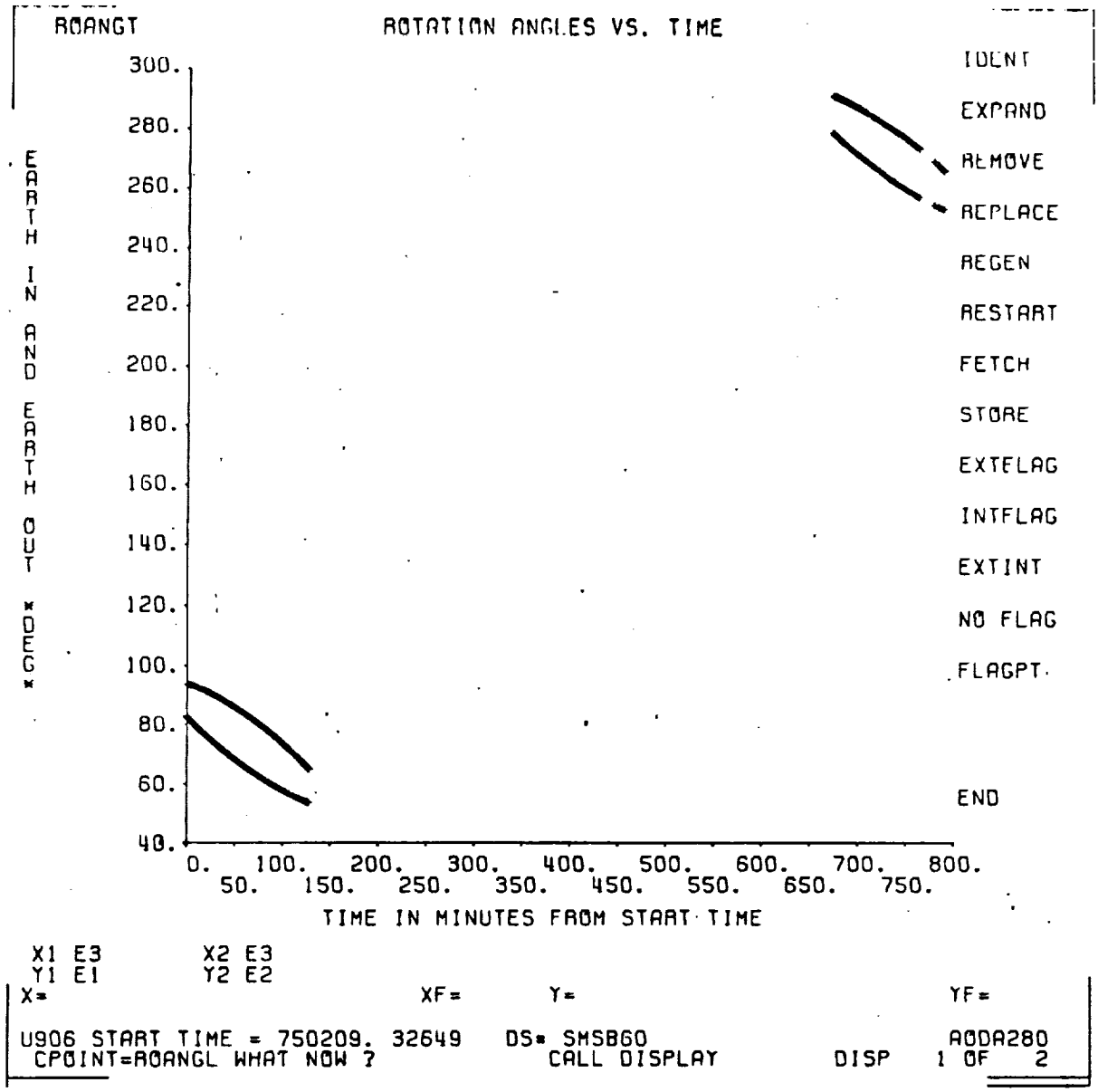

Figure 3-23. DS# SMSB60 Data Plots (3 of 8)

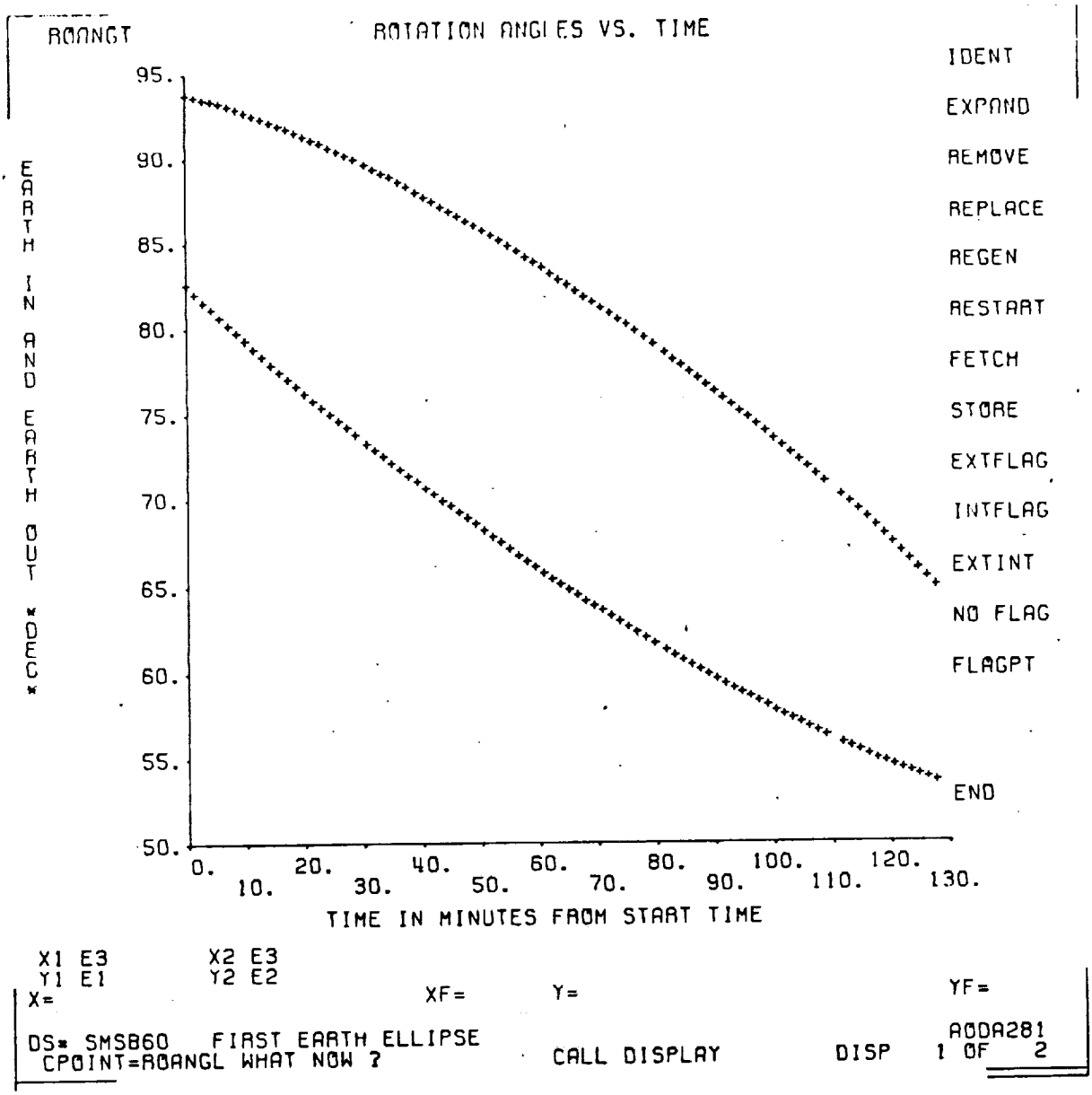

Figure 3-23. DS# SMSB60 Data Plots (4 of 8)

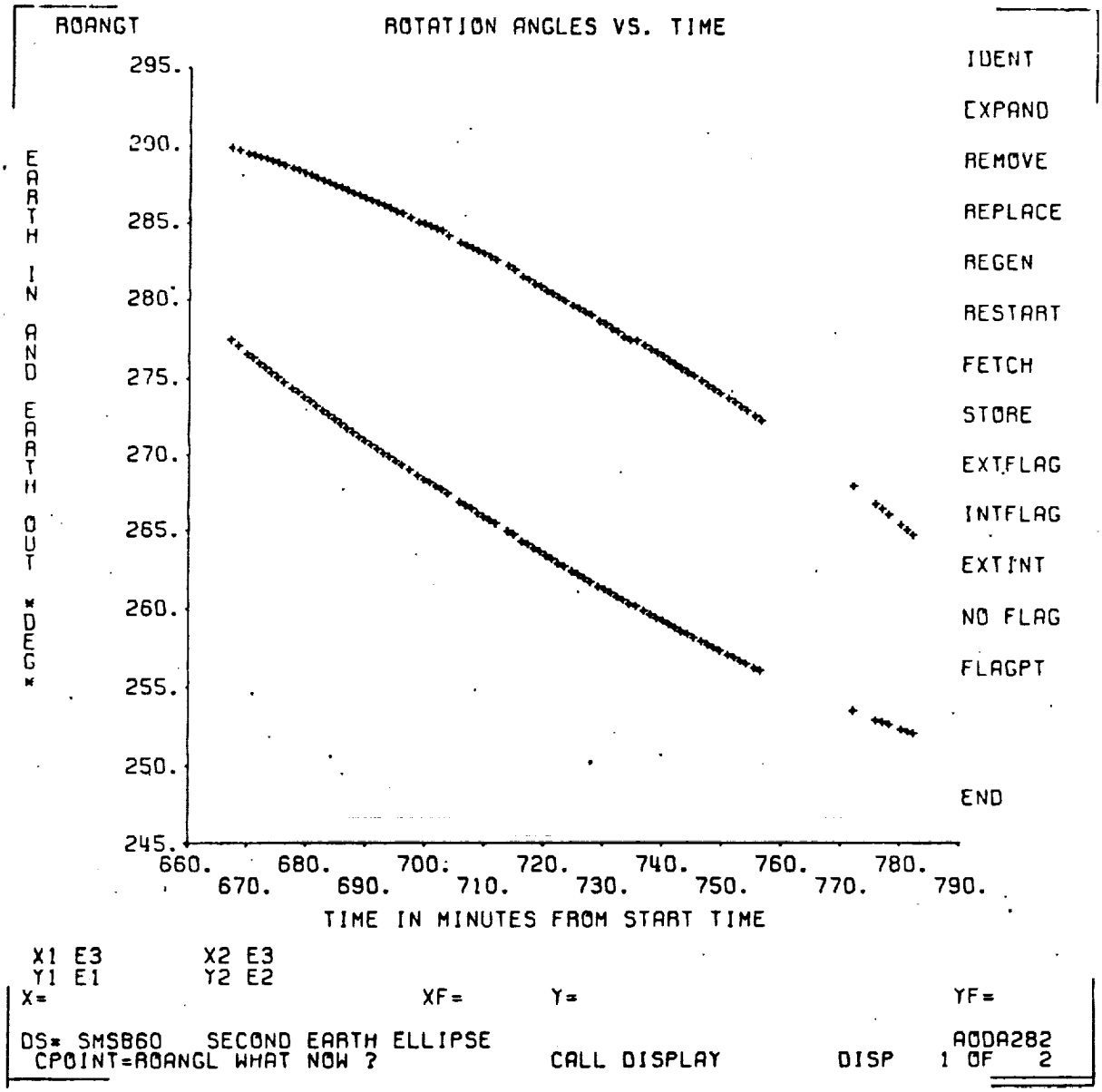

Figure 3-23. DS# SMSB60 Data Plots (5 of 8)

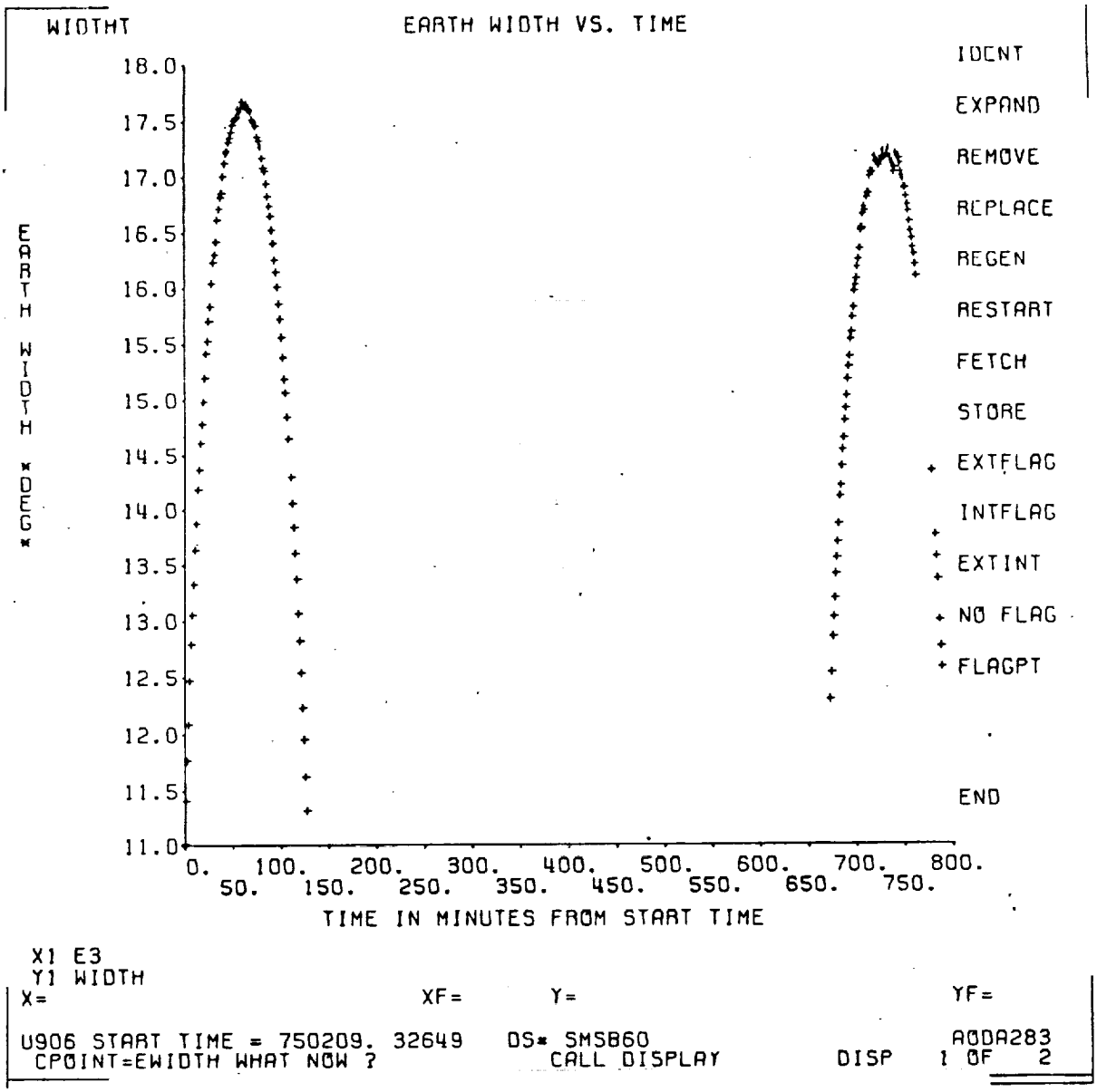

Figure 3-23. DS# SMSB60 Data Plots (6 of 8)

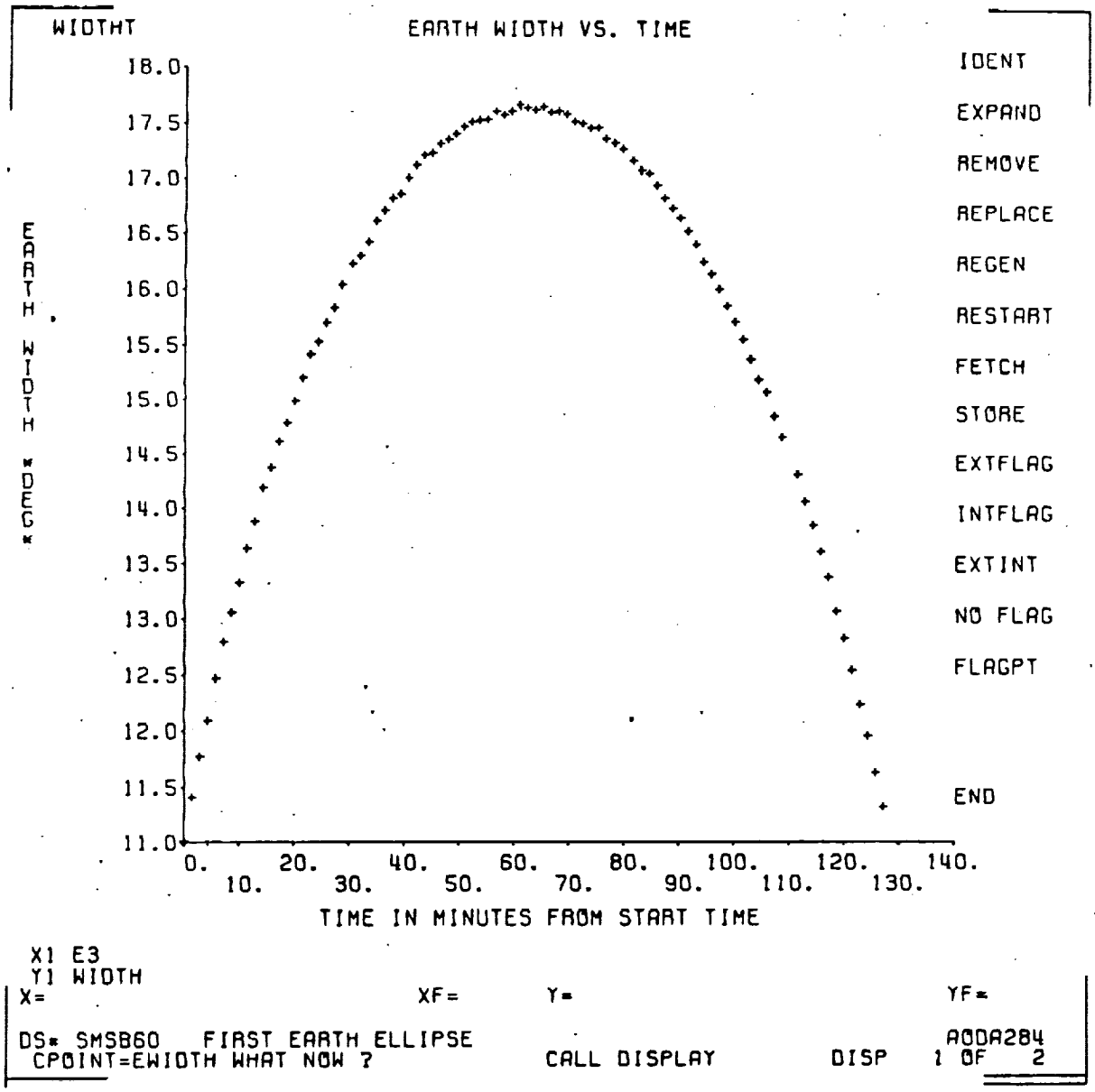

Figure 3-23. DS# SMSB60 Data Plots (7 of 8)

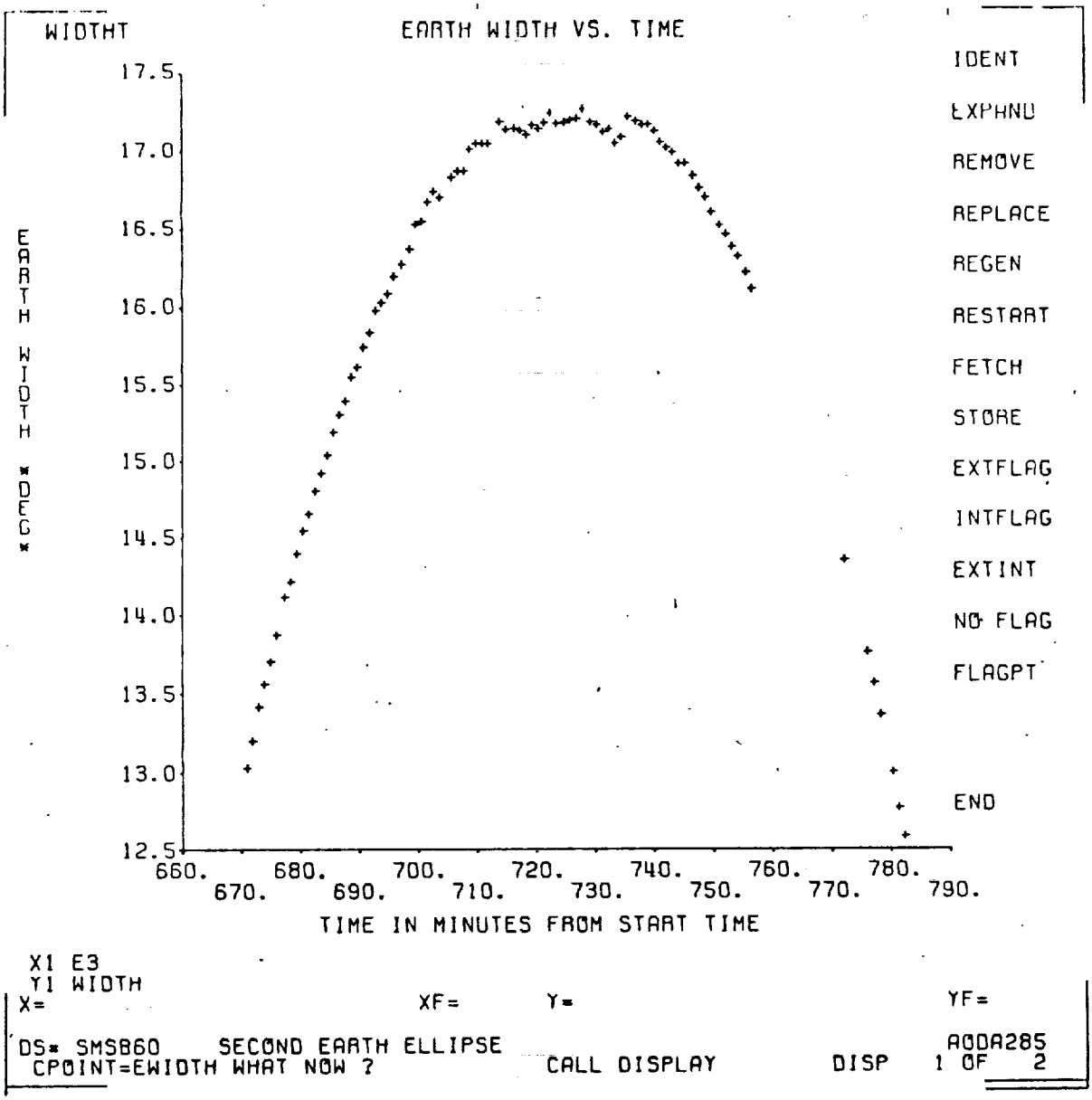

Figure 3-23. DS# SMSB60 Data Plots (8 of 8)

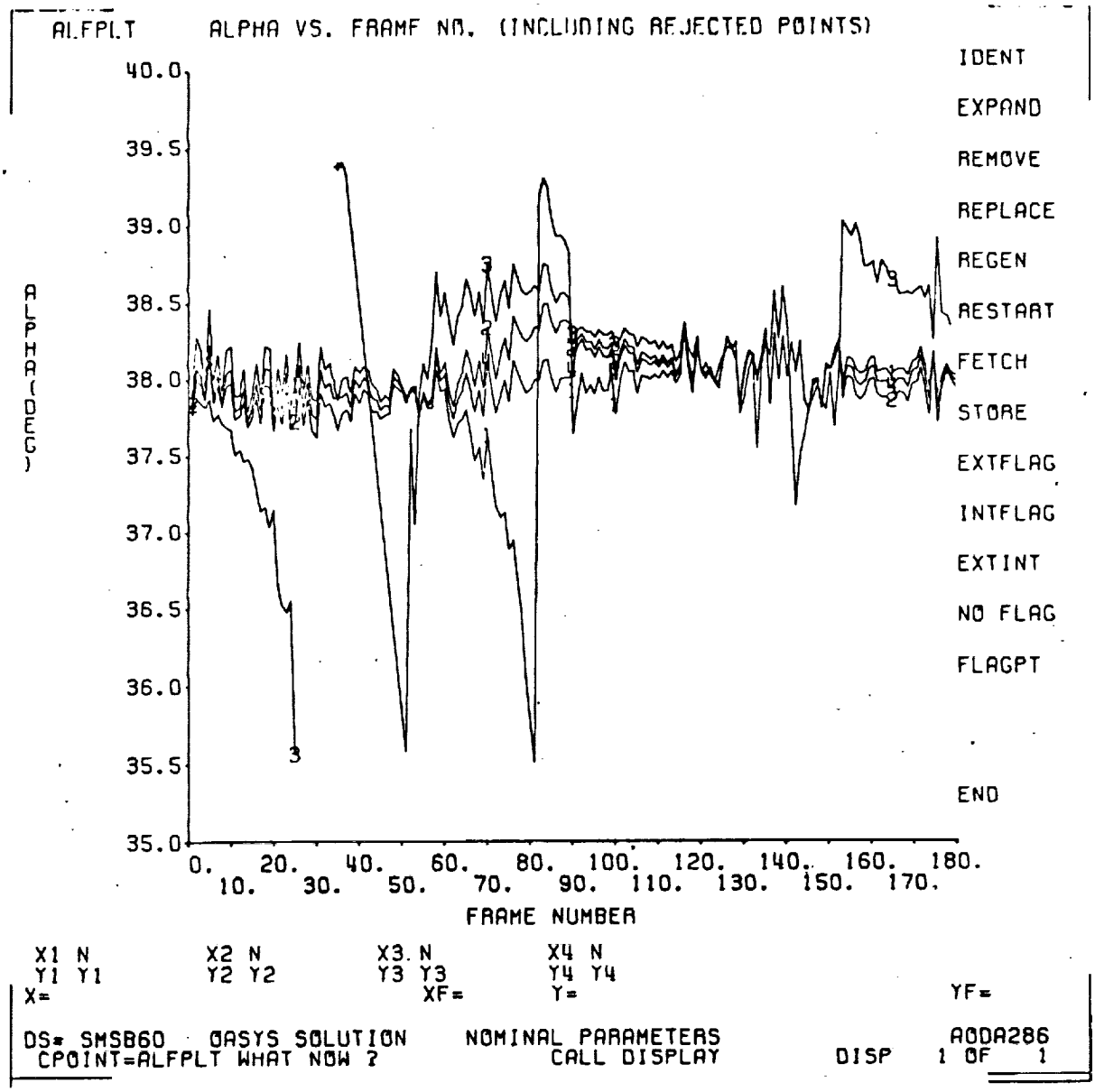

Figure 3-24. DS# SMSB60 Comparison of OASYS Solutions With Nominal and OABIAS Parameters (1 of 4)

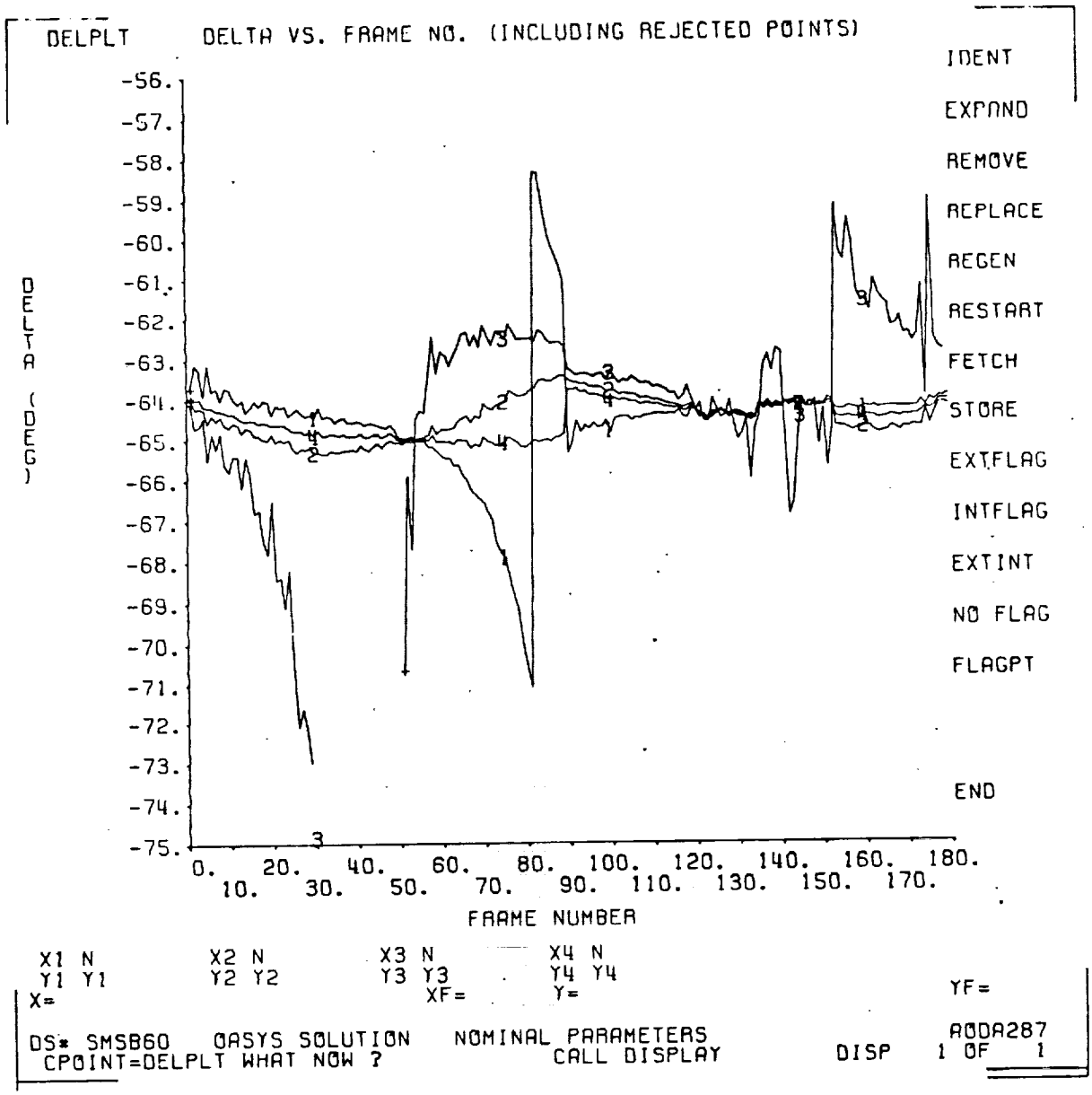

Figure 3-24. DS# SMSB60 Comparison of OASYS Solutions With Nominal and OABIAS Parameters (2 of 4)

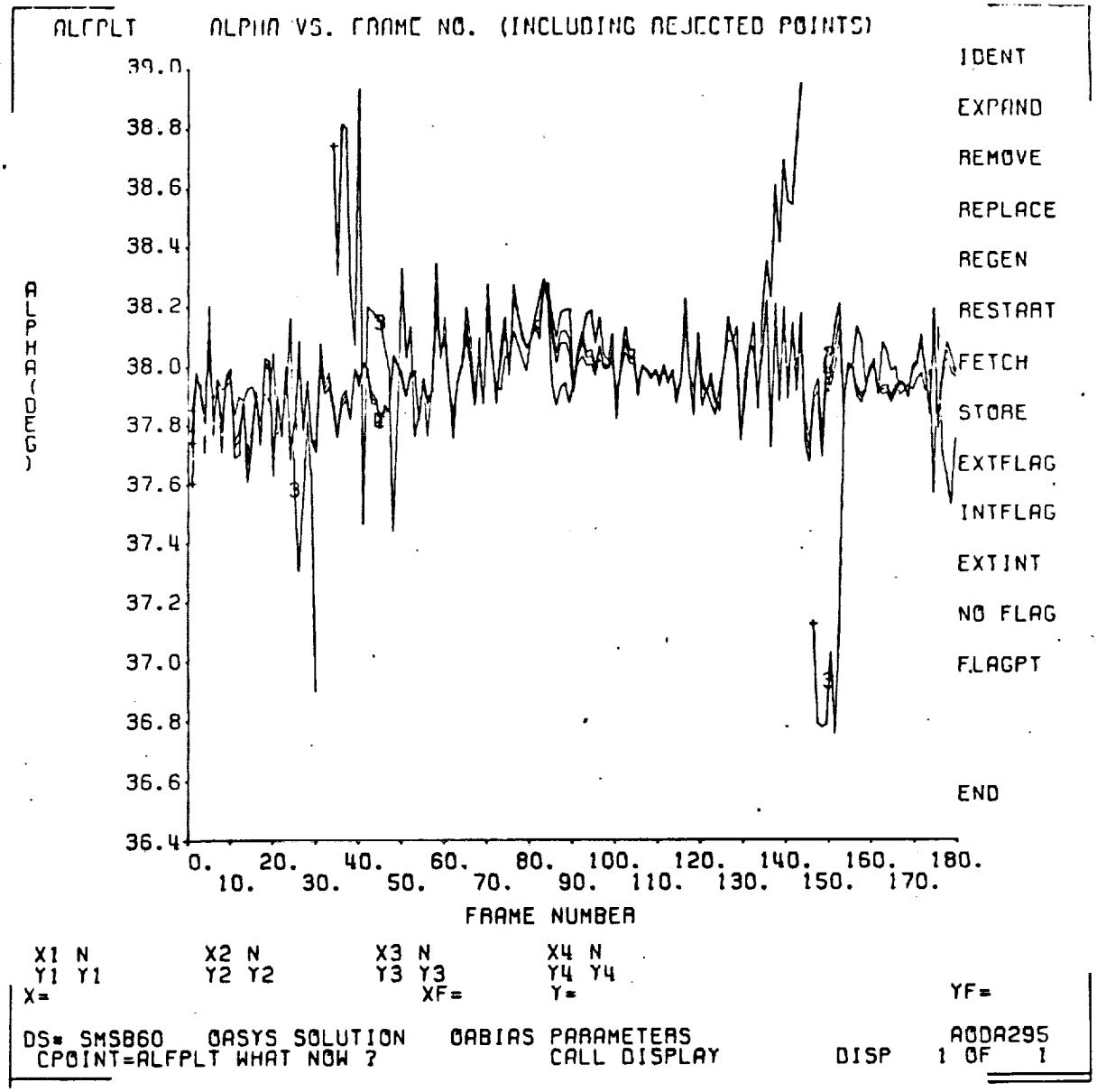

Figure 3-24. DS# SMSB60 Comparison of OASYS Solutions With Nominal and OABIAS Parameters (3 of 4)

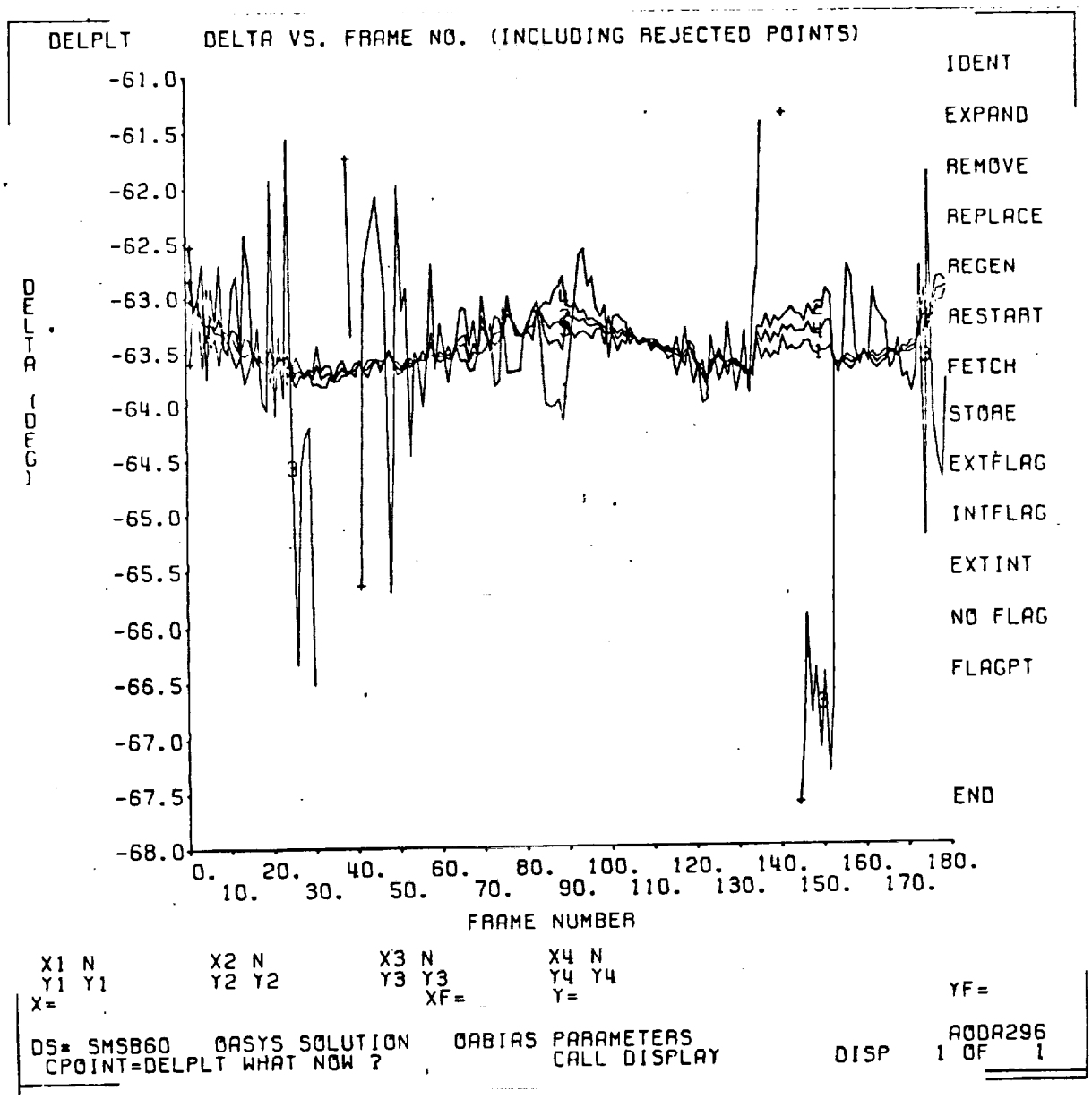

Figure 3-24. DS# SMSB60 Comparison of OASYS Solutions With Nominal and OABIAS Parameters (4 of 4)

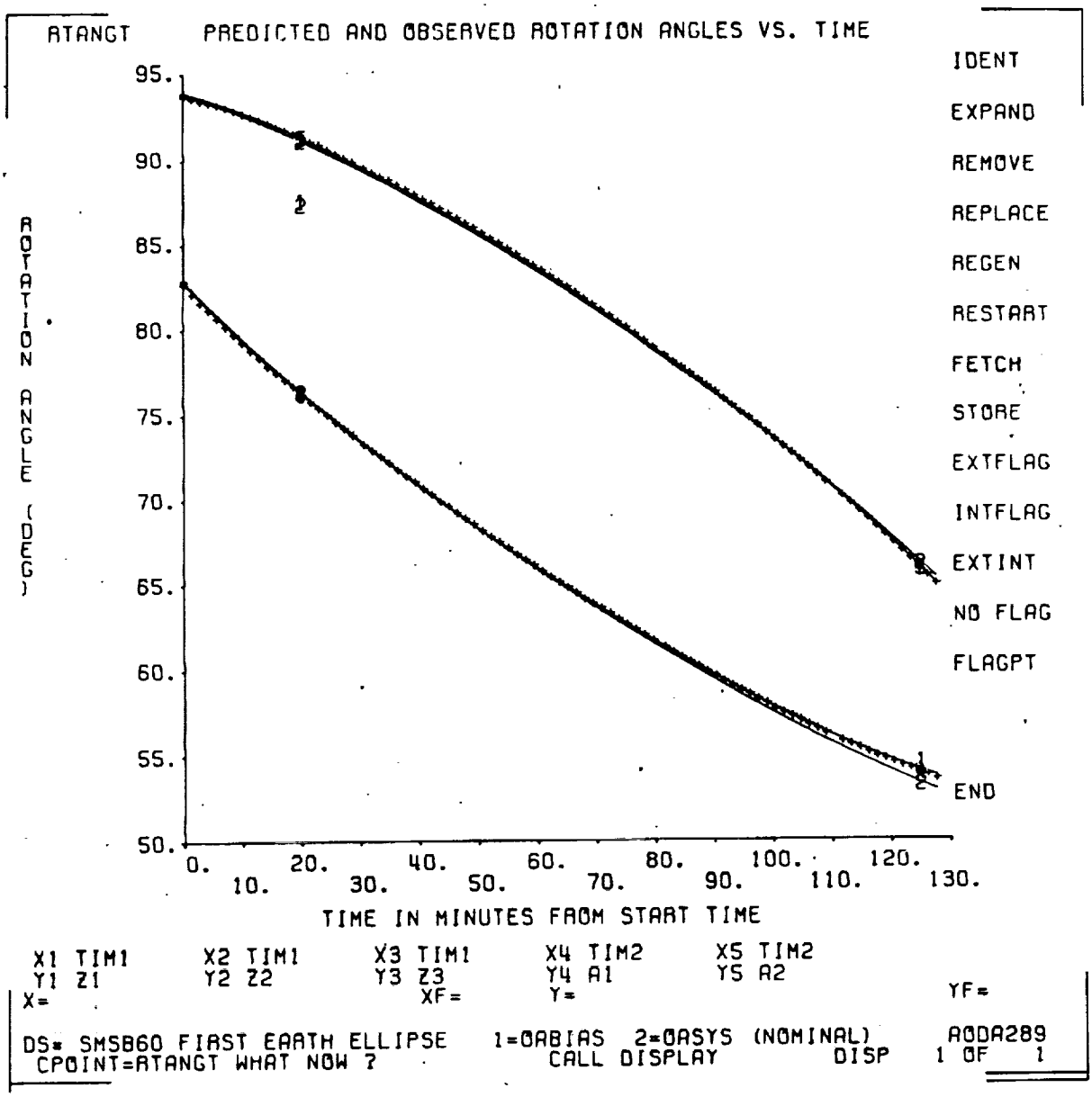

Figure 3-25. DS# SMSB60 Rotation Angle and Earth Width Plots for Nominal and OABIAS Solutions (1 of 6)

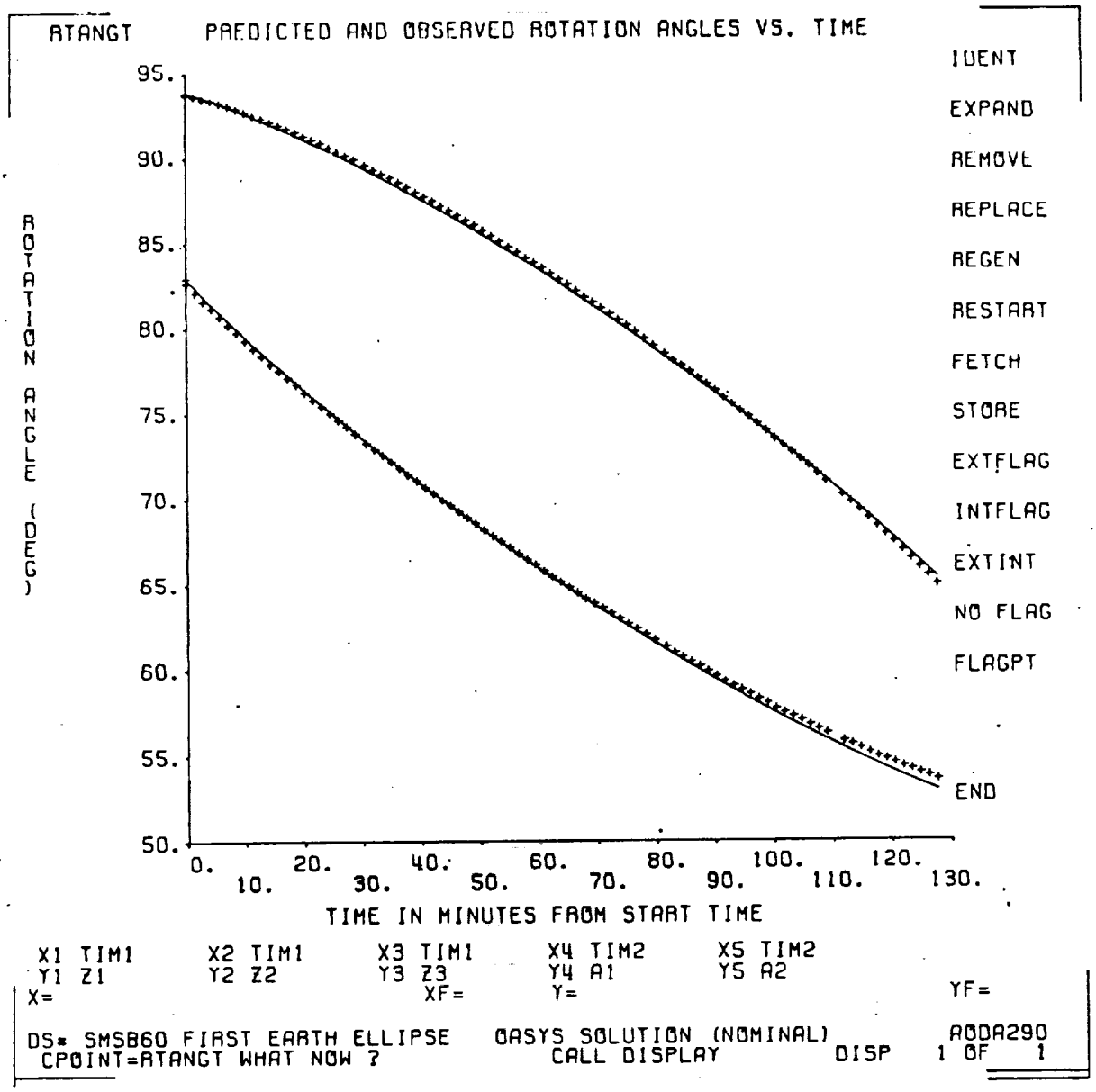

Figure 3-25. DS# SMSB60 Rotation Angle and Earth Width Plots for Nominal and OABIAS Solutions (2 of 6)

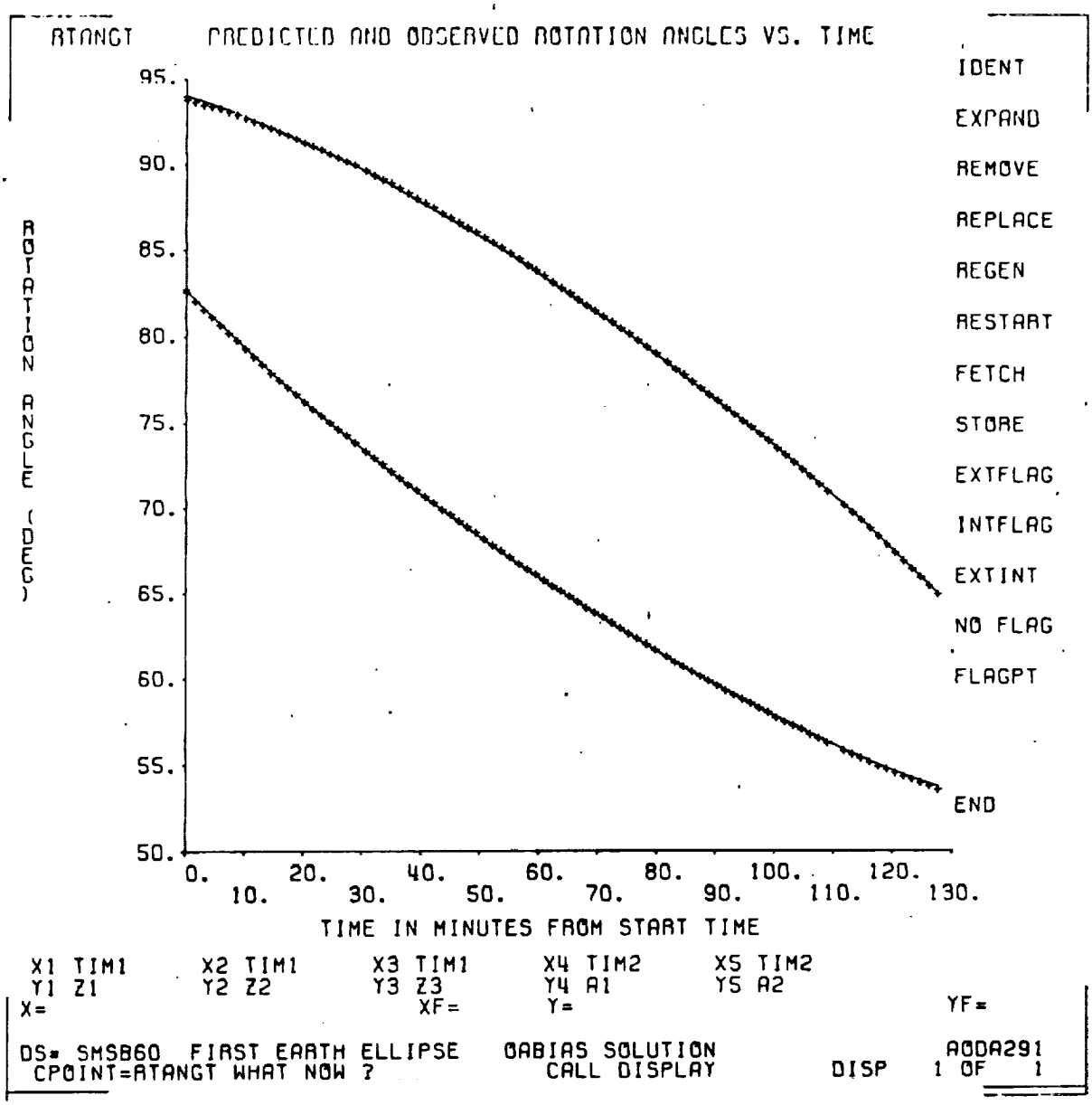

Figure 3-25. DS# SMSB60 Rotation Angle and Earth Width Plots for Nominal and OABIAS Solutions (3 of 6)

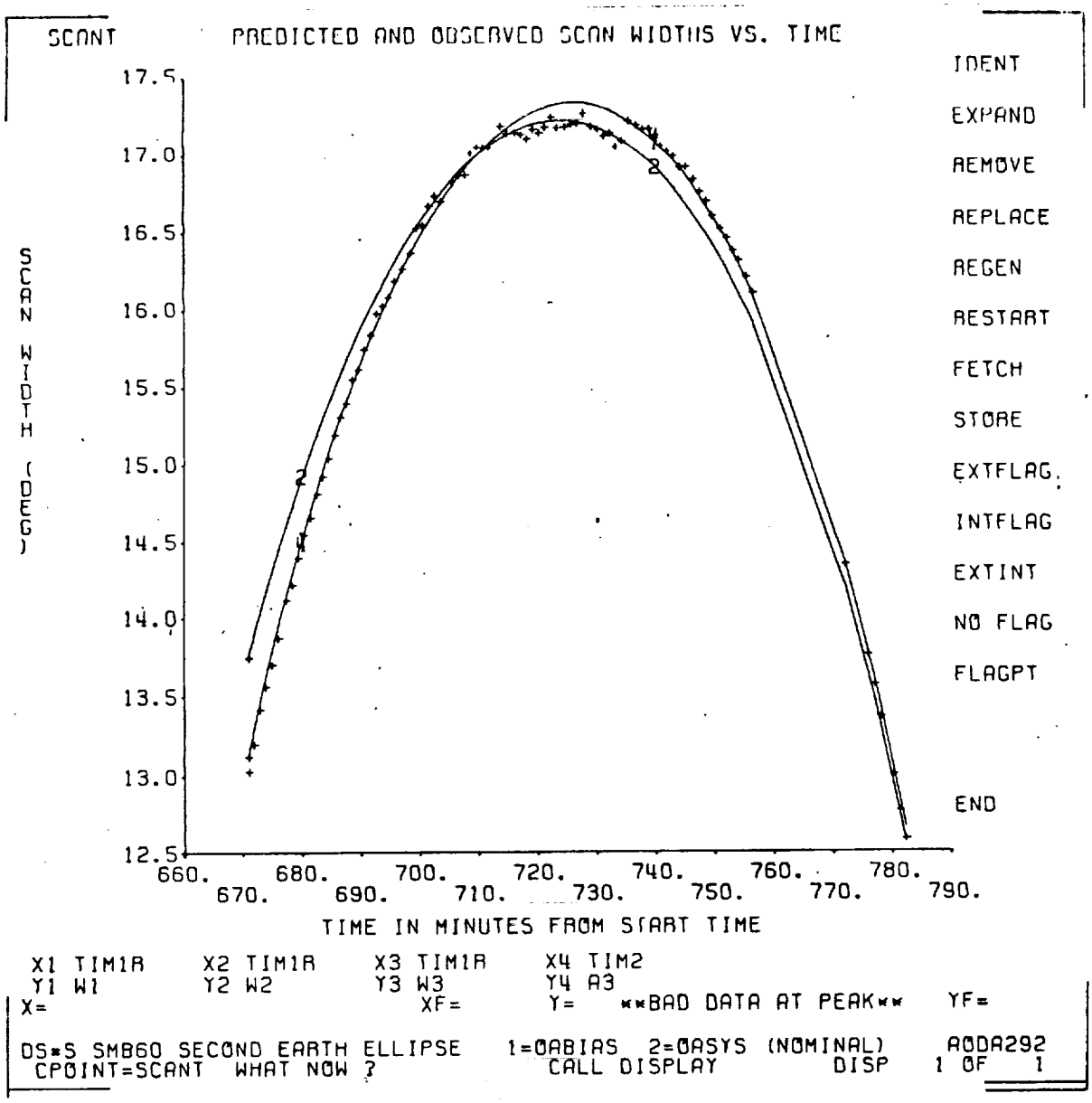

Figure 3-25. DS# SMSB60 Rotation Angle and Earth Width Plots for Nominal and OABIAS Solutions (4 of 6)

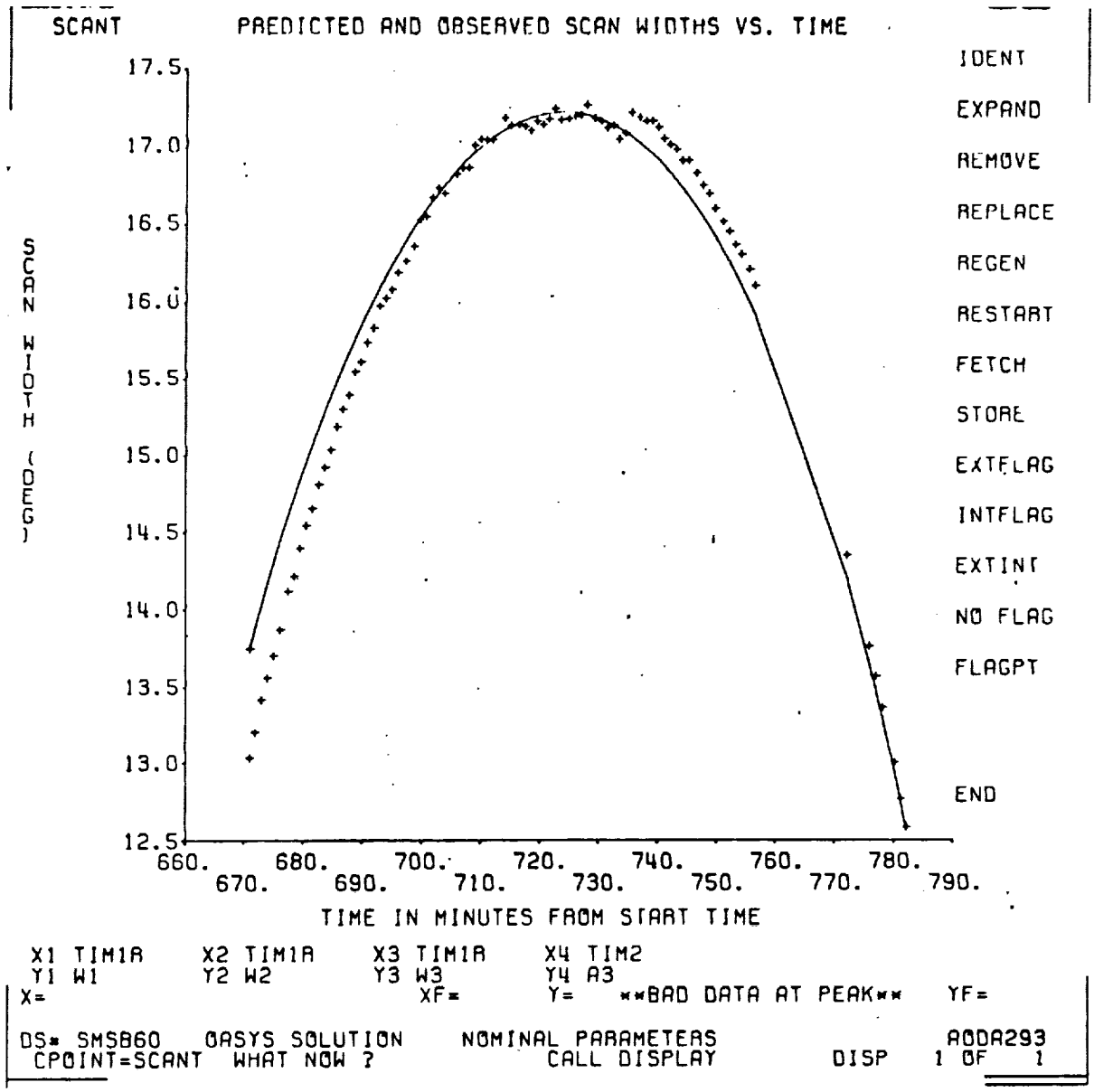

Figure 3-25. DS# SMSB60 Rotation Angle and Earth Width Plots for Nominal and OABIAS Solutions (5 of 6)

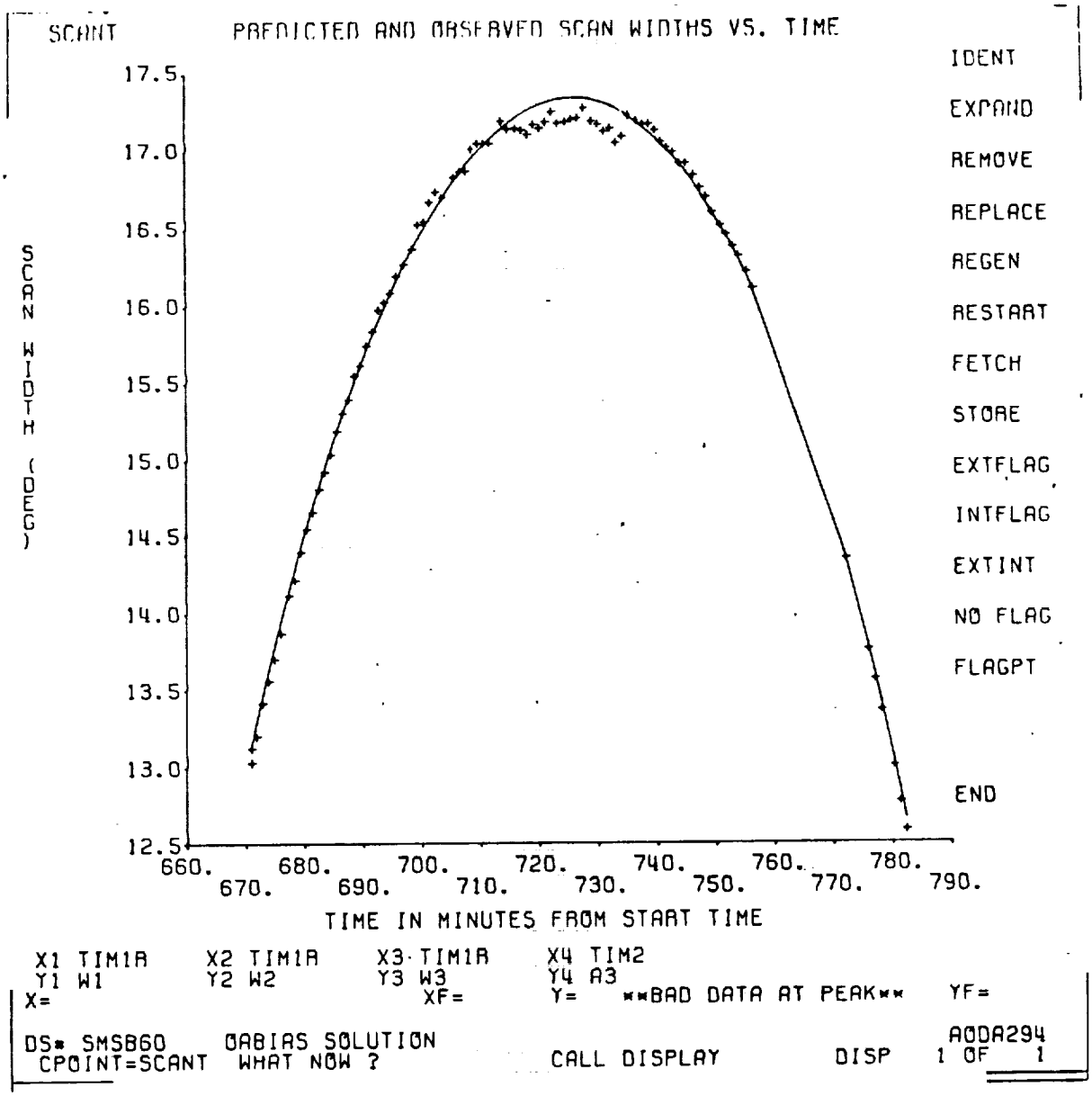

Figure 3-25. DS# SMSB60 Rotation Angle and Earth Width Plots for Nominal and OABIAS Solutions (6 of 6)

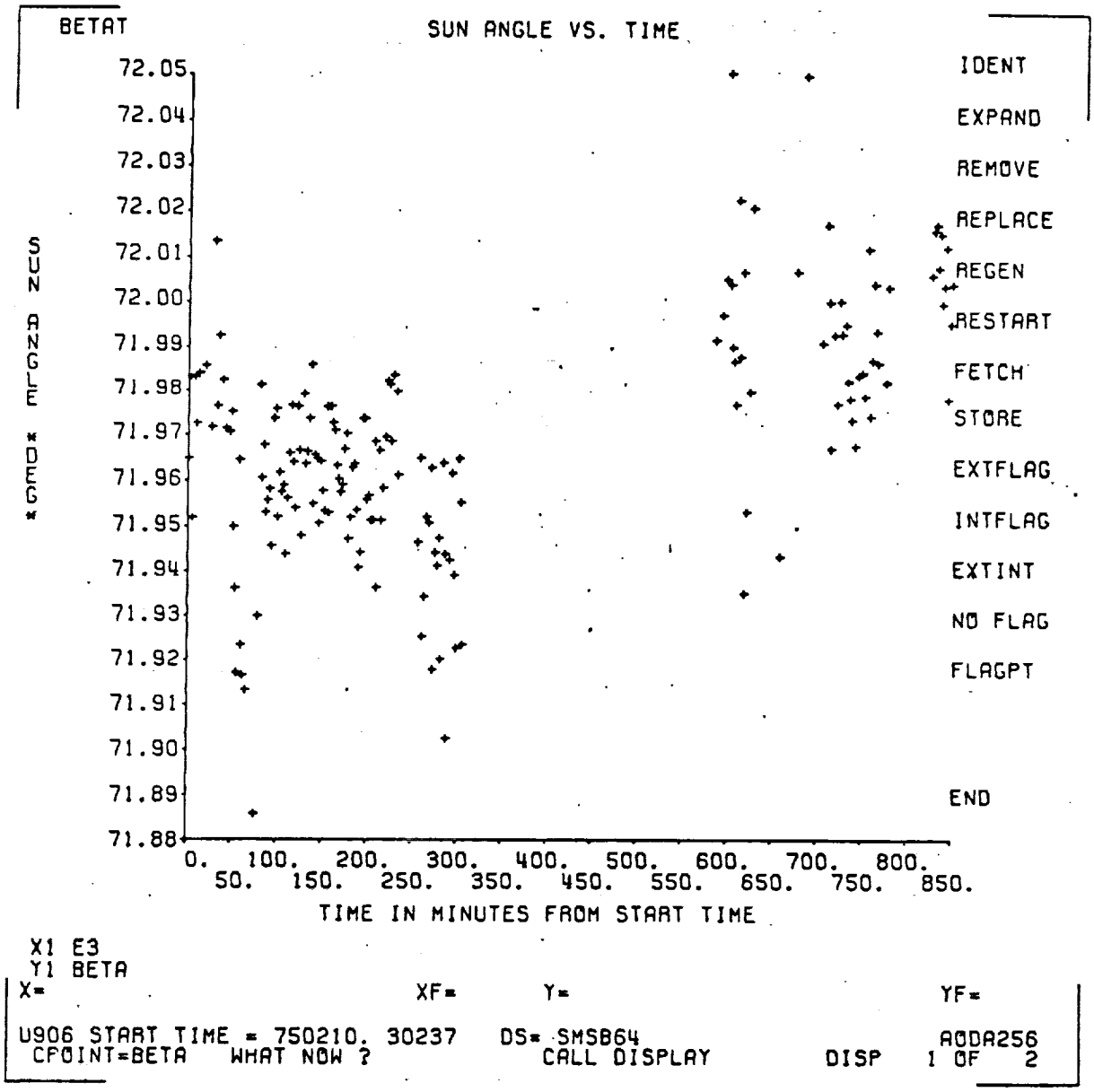

Figure 3-26. DS# SMSB64 Data Plots (1 of 3)

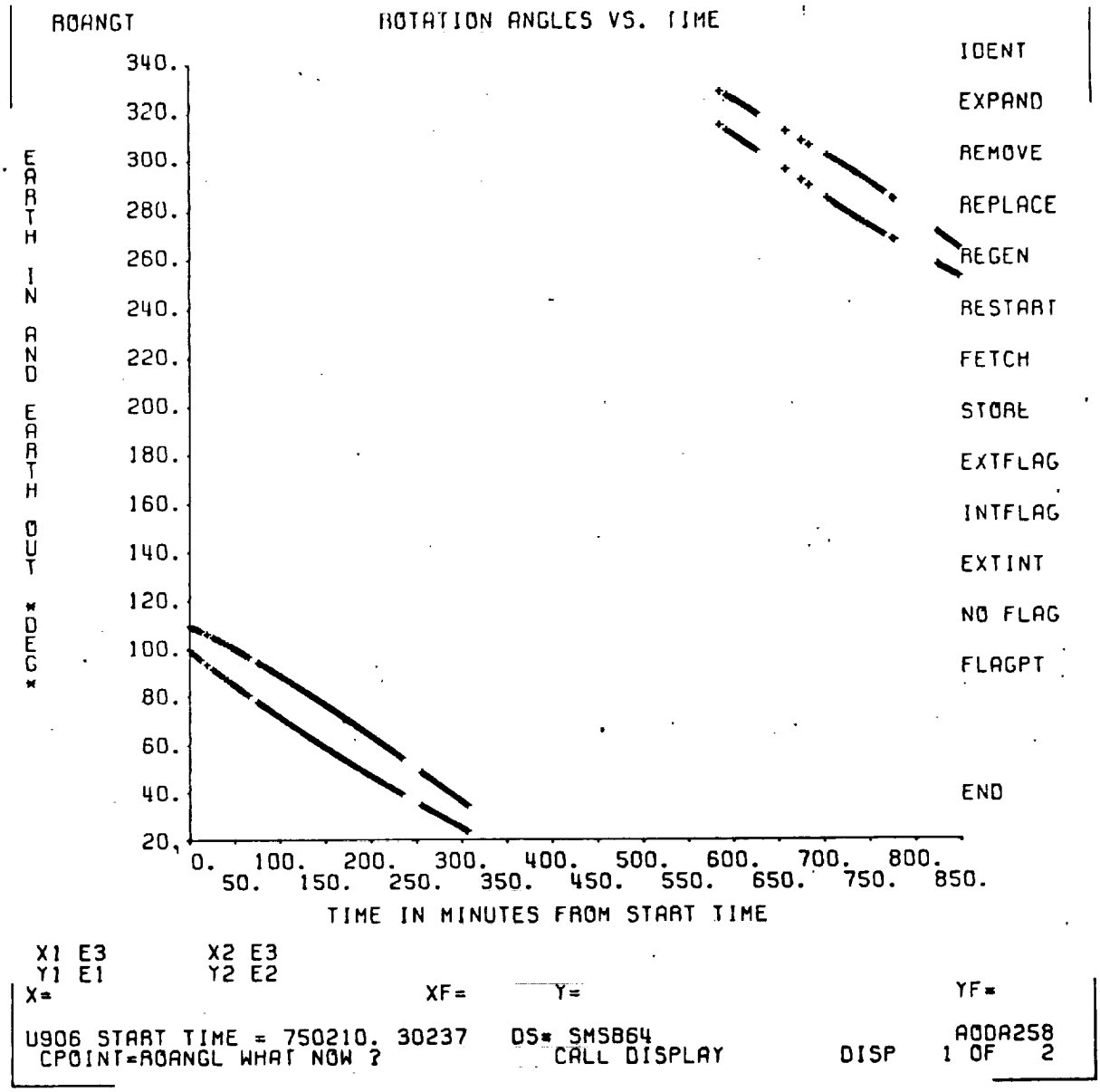

Figure 3-26. DS# SMSB64 Data Plots (2 of 3)

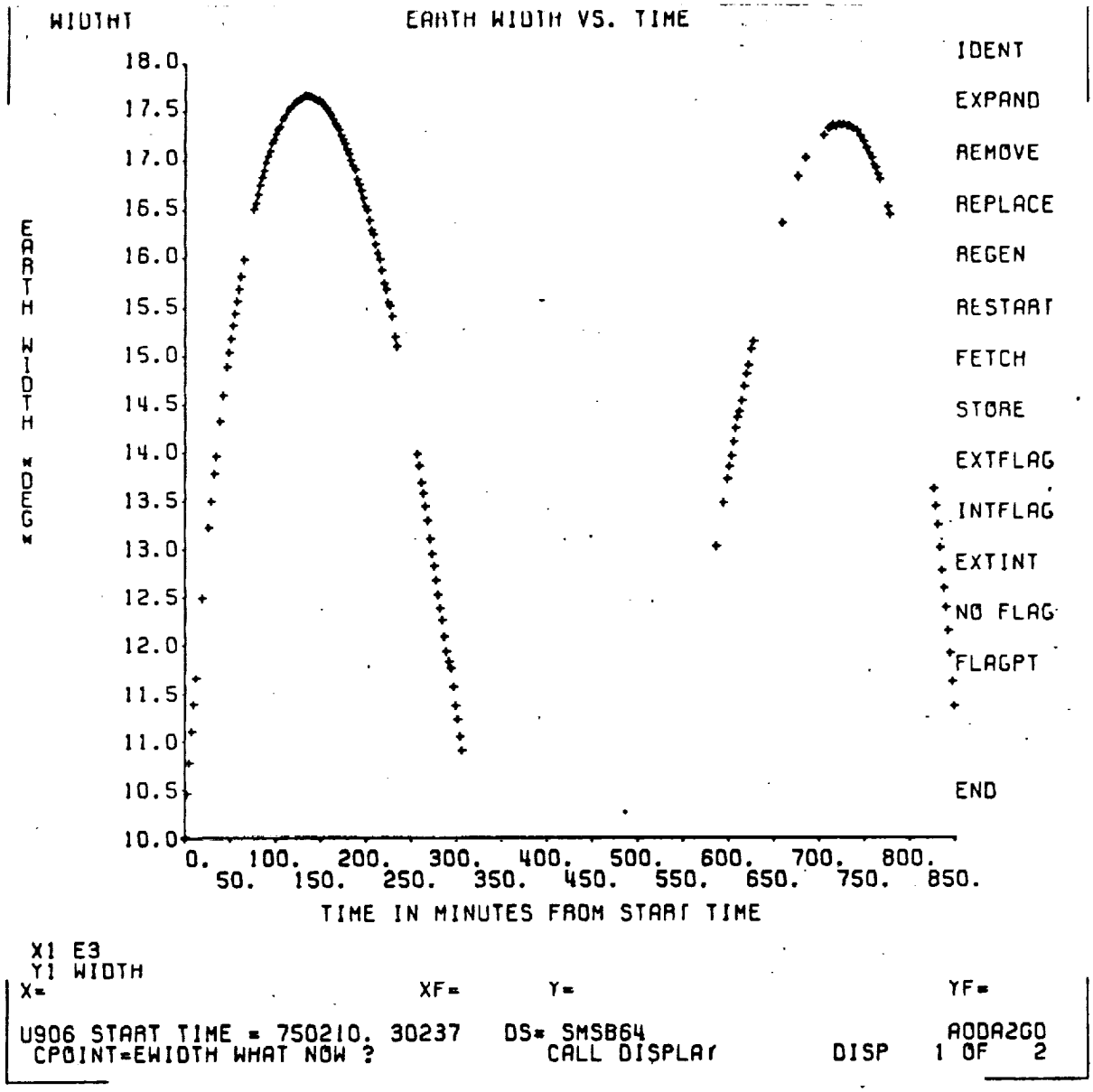

Figure 3-26. DS# SMSB64 Data Plots (3 of 3)

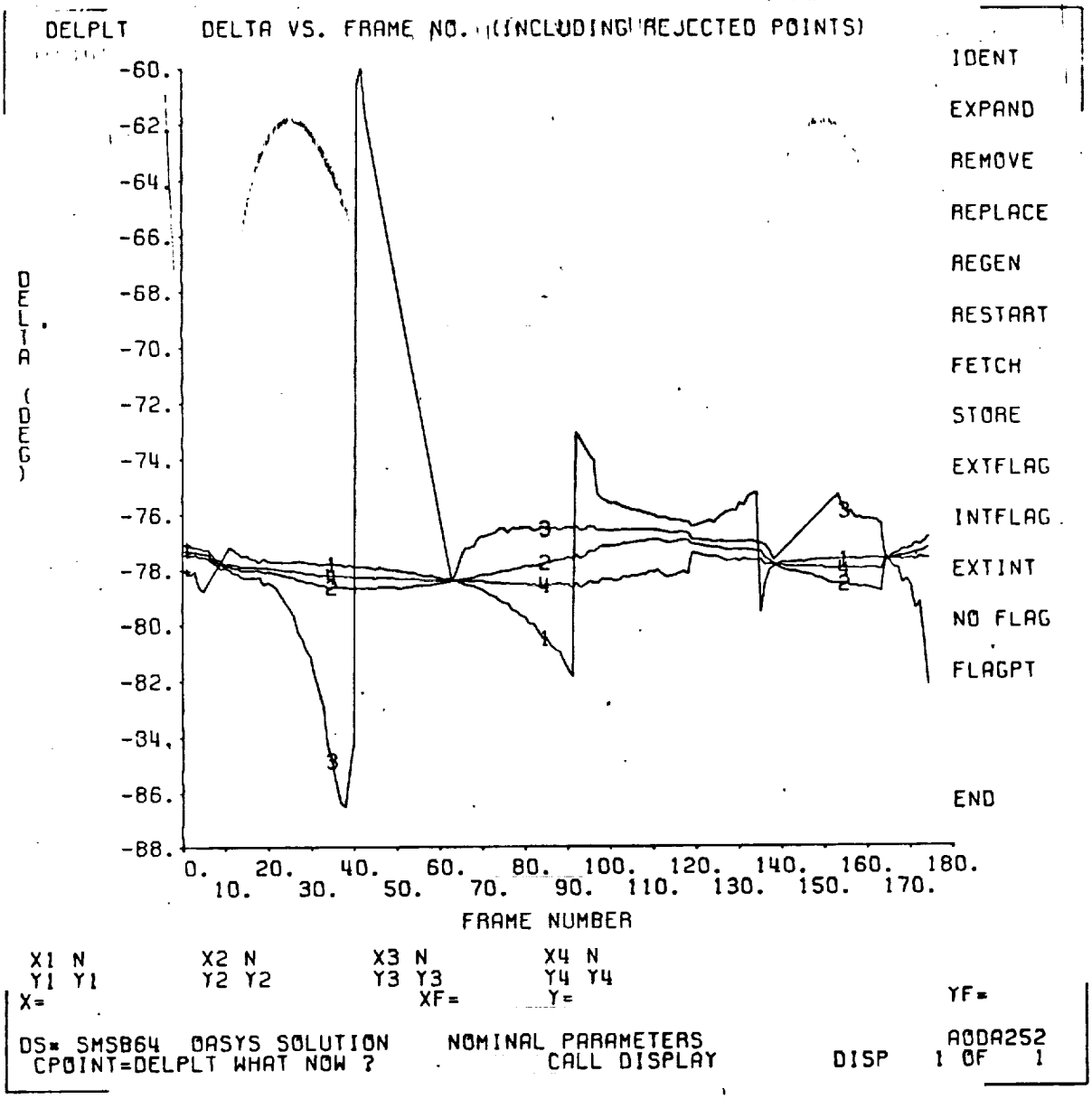

Figure 3-27. DS# SMSB64 Comparison of OASYS Solutions With Nominal and OABIAS Parameters (1 of 2)

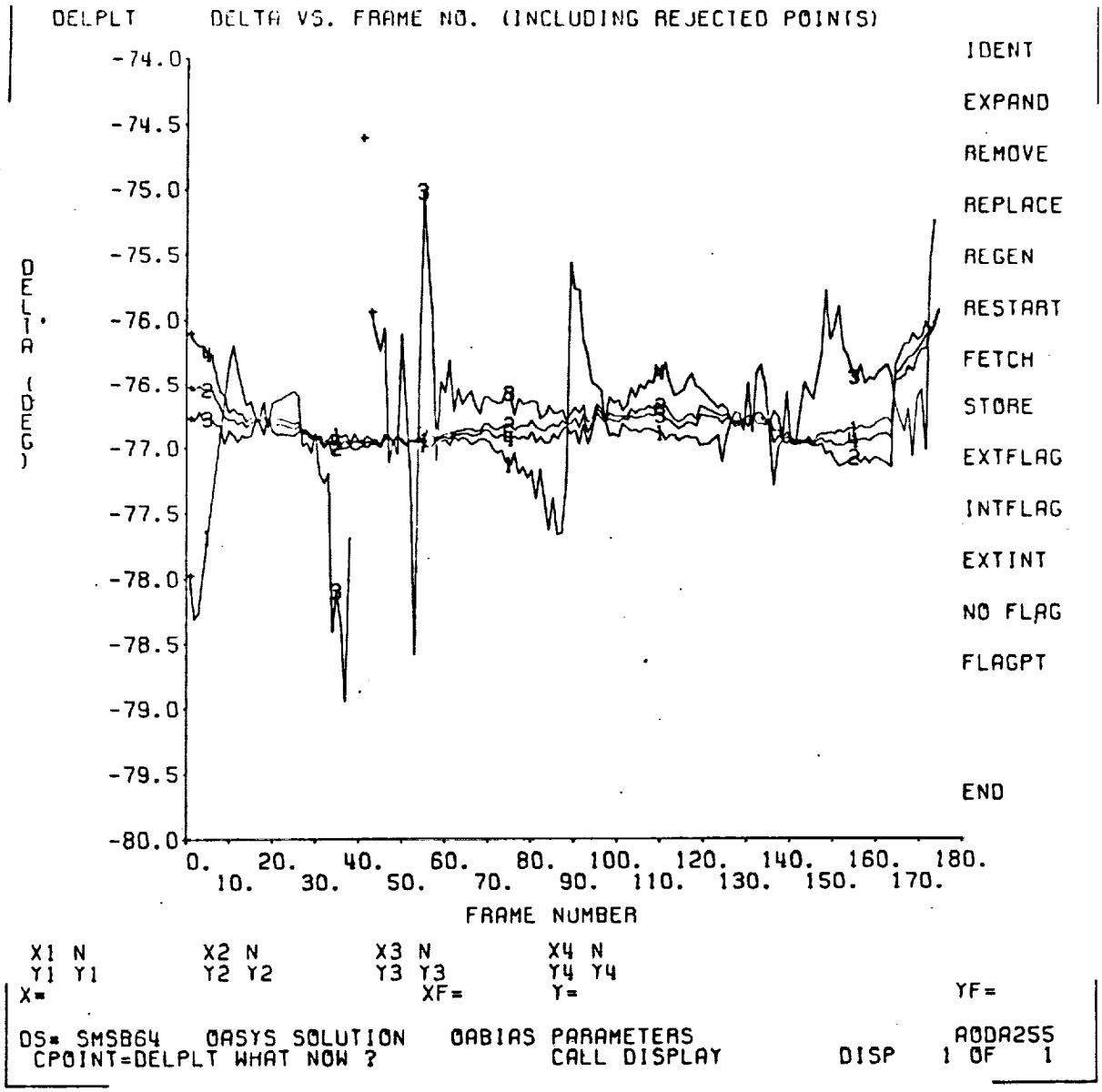

Figure 3-27. DS# SMSB64 Comparison of OASYS Solutions With Nominal and OABIAS Parameters (2 of 2)

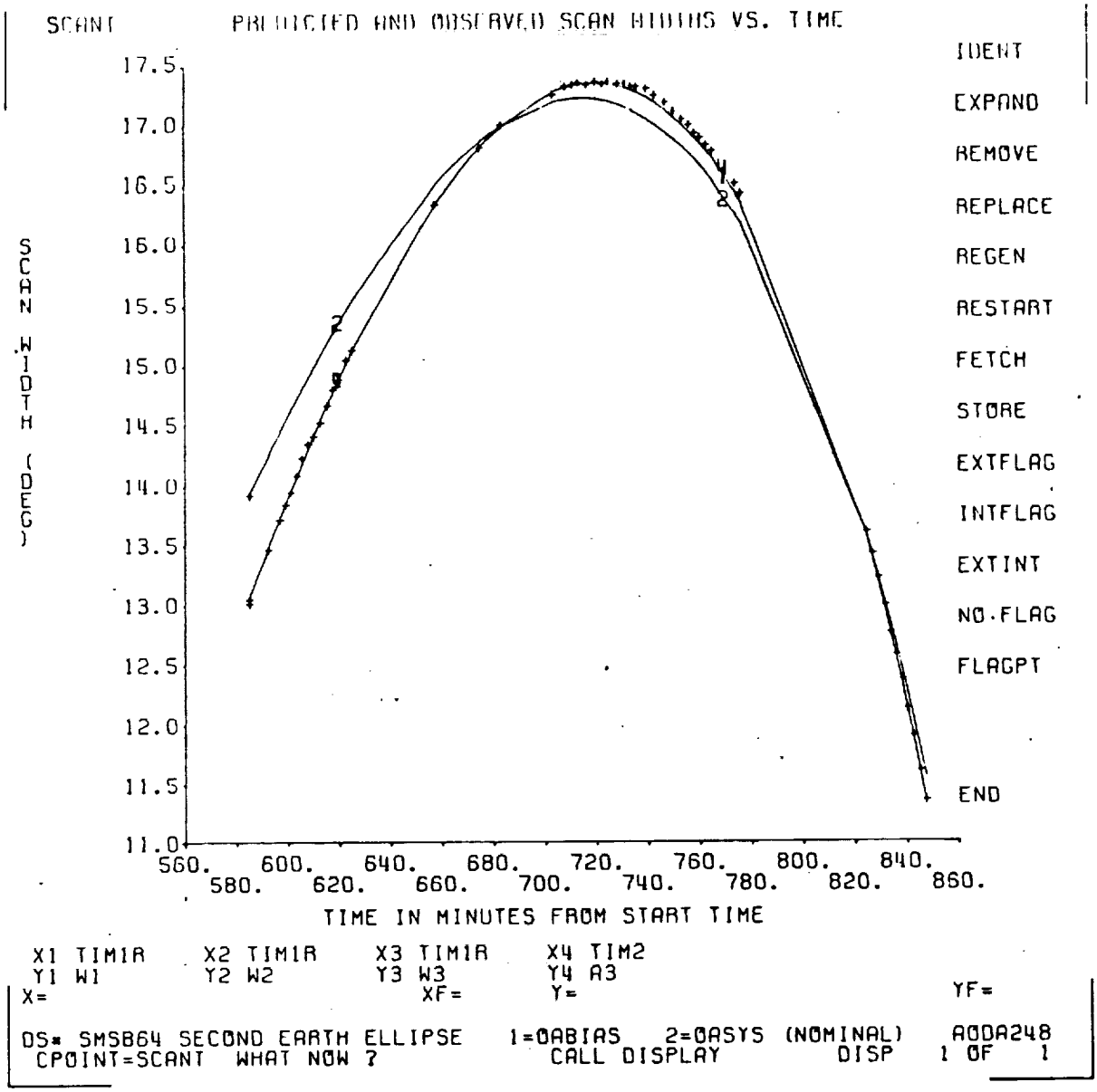

Figure 3-28. DS# SMSB64 Earth Width Plots for Nominal and OABIAS Solutions

3.4.3.2 Earth Sensor 2 Biases

The Earth sensor 2 (ES2) biases were determined from only one data set, DS#63. The results are listed in Table 3-5 and the corresponding plots are given in Figures 3-29 to 3-31 . Data points with Earth-width below 10^{o} have been removed from the data due to the pagoda effect. Aside from the pagoda effect, there is no other abnormal behavior apparent in this data set. In obtaining the biases, $\Delta\phi^{I}$ was fixed at the same value as $\Delta\phi^{0}$ in order to get convergence. As can be seen from either the lower part of Table 3-5 or Figures 3-30 and 3-31, the OABIAS results give a much better fit to the data and more reliable attitude solutions than the nominal parameters. However, the biases obtained in this data set have relatively higher uncertainties than those obtained from other drift orbit data. This may be due to the fact that this data set does not contain full coverage across the diameter of the Earth (see Figure 3-29 (3)) which is important in bias determination (see Reference 5).

Table 3-5. Earth Sensor-2 Bias Determination Results

OABIAS Bias Result

DS#			63		
Orbit			Drift Orbit 3		
Biases			Value	Statistical Unc.	Total Unc.
$\Delta\gamma$			.38	.096	.566
$\Delta\varphi$			$\lvert-.38\rvert$	$\lvert.054\rvert$	$\lvert.319\rvert$
$\Delta\phi$			$\lvert-.38\rvert$	$\lvert.054\rvert$	$\lvert.319\rvert$
$\Delta\rho$			.06	.040	.236
Comparison of OABIAS and Nominal Parameters					
OASYS			Using Nominal Parameters	Using OABIAS Results	
Deter-ministic Results	Right Ascension, α (Deg)		35.44	35.16	
	Declination, δ (Deg)		-77.41	-76.64	
	Standard Deviation	Arc Length	.46	.19	
		α	.60	.27	
		δ	.44	.18	
Fit to Data	Rot. Angle	Mean Residual	.122	.001	
		STDV	.249	.140	
		% of Good Fit	50%	100%	
		Maximum Deviation	.4	-	
	Central Body Width	Mean Residual	-.146	.005	
		STDV	.321	.037	
		% of Good Fit	10%	90%	
		Maximum Deviation	.7°	.03°	

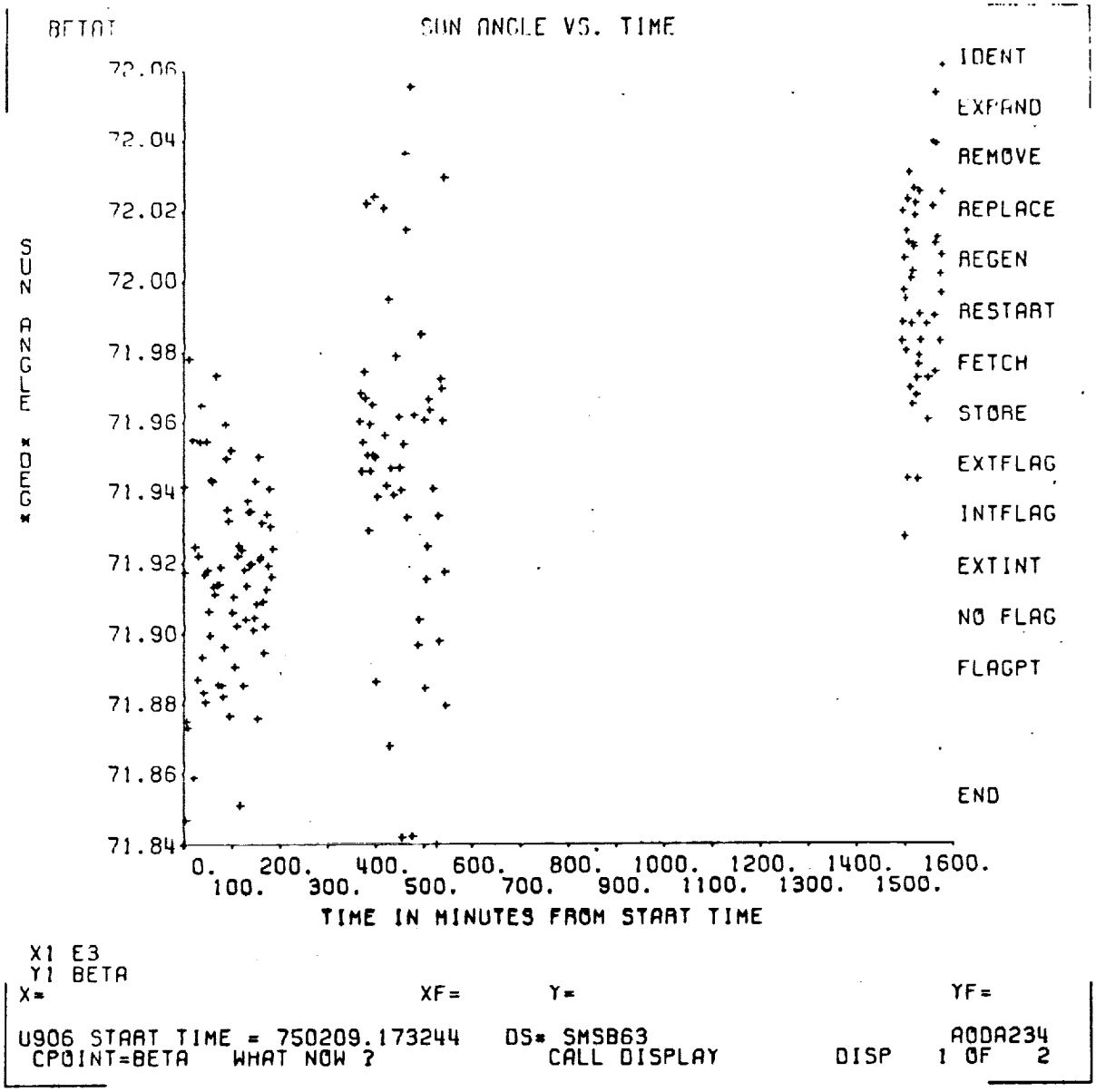

Figure 3-29. DS# SMSB63 Data Plots (1 of 3)

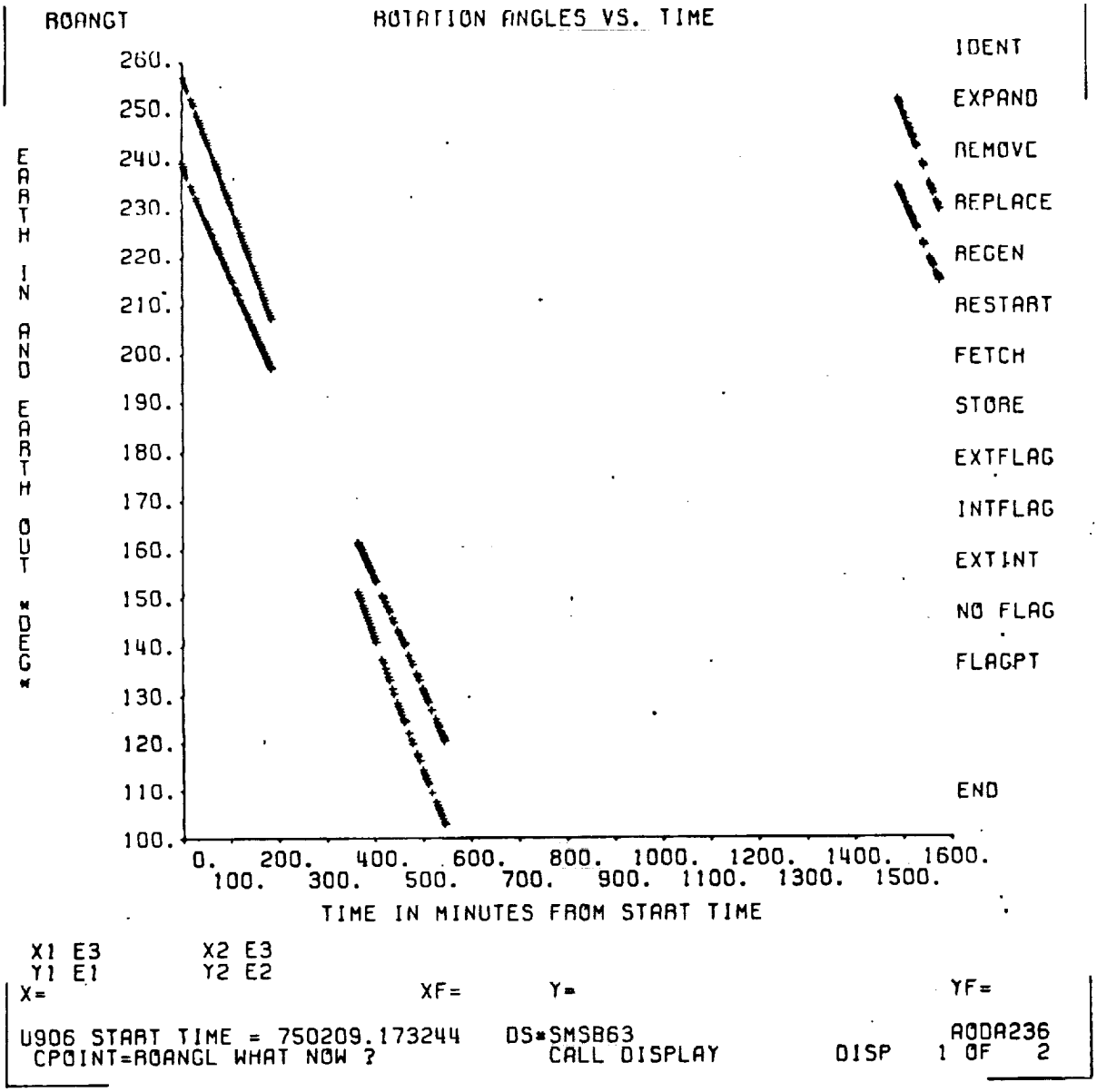

Figure 3-29. DS# SMSB63 Data Plots (2 of 3)

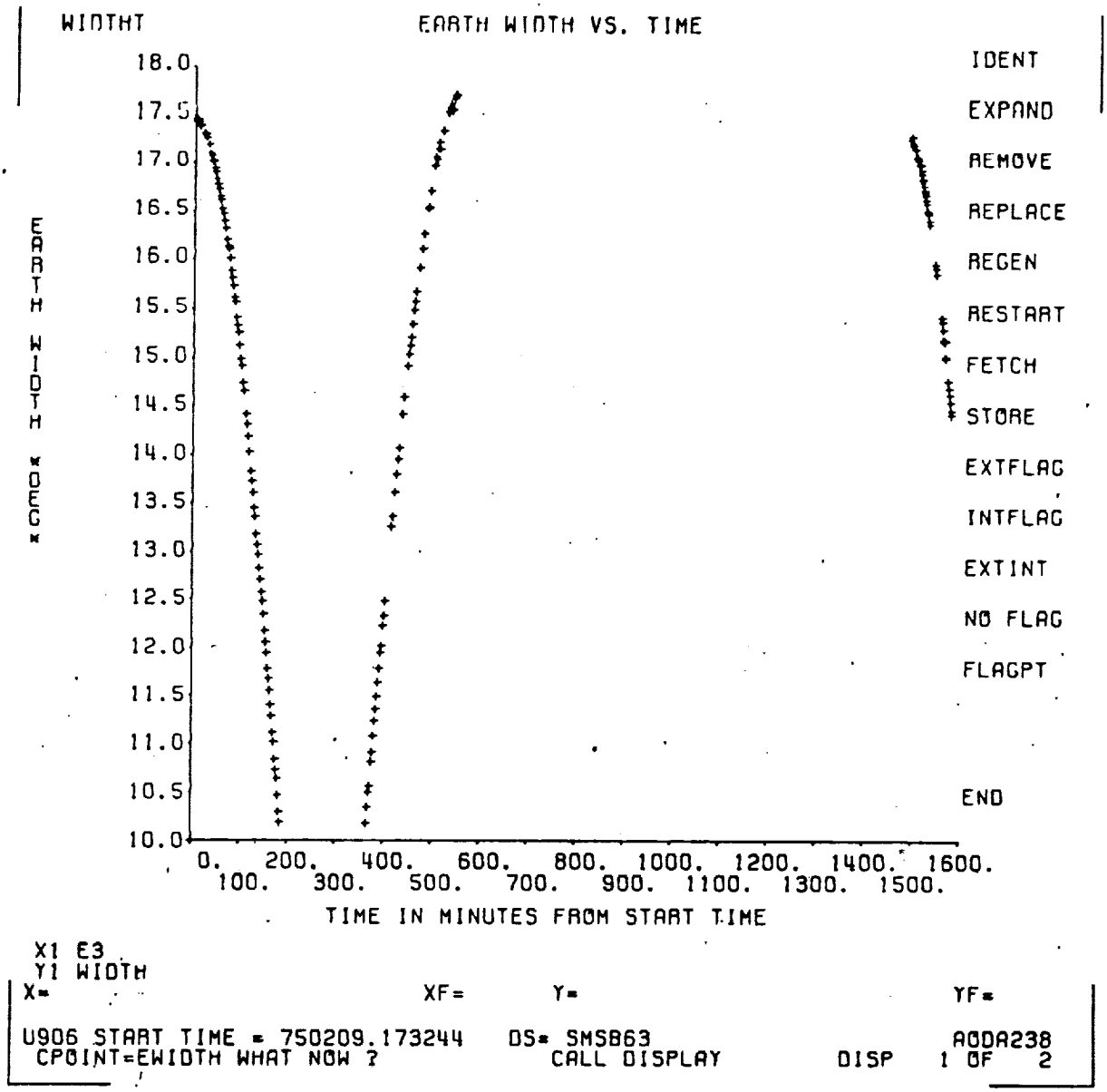

Figure 3-29. DS# SMSB63 Data Plots (3 of 3)

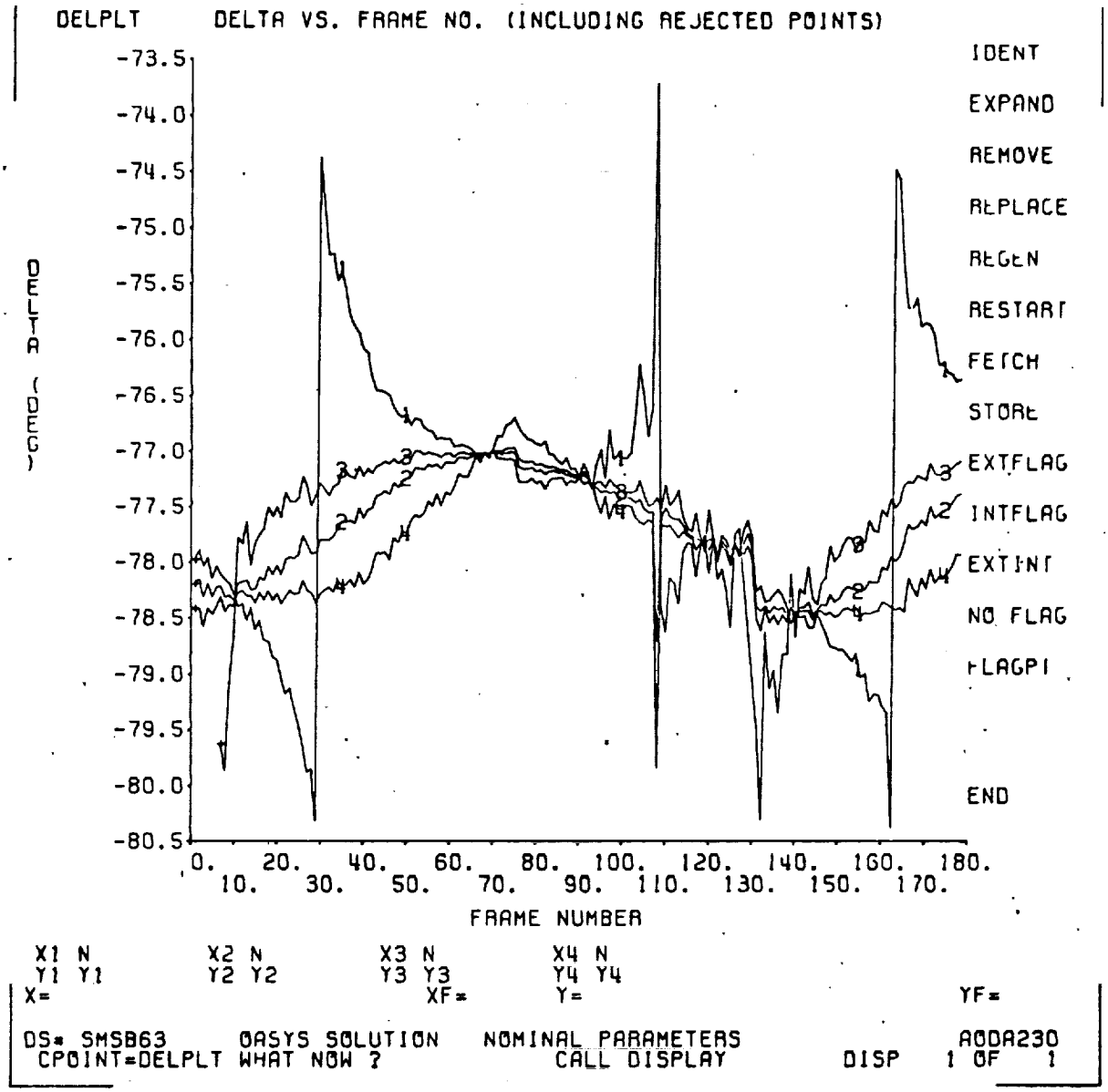

Figure 3-30. DS# SMSB63 Comparison of OASYS Solutions With Nominal and OABIAS Parameters (1 of 2)

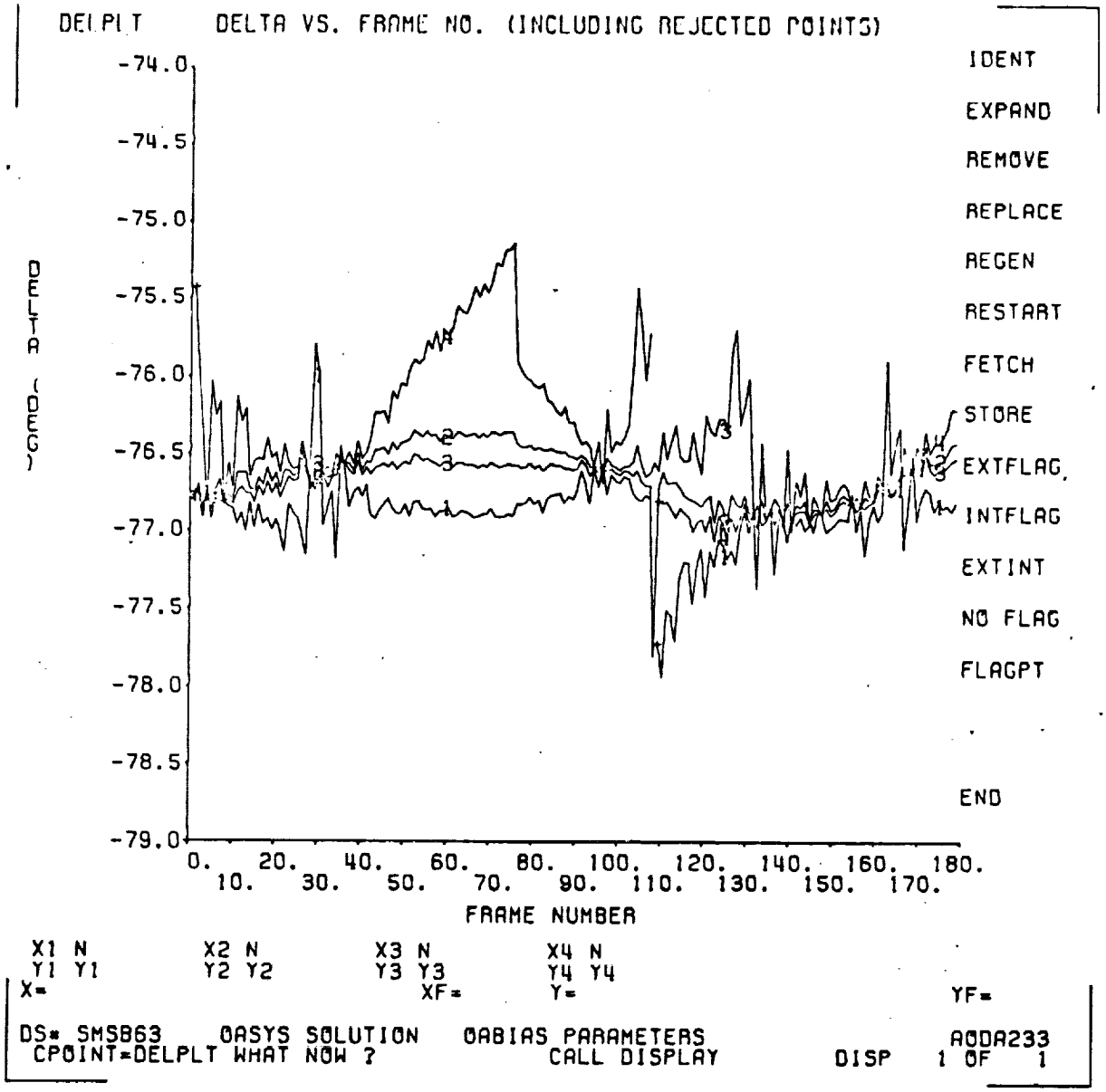

Figure 3-30. DS# SMSB63 Comparison of OASYS Solutions With Nominal and OABIAS Parameters (2 of 2)

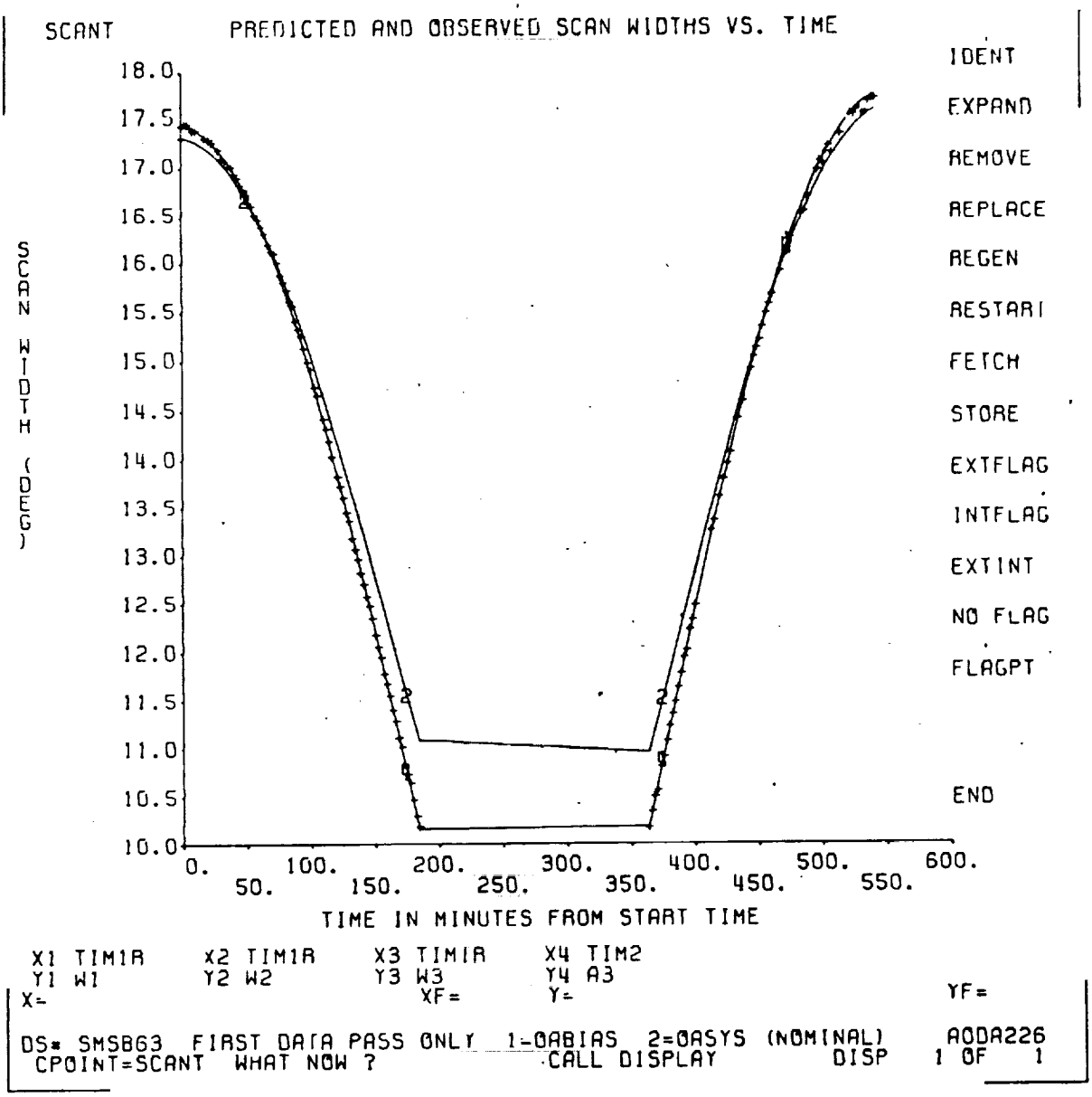

Figure 3-31. DS# SMSB63 Earth Width Plots for Nominal and OABIAS Solutions (1 of 3)

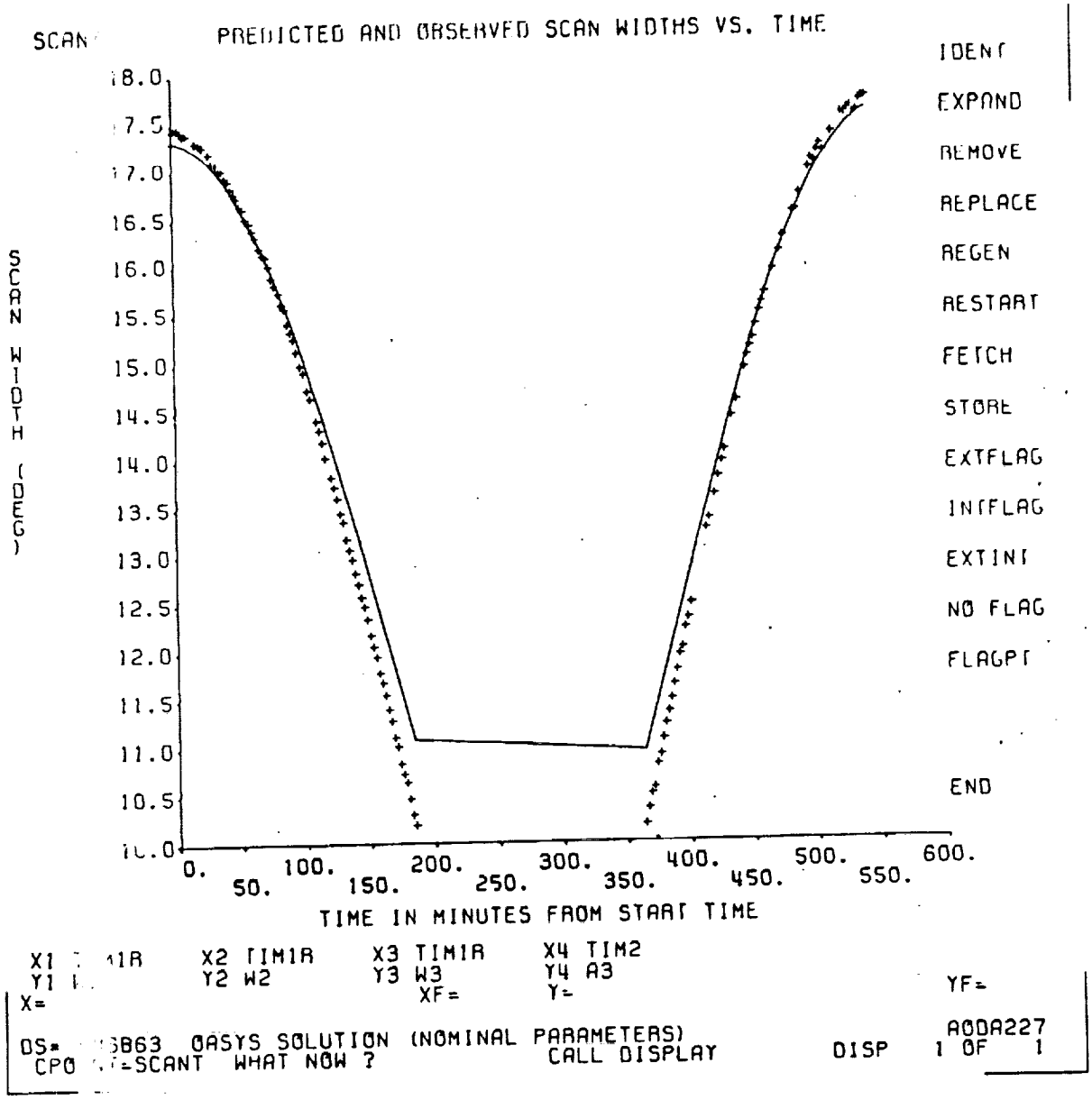

Figure 3-31. DS# SMSB63 Earth Width Plots for Nominal and OABIAS Solutions (2 of 3)

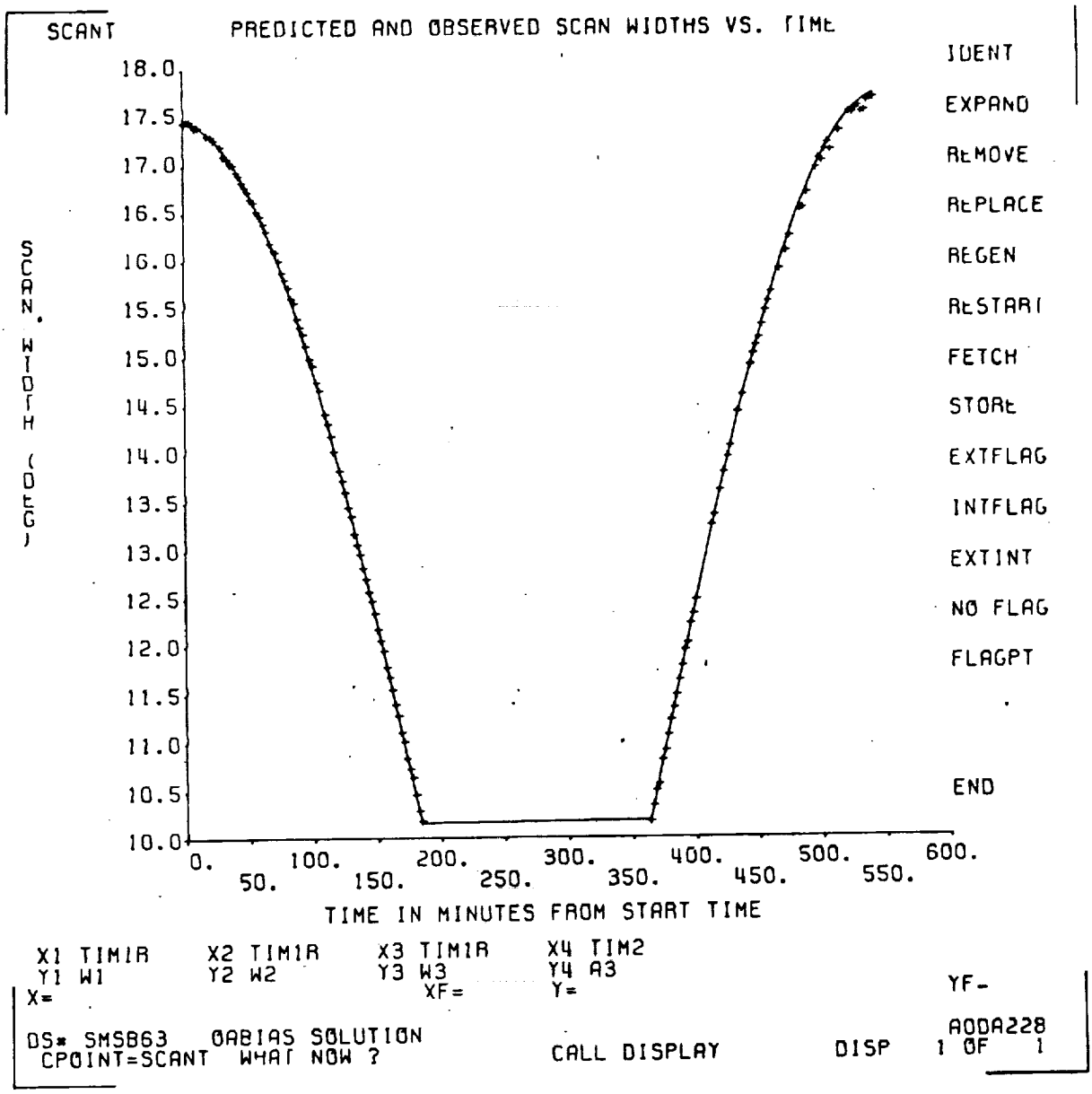

Figure 3-31. DS# SMSB63 Earth Width Plots for Nominal and OABIAS Solutions (3 of 3)

3.4.3.3 Earth Sensor-3 Biases

The only data set used in Earth sensor-3 bias determination is DS#53 in the transfer orbit. As previously discussed the transfer orbit data in general has poor data quality and little geometrical variation. Therefore the biases determined have large uncertainties. Table 3-6 and Figures 3-32 to 3-34 show the bias determination results and selected plots for this data set. Again, $\Delta\phi^I$ was fixed at the same value as $\Delta\phi^0$. From the comparison of OABIAS and nominal parameters given in the lower part of the table, it is not obvious which solution gives a better fit to the data. Although the OABIAS solution fits the rotation angles better, it shows a slightly larger mean residual and standard deviation in the Earth-width fit. Therefore it is hard to verify the existence of any bias for this Earth sensor. This is consistent with the bias results listed in the upper part of the table where none of the biases differs from zero by more than its uncertainty.

Table 3-6. Earth Sensor-3 Bias Determination Results

OABIAS Bias Result

DS#	53		
Orbit	Transfer		
Biases	Value	Statistical Uncertainty	Total Uncertainty
$\Delta\gamma$	.30	.11	.65
$\Delta\Theta^I$	.23	.07	.41
$\Delta\Phi^\circ$	.23	.07	.41
$\Delta\rho$	.01	.04	.24

Comparison of OABIAS and Nominal Parameters

OASYS			Using Nominal Parameters	Using OABIAS Results
Deterministic Results	Right Ascension, α (Deg)		24.54	24.33
	Declination, δ (Deg)		-19.63	-19.92
	Standard Deviation	Arc Length	.11	.11
		α	.08	.08
		δ	.08	.08
Fit to Data	Rot. Angle	Mean Residual	-.024	-.012
		STDV	.100	.089
		% of Good Fit	100%	100%
		Maximum Deviation	-	-
	Central Body Width	Mean Residual	-.014	-.021
		STDV	.079	.085
		% of Good Fit	100%	100%
		Maximum Deviation	-	-

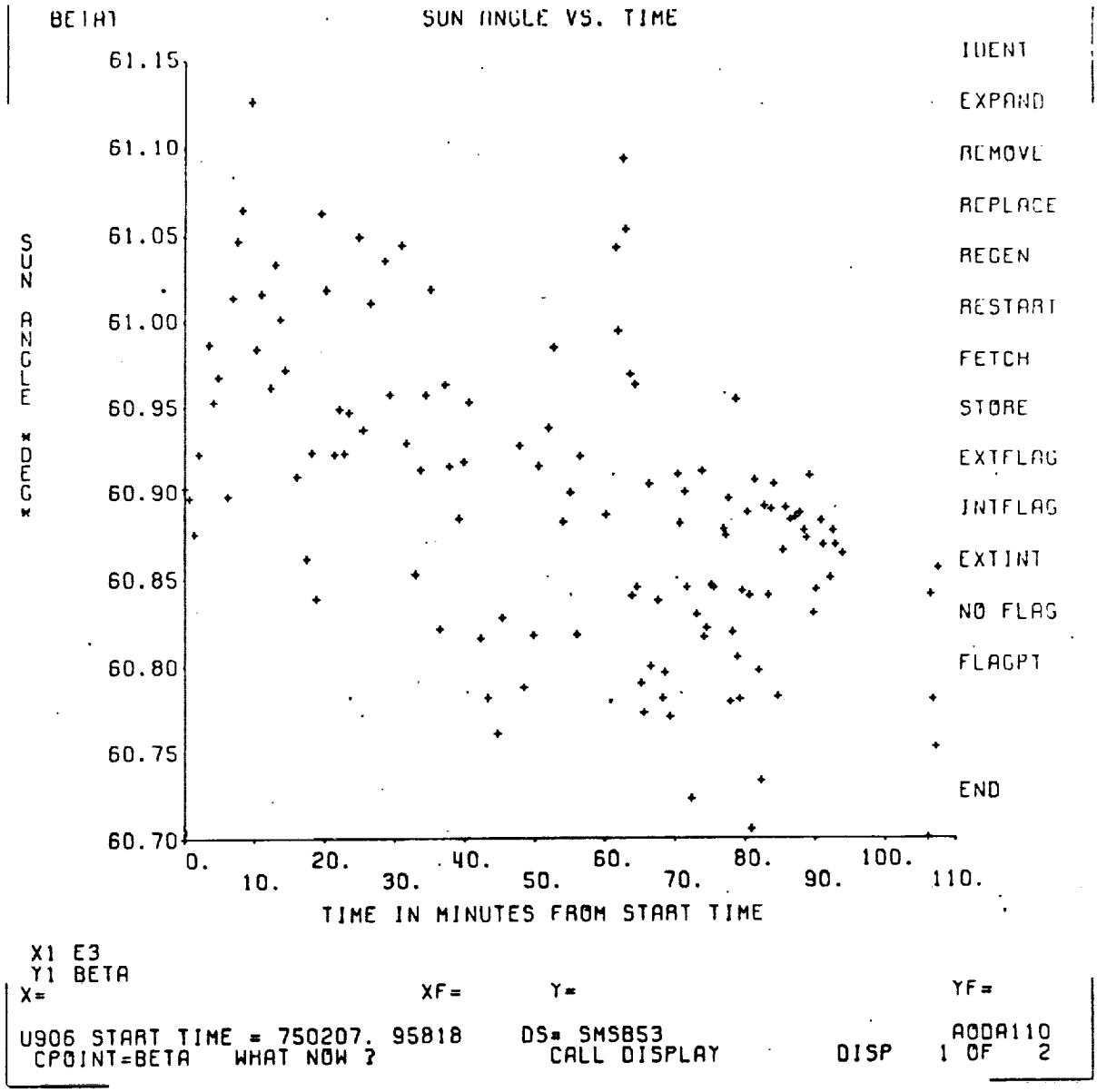

Figure 3-32. DS# SMSB53 Data Plots (1 of 3)

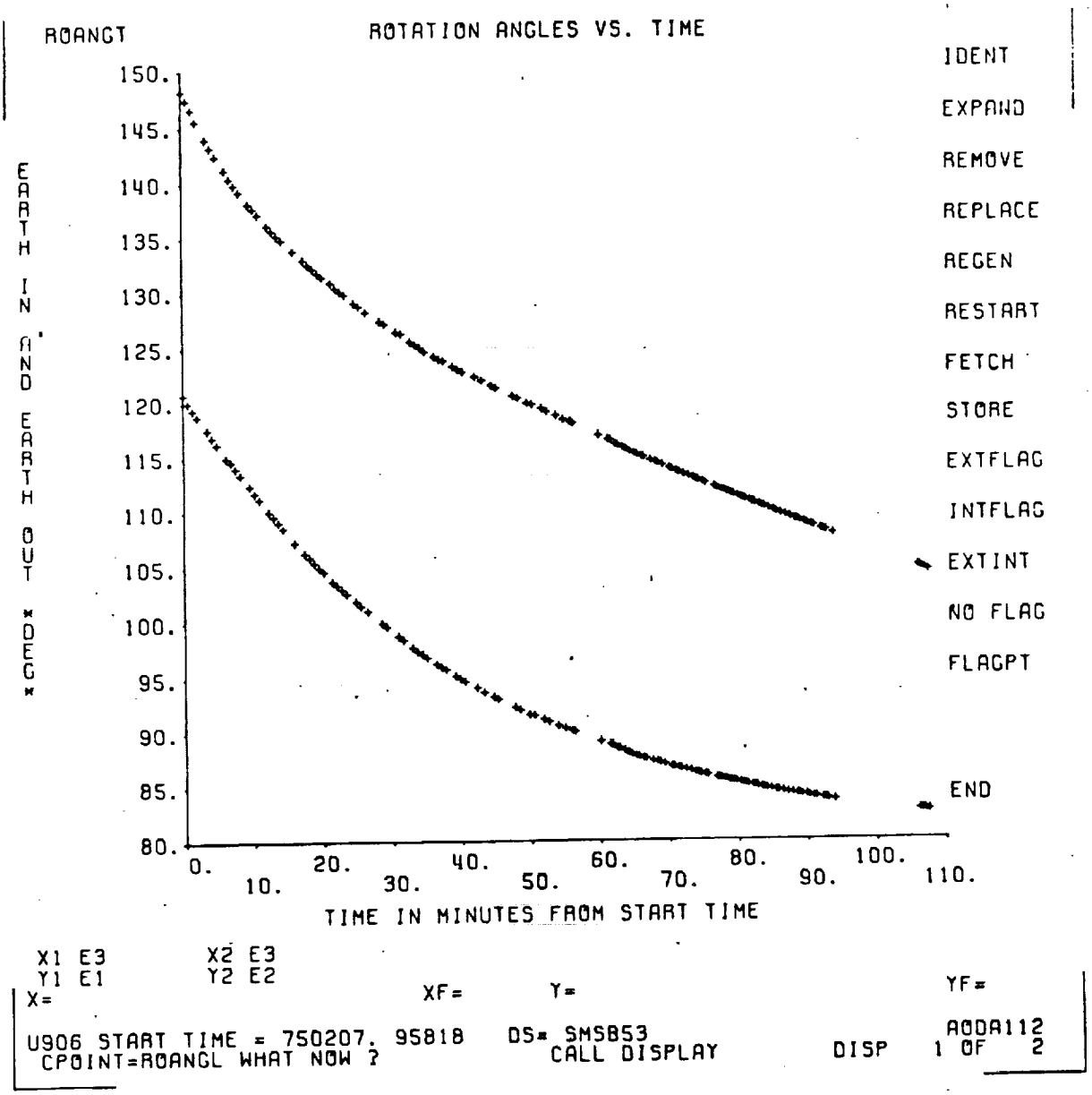

Figure 3-32. DS# SMSB53 Data Plots (2 of 3)

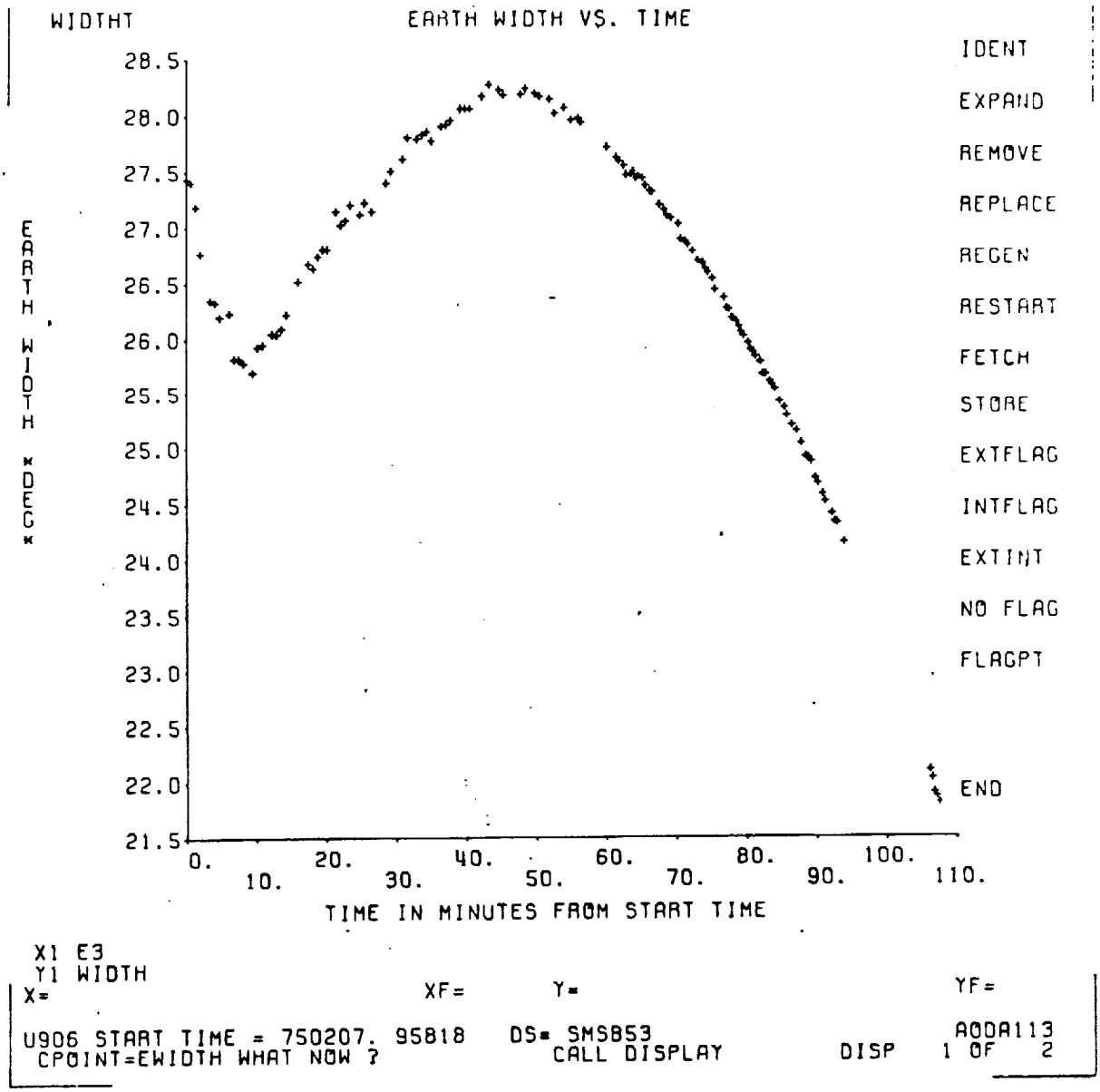

Figure 3-32. DS# SMSB53 Data Plots (3 of 3)

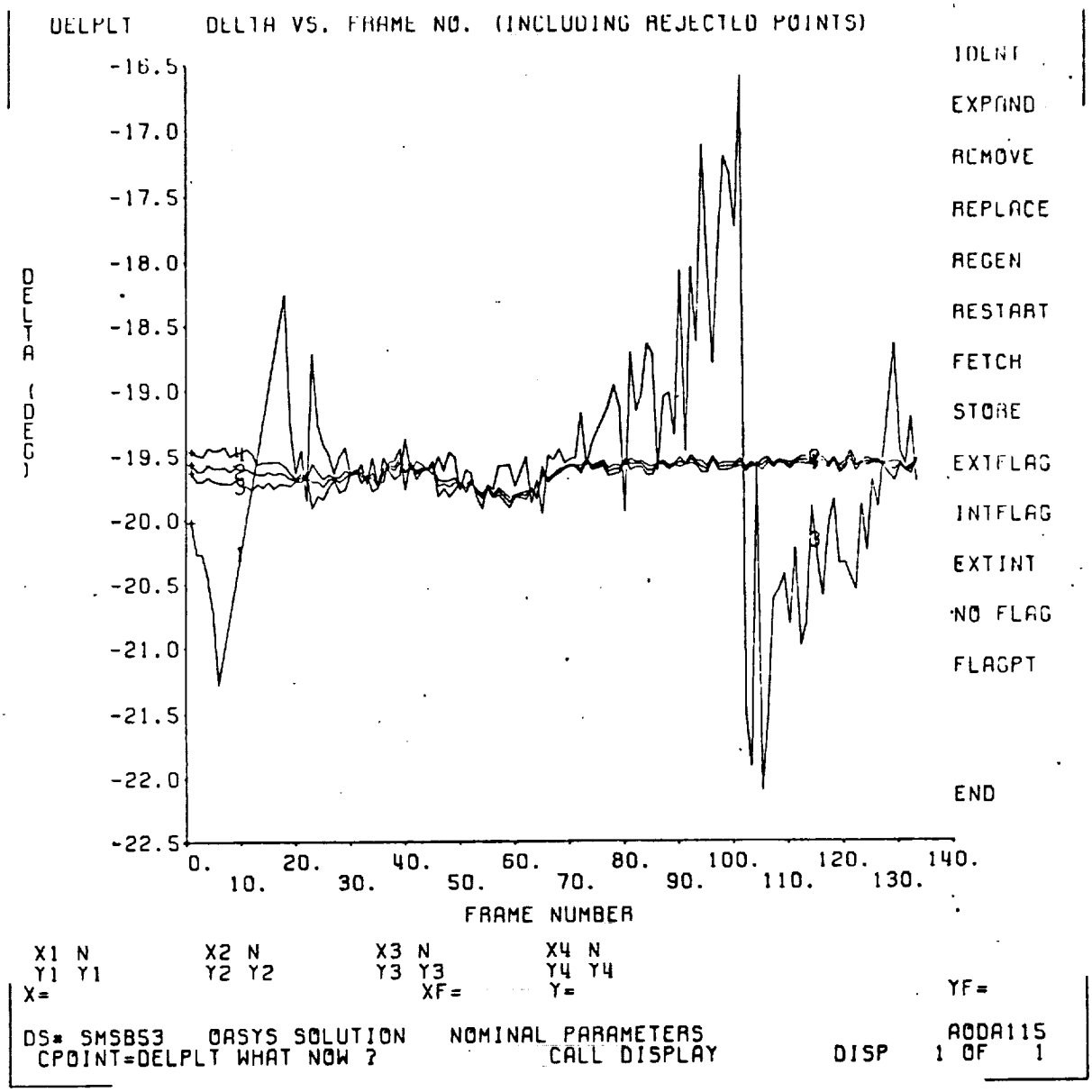

Figure 3-33. DS# SMSB53 Comparison of OASYS Solutions With Nominal and OABIAS Parameters (1 of 2)

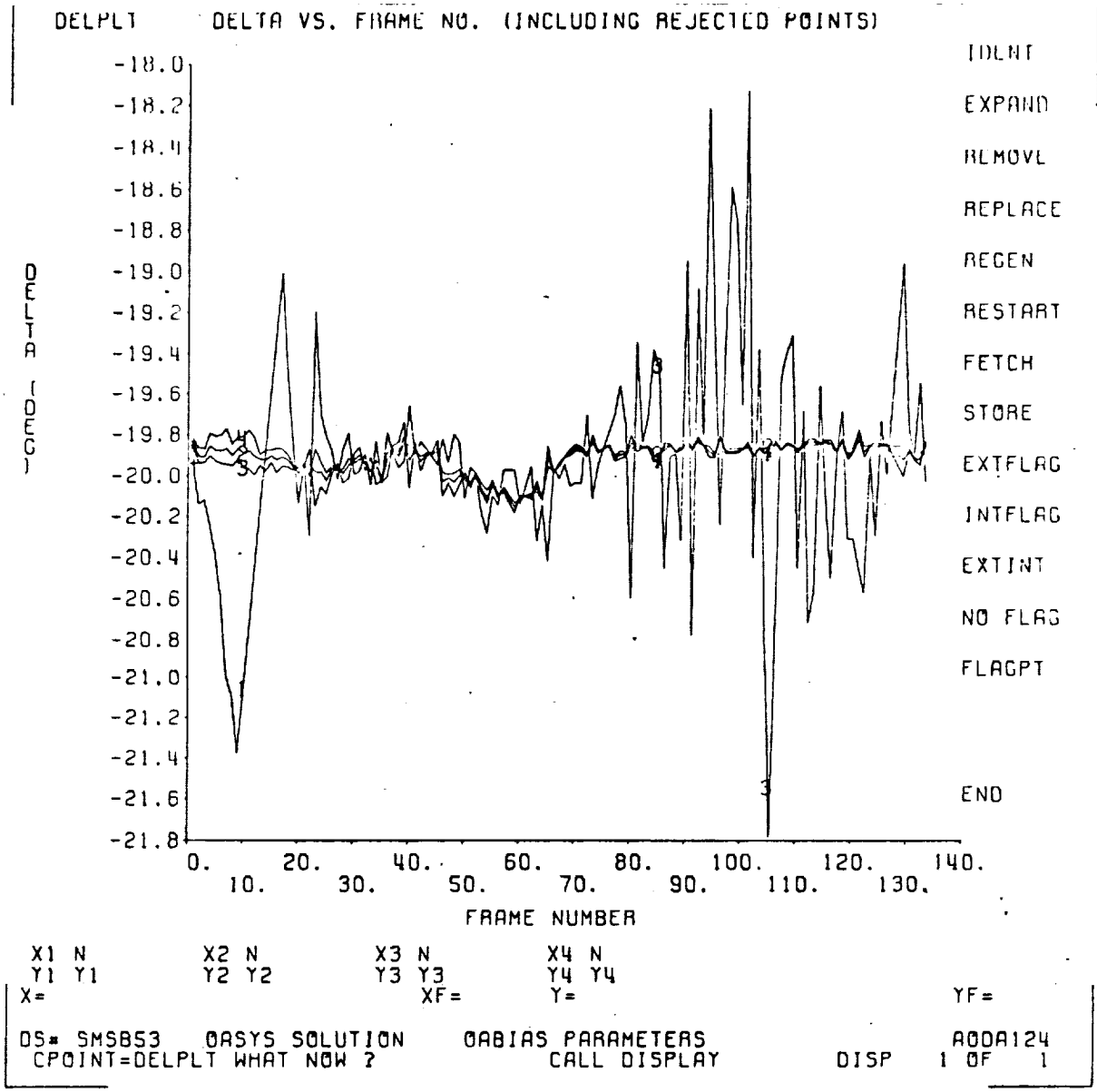

Figure 3-33. DS# SMSB53 Comparison of OASYS Solutions With Nominal and OABIAS Parameters (2 of 2)

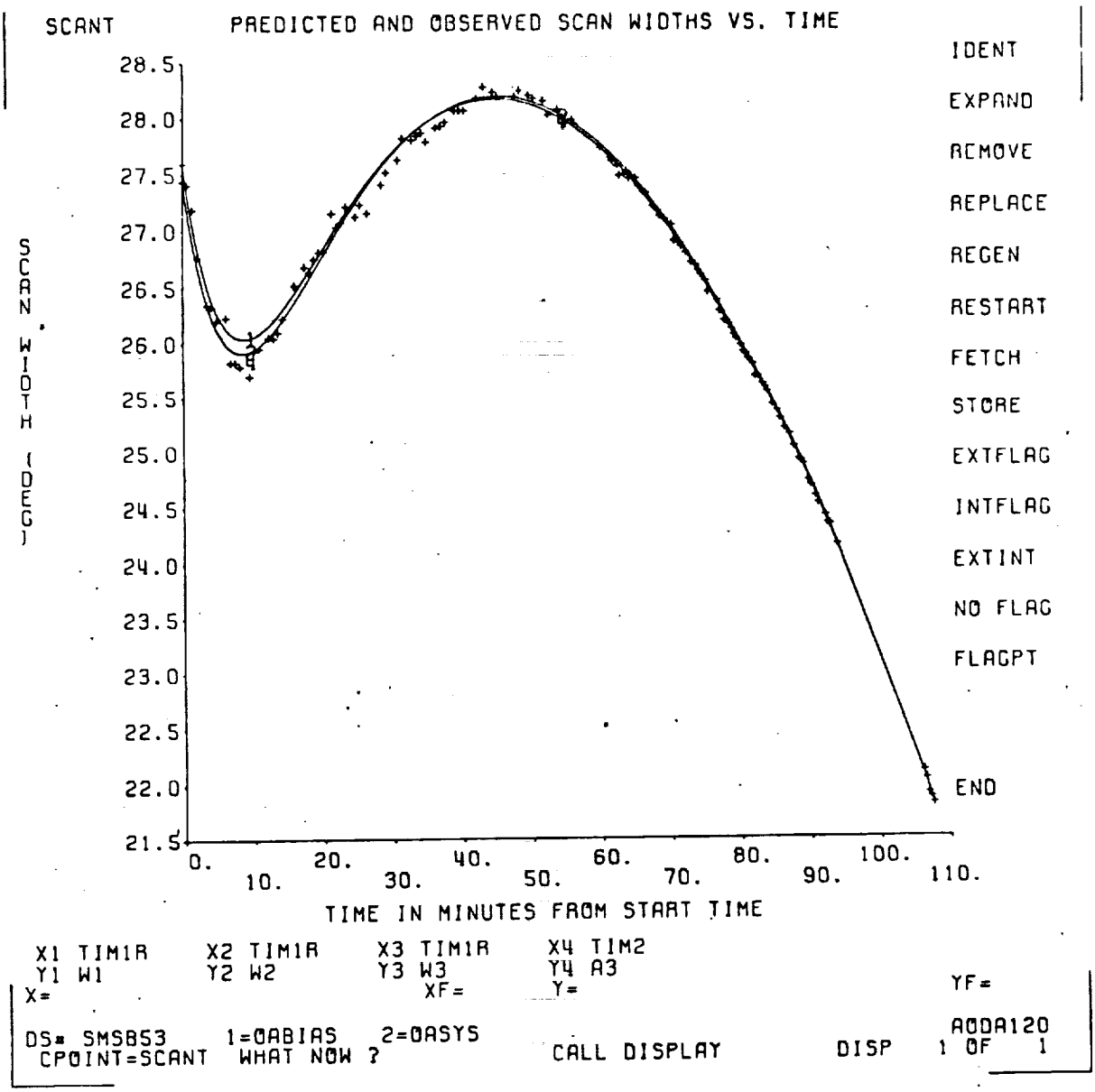

Figure 3-34. DS# SMSB53 Earth Width Plot for Nominal and OABIAS Solutions

3.4.3.4 Earth Sensor 4 Biases

Two data sets were available for Earth sensor 4 bias determination. One is DS#52 in the transfer orbit and the other is DS#59 in the second drift orbit. The bias determination results and the comparison of OABIAS and nominal parameters are given in Table 3-7. Again, the transfer orbit results are more uncertain than the drift orbit results and therefore are more lightly weighted in obtaining the mean values (see Section 3.5). In both data sets, $\Delta\phi^I$ was constrained to the same as $\Delta\phi^0$. The comparison table shows that the OABIAS results are much better than the nominal parameters, especially in DS#59.

Figures 3-35 to 3-37 and 3-38 to 3-40 are the data plots and predicted vs observed plots for DS#52 and 59 respectively. The Sun angle data of DS#52 (Figure 3-35(1)) shows strong systematic variations similar to that of DS#51 (Figure 3-20(1)). The poor quality of the OASYS deterministic results with OABIAS parameters obtained in DS#52 (Figure 3-36 (2)) implies a low reliability for these parameters. Although they are better than nominal parameters, there are still some systematic residuals remaining in the data. DS#59 is a very good data set except for the small glitches in the Sun angle data (Figure 3-38(1)). This data glitch did not affect the OABIAS solution as can be seen from Figure 3-39(3). The superiority of the OABIAS solution over the nominal solution on this data set is clear from Figures 3-39 and 3-40. In Figure 3-39 (1) and (2), the attitude solutions determined by the four different models exhibit dispersion over a very wide range while in Figure 3-39 (3) and (4), the four attitude solutions give constant attitudes within the data noise.

FOLDOUT FRAME 1

OABIAS Bias Result

DS#	52	
Orbit	Transfer	
Biases	Value	Statistica Unc.
$\Delta\gamma$	.44	.082
$\Delta\phi$	-.20	.056
$\Delta\phi$	-.20	.056
$\Delta\rho$	-.06	.030

Comparison of OABIAS and Nominal Parameters

OASYS				Using Nominal Parameters	U
Deter-ministic Results	Right Ascension, α (Deg)			25.06	
	Declination, δ (Deg)			-20.03	
	Standard Deviation		Arc Length	.41	
			α	.11	
			δ	.39	
Fit to Data	Rot. Angle	Mean Residual		.030	
		STDV		.150	
		% of Good Fit[3]		90%	
		Maximum Deviation[4]		.2°	
	Central Body Width	Mean Residual		-.110	
		STDV		.187	
		% of Good Fit[3]		50%	
		Maximum Deviation[4]		.2°	

FOLDOUT FRAME 2

Table 3-7. Earth Sensor-4 Bias Determination Results

	59			Weighted Mean	Unc. of the Mean
	Drift 2				
Total Unc.	Valve	Statistical Unc.	Total Unc.		
.484	-.01	.022	.130	.020	.126
.330	-.40	.028	.165	-.360	.148
.330	-.40	.028	.165	-.360	.148
.177	.03	.015	.089	.012	.080

sing OABIAS Results	Using Nominal Parameters	Using OABIAS Results
24.69	38.13	37.96
-19.57	-14.05	-63.51
.29	.39	.09
.11	.13	.10
.27	.39	.08
.023	.217	-.034
.131	.342	.084
90%	50%	100%
.2°	.5°	-
-.053	.407	.048
.155	.509	.064
65%	0%	40%
.2°	.5°	.03°

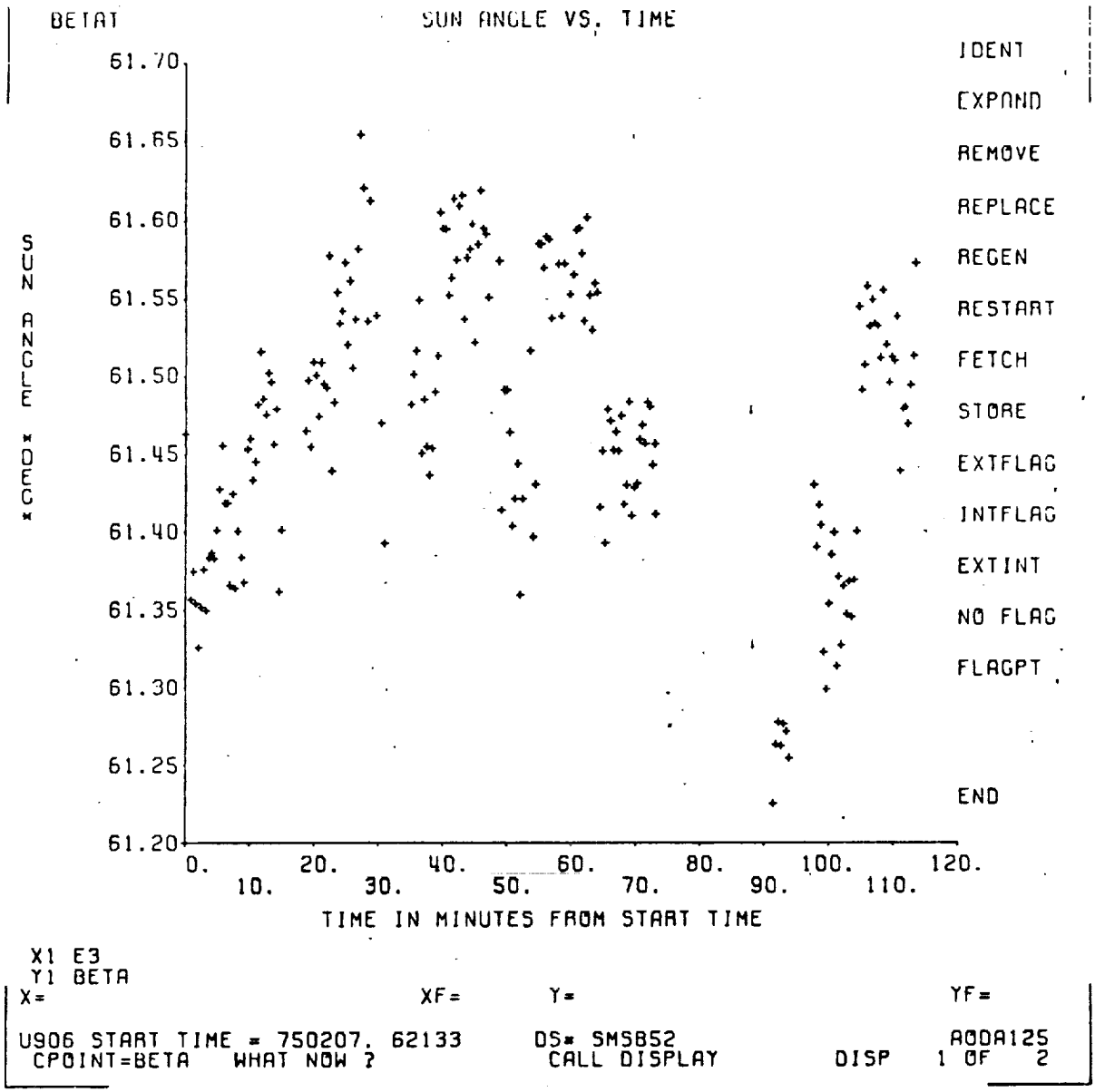

Figure 3-35. DS# SMSB52 Data Plots (1 of 2)

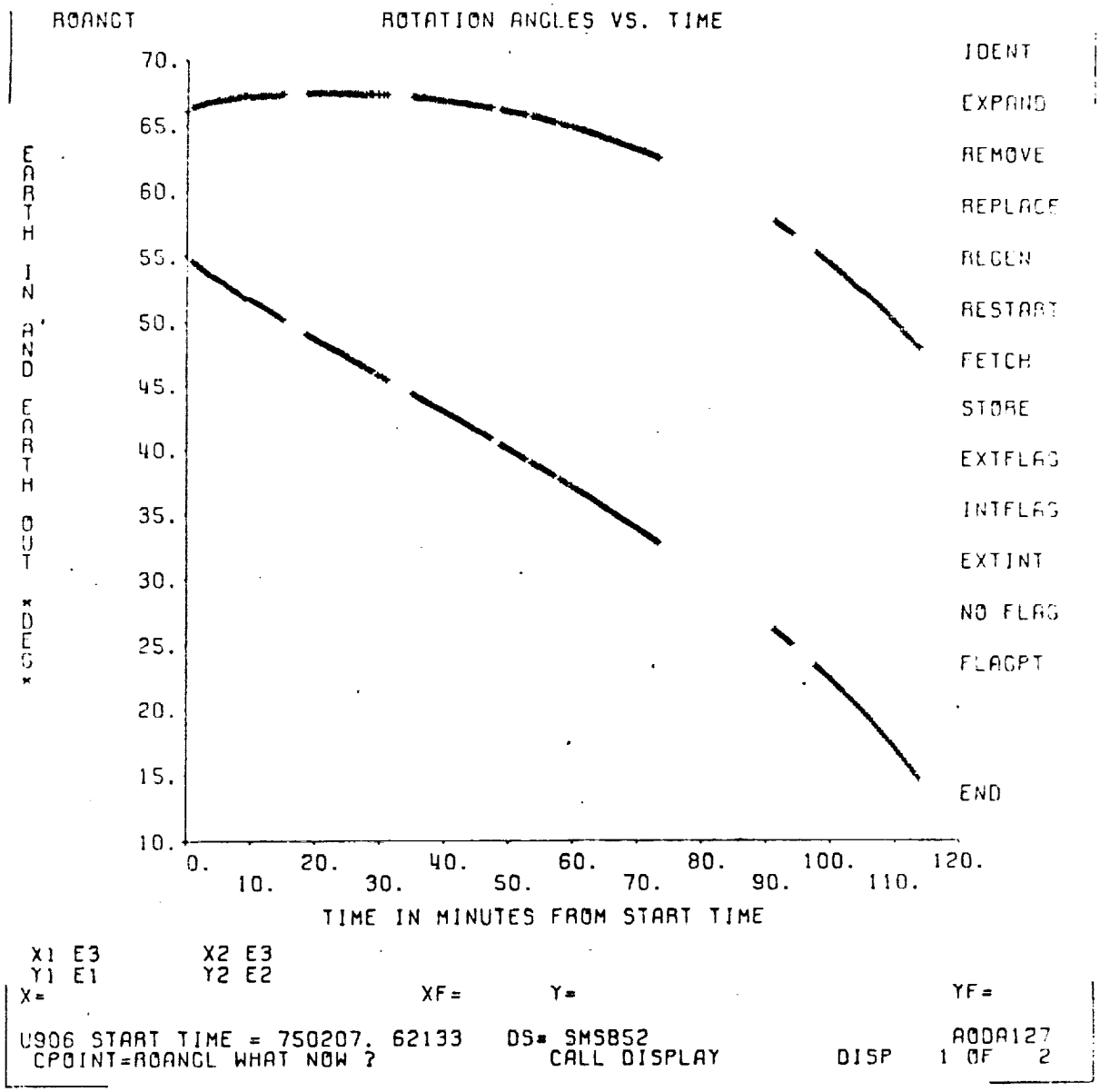

Figure 3-35. DS# SMSB52 Data Plots (2 of 3)

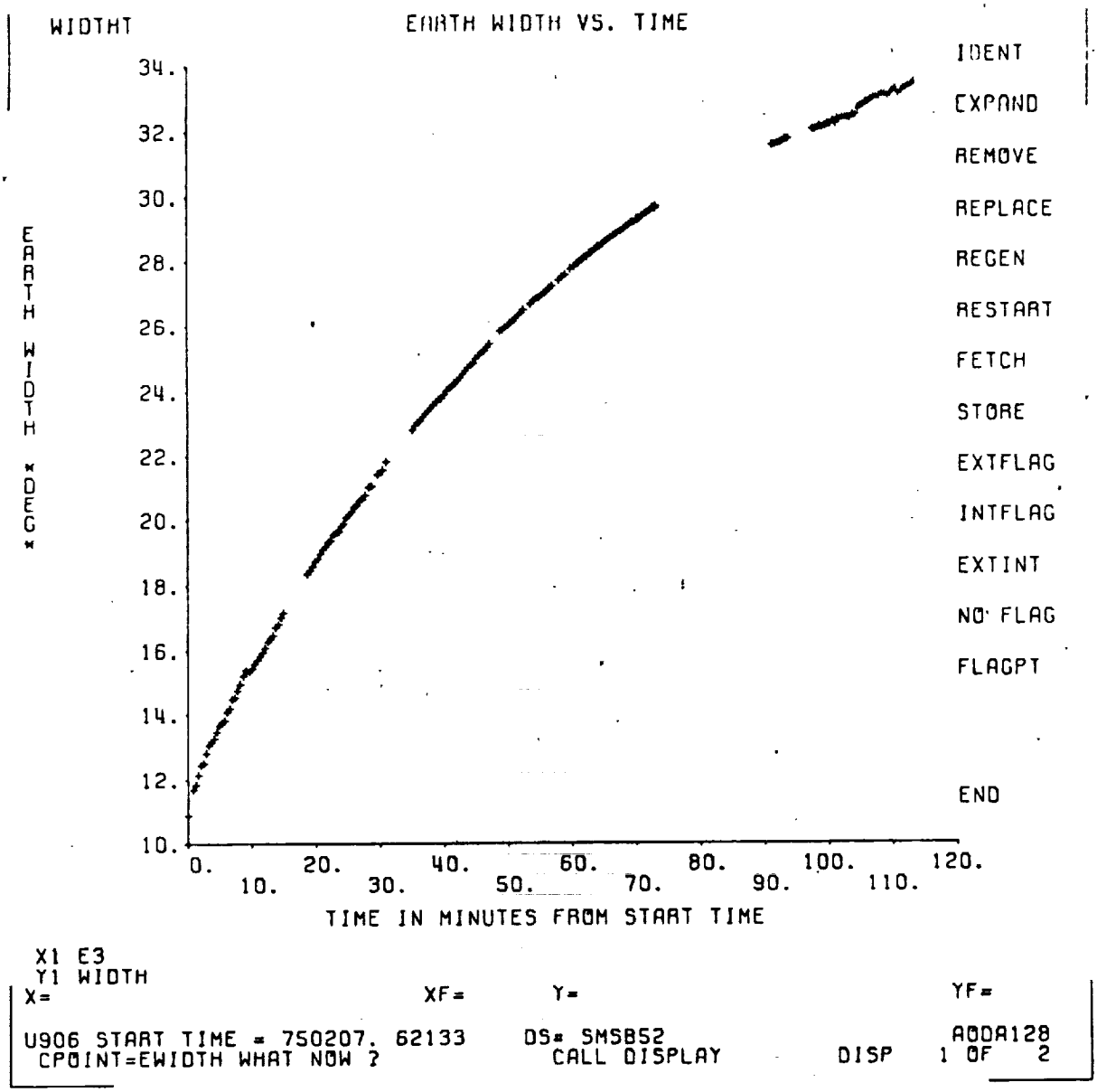

Figure 3-35. DS# SMSB52 Data Plots (3 of 3)

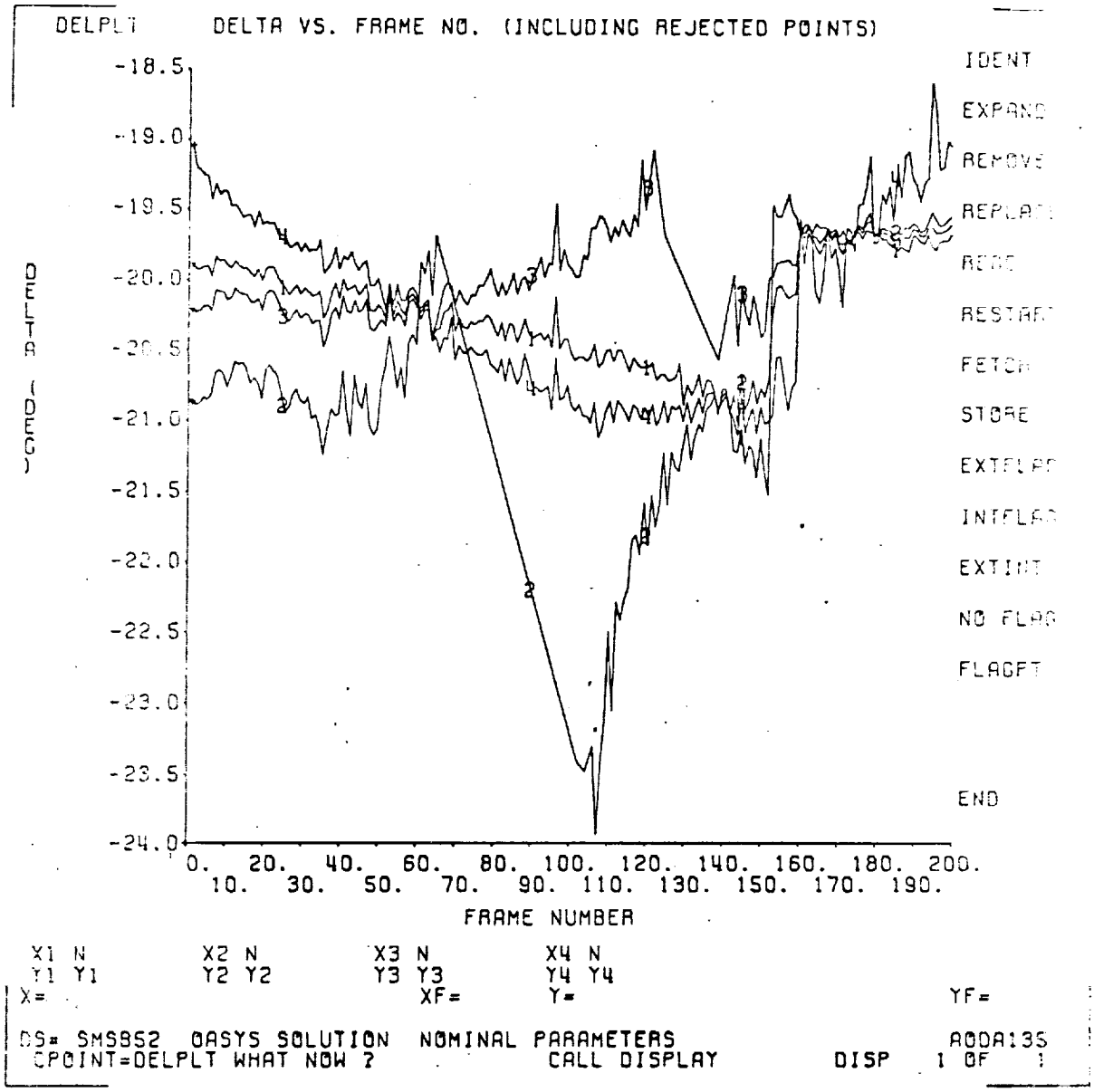

Figure 3-36. DS# SMSB52 Comparison of OASYS Solutions With Nominal and OABIAS Parameters (1 of 2)

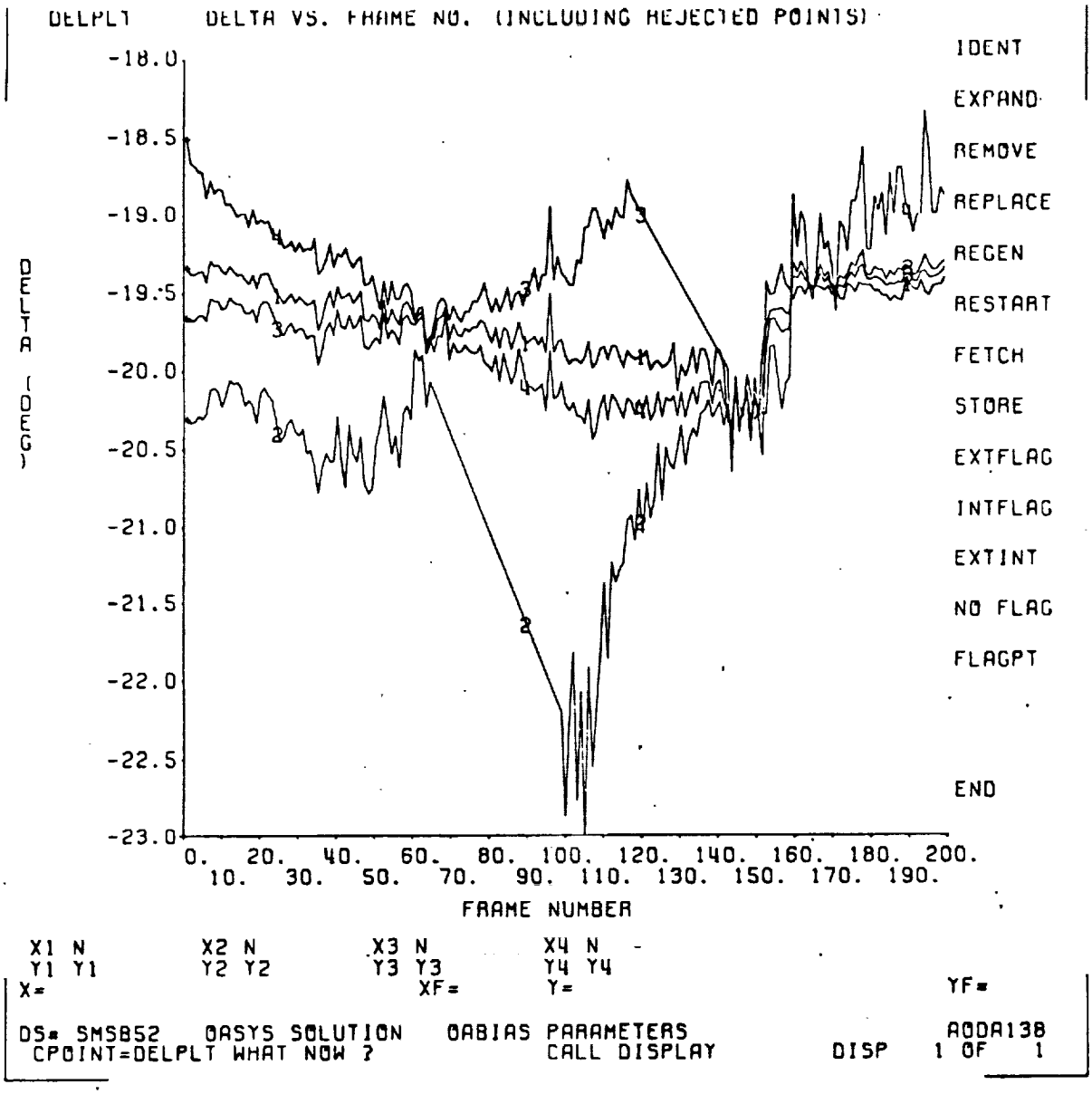

Figure 3-36. DS# SMSB52 Comparison of OASYS Solutions With Nominal and OABIAS Parameters (2 of 2)

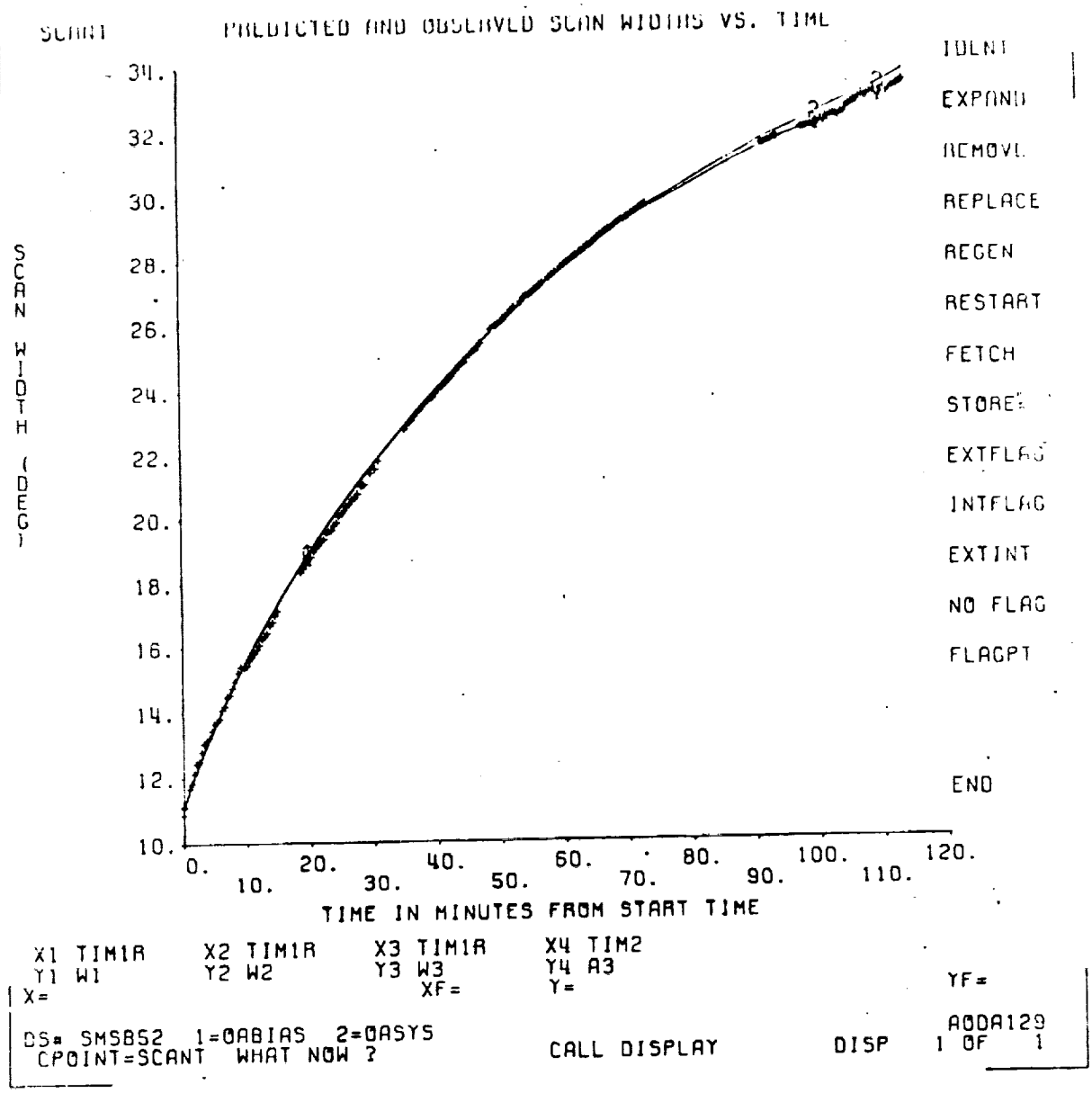

Figure 3-37. DS# SMSB52 Earth Width Plot for Nominal and OABIAS Solutions

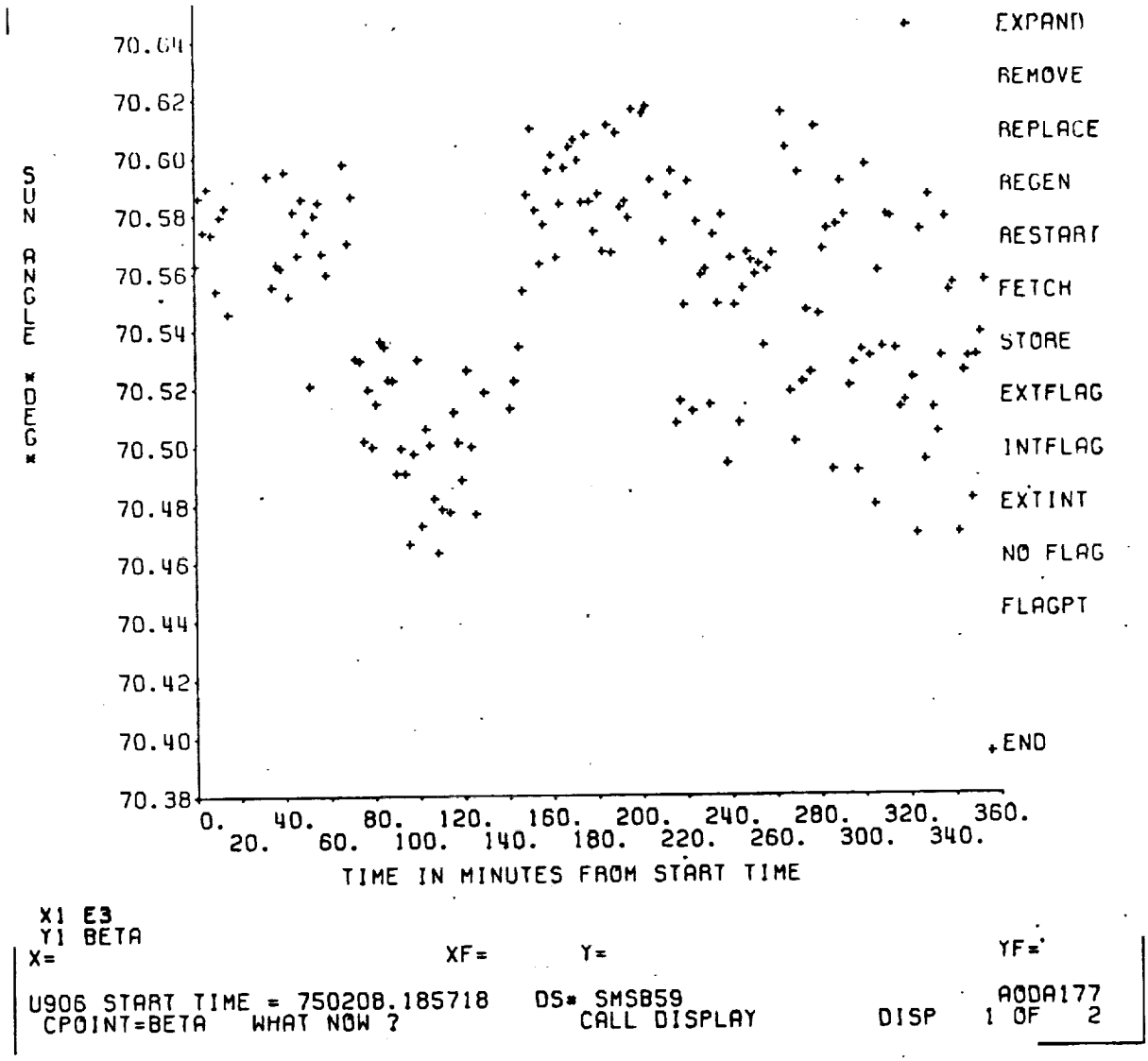

Figure 3-38. DS# SMSB59 Data Plots (1 of 3)

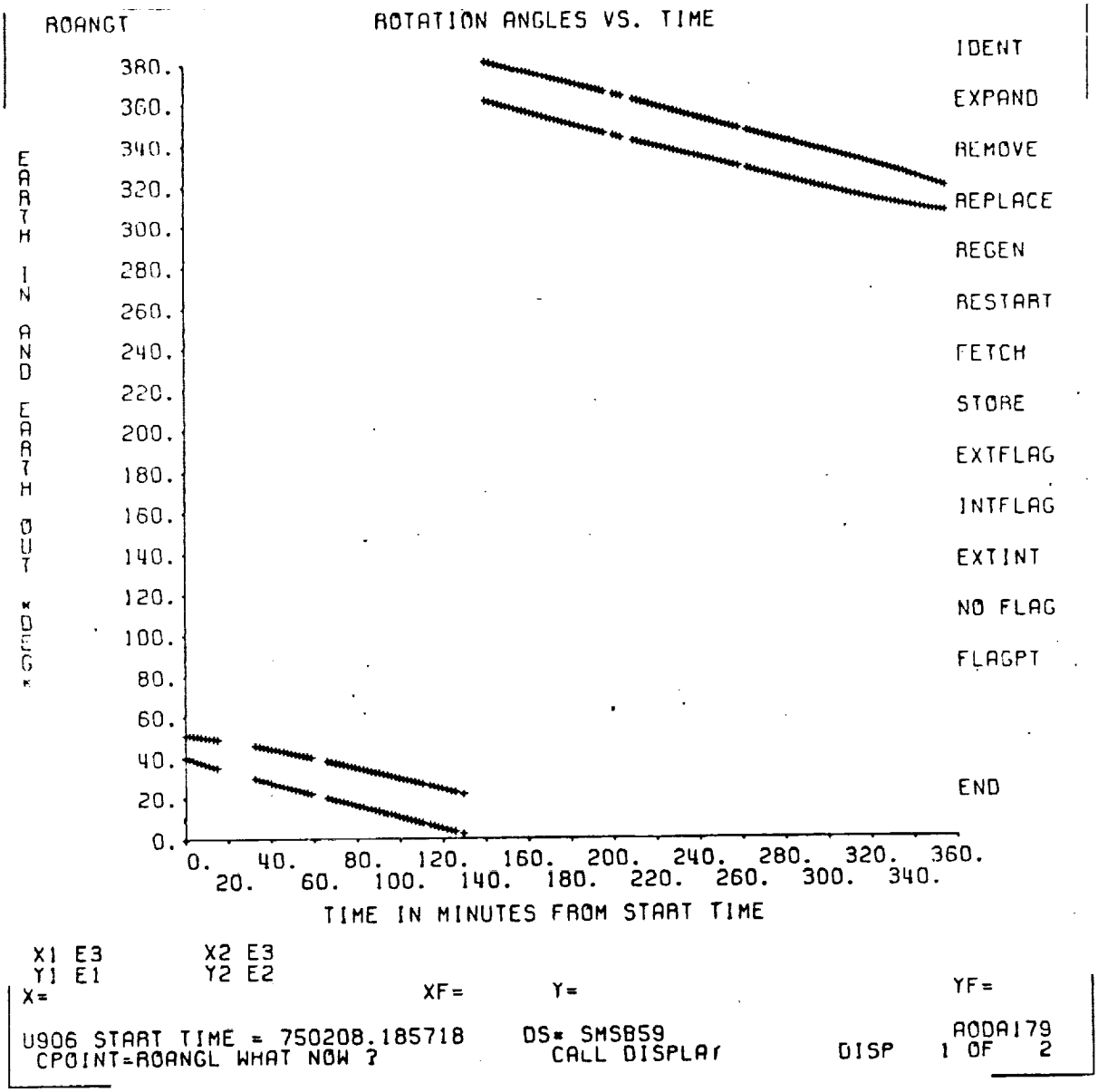

Figure 3-38. DS# SMSB59 Data Plots (2 of 3)

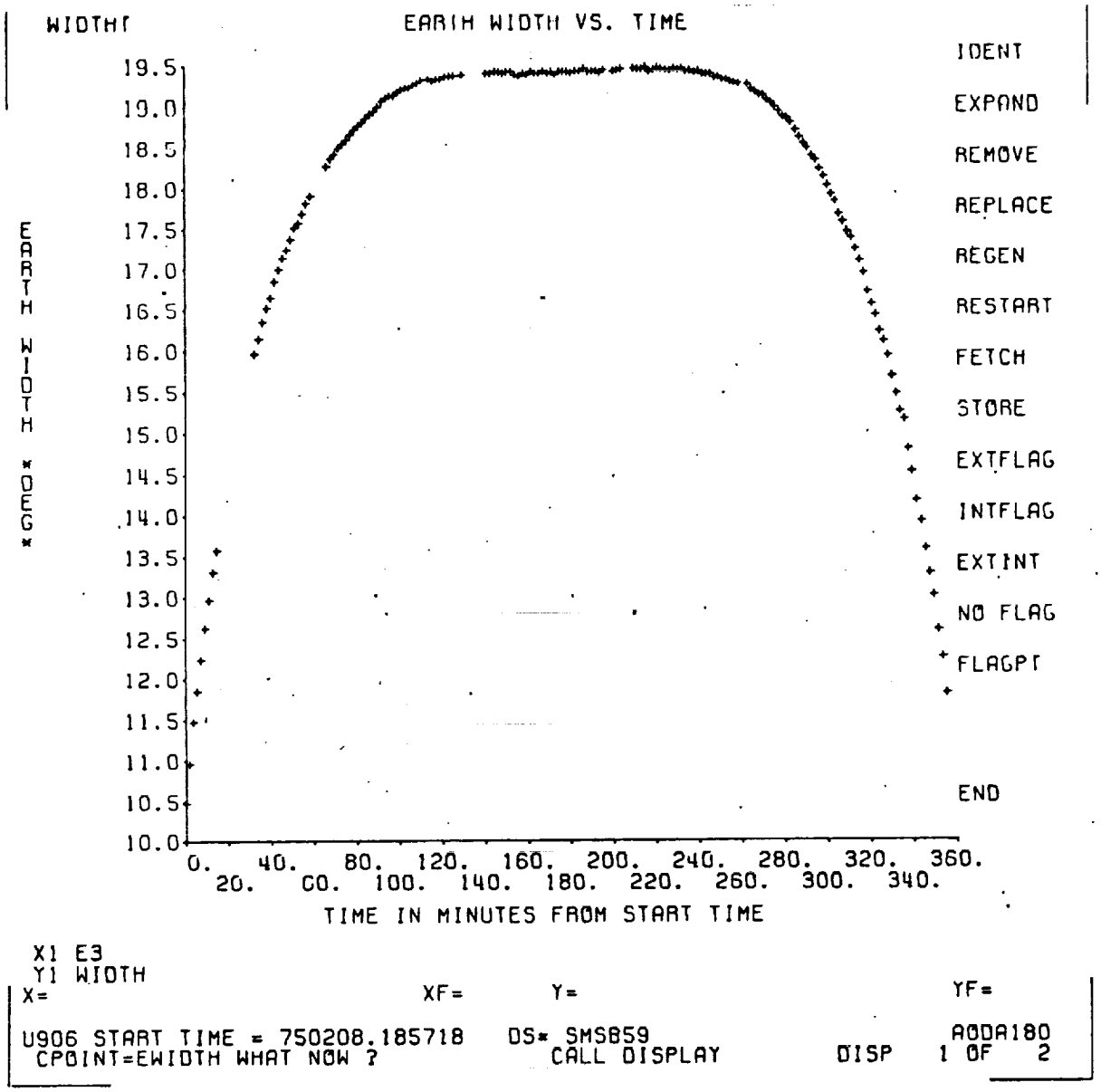

Figure 3-38. DS# SMSB59 Data Plots (3 of 3)

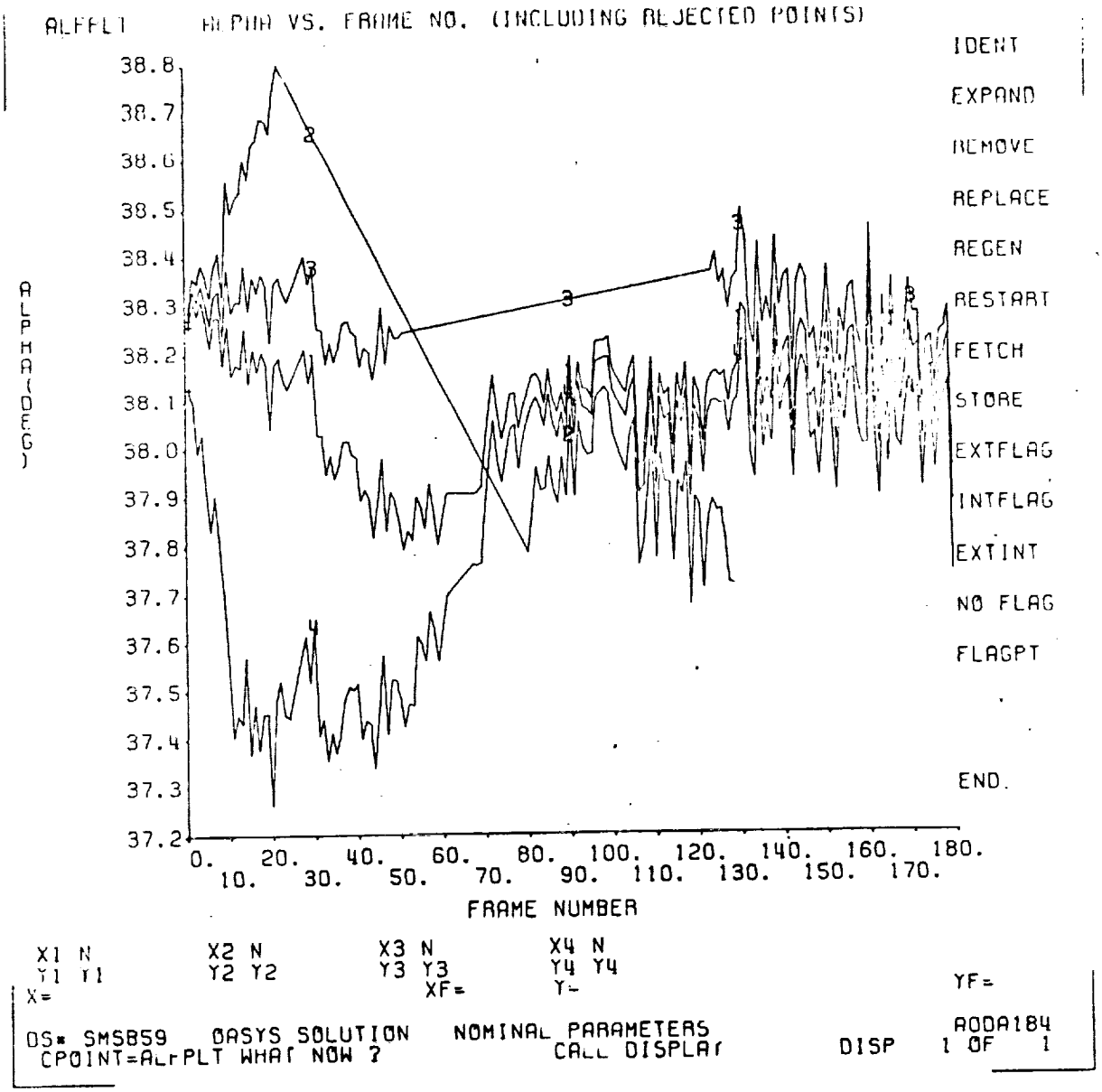

Figure 3-39. DS# SMSB59 Comparison of OASYS Solutions With Nominal and OABIAS Parameters (1 of 4)

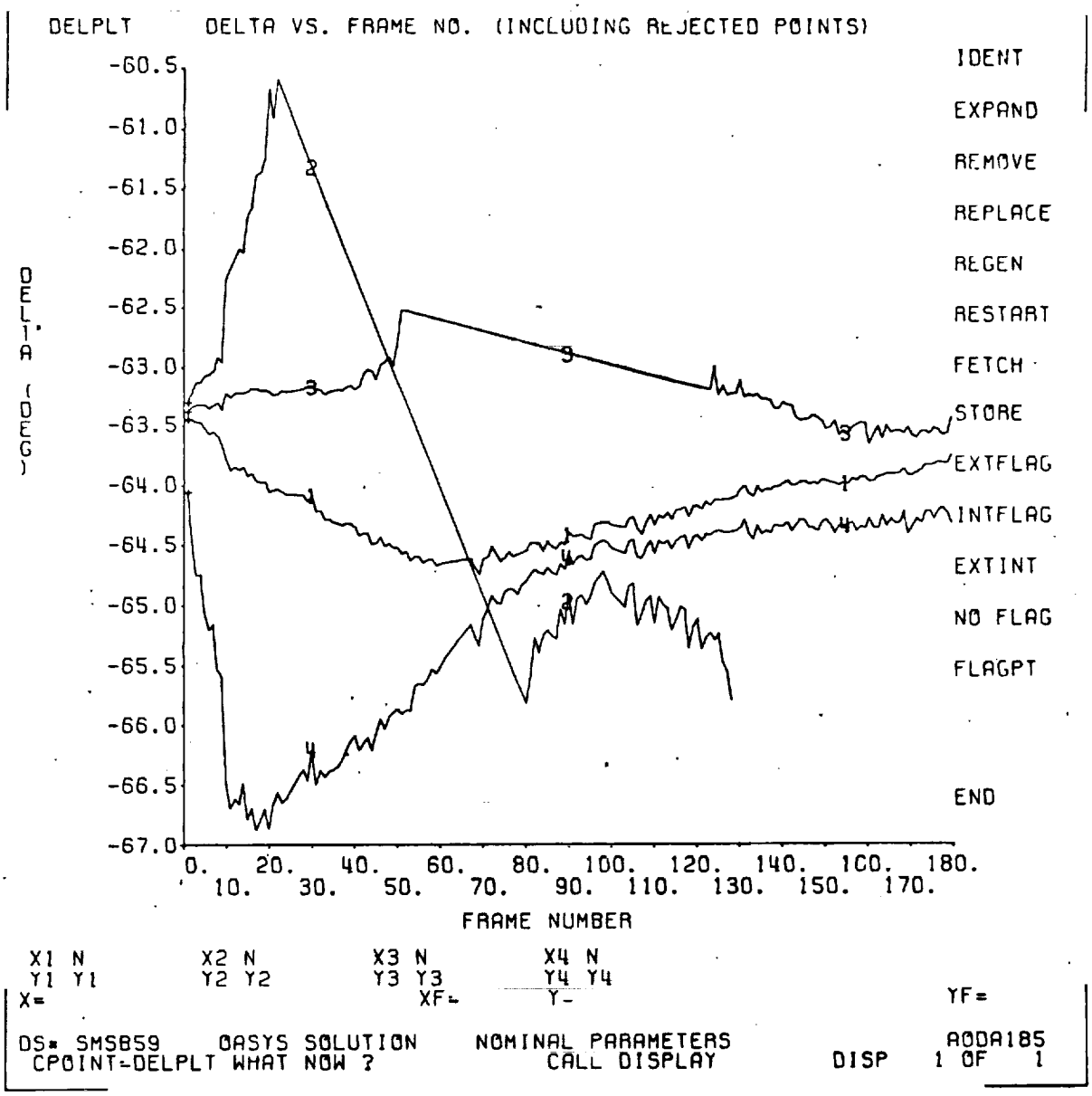

Figure 3-39. DS# SMSB59 Comparison of OASYS Solutions With Nominal and OABIAS Parameters (2 of 4)

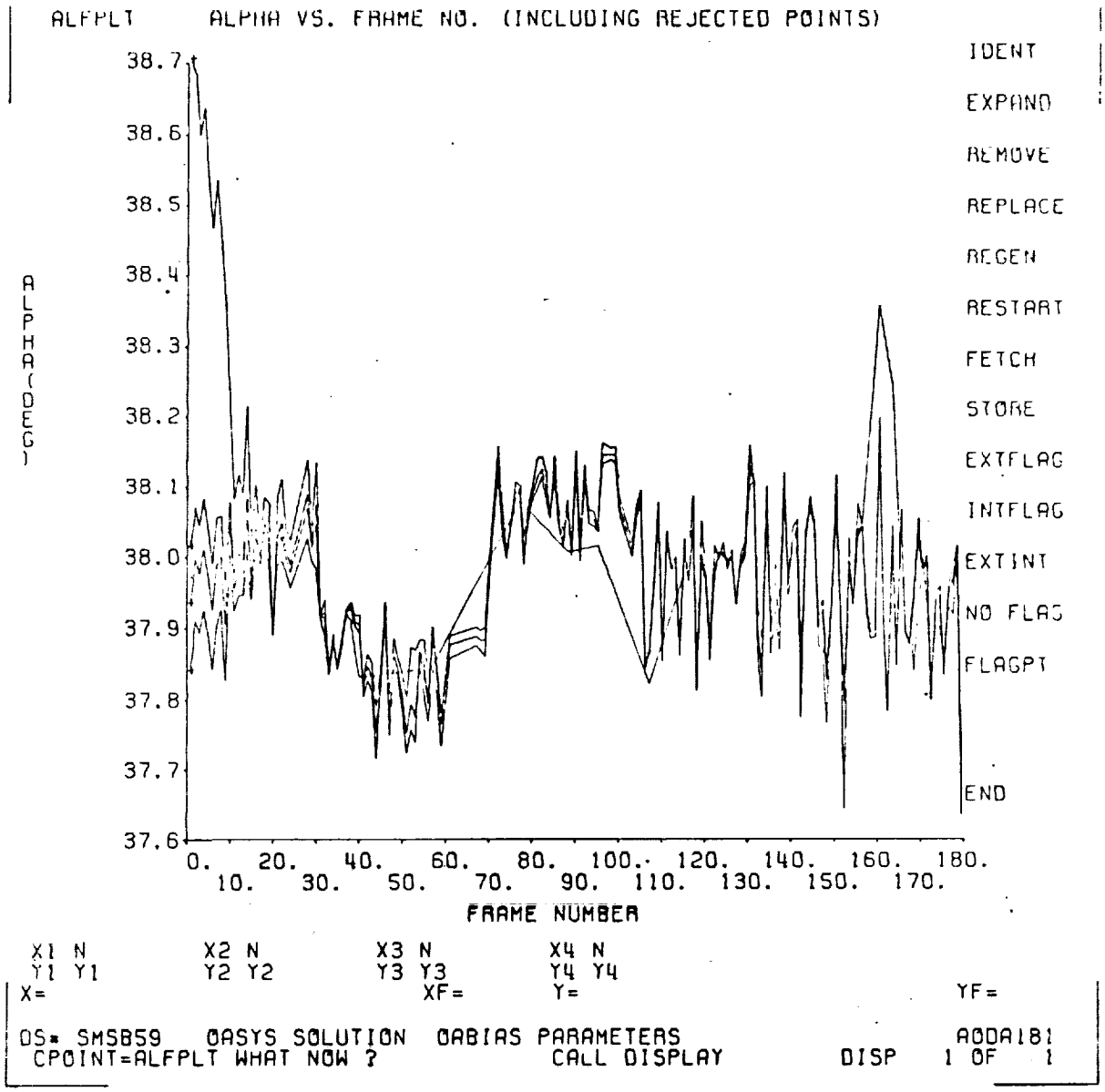

Figure 3-39. DS# SMSB59 Comparison of OASYS Solutions With Nominal and OABIAS Parameters (3 of 4)

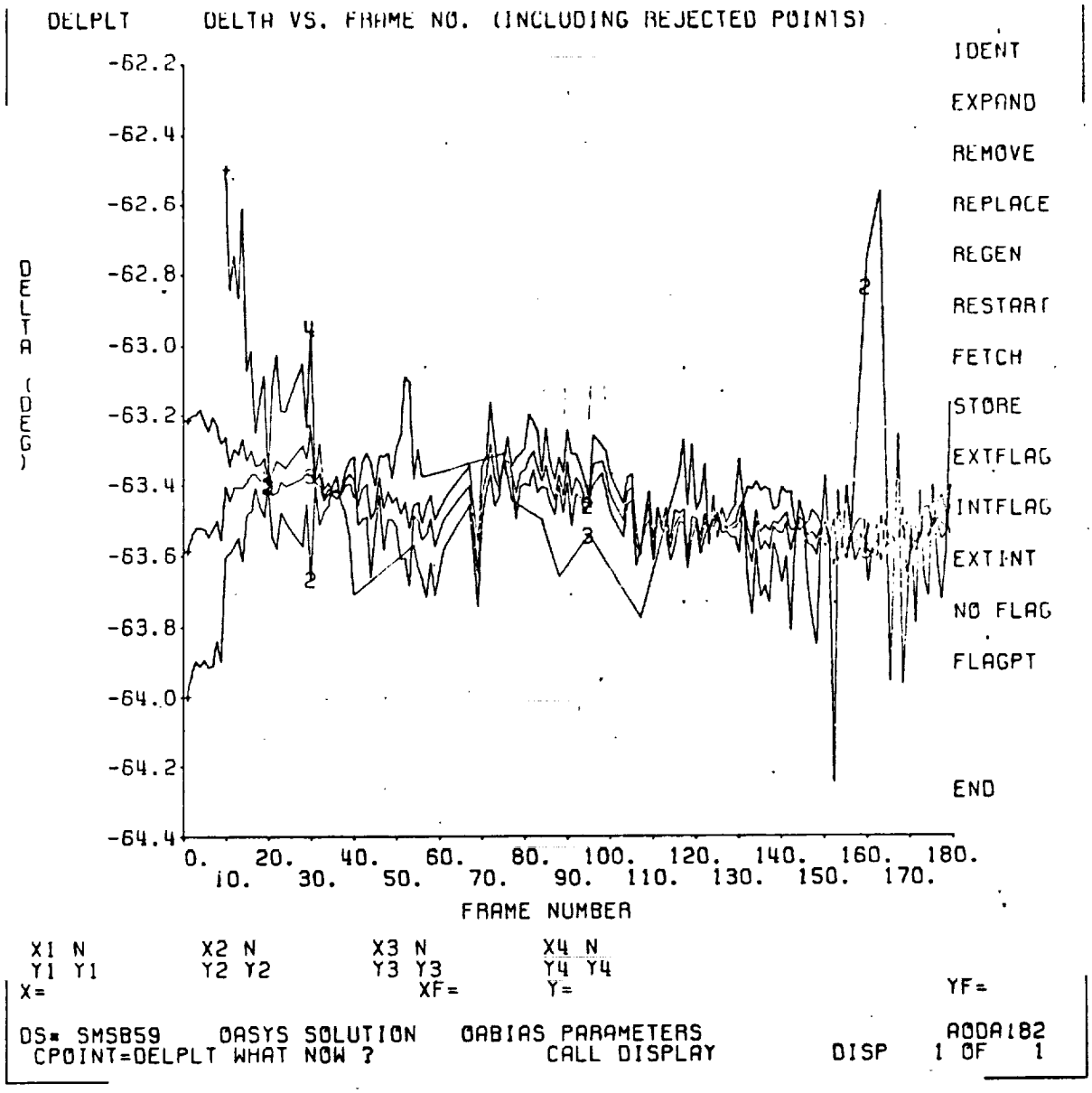

Figure 3-39. DS# SMSB59 Comparison of OASYS Solutions With Nominal and OABIAS Parameters (4 of 4)

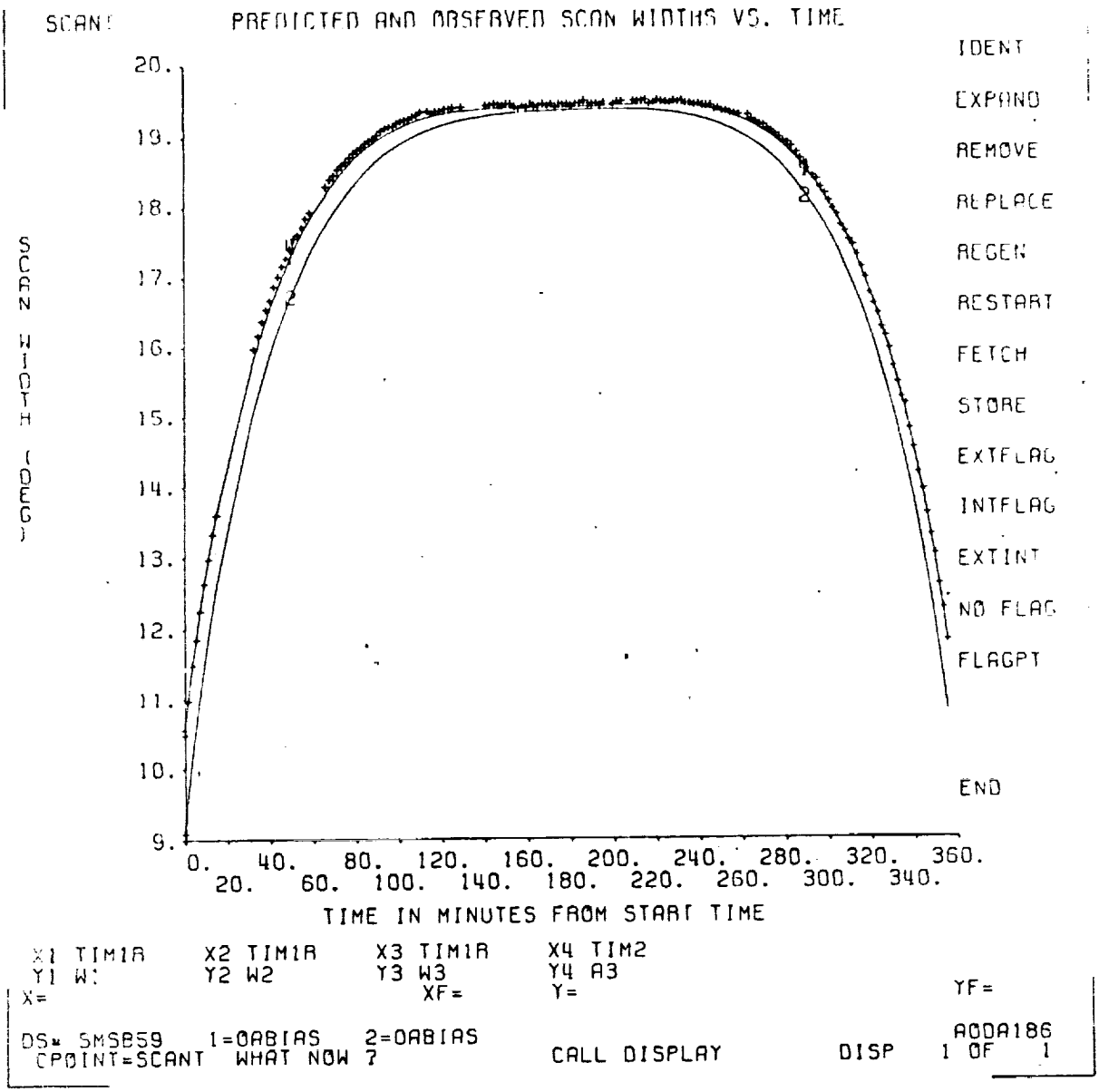

Figure 3-40. DS# SMSB59 Earth Width Plot for Nominal and OABIAS Solutions

3.4.3.5 Earth Sensor-5 Biases

The only data set available for bias determination on Earth Sensor 5 is DS#55. As pointed out in Section 3.3, this data set exhibits a very strong pagoda effect which extends to an Earth width of about 21°. This Earth width is 80 percent of the Earth's diameter as seen by ES5 and thus seriously interferes with bias determination efforts. It was not possible to get reliable bias results for this data set until processing of the remainder of the SMS-2 data had been completed. It was then possible to fix the Sun angle bias at its measured mean value of -0.185° (see Section 3.4.4) and solve for the remaining biases. The bias determination results so obtained are shown in Table 3-8. Again, the lower part of the table shows that the OABIAS results are much superior to the nominal parameters.

Most of the relevant plots for this data are included in the discussion of the pagoda effect in Section 3.3. For the remaining plots, see Reference 11.

Table 3-8. Earth Sensor-5 Bias Determination Results

OABIAS Results

DS#	55		
Orbit	Drift Orbit I		
Biases	Value	Statistical Uncertainty	Total Uncertainty
$\Delta\gamma$	.27	.011	.067
$\Delta\Omega^I$	-.15	.029	.171
$\Delta\Omega^\circ$	-.32	.029	.171
$\Delta\rho$	-.01	.011	.065

Comparison of OABIAS and Nominal Parameters

			Using Nominal Parameters	Using OABIAS Results
	Right Ascension, α (Deg)		26.55	26.34
	Declination, δ (Deg)		-19.81	-19.74
	Standard Deviation	Arc Length	.30	.09
		α	.06	.05
		δ	.30	.07
Fit to Data	Rotation Angle	Mean Residual	.215	-.016
		STDV	.381	.098
		% of Good Fit[3]	0%	90%
		Maximum Deviation[4]	0.7°	.1°
	Central Body Width	Mean Residual	.443	.005
		STDV	.574	.065
		% of Good Fit[3]	0%	100%
		Maximum Deviation[4]	.4°	-

ORIGINAL PAGE IS OF POOR QUALITY

3.4.4 Sun Sensor Biases

Although there are two Sun sensors on board SMS-2, only one of them, Sun sensor-2 (SS2) was used during the early portion of the mission covered by this report. Therefore all of the Sun angle biases determined from the SMS-B data sets are for SS2. The only information available for SS1 is from two "Sun sensor switch" experiments which are discussed later in this section.

Table 3-9 summarizes the OABIAS bias determination results for SS2. Six data sets contribute to this measurement; two from the transfer orbit (DS#52 and 53), two from drift orbit No. 2 (DS#59 and 60) and two from drift orbit No. 3. As usual, the results from the transfer orbit have high uncertainties and therefore have low weight in determining the mean. The results obtained from the four drift orbit data sets give good agreement within each orbit but shift by nearly $.1^{o}$ between the two orbits. This implies that systematic errors remain in the data or the orbit parameters as discussed in Section 3.4.2.

Figure 3-41 shows the Sun angle plots for the two Sun-sensor switch experiments. Figure 3-41 (1) shows data from the Sun sensor switch performed during the transfer orbit. The Sun sensor was switched from SS2 to SS1 at approximately 15 minutes from the start time and was switched back to SS2 at about 50 minutes from the start time.

Note the two sharp changes of about 0.25^{o} on the Sun angle measurements corresponding to the two switches. Exact measurements of the magnitudes of these jumps are not meaningful because of the strong systematic variations of the Sun angle data during this time span due to spin axis attitude motion. The normal drift rate of the Sun angle for this time span should be -0.0006^{o}/min., which means a decrease of about 0.04^{o} for the plot period of 65 minutes, while the data shows an increase of about 0.5^{o} for the same period of time.

Table 3-9. OABIAS Bias Result for Sun Sensor-2

DS#	Orbit	$\Delta\beta$	Statistical Uncertainty	Total Uncertainty	Weighted Mean	Uncertainty of the Mean
52	Transfer	-.29	.08	.472	-.185	.044
53	Transfer	-.23	.09	.530		
59	Drift 2	-.13	.015	.088		
60	Drift 2	-.14	.015	.088		
63	Drift 3	-.25	.024	.141		
64	Drift 3	-.22	.012	.071		

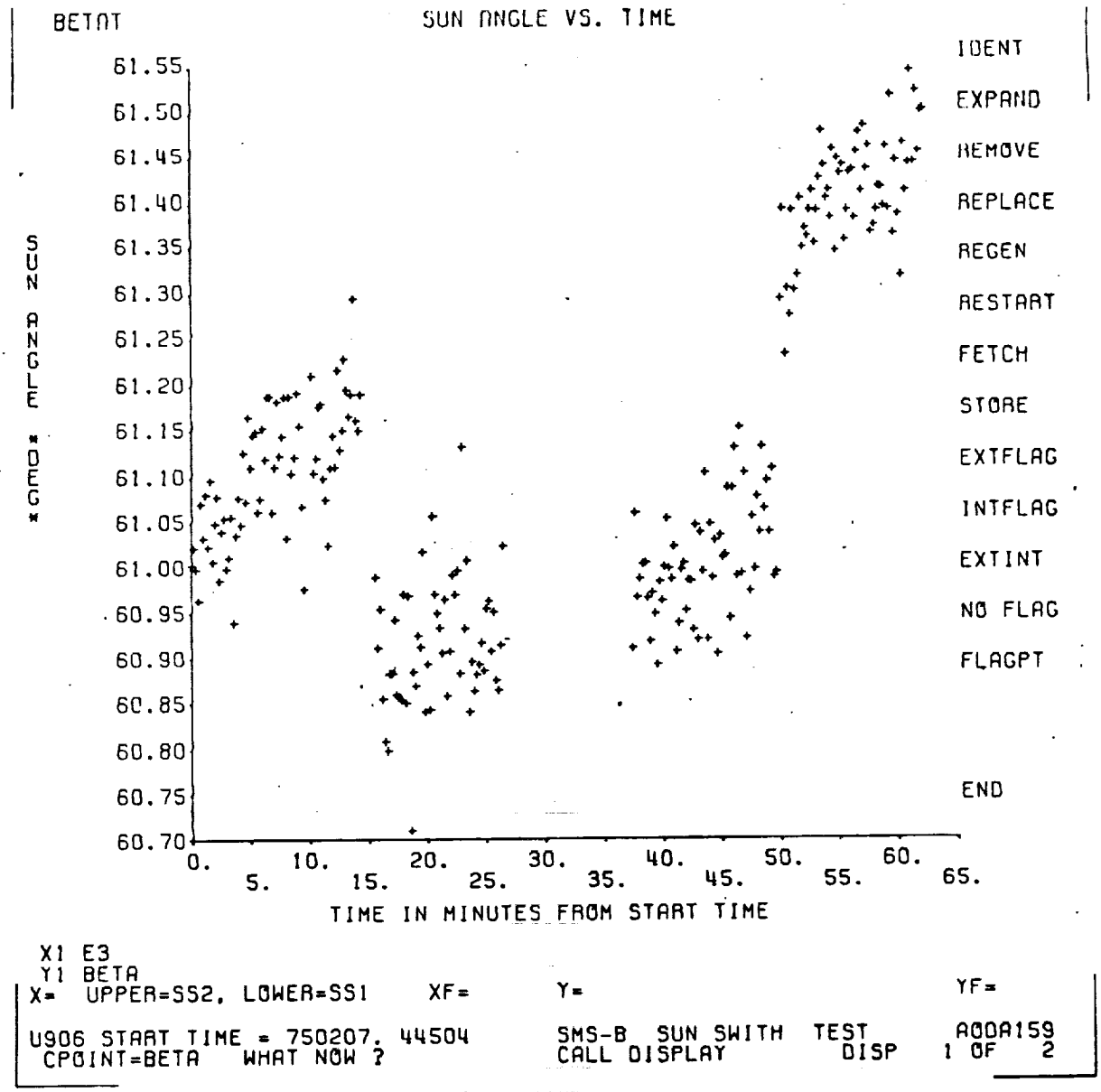

Figure 3-41. Sun Sensor Switch Experiments (1 of 2)

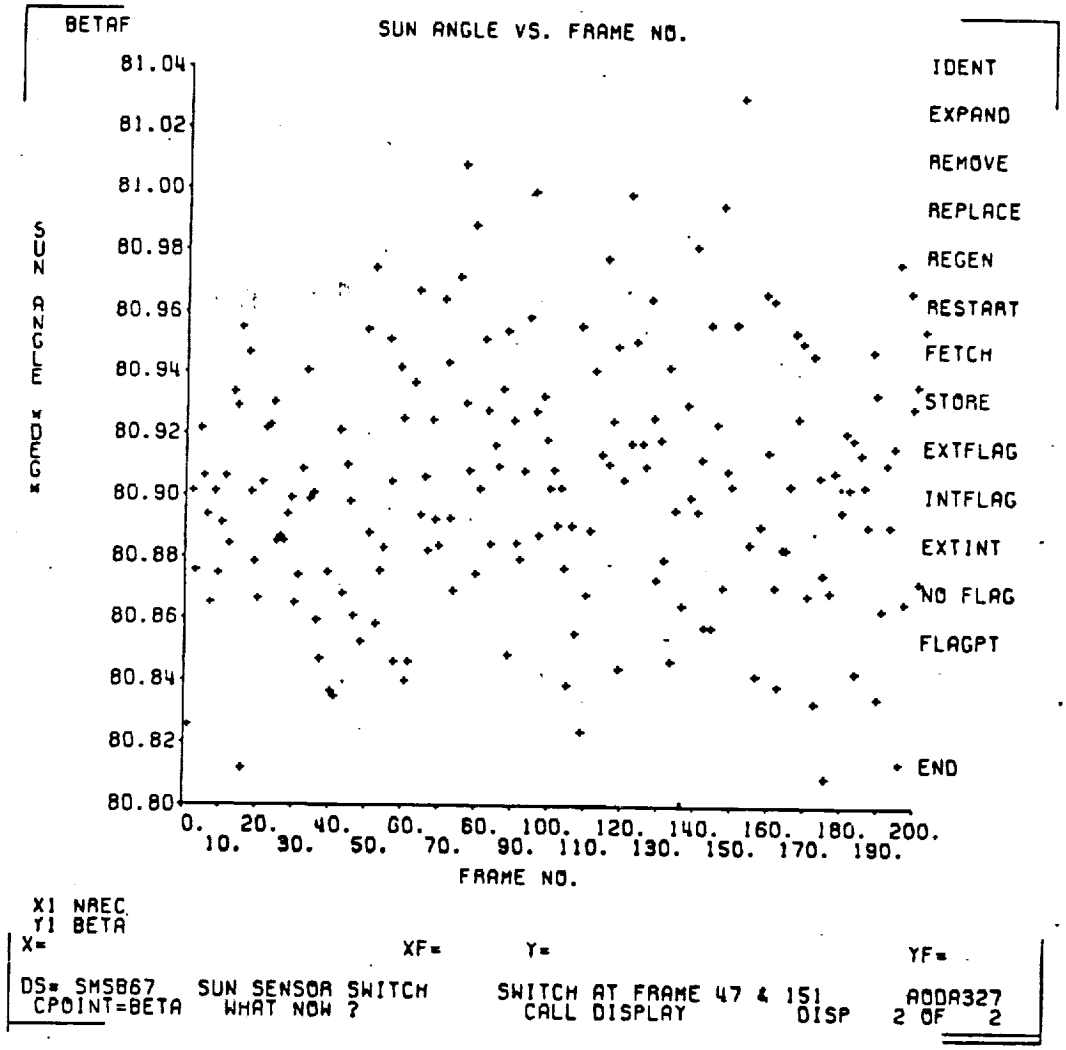

Figure 3-41. Sun Sensor Switch Experiments (2 of 2)

The discrepancy of about 0.25^{o} between the two sensors may be due to a mounting misalignment or it may be due to the fact that at a Sun angle of about 60^{o}, the Sun is at the end of the field of view of SS1[1]. Thus, an inaccurate calibration at the edges of the field of view is possible.

Another Sun-sensor switch performed in the mission orbit is shown in Figure 3-41 (2). Here the Sun sensor was switched from SS2 to SS1 and back to SS2 at frames 47 and 151, respectively. The Sun angle measured by Sun Sensor 1 is larger than that measured by Sun Sensor 2 by 0.02 ± 0.006 degrees.

In summary, the SS2 bias was determined from six data sets in three different orbits. A mean value of $-0.185^{o} \pm .044^{o}$ was obtained where the main part of the uncertainty comes from the systematic variations from orbit to orbit. The SS1 bias has not been directly determined. However, through a Sun sensor switch experiment performed in the mission orbit, SS1 appears to have the same bias as SS2 to within 0.02 degrees.

Note that if there is any error in the calibration of the Sun sensors, it is possible that the Sun sensor biases are Sun angle dependent. All of the Sun angles for the 8 OABIAS data sets used for this report lie between 60^{o} and 72^{o}. Due to this limited range of Sun angles, we are not able to tell whether the Sun angle bias is constant or Sun angle dependent.

---

[1] The field of view of each Sun sensor is approximately 120^{o} extending from either the positive or negative spin axis to 30^{o} beyond the spin plane. Thus, either Sun sensor may be used for Sun angles between 60^{o} and 120^{o}.

3.5 DETERMINATION OF UNCERTAINTIES

An important part of the present work on SMS-2 sensor behavior is the uncertainty analysis. In performing this analysis, a systematic procedure was developed to best evaluate the uncertainties of all the parameters given in this report. The evaluation was based entirely on the numerical results determined from data sets available. No subjective estimates were used in the process reported here.

The OABIAS processing for each data set results in a set of output uncertainties for the spin axis attitude components and biases. These uncertainties are the statistical uncertainties due to the noise of the data and the quality of the fit to the data. They correspond to the minimum uncertainties for the parameters in the sense that they do not include any unknown correlated systematic variation. The best way to estimate the total uncertainties of the parameters determined including all possible systematic variations, is to determine repeatedly the same parameters by processing different data sets which are from different orbits and different attitudes. Systematic variations are not always observable within a single data set. However, they are usually apparent when more data sets involving the same sensors are processed. Whether or not there exists any systematic variation can be seen in the dispersion of the solutions for the same parameters. If the solutions differ by more than the statistical uncertainties, the presence of systematic errors in the solutions is indicated. The more solutions that are available for the same parameter, the better is the information that can be obtained for the systematic uncertainties. Among the OABIAS parameters determined from the eight SMS-2 data sets, the Sun angle bias is the one most frequently solved for (see Table 3-2). Therefore, a quantitative method of extracting the effect of systematic variations on all solved for parameters is from a study of the dispersion of Sun angle bias solutions.

The following steps were followed in determining the uncertainties of the para-

meters reported in the present work. The first step was to obtain a weighted mean value for the Sun angle bias. In order to do this, correct weights were determined for the six solutions given in Table 3-8. Although the total uncertainty of each solution was not known, it is reasonable to use the statistical uncertainties for the relative weights because the statistical uncertainties do reflect the quality of the data and the goodness of the fit. Once the relative weights are available, the mean value can be obtained immediately from the following relation:

$$\overline{\Delta\beta} = \frac{\sum_i W_i' (\Delta\beta_i)}{\sum_i W_i'} \qquad (3\text{-}1)$$

Where the index, i, indicates the six individual solutions and W_i' is the relative weight of the i^{th} solution defined as the inverse of the square of its statistical uncertainty. After $\overline{\Delta\beta}$ was determined, the next step was to evaluate the expected error in $\overline{\Delta\beta}$. From statistical theory (for example see Reference 8), the uncertainty of the mean can be obtained from the relative weights and the dispersions of the individual solutions by the following equation:

$$\sigma^2_{\overline{\Delta\beta}} = \frac{\sum_i [W_i' (\Delta\beta_i - \overline{\Delta\beta})^2]}{(N-1) \sum_i W_i'} \qquad (3\text{-}2)$$

where N is the total number of observations which is 6 in the present case. The accuracy of $\sigma_{\overline{\Delta\beta}}$ depends strongly on N . The larger N is, the more accurately $\sigma_{\overline{\Delta\beta}}$ can be determined. Once $\sigma_{\overline{\Delta\beta}}$ was obtained, the overall uncertainties of the individual solutions were calculated as follows (see Reference 8).

$$\sigma_i^2 = \sigma^2_{\Delta\beta} \left(\frac{\sum_i W_i'}{W_i'} \right) \qquad (3\text{-}3)$$

Thus, from a set of relative weights obtained from the statistical uncertainties, the mean, the uncertainty of the mean, and the total uncertainties of the individual solutions for the Sun angle bias were determined by using Equations 3-1

through 3-3.

The ratio between the total uncertainty and the statistical uncertainty is the same for all six solutions (i.e., independent of i) as can be seen by substituting Equation 3-2 into Equation 3-3, which gives

$$\sigma_i^2 = \frac{\sum_i [W_i'(\Delta\beta_i - \Delta\beta)^2]}{(N-1)\,W_i'} = (\sigma_i') \frac{\sum_i [W_i'(\Delta\beta_i - \bar{\Delta\beta})^2]}{N-1}$$

or

$$\left(\frac{\sigma_i}{\sigma_i'}\right)^2 = \frac{\sum_i [W_i'(\Delta\beta_i - \bar{\Delta\beta})^2]}{N-1} = C^2 \qquad (3\text{-}4)$$

In Equation 3-4, σ_i' is the statistical uncertainty for the ith solution and C is a constant independent of i, which gives the proportionality between the statistical uncertainty and the total uncertainty. In the present case, C is fairly high with a value of 5.9. This means that the major part of the uncertainty is due to the systematic variations.

Once C was obtained, the method used to estimate the total uncertainties for the solutions of other parameters was to assume the same proportionality constant C. That is, each statistical uncertainty was multiplied by the derived constant C to obtain the total uncertainty. This corresponds to the assumption that the systematic variations in the Sun angle bias measurements have the same physical cause as the systematic variations in other state vector elements. With the total uncertainties determined, the weighted mean and the uncertainty of the mean for each parameter were then claculated through the following equations (see Reference 8).

$$W_i = \frac{1}{\sigma_i^2} \qquad (3\text{-}5)$$

$$\bar{x} = \frac{\sum_i W_i x_i}{\sum_i W_i} \qquad (3\text{-}6)$$

$$\sigma_{\bar{x}}^2 = \frac{1}{\sum_i W_i} \qquad (3\text{-}7)$$

Where x is the individual parameter, i indicates the different solutions for the parameter x, $\bar{x}$ is the weighted mean, and $\sigma_{\bar{x}}$ is the uncertainty of the mean.

All results listed in the tables given in Sections 3.4.3 and 3.4.4 were obtained following the procedures described above. Note that the relative uncertainties should be much more reliable than the absolute total uncertainties since the former are based on the statistical uncertainties determined from processings of about 200 data points while the latter are determined from only 6 observations. Specifically, for an uncertainty σ determined from 200 data points, the 95 percent confidence interval for the uncertainty is 0.91σ to 1.11σ, which is a small interval of about 0.2σ. (See, for instance, Reference 9). On the other hand, the 95 percent confidence interval for an uncertainty σ determined from 6 data points ranges from 0.62σ to 2.45σ. This gives an interval of about 1.83σ which is 9 times as large as that determined from 200 data points. This means that the relative uncertainties given in this report should be 9 times as reliable as the absolute uncertainties.

SECTION 4 - CONCLUSIONS AND RECOMMENDATIONS

4.1 CONCLUSIONS

The principal conclusions are that the SMS-2 attitude sensors performed adequately with no biases in excess of 0.4 degrees and that all necessary biases for accurate determination of attitude were successfully determined in near real-time by the Optical Aspect Bias Determination System, OABIAS. In addition, new statistical and geometrical procedures developed for predicting and measuring the determinability of biases were effective in both planning and carrying out an extensive program of bias determination which resulted in obtaining sensor bias measurements for all five SMS-2 Earth horizon sensors and Sun sensor-2. Following are the specific conclusions resulting from the SMS-2 analysis:

1. Counting both Earth-in and Earth-out azimuth biases as a single parameter, there are seven sensor parameters that differ from their nominal prelaunch value by more than the uncertainty in the data. These are:

   a. Sun sensor 2:

      Sun angle bias = -0.19 ± 0.04 degrees

   b. Earth horizon sensor 1 (+4 degrees):

      Sensor mounting angle bias = $+0.08 \pm 0.05$ degrees

      Azimuth bias = -0.37 ± 0.08 degrees

   c. Earth horizon sensor 2 (-4 degrees):

      Azimuth bias = -0.38 ± 0.32 degrees

   d. Earth horizon sensor 4 (-25 degrees):

      Azimuth bias = -0.36 ± 0.15 degrees

   e. Earth horizon sensor 5 (-48 degrees):

      Sensor mounting angle bias = $+0.27 \pm 0.07$ degrees

      Azimuth bias = -0.24 ± 0.17 degrees

All uncertainties are 95% confidence level (2σ). If it is assumed that the azimuth biases are all produced by some common cause, such as a misalignment of the reference azimuth or an advance in the triggering time of the sensor electronics, then the measurement value of this "common azimuth bias" is -0.35 ± 0.06 degrees.

2. A major systematic anomaly referred to as the pagoda effect occurs in the SMS-2 sensor data. The effect is most noticeably characterized by a sharp upturn in the Earth-out rotation angle plots as the scan of an horizon sensor enters or leaves the disk of the Earth. Although less evident when away from the edge of the disk, the pagoda effect produces observable systematic variations in rotation angle data whenever the sensor crosses a chord of the Earth's disk less than approximately 11 arc degrees in length. These data must then be discarded for attitude and bias determination purposes. This loss of data is particularly serious in that it covers a substantial portion of the geometrically valuable data used for bias determination. Any significant increase in the pagoda effect on future missions could interfere with or curtail systematic bias determination procedures unless the effect is adequately modeled. The pagoda effect is in good qualitative agreement with simulated data based on modeling the response of horizon sensor electronics. Work on obtaining quantitative agreement is in progress.

3. The prelaunch analysis procedures initiated with SMS-2 were successfully used to increase the effectiveness of bias determination procedures as follows:

   a. The bias and attitude determination geometry plots described in Section 2.2 reduced the number and variety of simulation runs that were needed for prelaunch analysis, even though numerous simulation runs were made to verify the conclusions reached from the geometry plots. As a consequence bias and attitude determin-

ability studies were carried out prior to launch for the Apogee Motor Firing attitude in both the transfer and drift orbit and for effectively all attitudes between AMF attitude and orbit normal in the drift orbit. This contrasts with SMS-1 for which bias determinability studies were confined nearly entirely to the AMF attitude in the transfer orbit.

b. The determinability of attitude and bias components was correctly predicted for sensors and geometries considered in the prelaunch analysis, with the exception of bias components for Earth horizon sensor-5 (-48 degrees) in the post AMF drift orbit. This exception appears to be directly attributable to the strong pagoda effect for this sensor which necessitated discarding data for all scan widths less than 80% of the Earth's diameter.

The prelaunch analysis was used to plan and carry out a successful sequence of bias determination activities during the course of maneuvering the spacecraft from AMF attitude to orbit normal.

4. New systematic procedures used for determining the statistical uncertainty due to the noise on the data and the quality of the fit to the data were effectively used in three ways: to improve the accuracy of the overall uncertainties in the attitude and bias parameters; to evaluate the effectiveness of different pre-averaging procedures; and to identify residual systematic errors in the data as described below.

5. The procedure of using multiple intermediate attitudes for bias determination purposes while maneuvering the spacecraft attitude to orbit normal was very successful. Specifically, this allowed the identification of some systematic residual errors between data sets which consequently increased the accuracy of the overall uncertainties and improved the general confidence in the results. Systematic residuals were clearly identifiable in the attitude sensor data. The

comparison of data from different sensors in the same orbit and the same sensors in different orbits suggests that the major component of the systematic variations may be residual errors in the orbit parameters. This implies that sufficiently accurate information to further refine orbit parameters may be available in the attitude sensor data, if both attitude and orbit estimates are based on approximately one orbit of data.

4.2 RECOMMENDATIONS

The recommendations in this section are based on the conclusions of the previous section and on the experience gained in the SMS-2 prelaunch and postlaunch. analysis. The order is not intended as a measure of relative priority. However, the first recommendation on the modeling of sensor electronics is, in the opinion of the authors, the most important one in that an unmodeled pagoda effect only slightly larger than that observed on SMS-2 could seriously hamper systematic procedures for attitude and bias determination. For example, a pagoda effect only 25% larger in Earth width would have resulted in no data at all being available for systematic determination of biases for ES5 on SMS-2.

The recommendations are:

1. Analysis should continue on the modeling of sensor electronics. Specifically, the analysis should include at least the following three elements:

   a. Quantitative analysis of the pagoda effect in SMS-2 sensor data to determine the degree to which the effect can be accurately modeled in terms of electronic response of the horizon sensor or other parameters.

   b. Determination of other effects which might be expected to result from anomalies in electronic response. This would specifically include an estimate of the azimuth bias which could result from electronic delays in horizon triggering times.

c. Determination and implementation of the most effective procedure for incorporating modeling of the sensor electronics into the Optical Aspect Bias Determination System, OABIAS, so that portions of the data which exhibit systematic variations due to the pagoda effect may be retained for attitude and bias determination purposes. It is not envisioned that electronic parameters would be incorporated into the OABIAS state vector for systematic measurements of their values at this time. Rather, it is recommended that sensor electronic response be taken into account in the same fashion as the oblateness of the Earth. That is, electronic parameters would be specified in one or more Namelist displays and would be used to determine a small final correction to predicted data prior to comparison with observed data.

The above analysis should result in the specification of parameters to be provided or calibration experiments to be performed that would provide the necessary information for determining the electronic response of any spacecraft attitude sensor prior to launch. Thus, electronic parameters would be treated in the same fashion as mounting angle parameters in that nominal values would be specified and final measured values would be provided prior to launch. A preliminary list of the appropriate parameters for specifying the response of horizon sensor electronics which determine horizon crossings by effectively differentiating the intensity of the illumination falling on the sensor and then triggering on the derivative signal is as follows:

(1) The form of the transfer function of the sensor electronics should be specified, as is done in the SMS Phase C Design Report (Reference 10), Section 4.3.2.2.

(2) The nominal and measured values of any parameters used in the transfer function should be given. In the case of the transfer

function from the SMS Phase C Design Report, this would entail specifying the following: preamplifier lower and upper cutoff, amplifier lower and upper cutoff, transformer lower cutoff, and detector response.

(3) The triggering mechanism and triggering level should be specified. "Mechanism" refers to the source of the pulse or pulses to establish the triggering level, to any external constraints which are placed on whether a triggering is recorded, and to how the first triggering is obtained as the sensor first scans into the Earth.

2. Analysis of the effect of proposed orbit and attitude sequences on attitude and bias determination should be included in mission planning as soon as a tentative timeline has been identified. With the geometric analysis and bad numerical results discussed elsewhere, an effective preliminary analysis of the potential for accurate determination of attitude and sensor biases could be carried out quickly and economically.

The standardization of attitude sensors and sensor electronics would greatly improve the ability to model their response since calibration and bias information gained on one satellite could be used on other satellites. This would also increase the potential for successful bias determination, since bias determination is frequently carried out at times when the attitude and orbit are different from nominal mission orbit and attitude. Since bias determination activities are normally not a part of the mission timeline until relatively near the launch date, they have not been taken into account in planning the variety of conditions under which attitude sensors would be required to operate. On the other hand, standardized sensors require that their behavior be well understood for a variety of operating conditions.

4. Analysis and development of the Attitude and Bias Determinability Prediction System (BAD) should continue in order to provide specific numerical measures of the determinability and distinguishability of attitude and bias parameters and to aid in obtaining appropriate relative weights for the biases obtained in the post-launch analysis.

5. In an area closely related to the development of the BAD System, analysis should continue on the generation and evaluation of geometry plots. This should include at least a study of the geometry of Earth-in and Earth-out dihedral angles and a study of the relative size and extent of the poor geometry regions. Procedures should be implemented for computer generation of geometry plots, so that they may become a regular part of bias and attitude determination analysis. It is specifically recommended that, at the present time, a self-contained system not dependent on interactive graphics be implemented for generation of geometry plots on the Cal Comp plotter. It is further recommended that consideration be given to the future development of an interactive graphics system for the prediction of bias and attitude determinability. Such a system would incorporate both the geometry plot techniques for overall immediate evaluation of geometric situations and the BAD analytic techniques for the development of specific numerical information.

6. Analysis should be undertaken on the effect of pre-averaging of data, particularly with respect to its effect on bias determination. The specific goal here is to increase the amount of information that can be gained from the attitude data without introducing any unwanted correlations or destroying the statistical independence of the data. This should be accomplished without greatly increasing the computer resources as would be required by increasing the number of points processed through OABIAS by a factor of 10 to 50.

7. Two minor modifications should be made to the OABIAS system prior to the next operational use of the program: These modifications are:

   a. Provide an option to constrain the Earth-in and Earth-out azimuth biases to have the same value.

   b. Provide an option for the automatic updating of the initial estimates of the data noise used to weight OABIAS observation models.

APPENDIX A - SMS ATTITUDE DETERMINATION HARDWARE DESCRIPTION

A.1 SPACECRAFT DESCRIPTION

The geometric structure of the SMS spacecraft is a cylinder 190.5 centimeters in diameter and 344 centimeters in length from the top of the magnetometer to the bottom of the apogee boost motor (ABM), as shown conceptually in Figure A-1. The spacecraft has a nominal launch weight of 626 kilograms. The primary structural member is a thrust tube located in the center of the cylinder. The radiometer/telescope instrument, extending the length of the spacecraft, is located in and supported by the thrust tube. The scanning mirror looks out through an opening in the cylindrical solar array of the spacecraft with a clear field of view of the Earth. The radiation cooler is mounted on the end of the spacecraft with a clear view of space. Solar panels form the outer walls of the spacecraft. An equipment shelf contains most of the spacecraft electronics. The ABM is attached to the thrust tube and covers the radiation cooler area. It is ejected by ground command, immediately after the AMF. In addition to the ABM, the spacecraft has an auxiliary hydrazine propulsion system. The hydrazine control system is capable of performing attitude and orbit adjustment maneuvers in the transfer, near synchronous, and synchronous orbits. This system consists of two 5-pound axial jets; two 5-pound radial jets; and two 0.5-pound vernier jets. A schematic drawing of this auxiliary propulsion system is presented in Figure A-2. These control jets can either be fired individually, or the two axial jets or the two radial jets can be fired simultaneously.

A.2 ATTITUDE DETERMINATION AND CONTROL SYSTEMS, ADAC

Attitude and stabilization control of the SMS spacecraft is maintained through the operation of an attitude determination and control (ADAC) system and an auxiliary propulsion system (APS) on-board the spacecraft (see Reference 10).

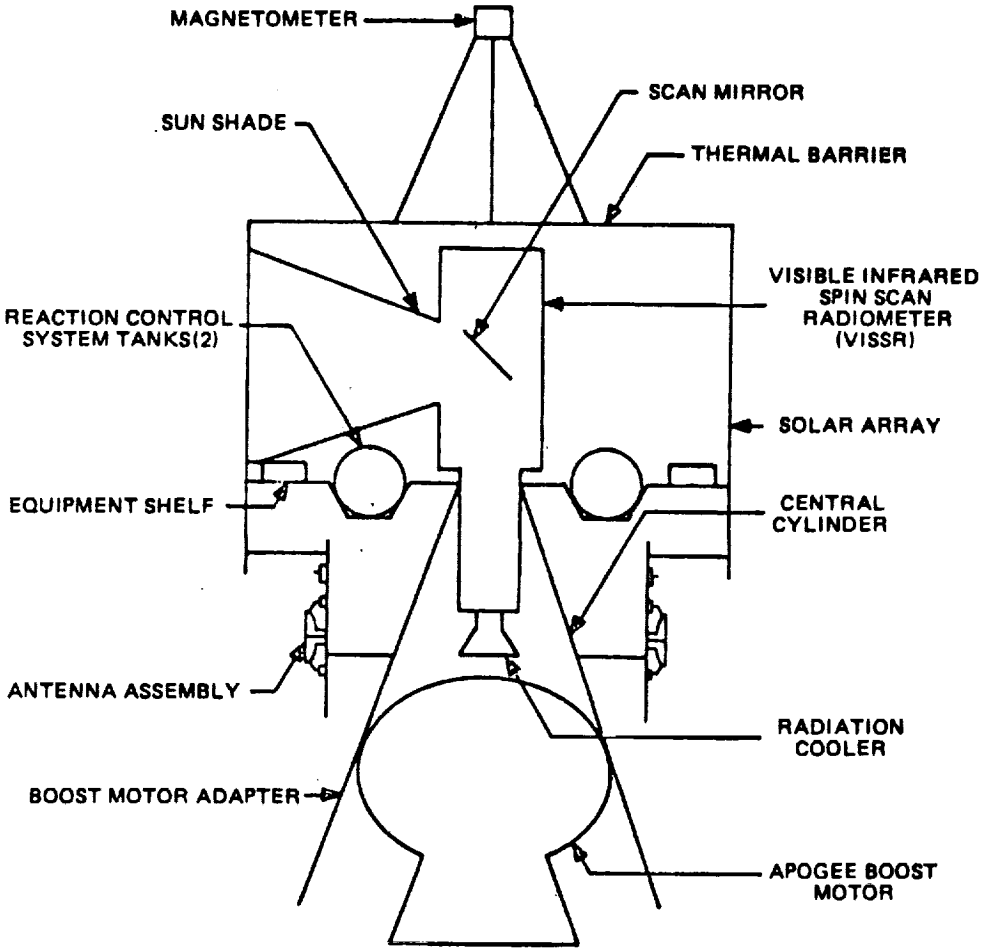

Figure A-1. Schematic View of SMS Spacecraft

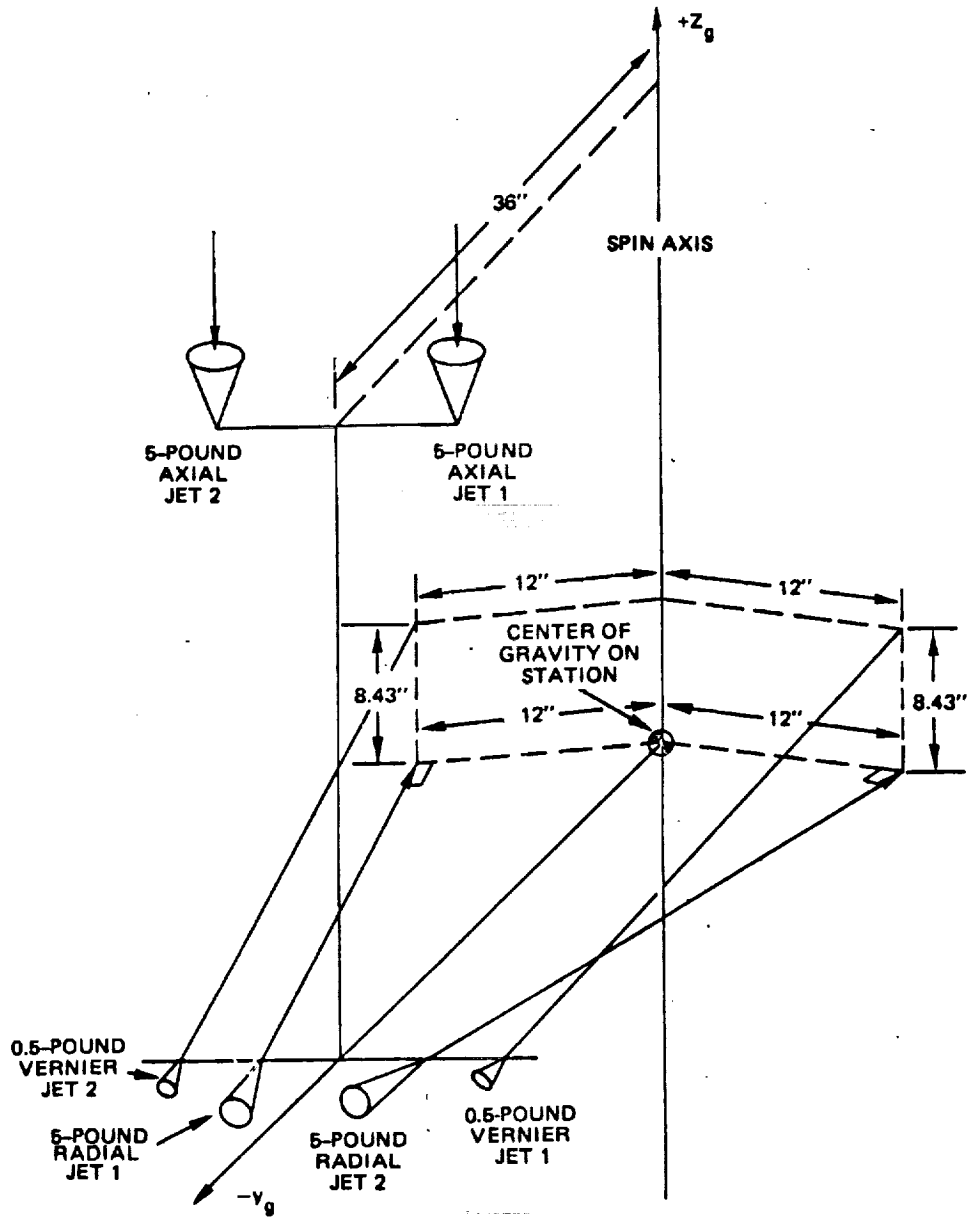

Figure A-2. Auxiliary Propulsion System Schematic

These systems are operated either automatically on the spacecraft or by commands from the ground stations. Spacecraft attitude and stabilization control consists of active and passive nutation control, injection velocity correction, fine and coarse spin-axis precession, fine and coarse attitude control, spin-rate and spin-speed control, station acquisition and changing, and east-west stationkeeping.

The ADAC system consists of Earth, Sun, and nutation sensors, an electronics unit, a valve driver unit, and a passive nutation damper. The outputs of the Earth, Sun, and nutation sensors are conditioned by the ADAC electronics unit and sent to the ground station via telemetry. These data are smoothed and processed on the ground to give an accurate measurement of spacecraft spin axis orientation, spin rate, and attitude before and after programmed maneuvers.

The ADAC system provides fixed-angle referenced timing signals to the Visible/Infrared Spin Scan Radiometer (VISSR) system and to the VISSR digital multiplexer. Also, the ADAC system provides Earth centroid data, and, in sunlight, provides Sun angle referenced data to the Sun Environment Monitor.

The ADAC system either performs or aids in performing the following functions during the transfer orbit phase:

a. Spin axis orientation.
b. Spin rate determination.
c. Nutation sensing.
d. Active nutation damping

The ADAC system either performs or aids in performing the following functions after ABM burn and separation:

a. In the sunlit portions of the orbit:

    (1) Antenna control
    (2) Spin axis orientation determination.

(3) Spin rate determination.

(4) Angle-referenced timing.

(5) Nutation sensing.

(6) Passive nutation damping.

b. In the eclipse portions of the orbit:

(1) SEMS timing.

(2) Antenna control timing.

(3) Nutation sensing.

(4) Passive nutation damping.

(5) Antenna control with other than sun sensor derived reference.

A.2.1 Attitude Determination Sensors

Spin axis orientation is determined by measurements made by Earth and Sun sensors. These sensors are intended to measure the spin axis orientation in the transfer orbit to an accuracy of ±1.0 degree and in the synchronous orbit to an accuracy of ±0.1 degree.

A.2.1.1 Earth Sensors

There are five Earth horizon sensors mounted and positioned in reference to the orbital spin plane as follows:

a. ES1 = $+4^{o}$ above spin plane (towards +Z axis).

b. ES2 = -4^{o} above spin plane (towards -Z axis).

c. ES3 = $+20^{o}$ above spin plane (toward +Z axis).

d. ES4 = -25^{o} below spin plane (towards -Z axis).

e. ES5 = -48^{o} below spin plane (towards -Z axis).

Here, the spin plane is the plane perpendicular to the spin axis and the +Z direction is the spin direction according to the right-hand-rule (as shown in Figure A-3). The measured values of their mounting angles and azimuth angles for SMS-2 are listed in Table A-1. The Earth sensors that are mounted at $+20^{o}$, -25^{o}, and -48^{o} with respect to the orbital spin plane are intended for use during the transfer orbit only and are turned off in mission orbit after the spacecraft is brought to orbit normal. The two Earth sensors mounted $+4^{o}$ and -4^{o} with respect to the orbital spin plane are used during synchronous orbit operations. The output of the Earth sensors is a measure of Earth width, translated by the ADAC electronics unit into instantaneous roll attitude angle data.

The Earth sensors are infrared sensors sensitive to radient energy in the 14-to-16 micron region. The sensor field of view (FOV) is rectangular, approximately 1.1^{o} on a side. As the FOV sweeps across the Earth disk, the radiance discontinuities between Earth and space at the ends of the scanned chord are sensed by the sensor, which produces an analog output as shown in Figure A-4. The analog output from the sensor is a positive pulse followed by a negative pulse, corresponding to the leading and trailing horizon crossings, respectively. The centroid of this two-pulse signal is the apparent Earth center (ignoring the oblateness of the Earth). This point lags the actual Earth center by a known amount because of the time constant of the sensor response. This delay, which has a magnitude of about 0.25^{o} in synchronous orbit, is accurately measured for each Earth sensor, and compensated for during the mechanical alignment.

A.2.1.2 Sun Sensors

Two redundant Sun sensors provide a measurement of spacecraft spin axis orientation with respect to the Sun line, a reference pulse for spacecraft thruster

Table A-1. Measured Sensor Elevation and Azimuth Angles for SMS-2

Sensor	Elevation	Azimuth Angles (+ in direction of spin)		
		Relative to SS1	Relative to SS2	Absolute: From +X axis
SS1	-	0^{o}	$.0056^{o}$	229^{o} 3' 18" (229.0550^{o})
SS2	-	$-.0056^{o}$	0^{o}	229^{o} 2' 58" (229.0494^{o})
ES1	3^{o} 58' 31" (3.9753^{o})	-77.1711^{o}	-77.1655^{o}	151^{o} 53' 2" (151.8839^{o})
ES2	-4^{o} 0' 43" (-4.0119^{o})	-77.1861^{o}	-77.1805^{o}	151^{o} 52' 8" (151.8689^{o})
ES3	20^{o} 0' 15" (20.0042^{o})	96.4372^{o}	96.4428^{o}	325^{o} 29' 32" (325.4922^{o})
ES4	-24^{o} 59' 21" (-24.9892^{o})	91.4397^{o}	96.4453^{o}	325^{o} 29' 41" (325.4947^{o})
ES5	-47^{o} 59' 41" (-47.9947^{o})	168.9778^{o}	168.9834^{o}	38^{o} 1' 58" (38.0328^{o})

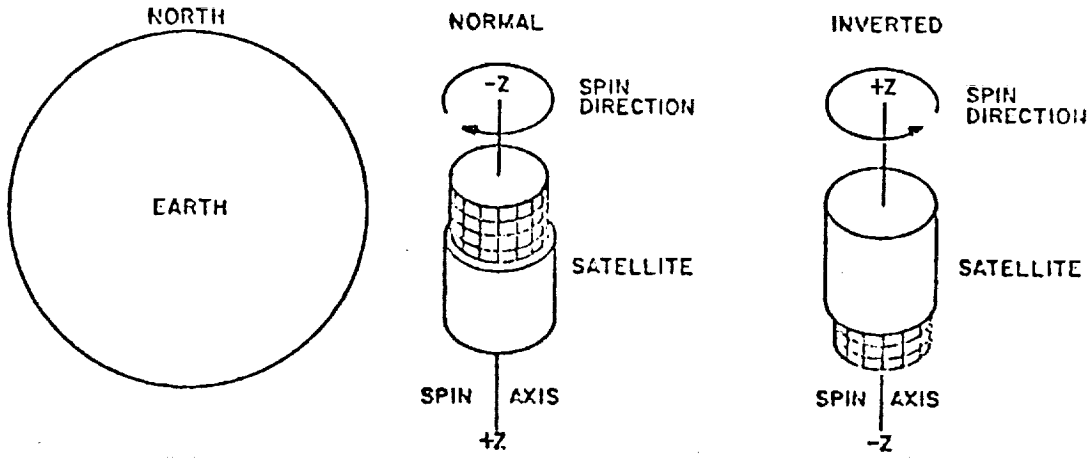

Figure A-3. Spacecraft Spin-axis Orientation

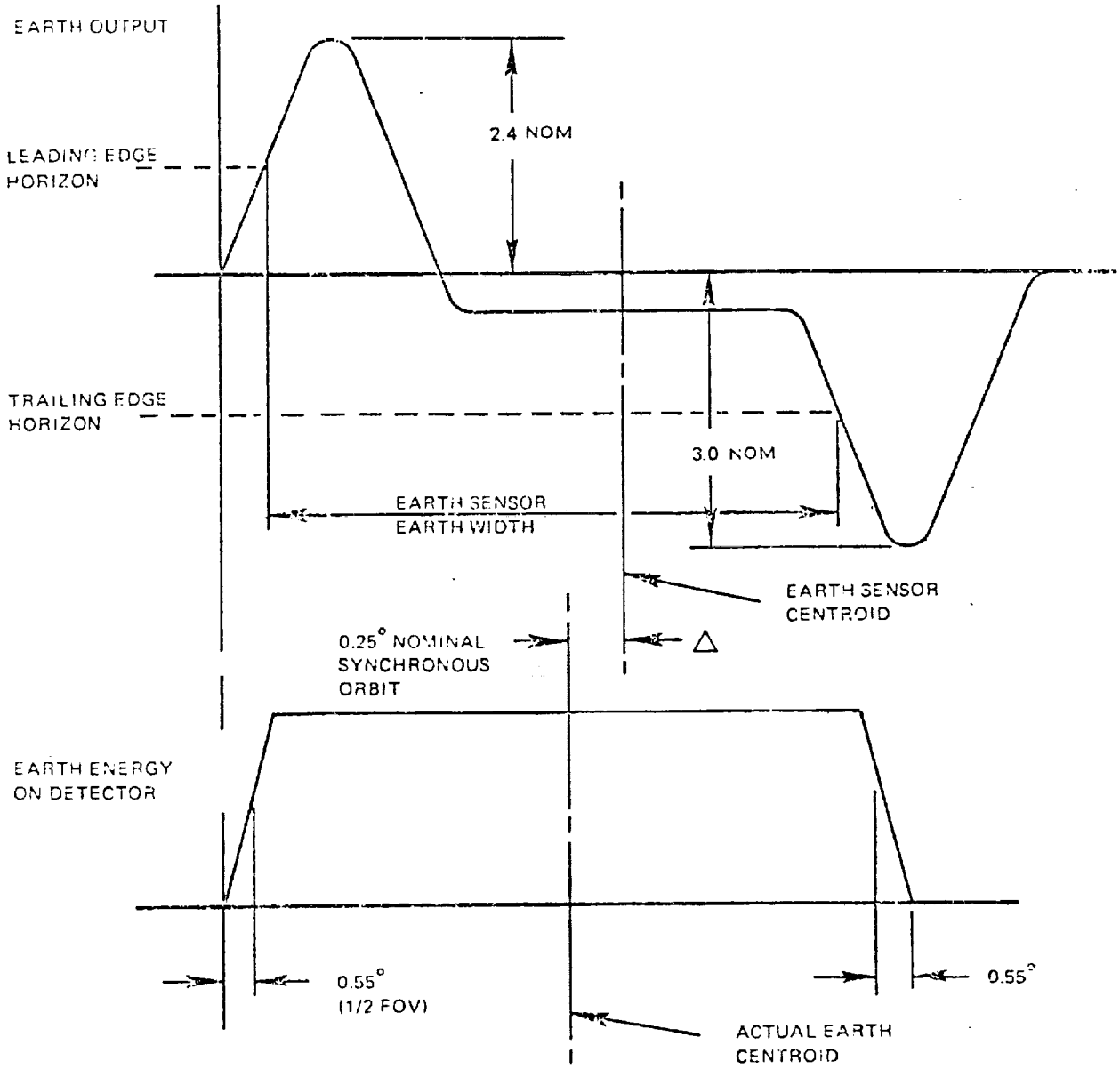

Figure A-4. Input Energy Profile and Sensor Response

ground command timing, and reference pulses for the VISSR system. The sensor output is sent to the ADAC electronics unit where it is formatted for input to the spacecraft telemetry system encoder to the VISSR system, and to the antenna control components.

The basic components of the Sun sensor are an entrance aperture, a shaped mask, and a silicon detector. These elements are arranged so that, with the sensor mounted on a spinning vehicle, the image of the Sun-illuminated entrance aperture is swept across the shaped mask. The shape of the mask determines the length of the output pulse generated by the silicon cell below the mask. The output pulse length varies in proportion to the angle between the Sun and the spin axis.

The sensor layout is shown in Figure A-5. The shape of the mask necessary to give a specified Sun angle-spin angle relationship is a function of aperture-to-mask spacing, the angle between the mask and the spin axis, and the effect of any refractive material in the optical path. The values used for the SMS sensors are 0.75 inch aperture-to-mask spacing and 20^{o} angle between the spin axis and mask plane. There is a 0.030 inch thick quartz window behind the aperture to keep the interior of the sensor free from dust and to provide a measure of radiation protection. The required relationship between Sun angle and spin angle is shown in Figure A-6. The mask shape required to give this relationship is given in Figure A-7.

The field of view (FOV) to be covered is defined in terms of the spin plane. The sensors must give data for Sun angles with respect to the spin plane of -87^{o} to $+87^{o}$. It is also required that redundant information be available between $+30^{o}$ and -30^{o}. Two sensors, each covering 117 degrees elevation (Sun angle), are used, as shown in Figure A-8. The output relationships from the two sensors are shown in Figure A-6. The leading edges of the FOVs are in a satellite meridian plane, containing the spin axis. This yields what is termed a "straight" leading edge. The first appearance of the Sun as detected

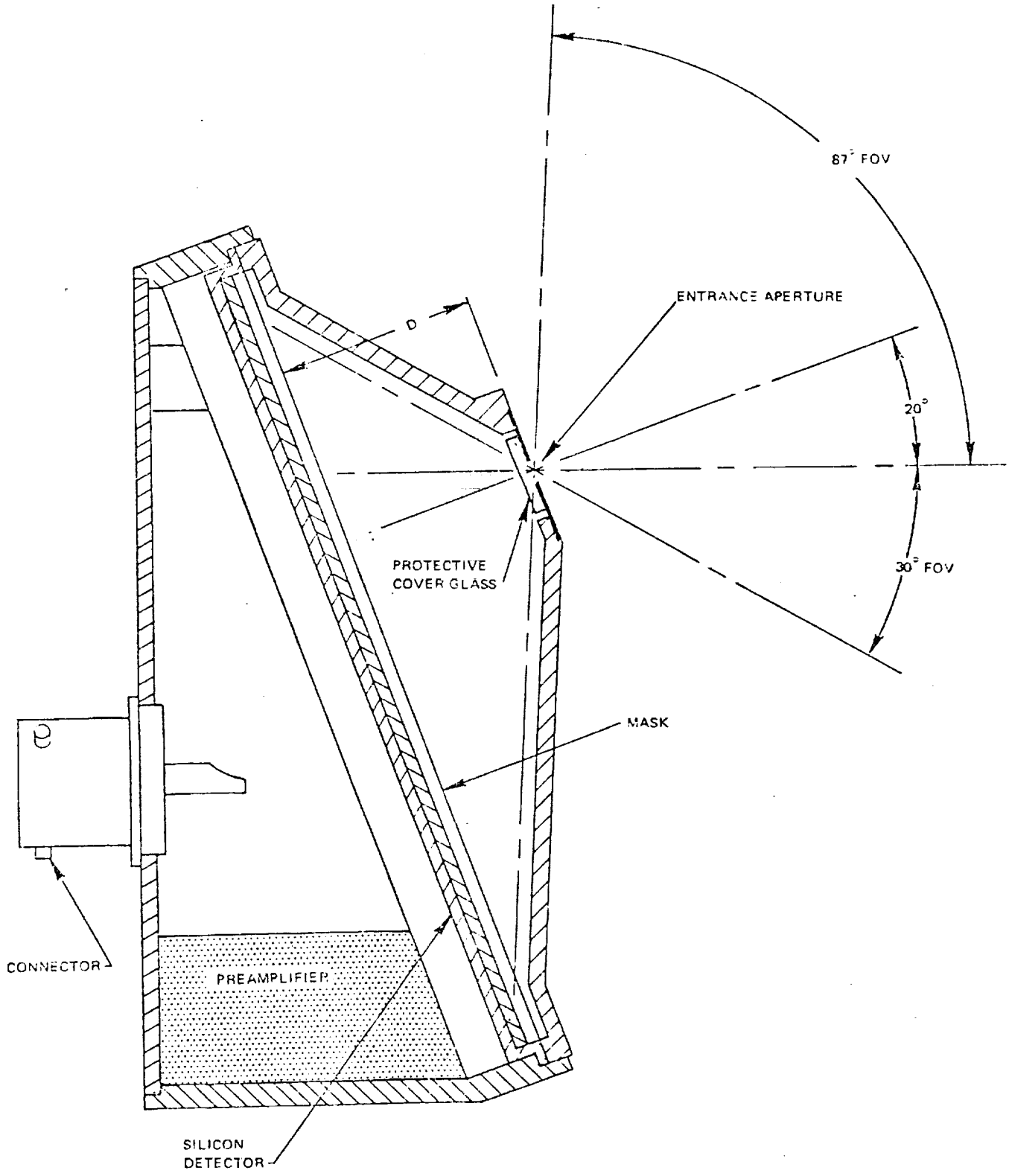

Figure A-5. SMS Sun Sensor

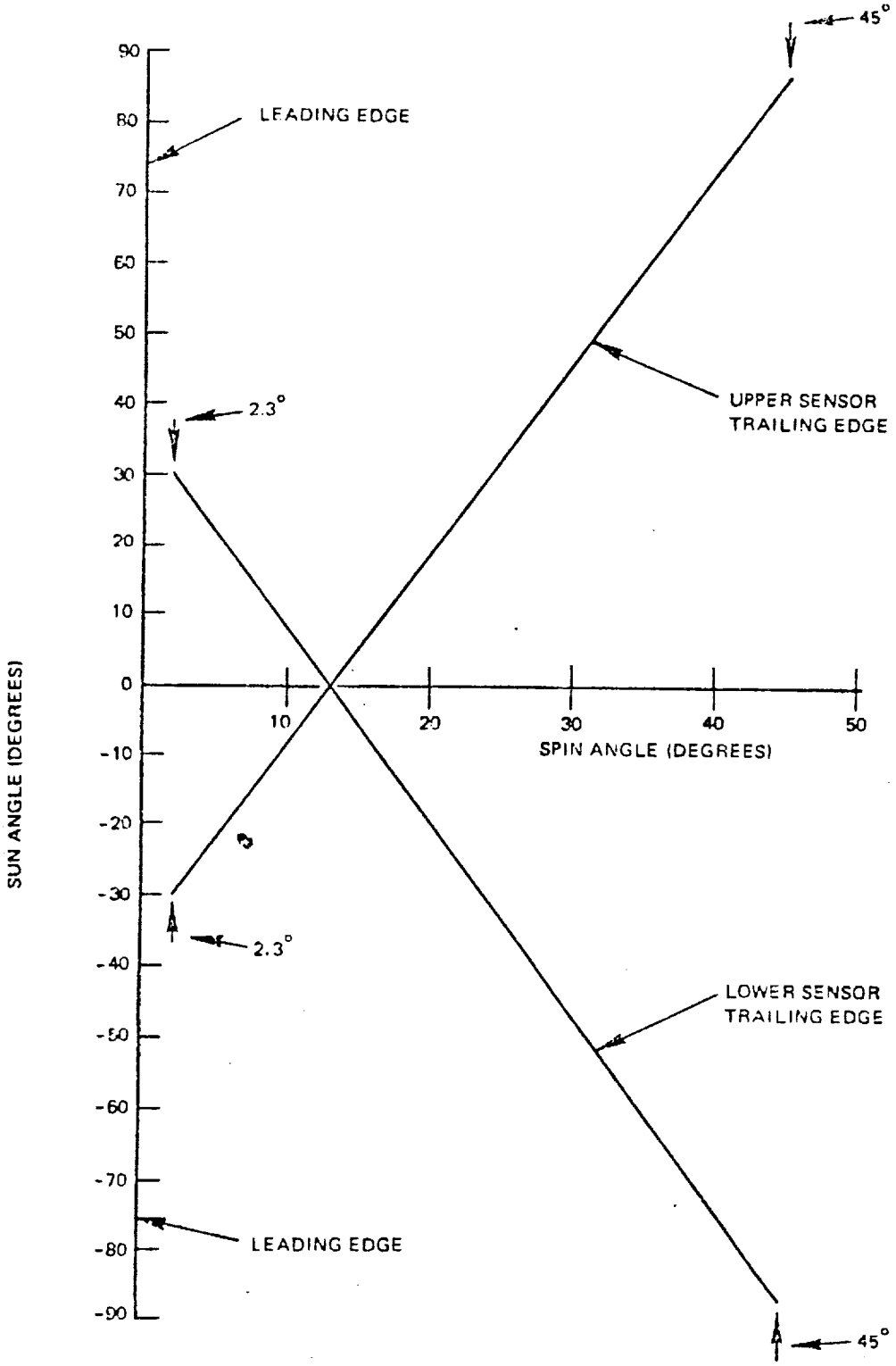

Figure A-6. Characteristics of Interval Between Leading and Trailing Edges (Pulsewidth)

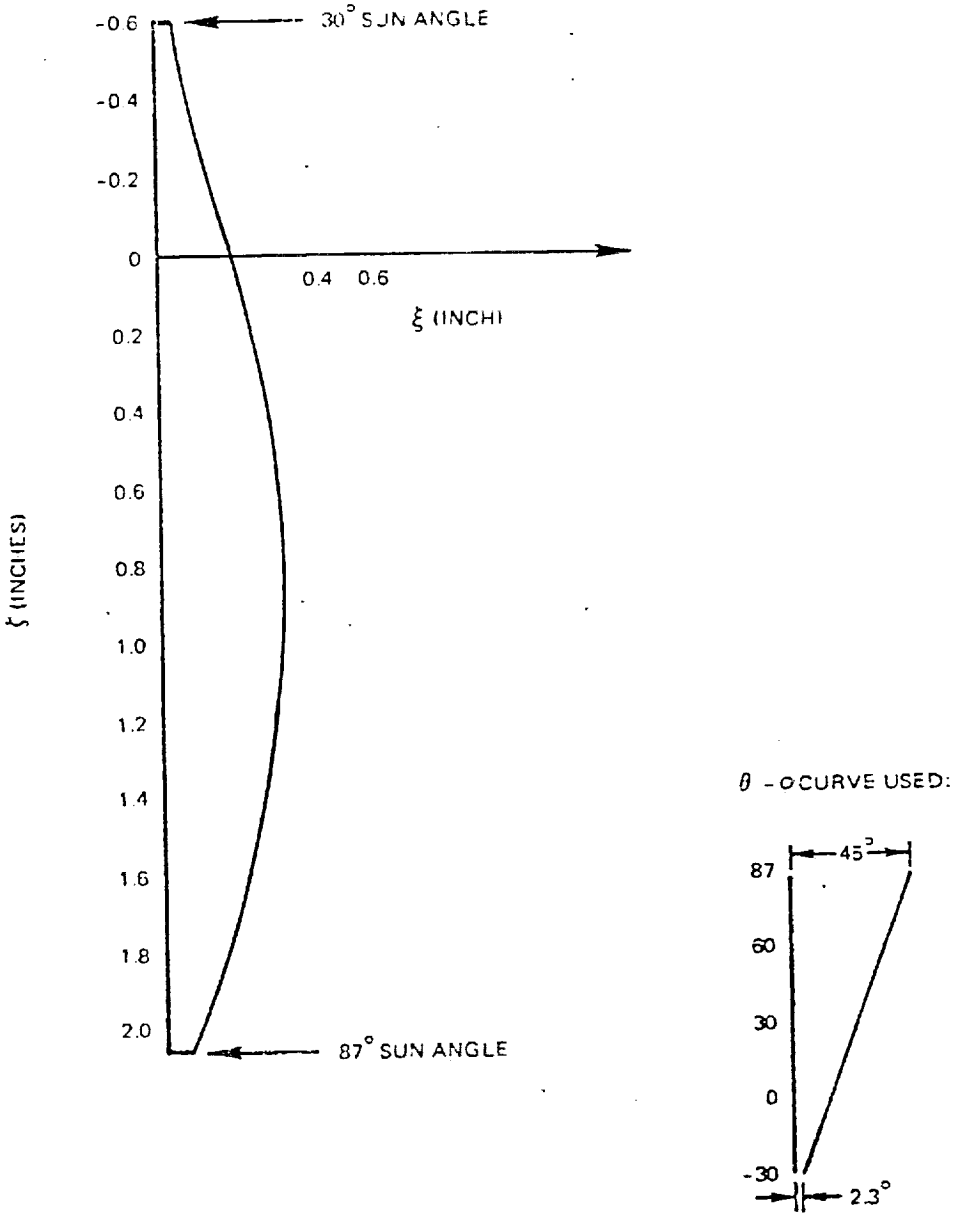

Figure A-7. Sun Sensor Mask Design for SMS

by the sensor occurs at the same azimuth angle with respect to the satellite for all Sun angles from -87 to $+87^{o}$. As can be seen from Figure A-6, the lower sensor is effectively a reflection of the upper sensor about the spin plane. The sensor output signal (the output of the internal preamplifier) is a pulse whose duration depends on Sun angle and spin rate. Predicted outputs for various Sun angles are shown in Figure A-9. The leading edge occurs at the same azimuth point independent of the slope of the trailing edge.

A.2.2 ADAC Electronics

The electronics specifications and design are taken from Reference 10.

A.2.2.1 Specifications

The Earth horizon sensor transfer function is

$$\left[\frac{1}{T_b s+1}\right]\left[\frac{T_1 s}{T_1 s+1}\right]\left[\frac{1}{T_2 s+1}\right]\left[\frac{T_3 s}{T_3 s+1}\right]\left[\frac{1}{T_4 s+1}\right]\left[\frac{T_5 s}{T_5 s+1}\right]$$

where T_b = 1.8 ms at 87.3 Hz (detector)

T_1 = 80 ms at 2 Hz (preamp lower cutoff)

T_2 = 0.238 ms at 670 Hz (preamp upper cutoff)

T_3 = 2.66 ms at 60 Hz (main amp, lower cutoff)

T_4 = 0.560 ms at 284 Hz (main amp, upper cutoff)

T_5 = 80 ms at 2 Hz (output transformer lower cutoff)

The ADAC signal conditioner converts the analog Earth sensor and Sun sensor signals into digital-pulse-type signals whose pulse position and pulse width contain the desired information. To maintain the required accuracy, the signals are threshold-detected at a specified fraction of the (average) peak amplitude. The signal waveforms are given in Figures A-9 and A-4 for

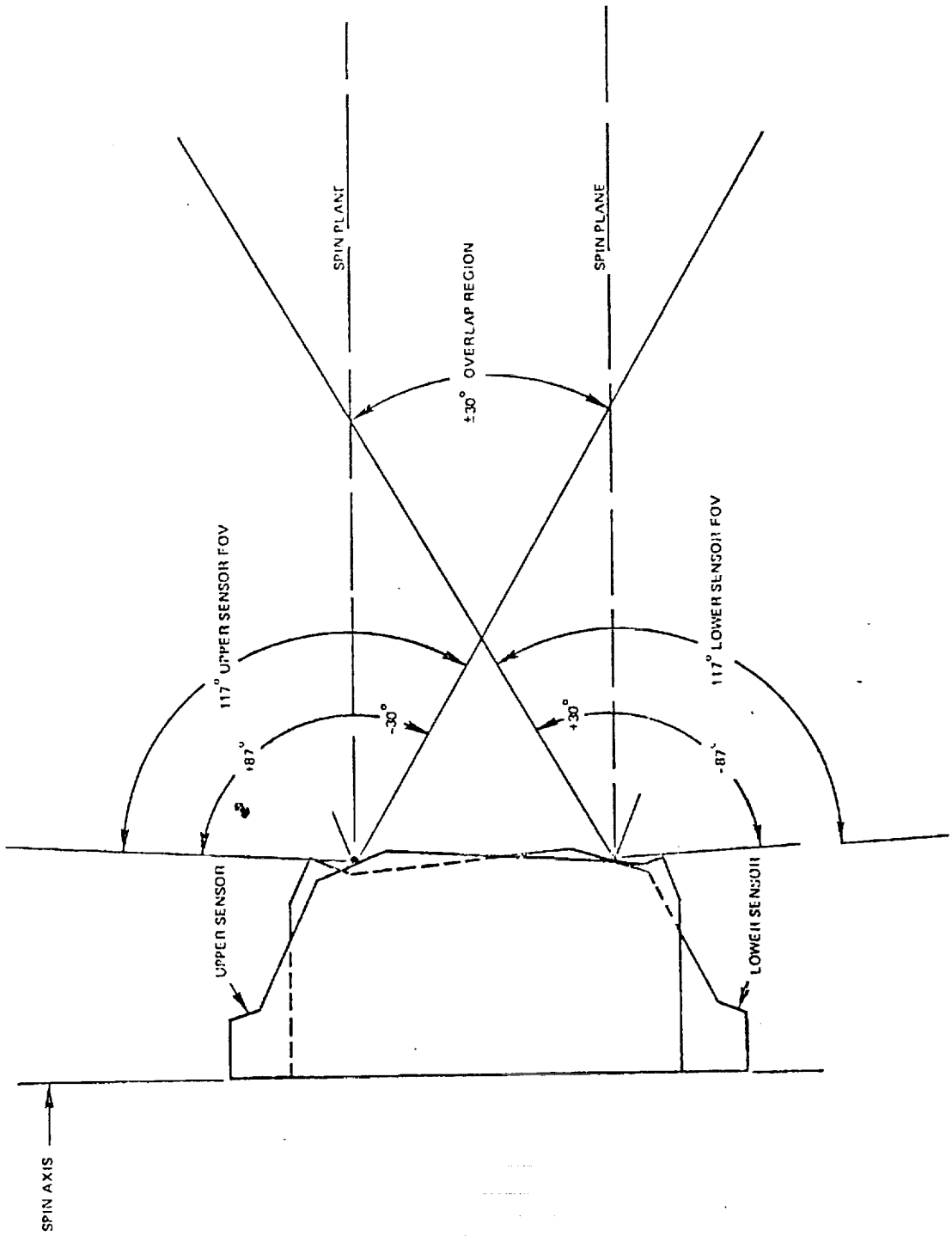

Figure A-8. SMS Sun Sensor FOV Layout

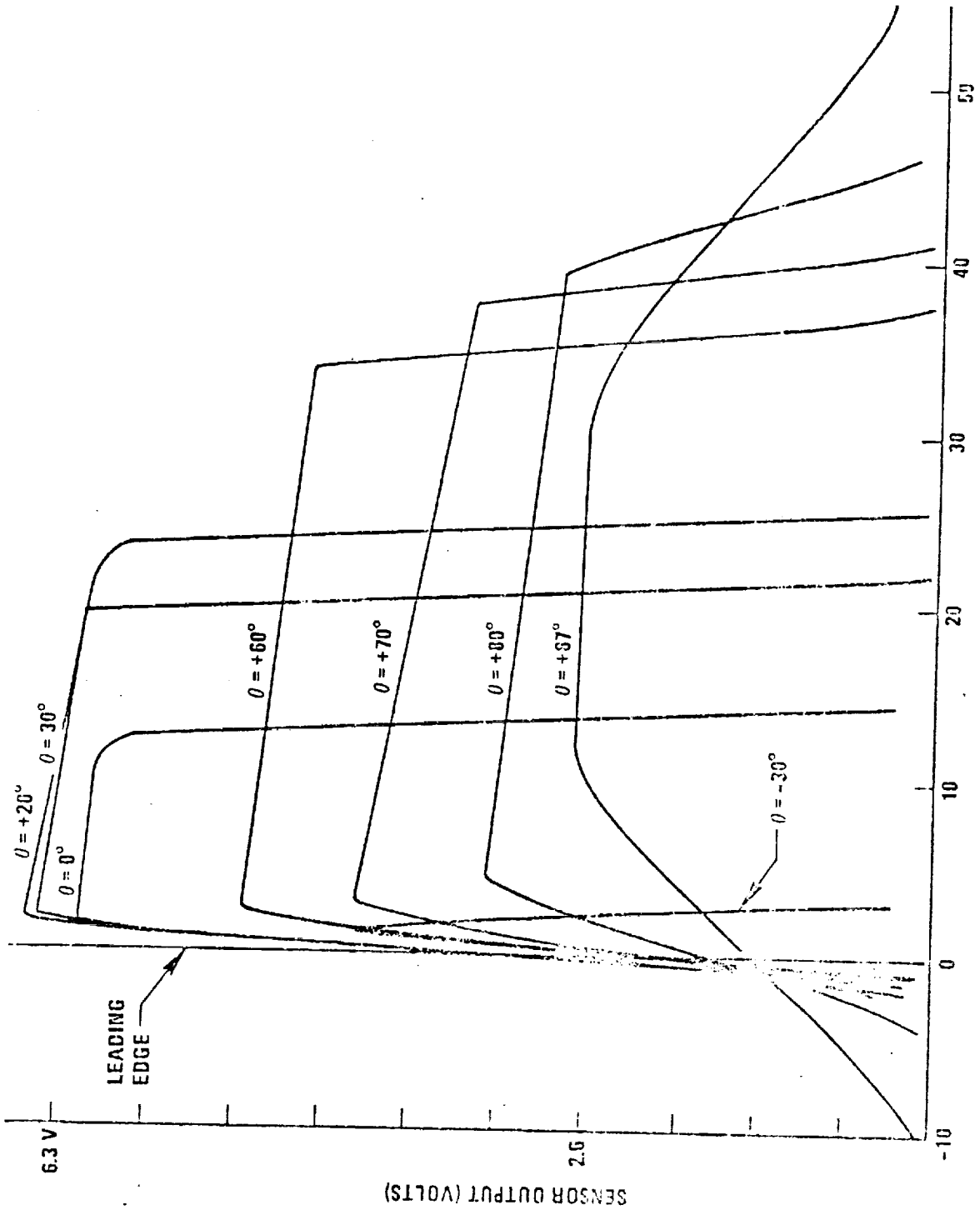

Figure A-9. Sensor Output Contours at Specified Sun Angles

the Sun sensor and Earth sensor, respectively. The electronics requirements are summarized below:

a. Sun Sensor (Identical for each sensor)

1.	Leading edge threshold	50% ±2% of peak
2.	Trailing edge threshold	50% ±2% of peak
3.	Leading edge jitter (including Sun sensor)	less than 1.0 μs pulse to pulse
4.	Output	digital pulse, standard logic levels

b. Earth Sensor (Identical for each sensor)

1.	Leading edge threshold	+50% ±5% of negative peak
2.	Trailing edge threshold	-60% ±5% of negative peak
3.	Output	digital pulse, standard logic levels

A.2.2.2 Design

The detailed block diagram of the signal conditioner is shown in figure A-10. Redundant preamplifiers, not shown, are located at the Sun Sensor for improving the signal-to-noise ratio. The preamplifier utilizes an integrated circuit operational amplifier with a 10 k Ω input resistor. The Sun Sensor is terminated into 1 k Ω resistance. Therefore, a short circuit in an amplifier input will not excessively load the sensor and will assure satisfactory operation of the alternate electronic circuits.

A peak detector uses the buffered signal, detects the average peak amplitude, and holds it in the form of a dc voltage for the threshold references. The threshold detector compares the buffered input signal with the peak detector output voltage scaled down to the desired 50% peak amplitude. When the threshold point is exceeded, an output logic pulse is generated until the signal drops below the trailing edge threshold. An ac positive feedback is used to prevent multiple triggering because of noise and also gives good rise and fall

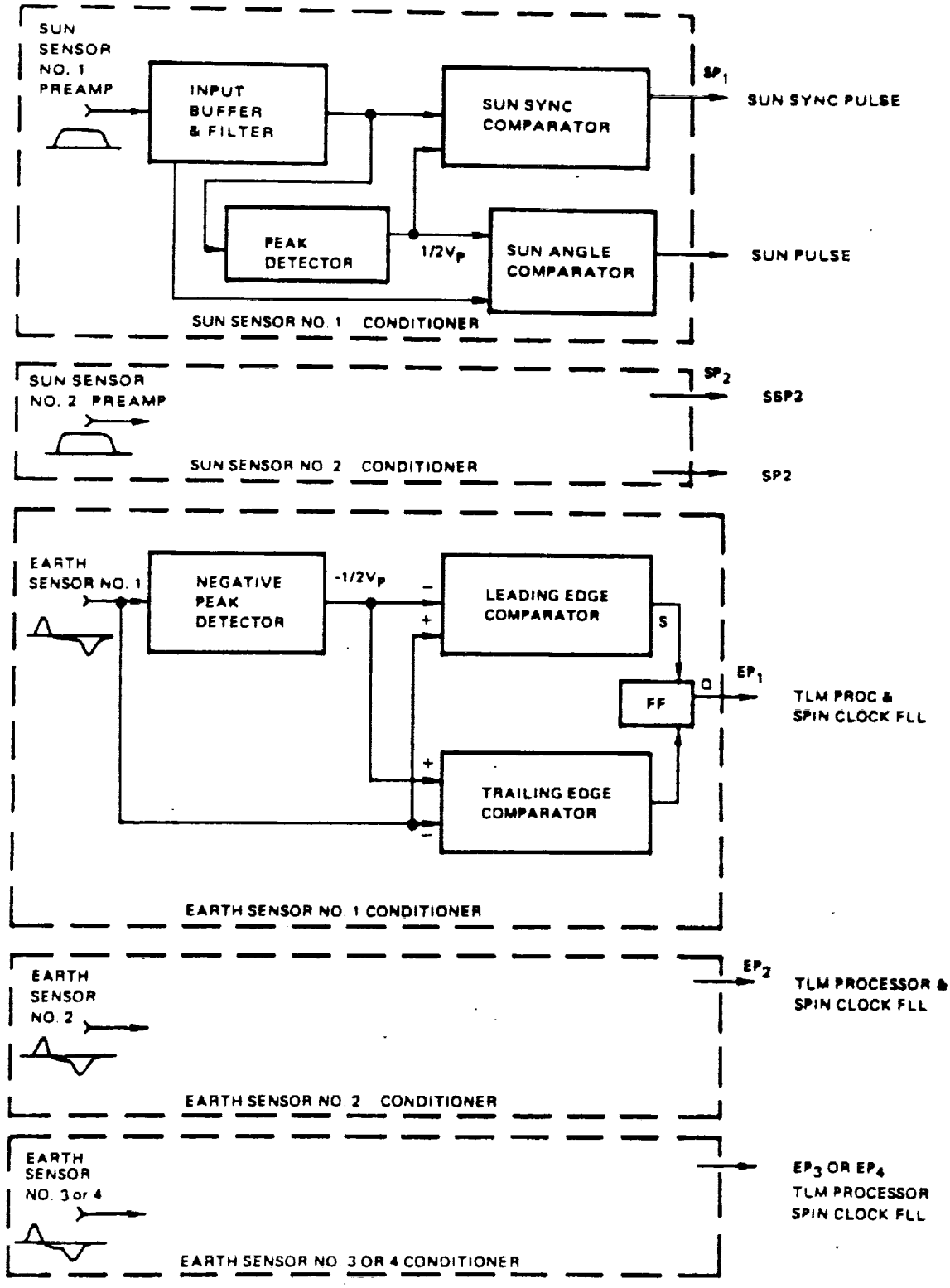

Figure A-10. ADAC Sensor Signal Conditioner

times to the output pulse. Two comparators are used, one for the Sun sync pulse (low jitter) and one for the Sun pulse (Sun angle measurement). Two identical circuits are employed, one for each sensor, to avoid switching low level sensor signals to a single detector and to provide electronics redundancy.

The Earth sensor signal is a buffered, bipolar analog signal resulting from the bandpass filtering of the Earth radiance pulse within the sensor electronics. The negative pulse is less susceptible to Moon interference because of orbit geometry, and it is peak detected by a circuit identical to that used in the Sun Sensor above. The output of the negative edge peak detector is fed to two comparators, one for the positive leading edge pulse and another for the negative trailing edge pulse.

The leading edge is used to set a flip-flop and the trailing edge resets it, thus generating a pulse representing a squared-up Earth radiance, as seen by the Earth sensors. This latter pulse is sent to the telemetry processor and is subsequently used for attitude determination and antenna pointing direction. Two identical circuits are used, one for each Earth Sensor. In addition, the input circuits are fault protected.

A.2.3 Nutation Control System

Prior to the ABM ignition and separation, the spacecraft has an unstable moment of inertial distribution which leads to a divergent nutational or coning motion. Two nutation sensors, which are redundant accelerometers located on the circumference of the spacecraft, measure the nutation angle with respect to the equatorial plane of the spacecraft. These sensors will provide measurements of the spacecraft nutation from third-stage separation to ABM ignition. The data are sent via the ADAC electronics unit and spacecraft telemetry system to the ground station. The ground station monitors the spacecraft nutation data. When the nutation exceeds predetermined limits, the station sends commands to the APS thrusters for damping the nutation.

REFERENCES

1. Computer Sciences Corporation, Document No. 3000-25600-01TR, Optical Aspect Bias Determination (OABIAS) System Description and Operating Guide, in preparation

2. --, Document No. 3000-06000-03TM, Optical Aspect Attitude Determination System (OASYS) Version 4.0 System Description and Operating Guide, M. A. Shear, December 1973.

3. --, Document No. 5035,22300-04TR, System Description and Operating Guide For The Orbit, Sun, and Attitude Geometry Program (OSAG), M. A. Shear, January 1972

4. --, Document No. 9101,13300-03TR, Optical Aspect Data Prediction (ODAP) Program, System Description and Operating Guide, Version 2.0, M. Joseph and M. A. Shear, October 1972

5. --, Document No. 3000-25600-02TR, Bias and Attitude Determinability Prediction System (BAD) Preliminary Analysis, L. C. Chen, K. S. Liu, and J. R. Wertz, in press

6. --, Document No. 3000-29100-06TN, SMS-B Attitude and Bias Determination Geometry, L. C. Chen, C. Chou, and J. R. Wertz, January 1975

7. --, Document No. 3000-27500-02TN, Synchronous Meteorological Satellite (SMS-B) Launch Window Data For January 30, 1975 Through February 15, 1975, S. Rosenburg, January 1975

8. P. R. Bevington, Data Reduction and Error Analysis For The Physical Sciences, New York, McGraw-Hill, 1969

9. J. E. Freund, Mathematical Statistics, Englewood Cliffs, N. J., Prentice-Hall, 1962

10. Philco-Ford Report No. WDL-TR4545, Synchronous Meteorological Satellite Phase C Design Report, June 1971

11. Computer Sciences Corporation Memorandum, OABIAS Analysis Plots For SMS-B, in press